

**INVESTIGATION OF WATER-BASED SILICA AND
ORGANICALLY MODIFIED SLICATE
SOL-GEL SYSTEMS**

By

ROBERT L. PARKHILL

Bachelor of Science

University of Central Oklahoma

Edmond, Oklahoma

1994

**Submitted to the Faculty of the
Graduate College of the
Oklahoma State University
In partial fulfillment of
the requirements for
the Degree of
DOCTOR OF PHILOSOPHY
December, 1999**

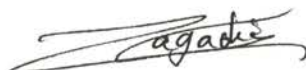
**INVESTIGATION OF WATER-BASED SILICA AND
ORGANICALLY MODIFIED SILICATE
SOL-GEL SYSTEMS**

Thesis Approved:

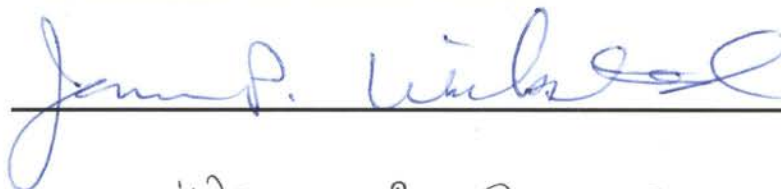


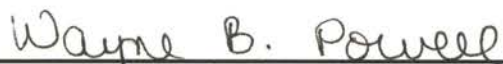
Thesis Advisor











Dean of the Graduate College

PREFACE

This study was conducted to address structural modifications associated with the development of a water-based sol-gel process. High concentrations of alcohol solvent used in traditional sol-gel methods have limited the full potential of sol-gel applications. With growing concerns on environmental issues, the sol-gel process must adapt to meet current and future environmental protection agency regulations. This work will provide a foundation for identifying structural formations associated with high water-content synthetic sol-gel processes. The specific objective of this research was to characterize silicate and organically modified silicate systems with respect to variations in water content, precursor use, curing temperature, and organic content. Water-based gels and films were characterized using ^{13}C and ^{29}Si Nuclear Magnetic Resonance (NMR), Fourier Transform Infrared spectroscopy (FT-IR), and Raman Spectroscopy.

ACKNOWLEDGMENTS

I wish to express my sincere appreciation to my advisor, Dr. Edward T. Knobbe for his intelligence, support, guidance, and friendship in my research at Oklahoma State University. My appreciation extends my doctoral committee—Drs. Edward T. Knobbe (Chair), Richard Bunce, Isabelle Lagadic, Nickalous Kotov, and James Wicksted – for their guidance and support in the completion of this research. I would like to also thank Dr. Richard Bunce, whose assistance and friendship was invaluable.

More over, I wish to express my sincere gratitude to those who provided suggestions and assistance for this study: Drs. Tammy Metroke, Andrew Vreugdendhil, Mike Donley, and Kai Dou.

I would also like to give special appreciation to my wife, Jami, for her understanding and support in my research, her comfort at times of difficulty, and love through the whole process. Special thanks also go to my mother and father, Fran and Bob, for their support, encouragement, love, and sacrifices made for me. Thanks also to my grandparent, James and Doe Splawn, to my sister, Lari Huey, as well as other family members, and friends for their words of encouragement.

Finally, I would like to thank the Department of Chemistry and Environmental Research Center for providing me with this research opportunity and their generous financial support as well as the Air Force Material Research Laboratory at Wright Patterson Air Force Base for its financial support and use of analytical equipment.

TABLE OF CONTENTS

Chapter	page
1. INTRODUCTION.....	1
The Problem.....	1
Purpose of Study.....	2
Limitations.....	2
Outline of Work.....	3
Conclusions.....	5
2. BACKGROUND	7
Sol-gel History	7
Sol-gel Process	8
Hybrid Ormosils	14
Conditions Influencing Structural Formations	17
Aqueous Phase Sol-gel Processing	26
3. EXPERIMENTAL METHODS AND PROCEDURES	29
General Overview of Sol-gel Processes	29
Overview of SiO ₂ Gel Preparation	32
Overview of SiO ₂ -Epoxide Ormosil Preparation	34
Thin Film Application and Monolithic Specimen Formations	38
Spectroscopic Characterization.....	39
4. INVESTIGATION OF WATER-BASED SILICA SOL-GELS BY ²⁹ Si AND ¹³ C SOLID STATE NMR.....	43
Introduction	43
Background	45
Results and Discussions.....	50
Conclusions.....	60

Chapter	page
5. RAMAN INVESTIGATION OF WATER-BASED SOL GELS AS A FUNCTION OF CURING TEMPERATURE.....	62
Introduction	62
Background	65
Results and Discussions.....	67
Conclusions.....	79
6. REFLECTANCE FT-IR INVESTIGATION OF SILICA THIN FILM COATINGS DERIVED FROM A WATER-BASED SOL GEL SYSTEM....	82
Introduction	82
Background	83
Results and Discussions.....	85
Conclusions.....	99
7. SOLID STATE ¹³ C AND ²⁹ Si NMR INVESTIGATION OF AN EPOXIDE-ORMOSIL SYSTEM AS A FUNCTION OF ORGANIC AND WATER CONTENT.....	100
Introduction	100
Background	105
Results and Discussions.....	113
Conclusions.....	133
8. RAMAN INVESTIGATION OF AN EPOXIDE ORMOSIL SYSTEM AS A FUNCTION OF CURING TEMPERATURE AND HYBRID CONTENT....	135
Introduction	135
Background	137
Results and Discussions.....	143
Conclusions.....	160

Chapter	page
9. REFLECTANCE FT-IR INVESTIGATION OF EPOXIDE ORMOSIL THIN FILMS DERIVED FROM A WATER-BASED SOL GEL PROCESS.	161
Introduction	161
Background	163
Results and Discussions.....	166
Conclusions.....	189
APPENIXES.....	191
APPENDIX A NMR SPECTRA AND TABLES OF SILICA GELS.....	191
APPENDIX B RAMAN SPECTRA AND TABLES OF SILICA GELS.....	196
APPENDIX C FT-IR REFLECTANCE SPECTRA AND TABLES OF SILICA GELS.....	202
APPENDIX D NMR SPECTRA AND TABLES OF ORMOSIL GELS.....	209
APPENDIX E RAMAN SPECTRA AND TABLES OF ORMOSIL GELS.....	218
APPENDIX F FT-IR REFLECTANCE SPECTRA AND TABLES OF ORMOSIL GELS.....	228
APPENDIX G MONITORING EPOXIDE CONTENT USING RAMAN.....	242
REFERENCES.....	244
VITAE.....	253

LIST OF TABLES

TABLE	Page
3.1 Reactant concentrations for TMOS derived silica sols with R values of 4, 8, 16, and 24.....	33
3.2 Reactant concentrations for TEOS derived silica sols with R values of 4, 8, 16, and 24.....	34
3.3 Reactant concentrations for 10% organic SiO ₂ -epoxide ormosil sols with R values of 4, 8, 16, and 24.....	36
3.4 Reactant concentrations for 20% organic SiO ₂ -epoxide ormosil sols with R values of 4, 8, 16, and 24.....	36
3.5 Reactant concentrations for 40% organic SiO ₂ -epoxide ormosil sols with R values of 4, 8, 16, and 24.....	37
3.6 Reactant concentrations for 60% organic SiO ₂ -epoxide ormosil sols with R values of 4, 8, 16, and 24.....	37
3.7 Reactant concentrations for 80% organic SiO ₂ -epoxide ormosil sols with R values of 4, 8, 16, and 24.....	37
4.1 Typical ²⁹ Si chemical shifts observed for tetra-oxide and tri-oxide silicate species.....	46
4.2 ²⁹ Si SP/MAS NMR peak positions and assignments for TMOS prepared silicate with R values of 4, 8, 16, and 24.....	50
4.3 ²⁹ Si SP/MAS NMR peak positions and assignments for TEOS prepared silicate with R values of 4, 8, 16, and 24.....	51
4.5 ²⁹ Si CP/MAS NMR peak positions and assignments for TMOS prepared silicates with R values of 4, 8, 16, and 24.....	54
4.6 ²⁹ Si CP/MAS NMR peak positions and assignments for TEOS prepared silicates with R values of 4, 8, 16, and 24.....	55

TABLE	Page
4.7 Density Measurements for TMOS and TEOS prepared silicate gels with R values of 4, 8, 16, and 24.....	57
5.1 Representative vibrational frequencies and assignments for observed bands in TMOS and TEOS derived sol gels.....	66
6.1 Representative vibrational frequencies and assignments for observed bands in TMOS and TEOS derived sol gels.....	84
6.2 Relative frequency shifts for the $\equiv\text{Si-O-Si}\equiv$ (L.O) peak in the TMOS and TEOS thin films prepared with R values of 4, 8, 16, and 24.....	97
7.1 ^{13}C NMR assignments for hybrid epoxide ormosils.....	111
7.2 Typical ^{29}Si chemical shifts observed for tetra-oxide and tri-oxide silicate species.....	113
8.1 Representative vibrational frequencies and assignments for observed bands in epoxide ormosil gels.....	138
9.1 Representative vibrational frequencies and assignments for observed bands epoxide based ormosil thin films coated on aluminum substrates.....	165
9.2 Peak assignments based on literature references.....	167

LIST OF FIGURES

FIGURES	Page
2.1 Overview of sol-gel preparations.....	10
2.2 Preferential sequence of hydrolysis in silicate system.....	20
2.3 Illustrative depiction of linear polymeric growth mechanism.....	20
2.4 Illustrative depiction of branched polymeric growth mechanism.....	21
2.5 Illustrative depiction of colloidal polymeric growth mechanism.....	22
3.1 General schematic representation of the water-based sol-gel process.....	29
3.2 Chemical structures of alkoxide reactants.....	32
3.3 Flow chart of epoxide ormosil preparation.....	35
4.1 Siloxane species characterized by representative “Q “ notation.....	46
4.2 ²⁹ Si SP/MAS NMR spectrum of silica gel prepared using TMOS and a R value of 4.....	50
4.3 ¹ H- ¹³ C CP/MAS NMR spectrum of TMOS gels prepared from R values of (a) 4 and (b) 8.....	53
4.4 ¹ H- ¹³ C CP/MAS NMR spectrum of TEOS gels prepared from R values of (a) 4 and (b) 8.....	53
4.5 Bimolecular and cyclization reactions.....	53
4.6 ¹ H- ²⁹ Si CP/MAS NMR spectrum of TMOS gels prepared from R=4 gel.....	54
4.7 Sol particulates and gel microstructures observed in water based gels.....	61
5.1 Numerical notation for siloxane ring structures.....	67

FIGURE	Page
5.2 Overlaid Raman spectra of SiO ₂ gels prepared using a TMOS solution with an R value of 4 cured at room temperature (RT), 60 °C, 150 °C, 300 °C, and 450 °C.....	68
5.3 Overlaid Raman spectra of SiO ₂ gels prepared using a TEOS solution with an R value of 4 cured at room temperature, 60 °C, 150 °C, 300 °C, and 450 °C.....	72
5.4 Overlaid Raman spectra of SiO ₂ gels prepared using a TMOS solution with an R value of 24 cured at room temperature, 60 °C, 150 °C, 300 °C, and 450°C.....	74
5.5 Overlaid Raman spectra of SiO ₂ gels prepared using a TEOS solution with an R value of 24 cured at room temperature, 60°C, 150 °C, 300 °C, and 450°C.....	75
5.6 Raman spectral comparison of low and high R valued gels for TMOS at room temperature and 450 °C.....	76
5.7 Relative intensities ratios between the 606 cm ⁻¹ and 800 cm ⁻¹ siloxane peaks observed in the TMOS and TEOS gels prepared with R values of 4, 8, 16, and 24. Results are shown as a function of curing at room temperature, 60 °C, 150 °C, 300 °C, and 450 °C.....	77
5.8 Relative intensities for the 1047 cm ⁻¹ nitrate peak observed in the TMOS gels prepared with a R value of 4, 8, 16, and 24. Results are shown as a function of curing at room temperature, 60 °C, 150 °C, 300 °C, and 450 °C...	79
6.1 Overlaid IR reflectance spectra of SiO ₂ thin film prepared with a TMOS solution using a R value of 4. Spectra presented are from films cured at room temperature, 60 °C, 150 °C, 300 °C, and 450 °C.....	88
6.2 Overlaid IR reflectance spectra of SiO ₂ thin film prepared with a TEOS solution using a R value of 4. Spectra presented are from films cured at room temperature, 60 °C, 150 °C, 300 °C, and 450 °C.....	89

FIGURE	Page
6.3 Overlaid IR reflectance spectra of SiO ₂ thin film prepared with a TMOS solution using an R value of 24. Spectra presented are from films cured at room temperature, 60 °C, 150 °C, 300 °C, and 450 °C.....	91
6.4 Overlaid IR reflectance spectra of SiO ₂ thin film prepared with a TEOS solution using a R value of 24. Spectra presented are from films cured at room temperature, 60 °C, 150 °C, 300 °C, and 450 °C.....	92
6.5 Relative intensities for the 940 cm ⁻¹ silanol peak observed in the TMOS and TEOS thin films prepared with R values of 4, 8, 16, and 24.....	93
6.6 Relative intensities for the 440 cm ⁻¹ ≡Si-O-Si≡ peak observed in the TMOS and TEOS thin films prepared with R values of 4, 8, 16, and 24.....	96
6.7 Relative intensities for the 800 ≡Si-O-Si≡ peak observed in the TMOS and TEOS thin films prepared with R values of 4, 8, 16, and 24.....	96
7.1 Glycidoxypropyltrimethoxysilane use in epoxide ormosil preparations.....	103
7.2 Siloxane species represented by “Q” and “T” notation.....	106
7.3 Reference to carbon nuclei with end group formations observed in the hybrid gels.....	112
7.4 ¹ H- ¹³ C CP/MAS NMR spectrum of 10% Epoxide Ormosil gels prepared with D values of 1, 2, 4, and 6.....	115
7.5 ¹ H- ¹³ C CP/MAS NMR spectrum of 80% Epoxide Ormosil gels prepared with D values of 1, 2, 4, and 6.....	120
7.6 ¹ H- ¹³ C CP/MAS NMR spectrum of 10%, 20%, 40%, 60%, and 80% epoxide ormosil gels prepared with D values of 1.....	122
7.7 ¹ H- ¹³ C CP/MAS/NMR spectrum of 60% epoxide ormosil gel prepared with D values of 1, 2, 4, and 6.....	124
7.8 Representative ²⁹ Si single pulse/MAS NMR spectrum of a 60% organic hybrid ormosil gel prepared with D values of 1 and 6.....	126

FIGURE	Page
7.9 Conversion efficiency in 10%, 20%, 40%, and 60% hybrid content gels prepared with D values of 1, 2, 4, and 6.....	127
7.10 Chemical structural of the organic networks formed in lower hybrid content gels with low and high D values.....	131
7.11 Chemical structural of the organic networks formed in the elevated hybrid content gels with low and high D values.....	133
8.1 Overlaid Raman spectra for the 10%, 20%, 40%, 60%, and 80% epoxide hybrid gels prepared with D values of 1 and cured at room temperature.....	147
8.2 Overlaid Raman spectra of the fingerprint region for 10%, 20%, 40%, 60%, and 80% epoxide hybrid gels prepared with an D value of 1 and cured at room temperature.....	148
8.3 Overlaid Raman spectra for the epoxide hybrid gels prepared with D values of 6 and cured at room temperature.....	152
8.4 Raman spectra of the fingerprint region for the epoxide hybrid gels prepared with an D value of 6 and cured at room temperature.....	153
8.5 Spectral overlay of hybrid ormosil gels prepared with an D value of 1 cured at room temperature and 150 °C.....	156
8.6 Spectral overlay of hybrid ormosil gels prepare with a D value of 6 cured at room temperature and 150 °C.....	156
8.7 Raman spectra of the fingerprint region for the 80% epoxide hybrid gels cured at room temperature and 150 °C.....	158
9.1 Overlaid IR reflectance spectra of epoxide-based ormosil thin film prepared using an D value of 1 and cured at room temperature.....	169
9.2 Overlaid IR reflectance spectra of epoxide-based ormosil thin film prepared using a D value of 1 cured at room temperature (enlargement).....	170

FIGURE	Page
9.3 Overlaid IR reflectance spectra of epoxide-based ormosil thin film prepared using an D value of 6 and cured at room temperature.....	172
9.4 Overlaid IR reflectance spectra of epoxide-based ormosil thin film prepared using a D value of 6 cured at room temperature (enlargement).....	173
9.5 Overlaid IR reflectance spectra of 20% hybrid content ormosil film prepared using an D values of 1, 2, 4, and 6. Films were cured in air at room temperature.....	175
9.6 Overlaid IR reflectance spectra of 60% hybrid content ormosil film prepared using an D values of 1, 2, 4, and 6. Films were cured in air at room temperature.....	177
9.7 Overlaid IR reflectance spectra of 80% hybrid content ormosil film prepared using an D values of 1, 2, 4, and 6. Films were cured in air at room temperature.....	179
9.8 Overlaid IR reflectance spectra of 60% hybrid content ormosil film prepared using an D values of 1 and cured in air at room temperature, 60 °C, 150 °C, and 300 °C.....	182
9.9 Overlaid IR reflectance spectra of 60% hybrid content ormosil film prepared using an D values of 6 and cured in air at room temperature, 60 °C, 150 °C, and 300 °C.....	184
9.10 Overlaid IR reflectance spectra of 80% hybrid content ormosil film prepared using an D values of 1 and cured in air at room temperature, 60 °C, 150 °C, and 300 °C.....	186
9.11 Overlaid IR reflectance spectra of 80% hybrid content ormosil film prepared using an D values of 6 and cured in air at room temperature, 60 °C, 150 °C, and 300 °C.....	188

CHAPTER 1

INTRODUCTION

1.1 The Problem

Over the past decade, there has been a significant amount of research conducted in the area of sol-gel materials processes. Many suitable applications have been scaled up into commercialized processes. Others, however, have been overlooked due to environmental concerns of volatile organic content (VOC) emissions. The elevated concentration of alcohol solvents typically used in sol-gel preparations have limited the widespread use of sol-gel methods. With growing concerns on environmental issues, the sol-gel process must be adapted to meet current and future environmental protection agency regulations if it is to ever find a broad commercial user base. In order to meet such requirements, a water-based system must be developed capable of providing chemical and physical characteristics similar to those found in traditional alcohol based sol-gels. Since the sol-gel process is based largely on hydrolysis chemistry, however, dramatic change in water content will significantly alter the polymerization mechanisms and affect resulting structural properties in the sol-gel systems. Since very little research has been conducted in this area, the effects on the chemical and structural properties are unknown. This lack of basic knowledge limits the full potential of sol-gel processing and hampers its use in many potential applications. Thus, the sol-gel process must be

modified for use as a water-based system in order to be viewed as an environmentally compliant process.

1.2 Purpose of the Study

The research described herein addresses chemical issues associated with developing a water-based sol-gel system. The work will provide a foundation for identifying chemical and structural formations in high water-content synthetic processes. Both silicate and organically modified silicate (ormosil) systems have been investigated with respect to water content, precursor use, curing temperature, and organic content. In each system, gels and films have been characterized using ^{13}C and ^{29}Si Nuclear Magnetic Resonance (NMR), Fourier transform infrared (FT-IR) spectroscopy, Raman spectroscopy, and picnometry density measurements. Results of each study have been used to identify fundamental chemical species evolution, and to help elucidate structural developments that take place in sol-gel materials. Conclusions from the dissertation research will provide basic knowledge for the preparation and characterization of water-based sol-gel systems, and will establish a baseline from which future efforts can be initiated to develop an environmentally compliant, low VOC sol-gel process.

1.3 Limitations

The sol-gel process, which is based on inorganic polymerization reactions, is considered a unique chemical route for the synthesis of non-metallic materials. Metal alkoxide precursors provide a method for obtaining almost any type of metal oxide ceramic. Combinations between various metal alkoxides under different processing

conditions enable an endless variety of amorphous and ceramic networks to be prepared. The most promising feature of the process is the versatility in preparation methods. The polymerization mechanisms are influenced by a number of different variables, which can be controlled to modify the process. Since very little work has been conducted in the area of a water based systems, the effects of many of the preparation parameters have not been identified and impose limitations due to the overall complexity of the sol-gel process. For the purpose of this study, selected conditions were used and only simple variations in processing conditions were investigated.

1.4 Outline of Work

The thesis consists of 9 Chapters. Chapter 1 presents a general introduction to the significance of this work. Chapter 2 contains a brief overview of the sol-gel process and addresses topics of relevance to this study. It highlights reaction mechanisms for both silica and ormosil systems, and identifies the effects of processing conditions on polymeric growth mechanisms. Chapter 3 contains a detailed description of the experimental methods and procedures used in this study. A general discussion of sol-gel preparation techniques is presented, and detailed instructions are given regarding the preparation of water-based silica and epoxide organically modified silicate gels and thin films. Chapters 4, 5, and 6 present the results associated with the investigation of inorganic silica gels and films prepared using a novel water-based sol-gel process. Chapters 7, 8, and 9 present the results of investigating epoxide-based organically modified silicate gel monoliths and films prepared using a water-based sol-gel process.

Chapter 4 focuses on the study of silica gels, prepared via a water based approach, using solid state ^{13}C and ^{29}Si NMR methods in conjunction with picnometer density

measurements. Solid state NMR results were used to identify chemical speciation in the siloxane network as a function of water activity and precursor type. Results were used to propose gel growth mechanisms and essential gel structures. Density results were used to correlate packing efficiencies with conclusions based on the NMR data.

Chapter 5 is a comprehensive Raman study which examines the development of silica gels as a function of water content, precursor type, and curing temperature. Raman spectra were used to identify the degree of gel hydrolysis, bulk silanol content, surface silanol content, bulk densification, and surface densification. Results were used to identify densification mechanisms and to corroborate mechanisms and structures proposed in Chapter 4.

Chapter 6 is a reflectance FT-IR study of silica thin films prepared using the water-based sol-gel process. Single reflection FT-IR spectra were used to monitor chemical changes in the siloxane network. Results were correlated to species evolution and structural developments as a function of water content and curing temperature. Results of the FT-IR studies were used to differentiate between linear and cyclic polysiloxane growth mechanisms.

Chapter 7 is a solid state NMR study conducted to qualitatively assess the chemical processes that occur in water-based epoxide ormosil processes. Special emphasis is placed on discussions associated with the influence of epoxide decomposition on the overall hybrid microstructure. This study was performed in two parts. In the first part, cross-polarization ^1H - ^{13}C NMR experiments were used to identify and monitor epoxide stability, diol formation, epoxide-epoxide polymerization, and organic-inorganic cross-linking as a function of water activity and total organic content. Results indicated a tendency, in most cases, for epoxide decomposition and the formation of carbosiloxane

bonds. In part two, single pulse ^{29}Si NMR experiments were used to quantify siloxane species and determine local environments surrounding silicon nuclei. Conclusions drawn from each study were used to propose model structures for chemical species development and structural characterization in epoxide ormosil gels.

Chapter 8 is a complementary Raman study of epoxide ormosils aimed at further elucidating chemical and structural developments identified in Chapter 7, and to characterize the effects of curing temperature on the epoxide ormosil gels. Ormosil gels cured at 150 °C were studied to determine the degree of polymerization and for signs of epoxide decomposition.

Chapter 9 is a FT-IR reflectance study of epoxide ormosil thin films prepared using the water-based sol-gel process. This is also a complementary study targeted at the identification of chemical and structural developments in ormosil thin films as a function of water content, organic content, and curing temperature. Comparisons of FT-IR, Raman, and solid state NMR spectroscopic methods were used to identify and corroborate interactions developing as a result of carbosiloxane formation and epoxide decomposition.

5. Conclusion

Based on these studies, a fundamental knowledge base has been developed for comparatively simple water-based sol-gel systems. By identifying chemical modifications in conventional inorganic and 2-component hybrid systems, a basic set of reference points has been established for furthering the development of new water-based processing methods. The effects associated with water content, precursor use, curing temperature, and organic content were investigated to provide structural models for

tailoring water-based silicate and organically modified silicate systems. The basic chemical and structural knowledge gained from this research will provide a reference for future studies investigating other processing conditions and will aid in the development of new environmentally compliant sol-gel processes.

CHAPTER 2

OVERVIEW OF SOL-GEL METHODS

2.1 Sol-Gel History

The first publication of sol-gel science dates back to 1845, when Ebelmen reacted SiCl_4 with ethanol to form the alkoxide precursor, tetraethoxysilane (TEOS).¹ In the ensuing year, Ebelmen reported the hydrolysis of TEOS to yield a silicate solution, which could be drawn into fibers and cast into amorphous gels capable of producing optical elements.^{2,3} In 1860, Mendeleev followed up Ebelmen's results and published a novel mechanistic idea that the suggested the hydrolysis of SiCl_4 yields $\text{Si}(\text{OH})_4$, which undergoes condensation reactions in a polymeric fashion to form polysiloxanes.⁴ It is with these initial experiments that sol-gel science was born.

The initial investigation of sol-gel chemistry was an interesting contribution to science, but it was more often regarded as a laboratory curiosity. It wasn't until the 1930's that sol-gel science began to experience some of the widespread study it sees today. Sol-gel chemistry progressed as an area of basic research, but found limited in use in commercial applications. It wasn't until the "rediscovery" of monolithic gel formation, development of a thin film coating method, and the establishment of low-temperature gel-to-glass conversion processes in the late 1970's and early 1980's that sol-gel science began to flourish.

Sol-gel chemistry has proven to be a useful preparative method in a wide range of application areas, largely because it provides a low temperature route to the preparation of ceramic-phase materials. During the past 15 years, it has also been associated with the preparation of novel inorganic/organic hybrid materials, which are typically prepared

through the use of standard metal alkoxide and more recently developed organically modified metal alkoxide precursors. Presently, the sol-gel method is beginning to transition from the laboratory to commercial-scale utilization, as it provides an approach to the development novel coatings and bulk materials, using a low-temperature route, that possess unique chemical and mechanical properties. In many cases, sol-gel materials are not readily prepared by the any other chemical method. Thus, there is great interest in developing a more complete understanding of the fundamental relationships which exist between initial preparative conditions and final material properties. The research described herein seeks to develop a deeper chemical understanding of sol-gel selected systems.

2.2 Sol-gel Process

2.2.1 Sol-gel Basics

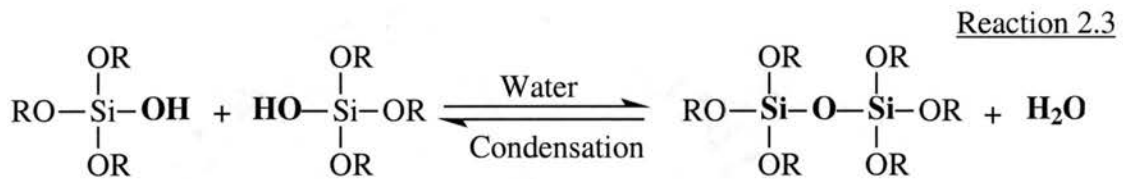
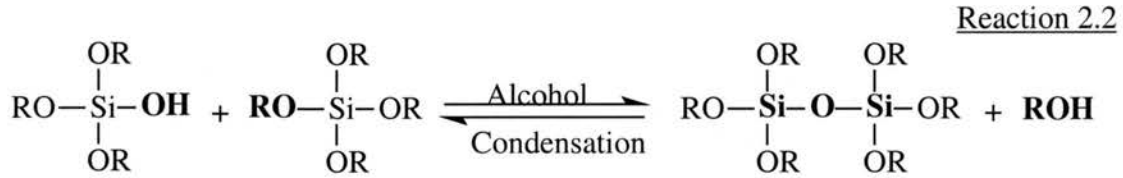
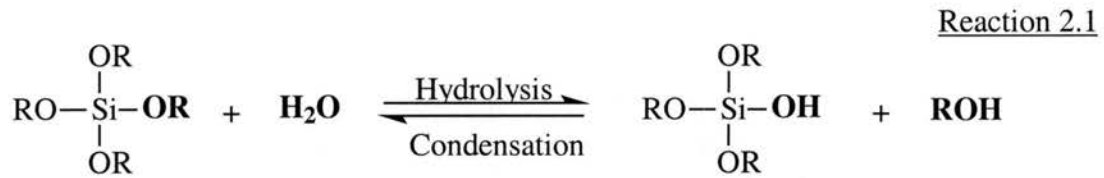
The sol-gel process, which in the most general sense is based on inorganic polymerization reactions, is considered a unique chemical route for the synthesis of ceramic-containing materials. The method provides a low temperature route for preparing ceramic material with excellent homogeneity, low sintering temperature, low impurity level, and tailorable physical features. The wide availability of many different metal alkoxide precursors provides a route to almost any type of ceramic composition. Combinations of various metal alkoxides enable unique amorphous networks to be prepared. With such a large potential for developing numerous types of ceramic systems, sol-gel science has developed into an extremely diversified field. Oxide materials of a variety of metals are now accessible as ceramic powders, fibers, glasses, thin film coatings, and monoliths. Applications reported in the literature have revealed sol-gel's wide diversity in fields such as corrosion protection, optical equipment, fiber development, ferroelectric material, bio-medical, and many others.⁶⁻¹⁰ The wide spread use has been attributed to the processes salient preparation and chemical aspects,

including: room temperature synthesis, chemical inertness, tailorability, and commercially demonstrated scale-up potential.

In the most basic sense, the sol-gel process is a method able to prepare inorganic network polymers at room temperature. The process is made up of 5 stages: sol preparation, gelation, aging, drying, and densification. In general terms, a metal alkoxide precursor undergoes hydrolysis and condensation reactions during sol initiation to form a solution containing oligomeric units and/or colloids. As the sol is aged, the inorganic network begins to grow and coalesce to form larger interconnected network. At some point the viscosity becomes large enough that the fluid is transformed to a rigid gel. Gels usually form a porous, three-dimensional matrix with alcohol and/or water solvents trapped in a metal oxide network. The drying process removes the solvent resulting in a porous ceramic network referred to as a xerogel. Curing can then be applied to initiate secondary reactions between residual hydroxyl groups and densification of the porous network. With elevated thermal treatment, the porous ceramic will collapse resulting in a high purity ceramic or glass material.

2.2.2 Sol-gel Chemistry

The sol-gel method consists principally of hydrolysis and condensation reactions, of alkoxy silane precursors to form a polymeric network of nanoporous gels. The reaction sequence typically proceeds through an acid- or base- catalyzed hydrolysis reaction, producing a hydrolyzed silane and an alcoholic by-product (Reaction 2.1). In the case of silicon alkoxide precursors, siloxane bridge formation occurs according to the condensation reactions shown in Reaction 2.2 and 2.3. As the condensation reactions proceed, an inorganic network polymer results from polysiloxane formation. The polycondensation reactions occur repeatedly, until the active silanol sites have formed a high density of siloxane bridges, usually slowing when a rigid gel is formed.



Alkoxide Precursors

R = OCH₃, OCH₂CH₃,.....

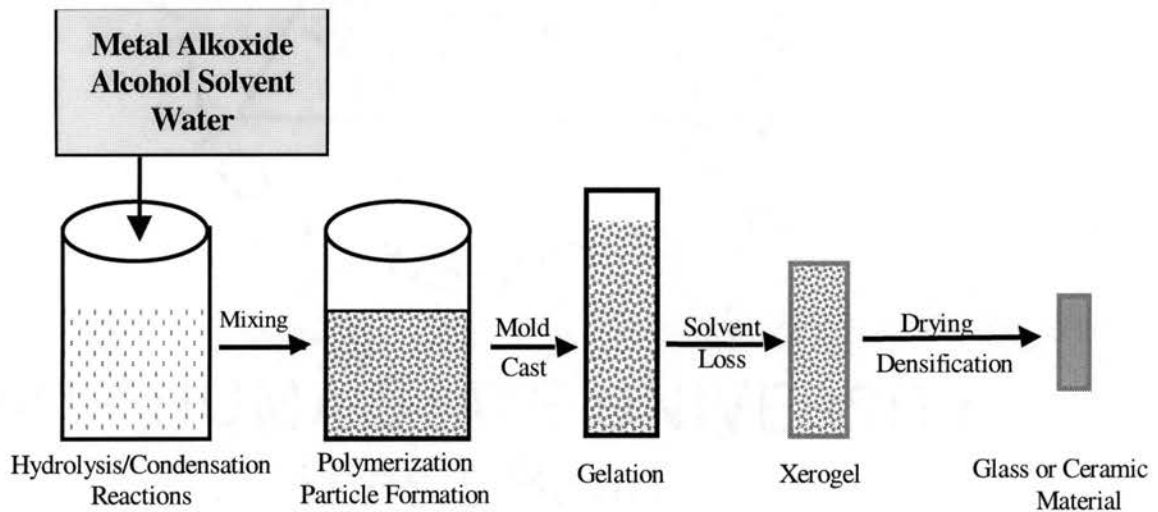


Figure 2.1 Overview of sol-gel preparations.

The reaction sequences presented, while illustrative, are substantially oversimplified with respect to the actual chemical processes involved. The sol is really a mixture of several competing reactions, including reverse reactions, which are more or

less kinetically favored under certain reaction conditions (i.e. alcoholysis & hydrolysis of siloxane bond). The system is complicated even further based on the use of tetrafunctional monomers which can lead to polymeric growth characterized by linear chains, highly branched 3-dimensional structures, or a mixture of network types. Even small variations in the reaction conditions can have profound effects on the polymeric growth mechanism and the eventual gel microstructure. In short, the sol-gel process is very complex process and highly dependent on processing conditions. A detailed review of the reaction mechanisms as understood 10 years ago is presented in the widely cited monograph entitled "Sol-gel Science and Technology".⁵

The kinetics and mechanistic of competitive hydrolysis and condensation reactions have been shown in numerous studies to influence and eventually determine the final gel micro-structure.¹¹ Experimental parameters such as catalyst type,¹²⁻¹⁴ solution pH,^{12,15,16} solvent content,^{17,18} water content,¹⁹⁻²⁹ temperature,^{30,31} and alkoxide precursor type^{5,32} are all known to effect reaction kinetics and, ultimately, the final gel microstructure. A wide variety of experimental conditions using variable pH and water/alkoxide ratios have been reported and postulated to reflect a variety of growth mechanisms and gel structures.^{12-15,19-29} Even though there is a wide diversity in experimental conditions between studies, a general consensus of three different gel condensation and network growth mechanisms are attributed to basic gel network formations: (1) growth of linear or weakly branched chains; (2), highly branched clusters, and (3) colloidal particles. Experimental conditions favoring each type of particulate formation will be discussed in section 2.4.

2.2.3. Acid and Base Catalyzed Reaction:

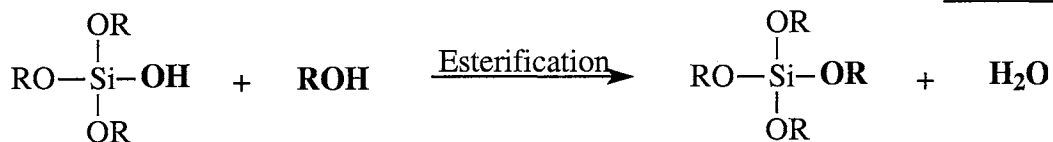
Acid- and base-catalyzed sol-gel processes for silica based systems exhibit opposite trends in hydrolysis and condensation reaction. The variation between the two reaction rates depends highly on the pH and water content. Under acidic preparation conditions, the hydrolysis rate increases with pH typically reaching a maximum at 2, while the condensation rate is minimized at low pH.¹¹ Base catalysis for silica based systems, on the other hand, tends to retard the hydrolysis reaction while accelerating condensation reactions.⁵ The variation between reaction rates directly alter the sequential polymeric growth of monomer and extend siloxane fragments. Gelation under acidic conditions slows the condensation reaction kinetics and tends to result in the development of linear and branched siloxane chains. Polymerization under base-catalysis, on the other hand, tends to result in gels composed of highly branched clusters and/or colloidal particles. The microstructure, which develops, is specific to the type of catalyst used, but other parameters such as water content, solvent, and exact pH have very influential effects on the final gel microstructure due to the effects on competing reaction kinetics. In a review of sol-gel processing, C.J. Brinker suggested that an acid-catalyzed hydrolysis reaction with low H₂O/Si ratios produces weakly branched “polymeric” networks, whereas base-catalyzed hydrolysis reactions with large H₂O/Si ratios tend to produce highly branched “colloidal” particles.^{5,11} Intermediate conditions produce mixed structures. Generally, acid catalyzed processes are used to prepare more dense films, and water activity is used as the primary method to control reaction kinetics and polymeric growth mechanisms. A more detailed review of growth mechanisms for an acid catalyzed system is present in section 2.4.

Mineral acids or ammonia are the most common catalyst reported in the literature. However, other catalysts such as acetic acid and other carboxylic acids, amines, and are also described. Choice of a catalyst and its relative concentration in the sol-gel process is an influential factor in the sol-gel process. Aelion et. al. observed that the rate and extent of the hydrolysis reaction of TEOS was influenced by the strength and concentration of the acid or base catalyst.^{33,34} They found that all strong acids behave similarly, whereas weaker acids required longer reaction times to achieve the same extent of reaction. The condensation reaction is influenced in much the same way. Since the reaction rates influence the reaction kinetics, the choice of catalyst is important in the overall development of the gel microstructure.

2.2.4. Esterification Reactions

Esterification is the reverse hydrolysis reaction in which an alcohol displaces a hydroxyl group to produce a water molecule (see Reactions 2.1 and 2.4). Studies examining the reesterification of polysiloxanes have indicated the reaction is strongly dependent on the pH. Reesterification rates increase in acidic media.^{26,35,36} Kinetic modeling and experimental results present by J. Ro and I. Chuno have shown the reesterification reaction rate is much slower than the hydrolysis reaction rate, but has a considerable effect in determining the overall process kinetics.¹⁹ Sol-gel preparative conditions employing a large excess of alcoholic solvent in the presence of acidic species result in the highest reesterification rates and a somewhat reduced overall hydrolysis rate.^{5,13,38} Sols prepared without the use of an alcohol co-solvent will limit the influence of the reesterification back-reaction. This ultimately impacts the final gel microstructure.

Reaction 2.4



2.3 Hybrid Ormosils

2.3.1 General Hybrid Ormosils

Novel inorganic/organic hybrid materials may be synthesized by the sol-gel process. Organically modified ceramic gels, or ormocer gels, are typically prepared using organically modified metal alkoxide precursors mixed with complementary metal alkoxides. Organically-modified silicates, or ormosils (a subset of the broad class of ormocers) are typically prepared using modified silicates and tetraalkoxysilane precursors. Alkoxysilane precursors, having functionalized organic moieties covalently bonded to a silicon atom, can be introduced in the reaction mixture in much the same way conventional ceramic sol-gels are prepared. The mild reaction conditions and low temperature processing allow organic moieties to be intimately incorporated into the inorganic network. The availability of various types of organic functional groups provides a vast array of possible chemical compositions and characteristics which can be developed. The incorporation of organic functional groups into the inorganic network enable selected properties, such as flexibility and/or modulus of elasticity, to be optimized for particular applications. Flexibility can be introduced by the incorporation of organic oligomeric polymeric material into the organic network, which reduces structural strains in the oxide network, while still retaining selected attributes, such as hardness and/or chemical resistance, which are typically associated with ceramic materials. The introduction of organic groups into an inorganic network leads to new structure-property characteristics, thereby promoting the development of new applications from the resulting hybrid materials. With an endless possibility in variations of the organic compositions and content, hybrid systems have opened an entirely new

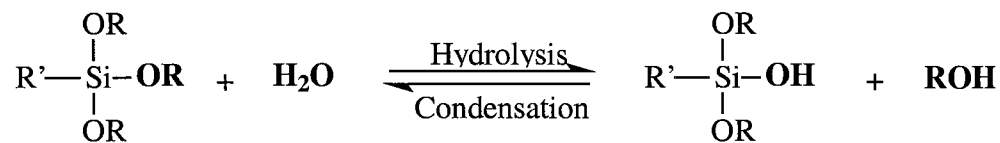
area of sol-gel processing, capable of improving traditional ceramic systems and extending sol-gel applications in to a whole new field of applications.

2.3.2 Ormosil Chemistry

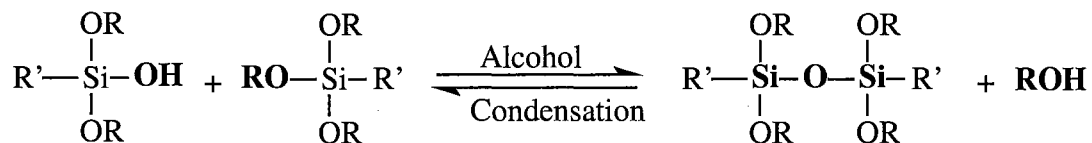
Ormosil systems are prepared by a series of reaction sequences similar to those previously described with the addition of one or more organic polymerization reactions. In an epoxide ormosil gel, the silicate portion of the precursor undergoes hydrolysis and condensation, tending to produce a condensed silica network with functionalized organic groups incorporated into the network (Reactions 2.5-2.7). Treatments are then applied to polymerize the organic functional groups and produce an additional network of organic bond formations. An example of hybrid organic-inorganic polymer formation from an epoxide-modified silicon alkoxide precursor is shown in Reaction 2.8. During polymerization of the epoxide group, the organic component cross-links creating an inner connected network of both inorganic and organic phases. The efficiency of organic polymerization is highly dependent on hybrid content, temperature, and organic distributions in the silica network.

In general, a typical hybrid sol-gel reaction mixture is comprised of a combination of the reactions (2.1-2.8) described in this chapter. The kinetics of each reaction type are determined by the specific reaction conditions.

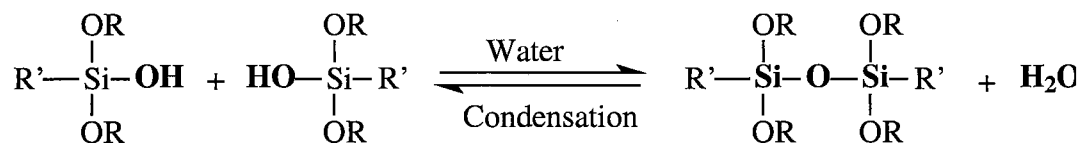
Reaction 2.5



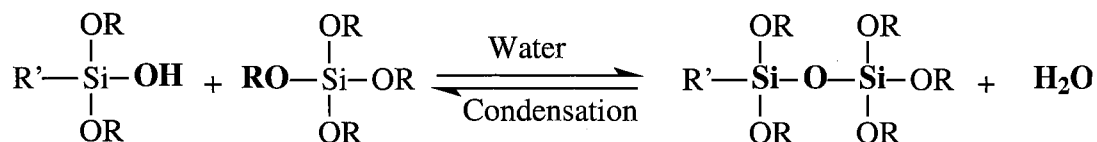
Reaction 2.6



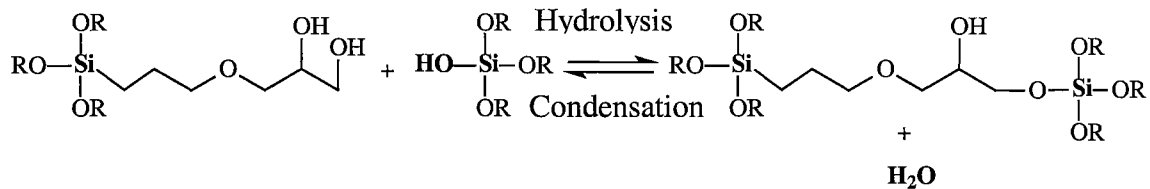
Reaction 2.7



Reaction 2.8

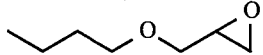


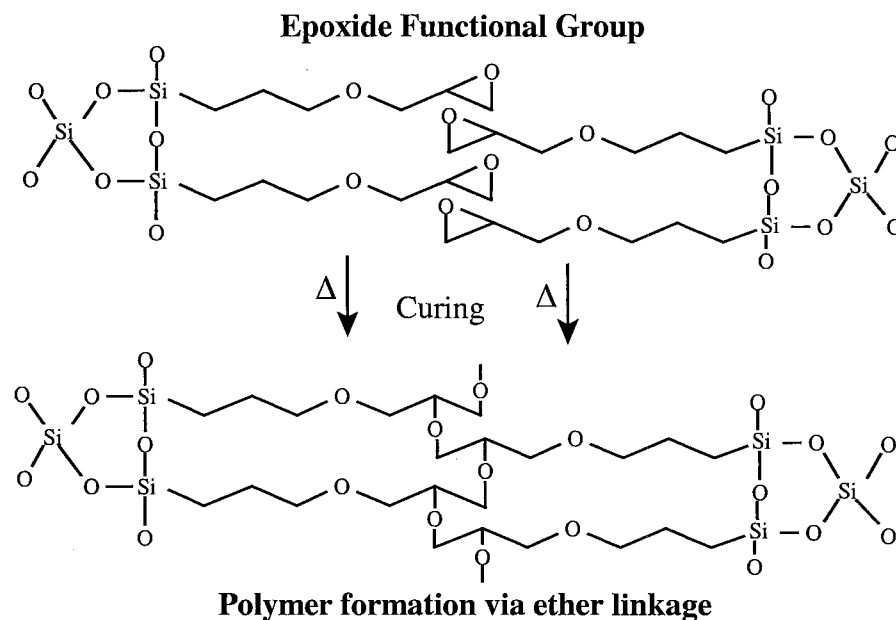
Reaction 2.9



Alkoxide Precursors

R = OCH₃, OCH₂CH₃,.....

R' = -CH₃, -CH=CH₂, ,



2.4 Conditions Influencing Structural Formations

2.4.1 Effects of Water Content on the Silica Network

The effects of water concentration in alcohol-based sol-gel systems have been extensively reported in the literature.¹⁹⁻²⁹ Studies have shown the water content directly influences reaction kinetics.^{15,19,26,39} The rate of hydrolysis in an acid catalyzed system has been identified to be orders of magnitude faster than the condensation reaction at low pH.^{15,20} The differences between hydrolysis and condensation reaction rates essentially determine the sequence in which the polymerization mechanism occurs. By controlling the condensation reaction and/or relative concentration of hydrolyzed species the polymeric sequence has been used to obtain various types of gel microstructures.

The concentration of hydrolyzed species in the sol is dependent on the water content. In a study by Aelion et al., the acid catalyzed hydrolysis of tetraethoxysilane (TEOS) was identified to be first-order with respect to H_2O .³³⁻³⁴ In conditions with rapid hydrolysis rates and first-order rate dependence with respect to H_2O , the concentration of

hydrolyzed species in solution is dependent on the relative amount of water added to the sol mixture. This implies that the water concentration indirectly controls the mechanism by which polymerization occurs. Based on these principles, the majority of sol-gel studies conducted have used low water concentrations to control reaction kinetics and obtain desired gel microstructures.

The activity of water in sol-gel preparations has traditionally been reported in the literature by the so-called "R value". Specifically, the R value indicates the $H_2O:M$ molar ratio, where M represents the metal center of a metal alkoxide. For example, an R value of 2 would indicate two moles of water were present for each silicon alkoxide precursor equivalent present in the reaction mixture. "R" value terminology has also been extended to include non-silicon based metal alkoxide precursors, such as titanium tetraalkoxides.

The activity of water in hybrid sol-gel preparation has been modified to account for variations associated with using organically-modified trialkoxysilane precursors. Since R value terminology is based on the use of tetraalkoxysilane precursors, mixtures of tri- and tetraalkoxy metal precursors could lead to uncertainties in the actual water content used in a gel preparation depending on the relative ratio of the tetra- and trialkoxysilane precursors. Therefore, the use of R value in hybrid preparations would not truly represent the actual water content as a function of reactive alkoxy functionality. To account for such variations, a modified "D value" terminology has been employed in this work to indicate the true H_2O :alkoxide molar ratio. The "D value" nomenclature is independent of effects caused by the use of two (or more) different alkoxide precursors. A D value of 1 for a tetraalkoxy silane precursor corresponds to an R value of 4, indicating the use of 4 moles of water for every mole of tetraalkoxysilane. In the case of a 50:50 mixture of tri- and tetraalkoxy silanes, a D value of 1 would indicate 1 mole of water was present for each molar alkoxide equivalent, or 7 total moles of water for a mixture containing 1 mole of trialkoxysilane and 1 mole of tetraalkoxy silane. The need for D notation arises from the fact that an R value of 4 for example, in a mixed system

does not define the total ratio of moles of water to the number of molar equivalents in a mixed trialkoxysilane/tetraalkoxysilane system. In order to establish a fixed ratio of molar water activity as a function of molar alkoxide equivalents, the hybrid gel preparations described in Chapters 7, 8, and 9 utilize the D value nomenclature.

$$R \text{ value} = \frac{\text{total molar equivalents of water}}{\text{total molar equivalents of silane}} \quad \text{Equation 2.1}$$

$$D \text{ value} = \frac{\text{total molar equivalents of water}}{\text{total molar equivalents of alkoxide}} \quad \text{Equation 2.2}$$

Several studies conducted on the effects of water content have identified three general types of growth mechanisms and gel structures.^{11,16,21,27,30} Low water content gels, identified with H₂O/silane ratios (R values) of less than 4, were reported to favor development of entangled linear or weakly branched chain fragments. Intermediate R values, those ranging from 4 to 10, were reported to favor highly branched fragments and/or clusters. Systems with elevated R values, typically greater than 10, have been reported for gels composed of both highly branched clusters and/or small particles.

2.4.1.1 Low water content Sols

Preparations of low water content sols (e.g., R values of less than 4) have been previously correlated with a growth mechanism that features the entanglement of polymeric linear or weakly branched chain formations. Limiting the amount of water available for alkoxide hydrolysis results in a sol mixture having a limited concentration of hydrolyzed species. Such conditions preferentially favor the hydrolysis of less structurally hindered alkoxide species (i.e. monomers, dimers, trimers, etc.). In a study conducted by Brinker, the growth mechanism in a low R-valued gel was explained using simple steric models in which metal alkoxide monomers were more readily hydrolyzed

than dimers or oligomer chain ends; these, in turn, were more readily hydrolyzed than inner chain alkoxide groups (reference Figure 2.1).^{5,16} Observations of preferential hydrolysis ordering of this type implies that linear chain development tends to be favored over branch formation under low R value conditions (limited water activity). In addition, the initial consumption of water through hydrolysis and slow subsequent water elimination after condensation provides conditions that are very suitable for linear chain growth. It is hypothesized that gelation occurs in such systems as the linear chains become entangled. Upon solvent evaporation, chain entanglement occurs and a dense microporous siloxane network is formed. Thus, the combination of preferential hydrolysis and control of hydrolyzed species content provides optimized conditions for linear chain growth.

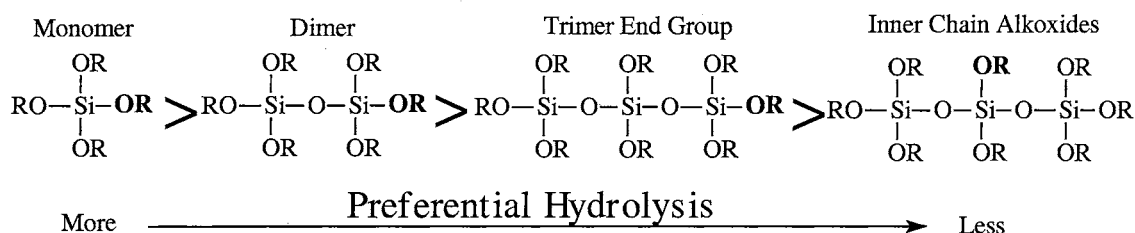


Figure 2.2. Preferential sequence of hydrolysis in silicate systems.

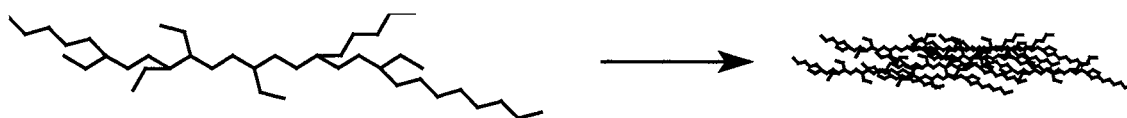


Figure 2.3. Illustrative depiction of linear polymeric growth mechanism.

2.4.1.2 Intermediate water content sols

An increase in the water content leads to greater degree of early stage hydrolysis, reportedly leading to elevated branching in the polymerizing polysiloxane chains. Gels formed from sols having intermediate R values (e.g., those between 4 and 10) have been previously shown to exhibit growth mechanisms characterized by highly branched structures.^{5,27,30} Elevated water content leads to increased hydrolysis rates and a greater number of hydrolyzed species in the growing oligomeric fragments. Unlike sols with limited water available for hydrolysis, a strong preference for hydrolysis of monomeric alkoxide species does not exist when an abundance of water is available for early stage hydrolysis. Thus, slow hydrolysis kinetics no longer controls the polymeric growth mechanism. Chain branching begins to develop as a result of alkoxide species hydrolysis occurring at points all along the growing chain fragments rather than at the less sterically-hindered end group positions. The increase in hydrolyzed fragments provides additional sites for polymeric growth in multiple directions. The extent of branching determined by the relative hydrolysis and condensation reaction rates. Unlike the linear chains which are favored when water activity is low (e.g., R values less than 4), the highly branched chains/clusters which form with excess water are unable to interpenetrate one another during drying and shrinkage. These chain fragments act more like discrete particulates. Thus, gelation occurs for these systems through cluster coalescence and subsequent linkage formation. Upon xerogel formation, the more rigid network structure combined with a less efficient packing mechanism lead to a more open gel microstructure.

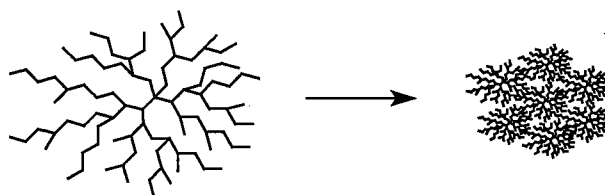


Figure 2.4. Illustrative depiction of branched polymeric growth mechanism.

2.4.1.3 High water content sols

Sol preparations using elevated water concentrations (e.g., an R value of 10 or more) have been identified with gel microstructures consisting of the nucleation of small colloidal particles that coalesce together to form a three dimensional network.^{93,183-185} Very high levels of water activity effectively increase the rate of hydrolysis to such an extent that the alkoxide species are essentially all completely hydrolyzed prior to any significant degree of condensation. Condensation reactions occurring after hydrolysis have been proposed to lead to linear chains followed by cyclization. The cyclization becomes favored based on an increase in the probability of an intramolecular reaction occurring prior to an intermolecular reaction. The shift to cyclization appears to be an affect of dilution and elevated concentration of hydrolyzed species. I. Strawbridge and co-workers indicated that such conditions are similar to those exhibited in the polymerization of monosilicic acid ($\text{Si}(\text{OH})_4$).²⁷ As described by Iler, silicic acid polymerization occurs through rearrangement of cyclic species into small densified particles which act as nuclei for further growth via an Ostwald ripening mechanism.⁴⁰ Under acidic conditions, the particle growth will continue until a size of 2-4 nm is reached at which point the rate of polymerization and depolymeration is slow and particle growth stops. Gelation and porous network formation then occurs through the coalescence of small particles into a three-dimensional polymer composed of dense colloids with interstitial voids.

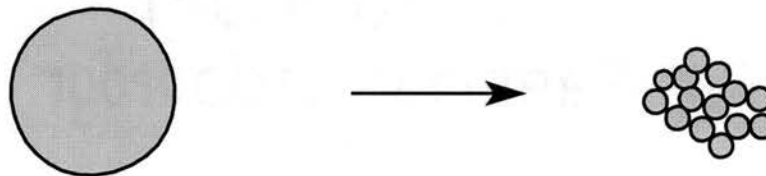


Figure 2.5 Illustrative depiction of colloidal growth mechanism.

2.4.2 Alkoxide Precursor Effects

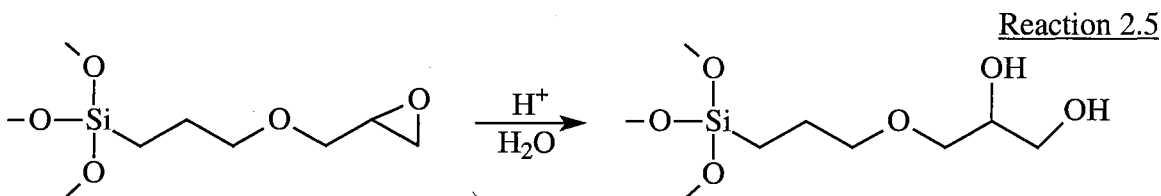
Alkoxide precursors can largely effect hydrolysis and condensation reaction kinetics through steric hindrance and electron donating or withdrawing (inductive) effects of the organic group. Short chain alkoxides, which have minimal steric hindrance and limited electron donating characteristics, react much faster than larger alkoxide species.^{5,16,32} Precursor sols incorporating small alkoxide side groups, such as tetramethoxysilane (TMOS), hydrolyze more readily than those incorporating larger alkoxide side groups (i.e., tetraethoxysilanes, (TEOS), tetrapropoxysilane, (TPOS), *etc.*) Studies by both Yamane et. al. and Chen et. al. have shown that hydrolysis rates decrease rather dramatically with increased alkoxide chain length.^{32,38} The sol hydrolysis kinetics can largely determine the resulting gel microstructure, as previously noted. Thus, the use of different alkoxide precursors in a sol-gel system effect reaction rates and alter resulting gel structures. One of the goals of this research is to characterize the chemical species which develop in sol-gel reaction mixtures as a function of precursor type, using complementary spectroscopic methods.

2.4.3 Effects of Water Content on Organic-Inorganic Hybrid Systems

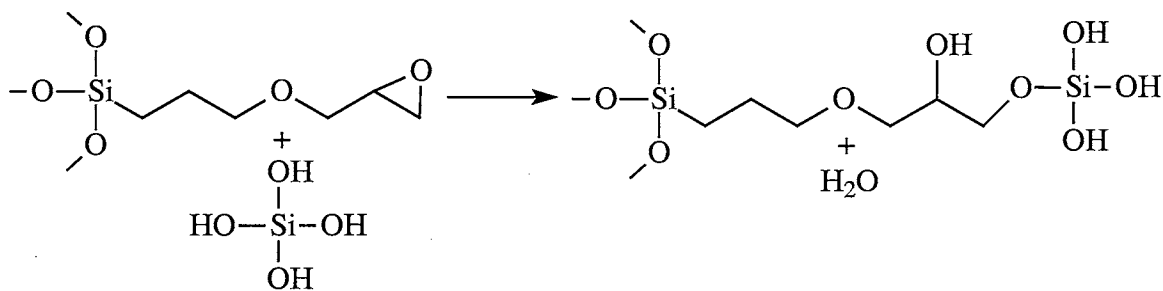
Although there has been a rapid increase in studies pertaining to ormosil preparation, the effects of high water content on hybrid systems is not well characterized or understood. Most hybrid systems reported in the literature have used comparatively low water concentrations, between 2 to 4 moles of water per mole of silane, which have little affect on the stability or solubility of the functionalized side chain (e.g. epoxide, vinyl, methyl methacrylate). With limited amounts of water present, the hydrolysis reaction consumes a large portion of the water rendering the organic functional group unaffected. Preparations using elevated water content, effect the chemical stability of certain organic moieties as well as the solubility of the ormoecer precursor. Hybrid systems prepared with hydrophobic functional groups (i.e. vinyl, methyl methacrylate)

can become phase separated in solution, whereas hybrid systems which are water soluble (i.e. epoxide) can decompose. Thus, it is of great interest to determine the effects and limitations of using a water-based process in the preparation of ormosil gels and to use spectroscopic methods to assess the underlying chemical and physical processes.

Epoxide ormosil gels, which are studied extensively in this research, have been shown to be unstable in an aqueous acid environments. Investigations by Schmidt et. al. on sol-gels prepared from glycidoxypropyltrimethoxysilane have shown that the epoxide functional group can undergo a ring-opening reaction to form diol end groups (Reaction 2.5).⁴¹⁻⁴³ Under acid condition with excess water, the epoxide will gradually decompose over time. Schmidt and Seiferling have also suggested that once diol has formed, an esterification reaction can occur with silanol groups to form a stable organic-inorganic linkage (Reaction 2.6).⁴⁴ This type of linkage has not been specifically described in the literature, but similar esterification reactions between TMOS and glycol have identified.⁴⁵ The term "carbosiloxane linkage" has been coined to describe the hybrid $\equiv\text{C}-\text{O}-\text{Si}\equiv$ bridge. In such gel systems, the ormosil chemical structure and macroscopic material properties will be significantly altered. Therefore, it is imperative to determine what types of chemical modifications will occur and how they will effect the physical properties of an ormosil system. An assessment of the fundamental relationship between molecular-level chemistry and the nature of the resulting gel structure serves as a main thematic focus of this research.



Reaction 2.6



2.4.4 Effects of Hybrid Content on the Silica Network

Structural effects arising from variations in the hybrid content are highly dependent on size and concentration of the organically modified silicate. A study conducted by Delattre and Babonneau on organically modified silicates mixed with tetraethoxysilane revealed an increase in the organically modified side size lead to a decrease in the condensation surrounding the modified silane precursor.⁴⁶ It was also shown that the addition of modified silicate resulted in an overall increase in the degree of condensation. The increase in condensation efficiency was attributed to the increase in local chain flexibility imparted by the organically-functionalized silanes. Since functionalized silanes often act as network modifiers, ormoecer-modified siloxane networks tend to be less rigid. They also pack more efficiently during drying and shrinkage, promoting a denser gel structure.⁴⁶ The silanol condensation reaction occurring around the modified silicate were inhibited due to the steric hindrance associated with the functional groups presence. Large concentrations of organics in the hybrid gel have been reported to induce phase separation. Work conducted by Witte et. al. on several organo-alkoxysilanes revealed homogenous distributions of the organic phase in hybrid gels with low organic content, where as in the hybrid systems which

posses substantially more organic component, phasic segregation of the modified silicate species occurred.⁴⁷ Thus, variations in the size and concentration of the functional group will clearly affect the overall degree of siloxane development and distribution of hybrid content in the ormosil microstructure.

2.5 Aqueous Phase Sol-gel Processing

Generally speaking, metal alkoxides have very limited solubility in water but are highly soluble in simple alcohols. Traditionally, sol-gel processing methods have relied on the use of alcoholic solvents to eliminate the formation of bi-phasic solutions, improve mixing, control structural properties, and improve thin film processing characteristics. Alcohol solvent use, however, is not a requisite condition of sol-gel chemistry. In some cases it is highly desirable to eliminate alcoholic solvents and reduce or eliminate VOC (volatile organic compound) emissions for those wishing to develop large-scale commercial processes. It has been shown that sol-gel hydrolysis and condensation reactions can proceed even without the immediate reactant miscibility that alcoholic solvent addition usually provides. Vigorous mixing of a bi-phasic solution can develop the necessary reaction interface between water and the alkoxide phase. As alkoxide precursor hydrolysis proceeds, the generated products (e.g., silanols and alcoholic by-products), which are water soluble, improve the reaction solution miscibility. Thus, in the absence of any added alcohol solvent a bi-phasic solution can homogenize after a period of vigorous mixing. Once a homogenous solution has been prepared, the sol can be cast into monolithic molds or applied by traditional dip-, spray-, or spin-coating methods.

This concept of preparing silica gels or glass “without a co-solvent” is not new, but relatively unexplored in the literature. Avnir and Kaufman questioned the need for “co-solvents” in 1986. They showed that transparent, homogenous, monolithic xerogels could be prepared using an entirely water-based process.³⁵ Due to processing challenges, however, water-based processing methods, have been largely avoided by the research community. This work will focus, in part, on the investigation of water-based sol-gel processes and the identification of structural and chemical developments with respect to processing conditions. It is hoped that this body of work and future studies in this area will serve as the key to development of new environmentally compliant water-based sol-gel processes that deliver materials having properties and performance characteristics which meet or exceed those of media prepared by traditional solvent based processes.

2.5.2 Thin Film Applications by a Water Based Processes

In addition to perturbing reaction kinetics, water content also effects sol wetting properties and surface tension. Unlike typical sol-gel derived solutions used for thin film coatings, which generally rely on the use of organic solvents, aqueous phase sols tend to have substantially greater surface tensions and poor substrate wetting properties. Methanol, for example, has a moderate surface tension (23 dynes/cm²), while water has a very high surface tension (72 dynes/cm²).⁴⁹ Solutions having large surface tensions generally result in poor substrate surface wetting characteristics due to the high surface energy between the solution substrate interface. Presently, lack of adequate film quality substantially limits the use of water based sol-gel processes for thin film applications.

Surfactant use in coating systems has been shown to be one of the primary mechanisms for improving film quality and extending film applications to water based

sol-gel systems. Currently, many industrial sources offer surfactants which can be tailored to a particular system for reducing surface tension and improving wetting. Recent studies in the area of protective coatings have utilized surfactants in a highly water-based sol-gel process to deposit thin films with surface qualities similar to alcohol derived films.⁵⁰⁻⁵⁴ In this study, commercial surfactants were used since the eventual use of a water-based commercialized sol-gel process for coatings technology will require additives to improve the film quality.

CHAPTER 3

EXPERIMENTAL METHODS AND PROCEDURES

3.1 General Overview of Sol Gel Preparation

The method for preparing pure SiO_2 and hybrid ceramic materials generally entails a five step process consisting of sol preparation, specimen processing (e.g., monolith casting or film application), gelation, drying, and densification. In general, the sol-gel process provides a very flexible route to the preparation of advance ceramic materials. Through control of precursor choice and reaction conditions, an essentially unlimited variety of ceramic and hybrid materials can be prepared and, in the case of coatings, applied to almost any type of desired substrate. A general schematic representation for a water-based sol-gel process is illustrated in Figure 3.1.

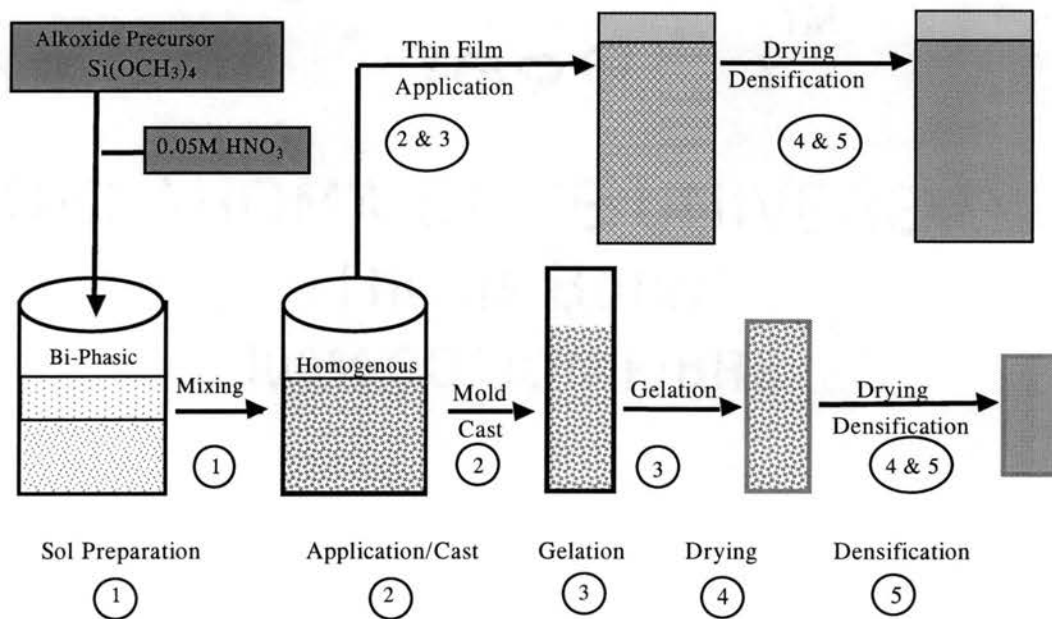


Figure 3.1: General schematic representation of the water-based sol-gel process.

Sol preparations(1) utilized in the experimental section were based on a solvent free technique originally reported by Avnir and Kaufman.³⁵ The process relies on using water as both a reactant and a solvent. Co-solvents such as methanol or ethanol, traditionally added to improve water immiscibility, were excluded to arrive at a composition with reduced VOCs. One of the key challenges of aqueous sol-gel preparation, however, is that the silicon alkoxide precursors are insoluble in water. Elimination of organic co-solvents, therefore, leads to the formation of bi-phasic reaction mixtures. It is at the interface between the alkoxide and the water phases where hydrolysis takes place. As hydrolysis continues, the insoluble alkoxide precursor is consumed, resulting in the formation of a water soluble silanol species and alcoholic by-products. Using vigorous mixing conditions, the bi-phasic solution becomes an emulsion thus increasing the relative interfacial surface area and accelerating the alkoxide hydrolysis rates. When a sufficient portion of the alkoxide precursor has been hydrolyzed, the reaction mixture becomes a homogenous single-phase sol (2). The condensing sol can be allowed to gel into a monolithic shape or it can be applied to a desired substrate and allowed to gel as a film.

Gelation proceeds as the hydrolyzed species condense(3), forming a porous, 3-dimensional network with entrapped residual solvent and water in the gel pores. As the residual water and alcohol by-products evaporate, the coalescence between sol fragments is accelerated leading to an increase in the degree of inorganic polymerization and network formation. After sufficient polymerization, a rigid 3-dimensional structure evolves with water and alcohol species remaining in the pore network.

The drying (4) and densification (5) steps are applied to remove residual by-products and to collapse the porous network. At low temperatures (<120°C), residual alcohol and water can be removed without substantially affecting the pore network. Such gels are referred to as xerogels. As curing temperatures increase, additional condensation reactions take place between adjacent silanol species, resulting in pore collapse. Densification and/or structural modifications in the siloxane network can occur over a broad temperature range depending on processing conditions. In conditions where sufficient heat is applied (i.e. up to approximately 1000 °C), structural densities equivalent to traditional melt glass can be obtained.

In this study, silica and organically-modified hybrid silicate gels were prepared using a water-based sol-gel method free of alcohol co-solvent. The systems were prepared using four different water concentrations and 3 types of alkoxide precursors. SiO₂ gels were prepared from tetramethoxysilane (TMOS) and tetraethoxysilane (TEOS) precursors. Epoxide ormosil gels were prepared using variable concentrations of glycidoxypropyltrimethoxysilane (GPTMS) and TEOS. Solid state ¹³C and ²⁹Si nuclear magnetic resonance (NMR), Raman spectroscopy, Fourier transform infrared spectroscopy (FT-IR), and pycnometer density measurements were used to elucidate structural formations as a function of water content, precursor use, hybrid content, and curing temperature. The focus of this study is to provide basic structural knowledge for water-based sol-gel systems and to advance the development of an environmentally compliant low volatile organic compound (VOC) sol-gel process.

3.2 Overview of SiO₂ Gel Preparation

Water-based SiO₂ gels were prepared using an acid-catalyzed process. Tetramethoxysilane (TMOS) and tetraethoxysilane (TEOS) were used as received from Aldrich chemicals. Each alkoxide precursor was mixed with four different water/silane ratios (R value). R values of 4, 8, 16, and 24 were used to provide an incremental distribution between literature-referenced low and high water values. The water source was a 0.05 M HNO₃ stock solution with a pH near 2. Mixing between the alkoxide precursor with water was different for each systems and is explained in sections 3.2.1 and 3.2.2. A total of eight sols were prepared with four different water concentrations and two different types of precursors.

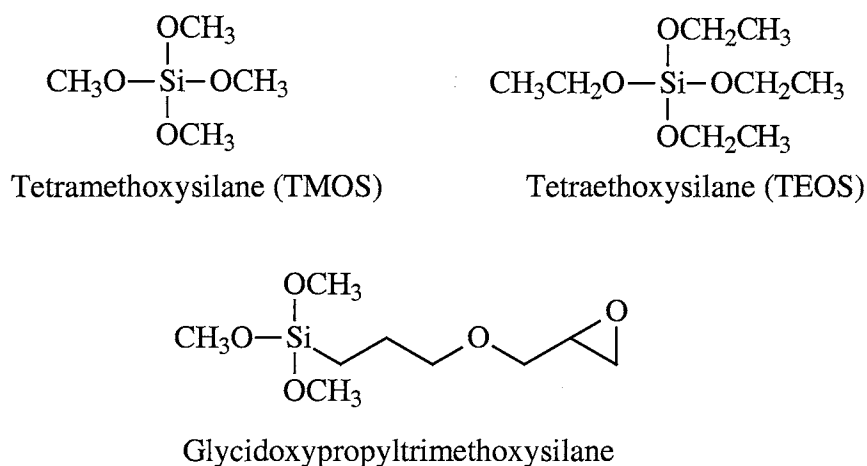


Figure 3.2 Chemical Structures of alkoxide reactants.

3.2.1 TMOS Sol Gel Preparation

Preparation of a typical TMOS silica sol-gel solution was performed as follows: 7.20 mL of 0.05 M HNO₃ was added dropwise to a closed container containing 14.90 mL

of TMOS. The addition rate was approximately 1 mL per minute. Upon completion of TMOS addition, the solution was stirred for 2 h in the closed container. After mixing, the solution was placed into a Teflon tank for dip-coating onto aluminum slides, or held in a closed container to be used for casting of monolithic specimens in 50-mL disposable beakers. Table 4.1 represents an overview of concentrations required to prepare R valued systems of 4, 8, 16, and 24.

Table 3.1: Reactant concentrations for TMOS derived silica sols with R values of 4, 8, 16, and 24.

Reactants	<u>R value</u>			
	4	8	16	24
TMOS	14.90 mL	14.90 mL	14.90 mL	14.90 mL
0.05 M HNO ₃	7.20 mL	14.40 mL	28.80 mL	43.20 mL

3.2.2 TEOS Sol Gel Preparation

Preparation of a typical TEOS silica sol-gel solution was performed as follows: 22.30 mL of TEOS was added directly into a beaker containing 7.20 mL of 0.05 M HNO₃. The resultant bi-phase solution was vigorously stirred at room temperature. The bi-phasic solution became a clear single-phase sol approximately 1 h after initial mixing. The solution was continually stirred for 2 h in the closed container. After thorough mixing, the solution was placed into a Teflon tank for dip-coating onto aluminum slides, or held in a closed container to be used for casting of monolithic specimens in 50-mL disposable beakers. Table 3.2 represents an overview of concentration required to prepare R valued systems of 4, 8, 16, and 24.

Table 3.2: Reactant concentrations for TMOS derived silica sols with R values of 4, 8, 16, and 24.

Reactants	<u>R values</u>			
	4	8	16	24
TEOS	22.30 mL	22.30 mL	22.30 mL	22.30 mL
0.05 M HNO ₃	7.20 mL	14.40 mL	28.80 mL	43.20 mL

3.2.2 Surfactant Addition

The FC-171 and FC-430 surfactants obtained from 3M were used as received. Stock solutions containing 1.0% (w/w) of FC-171 and 4.0% (w/w) of FC-430 were prepared and used accordingly. The surfactants were added to the sol in a drop-wise manner to obtain a final concentration of 0.05 % w/w of FC-171 and 0.20 % w/w of FC-430. The final solution was gently mixed using a pipette. The sol solutions were then immediately transferred to Teflon cells and dip-coated on aluminum slides.

3.3 Overview of SiO₂-epoxide Ormosil Preparation

Ormosil preparations were very similar to those used in the silica based system with only variations in the type of precursors used. Glycidoxypropyltrimethoxysilane (GPTMS) and tetraethoxysilane (TEOS) were obtained from Aldrich chemicals and used as received. The alkoxide precursors were mixed in appropriated concentrations to obtain hybrid gels with 10%, 20%, 40%, 60%, and 80% mole percent organic content. The organic mole percentages were derived using Equation 3.1. Reference to the carbon and silicon molar concentrations were based on the theoretical gel structures formed as a result of complete hydrolysis. D values (water/alkoxide) of 1, 2, 4, and 6 were used to

provide an incremental distribution between literature referenced low and high water values. The water source was a 0.05 M HNO₃ stock solution with a pH near 2. Acidic conditions were selected to catalyze the hydrolysis reaction. All of the sols were prepared under identical conditions except for variations in the GPTMS/TEOS ratios. A total of twenty sols were prepared with five different concentrations of organic content and four different water concentrations. An ormosil preparation flow chart is present in Figure 3.3.

Equation (3.1)

$$\text{Organic Content} = 100\% \times \frac{\text{Moles of Carbon}}{\text{Moles of Carbon} + \text{Moles of Silicon}}$$

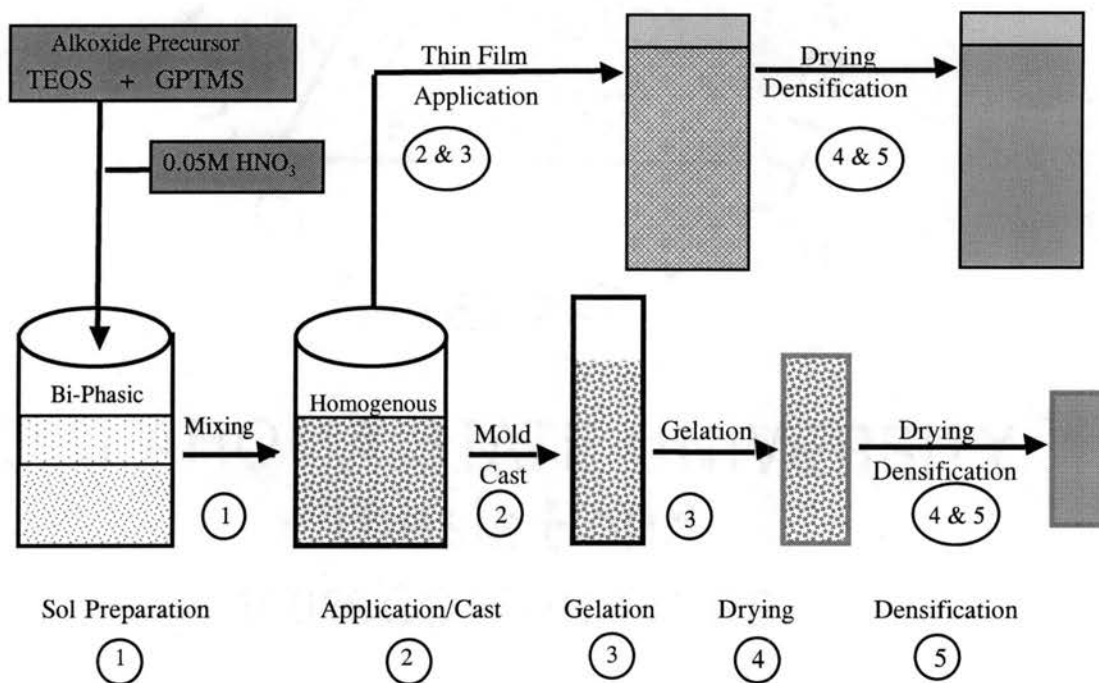


Figure 3.3 Flow chart of epoxide ormosil preparation.

3.3.1 Epoxide Ormosil Sol Gel Preparation

Preparation of a typical ormosil sol-gel solution was performed as follows: 11.15 mL of TEOS and 0.21 mL of GPTMS were placed in a beaker with 3.65 mL of 0.05 M HNO₃ acid. The resultant bi-phase solution was vigorously stirred to initiate hydrolysis and induce mixing. The bi-phasic solution became a clear single-phase sol approximately 1 h after initial mixing. The solution was continually stirred for 2 h in the closed container. The solution was removed and prepared for dip-coating onto aluminum slides and casting in 50-mL disposable beakers. Tables 3.3 through 3.7 represent sol-gel recipes twenty different sols prepared using R values of 4, 8, 16, and 24 with organic concentrations of 10%, 20%, 40%, 60%, and 80% mole percent.

Table 3.3: Reactant concentrations for 10% organic SiO₂-epoxide ormosil sols with D values of 1, 2, 4, and 6.

Reactants	<u>D values</u>			
	1	2	4	6
TEOS	11.15 mL	11.15 mL	11.15 mL	11.15 mL
GPTMS	0.21 mL	0.21 mL	0.21 mL	0.21 mL
0.05 M HNO ₃	3.65 mL	7.30 mL	14.60 mL	21.90 mL

Table 3.4: Reactant concentrations for 20% organic SiO₂-epoxide ormosil sols with D values of 1, 2, 4, and 6.

Reactants	<u>D values</u>			
	1	2	4	6
TEOS	11.15 mL	11.15 mL	11.15 mL	11.15 mL
GPTMS	0.48 mL	0.48 mL	0.48 mL	0.48 mL
0.05 M HNO ₃	3.72 mL	7.44 mL	14.88 mL	22.32 mL

Table 3.5: Reactant concentrations for 40% organic SiO₂-epoxide ormosil sols with D values of 1, 2, 4, and 6.

Reactants	<u>D values</u>			
	1	2	4	6
TEOS	5.58 mL	5.58 mL	5.58 mL	5.58 mL
GPTMS	0.69 mL	0.69 mL	0.69 mL	0.69 mL
0.05 M HNO ₃	1.97 mL	3.94 mL	7.88 mL	11.82 mL

Table 3.6: Reactant concentrations for 60% organic SiO₂-epoxide ormosil sols with D values of 1, 2, 4, and 6.

Reactants	<u>D values</u>			
	1	2	4	6
TEOS	5.58 mL	5.58 mL	5.58 mL	5.58 mL
GPTMS	1.84 mL	1.84 mL	1.84 mL	1.84 mL
0.05 M HNO ₃	2.25 mL	4.50 mL	9.00 mL	13.50 mL

Table 3.7: Reactant concentrations for 80% organic SiO₂-epoxide ormosil sols with D values of 1, 2, 4, and 6.

Reactants	<u>D values</u>			
	1	2	4	6
TEOS	2.23 mL	2.23 mL	2.23 mL	2.23 mL
GPTMS	4.42 mL	4.42 mL	4.42 mL	4.42 mL
0.05 M HNO ₃	1.80 mL	3.60 mL	7.20 mL	10.80 mL

3.3.2 Surfactant Addition

Concentrations of FC-171 and FC-430 surfactants were identical for those used in preparing silica gels. Stock solutions containing 1.0 % (w/w) of FC-171 and 4.0 % (w/w)

of FC-430 were prepared and used accordingly. The surfactants were added to the sol in a dropwise manner to obtain a final concentration of 0.05 % (w/w) of FC-171 and 0.20 % (w/w) of FC-430. The final solution was gently mixed using a pasteur pipette. The sol solutions were then immediately transferred to Teflon cells and dip-coated on aluminum slides.

3.4 Thin Film Application and Monolithic Specimen Formations

3.4.1 Dip-Coating Application

Aluminum slides were dipped into precursor sols using a Chematic Technology Inc. model 201 dip-coater. Prior to dipping, the substrates were polished with 400 and 600 grit silicon carbide sandpaper and sonicated in isopropanol. The sol gel coatings were applied using a single dip process. Approximately 30 mL of sol was transferred to the Teflon dipping cell. Dip-coating was done using a sol dwell time (time of immersion in sol mixture) of 10 seconds and a withdrawal speed of 10 cm/s into laboratory ambient air. Additional information on the fundamentals of sol-gel dipping process can be found in two different reviews by C.J. Brinker, et. al.^{56,57}

3.4.3 Casting of Monolithic Gels

Monolithic gels were prepared from sol solutions comparable to those used in the dip-coating process. Approximately 30 mL of sol was placed in a 50-mL polypropylene beaker. Parafilm was placed over the beaker and perforated to control the drying rate. The samples gelled between 1-3 days for low R and D/high silica gels and up to 2 weeks for the high R and D/high hybrid systems. In all cases, dried xerogels were transparent. Samples were ground using a mortar and pestle until a fine powder was obtained.

3.5 Spectroscopic Characterization

3.5.1 Experimental Nuclear Magnetic Resonance (NMR)

The ^{29}Si NMR spectra were obtained using a Chemagnetics 300MHz (7.06T) spectrometer operating with a 7.5mm 300VXP-144 double resonance (H-X) probe. Spectra were recorded at a resonance frequency of 59.8 MHz. Magic angle spinning was carried out, utilizing a spinning rate between 4 and 5 KHz. Both ^{29}Si single pulse and cross polarization experiments were conducted. Chemical shifts were referenced to an external standard of tetramethylsilane. Peak frequencies and intensities were deconvoluted using Chemagnetics Spinsight software.

The ^{29}Si single pulse experiments were performed using a single pulse sequence with proton decoupling. Xerogels were grounded to a fine powder and packed into the rotor. The $\pi/2$ pulse widths were 8 μs . The pulse delay time was 120 s. A total of 360 scans were collected to achieve acceptable signal to noise ratios.

The ^1H - ^{29}Si cross-polarization experiments were collected using a quasi-adiabatic cross-polarization sequence.⁵⁸ This pulse sequence is insensitive to the Hartmann-Hahn match condition and the MAS spinning speed. The $\pi/2$ pulse width used was 8 μs . The contact time was 8 ms. The pulse delay was 3 s. A total of 2000 acquisitions were obtained.

^1H - ^{13}C cross-polarization experiments were collected using a quasi-adiabatic cross-polarization sequence. The $\pi/2$ pulse width used was 4 μs . The contact time was 2 msec. The pulse delay was 1 s. A total of 10000 acquisitions were obtained.

3.5.2 General Raman and Infrared Spectroscopy

Raman and infrared spectroscopies are two techniques used to detect vibrational modes in both organic and inorganic materials. The methods induce molecules to undergo changes in their vibrational energy states by subjecting them to excitation radiation in selected spectral regions.⁵⁹⁻⁶¹ IR and Raman spectra are complementary techniques which exhibit similar vibrational characteristics, but with different intensities. The molecular vibrational intensities differ because of the different excitation mechanism and therefore different selection rules. Raman and IR absorption spectroscopies may be used to generate complementary information about bonding and structure in solid state specimens.

3.5.2(a) Experimental Single Reflectance Infrared Spectroscopy

Single reflectance infrared spectroscopy is a simple non-destructive method for acquiring infrared information. Thin films coated on reflective surfaces can be analyzed by transmitting IR irradiation through the sample and collecting at diffuse off-axis reflection. The method allows samples to be monitored over the complete spectral range without special requirements.

One of the primary disadvantages of single reflectance IR is sampling thickness requirements. Since the method relies on a single pass reflection, the sample must be thick enough to provide sufficient IR absorption. Normally, films of at least 500 nm thick are required to provide sufficient absorption.

Infrared spectra in this study were acquired using a Bruker Equinox 55 FT-IR operating with OPUS software equipped with a liquid nitrogen cooled MCT detector. A 30° single reflectance attachment from Spectra Tech was used to analyze the coated

aluminum slides. An uncoated aluminum slide was used to generate the baseline spectrum. The sampling area was 1 cm². A total of 64 scans were acquired with a spectral resolution of 4 cm⁻¹.

3.5.2(b) Experimental Raman

Raman analysis was performed using a FRA 106/RFS 100 Bruker FT-Raman spectrometer. Samples were ground into fine powders and packed into 1mm² sample cells. Sample excitation was obtained using a Nd:YAG laser operating at a wavelength of 1.06 μm and a power intensity between 100 and 500 mW. Photoemissions were collected with a germanium based photodiode cooled to 77 K. A total of 64 scans were performed using a spectral resolution of 4 cm⁻¹.

3.5.3 Density Measurements

Density measurements were obtained using an automated gas displacement pycnometer. The instrument determines the volume of a material by measuring the pressure change of known gas in two calibrated cell volumes. The correlation between volume and pressure is derived from the ideal gas law, $PV = nRT$, where P = pressure, V = volume, n = moles of gas, R = gas constant, and T = temperature. By using two cells with known volumes and measurable pressures, the volumetric displacement of an unknown solid sample can be measured through pressure differences.

Experimentally, an automated Micromeritics AccuPyc 1330 pycnometer operating with high purity helium gas was used. Prior to analysis, powder samples were vacuum dried at room temperature for 12 h and pre-weighed before analysis. The pycnometer consisted of two cells with standardized volumes. In one cell, helium gas was charged to

a preset pressure of 19.5 lbs/in² in order to standardize the concentration of gas (n). In the second cell, an unknown volumetric sample was placed in the cell at ambient pressure and purged with helium gas repeatedly in order to evacuate any solvents, which could alter pressure measurements. The charged cell was then released into the second cell. The pressure of the combined cells was measured using a gauge pressure transducer. The pressure indifference between the adjoined cells “with” and “without” the unknown sample was used to identify the volumetric displacement of the unknown sample. The final density was determined by dividing the volumetric sample displacement by the sample weight. A minimum of 10 measurements was carried out on each sample. Final densities were averaged and reported with a standard deviation of less than 0.005 g/cm³.

CHAPTER 4

INVESTIGATION OF WATER-BASED SILICA SOL-GELS BY ^{13}C AND ^{29}Si SOLID STATE NMR

4.1 Introduction

Solid state NMR spectroscopy (^{13}C and ^{29}Si) has been used extensively in characterizing sol-gel systems. Single pulse and cross-polarization experiments targeting silicon nuclei provide a direct method of acquiring both quantitative and qualitative information about the silica composition and the surrounding network microstructure. Single pulse ^{29}Si NMR/magic angle spinning (SP/MAS) experiments have been used in numerous studies to resolve the local environment of silica based materials and to provide compositional percentages of condensed species.⁶²⁻⁷⁰ Studies using supplemental ^1H - ^{13}C cross-polarization/magic angle spinning (CP/MAS) experiments have been used to identify the extent of the hydrolysis reaction and aid in differentiating between silanol and unhydrolyzed alkoxide silane species.^{44,63,70} Studies making comparisons between ^{29}Si SP/MAS results and ^1H - ^{29}Si CP/MAS experiments provide complementary information concerning the local environments surrounding condensed species.⁷⁰⁻⁷⁴ Spectral comparisons between SP and CP peak intensities can provide qualitative information concerning silanol distributions and structural formations. By utilizing 3 different solid state NMR experiments (^{29}Si SP/MAS, ^1H - ^{13}C CP/MAS, and ^1H - ^{29}Si CP/MAS), silica gels prepared under selected experimental conditions can be monitored to elucidate differences in the degree of hydrolysis and condensation, chemical composition, and structural sub-units associated with variations in sol gel growth mechanisms.

Parameters such as pH, catalyst type, solvent concentration, water content, precursor, and curing temperature have all been shown to influence the polymeric growth mechanism and subsequent gel microstructure in silicate gels.¹²⁻²⁸ Although there is a wide diversity in sol gel processing conditions, gel formation and growth are usually attributed to one or more of three general subunit types: (1) linear chains, (2) branched chain/fragments, and/or (3) dense colloidal particles. Gel microstructures derived from each subunit-type have been studied as a function of parameters such as chemical composition, silanol content, and gel density. NMR studies conducted on many of these systems have indicated that processing conditions, such as elevated water content and precursor type, can substantially alter particle or cluster development in the sol, effecting the final gel microstructure.^{65,68,74-77} SP/MAS and CP/MAS solid state NMR studies can provide great insight into evolving gel microstructures and growth mechanisms.

In this chapter, solid state ^{13}C and ^{29}Si NMR experiments and pycnometer density measurements were used to characterize silica gel formations as a function of initial water activity (R value) and precursor type. Gels having R values of 4, 8, 16, and 24 were prepared using TMOS and TEOS precursors. Single pulse and cross-polarization ^{29}Si NMR experiments were used to quantify siloxane species and to determine local environments surrounding silicon nuclei. Complementary ^1H - ^{13}C cross-polarization NMR analysis was used to identify the degree of hydrolysis and the presence of residual alcohol. Gel density measurements were used to support structural assignments associated with packing efficiencies and growth mechanisms. Local sol-gel chemistry and gel microstructure have been determined as a function of R value and precursor type. Polymer growth mechanisms have been classified as being derived from linear chains, branched chains/fragments, and/or spherical particles.

4.2 Background:

4.2.1 Solid State NMR

Solid state ^{29}Si NMR spectroscopy of silica glass has been extensively investigated over the past 20 years. Early studies on mineralogical samples by Lippma and co-workers demonstrated that the degree of condensation surrounding a silicate structure could be determined via high-resolution solid state ^{29}Si spectroscopy through isotropic chemical shifts.⁷⁴⁻⁷⁸ The authors of this early work developed a “Q” notation to label the various types of silicate structures observed. This “Q” notation has been widely used in subsequent literature. The symbol “Q” represents any given silicon-centered oxide tetrahedron; the numerical superscript is used to identify the number of attached silicate tetrahedra. For example “Q₁” represents a silicate species which has formed one $\equiv\text{Si-O-Si}\equiv$ linkage and has 3 nonbridging functionalities (e.g., silanol or alkoxide groups). As the subscript number increases, so does the number of siloxane linkages (and the number of nonbridging ligands is reduced). “Q₄”, therefore, refers to a silicon atom which is bonded to 4 other silicate tetrahedra through 4 bridging oxygen atoms. A complete representation of the “Q_n” species is illustrated in Figure 4.1. The notation provides a clear and flexible method by which to identify various silicate species.

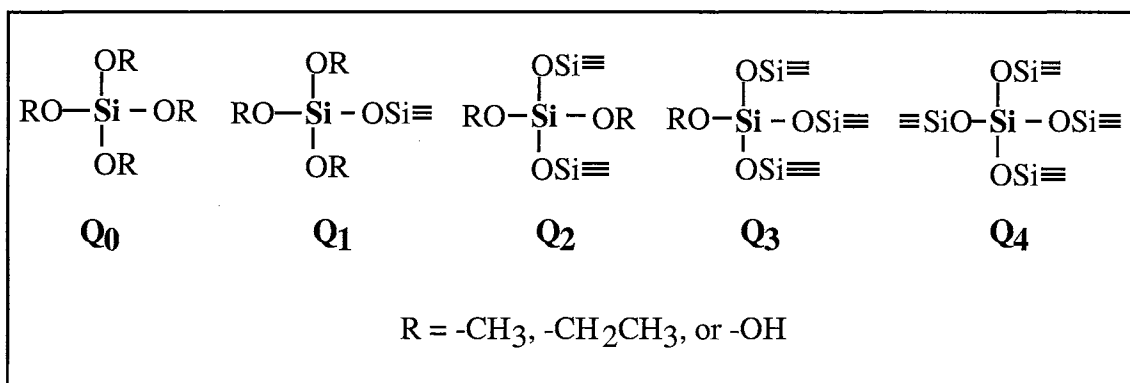


Figure 4.1: Siloxane species characterized by representative “Q” notation. Bold Si represents designated Q species.

In high resolution ²⁹Si NMR experiments, the chemical shifts for gels derived from tetra-alkoxide precursors have been observed typically between the range of -72.3 ppm and -115.0 ppm. In this region, peaks are well defined and incrementally separated based on the specific degree of condensed species. Reported isotropic ²⁹Si chemical shifts observed for Q_n silicate nuclei are presented in Table 4.1 with literature sources cited.

Table 4.1: Typical ²⁹Si chemical shifts observed for tetra-oxide and tri-oxide silicate species. Peak shifts are referenced against with a tetramethylsilane (TMS) standard.

Peak Type (Q _n)	Chemical Shifts	References
Q ₀	-72 ppm to -82 ppm	62-80
Q ₁	-82 ppm to -89 ppm	
Q ₂	-90 ppm to -98 ppm	
Q ₃	-100 ppm to -104 ppm	
Q ₄	-108 ppm to -115 ppm	

4.2.2 Single Pulse Experiments

Single pulse/magic angle spinning (SP/MAS) experiments on silica samples have been extensively used to elucidate local chemical environments, and to quantify siloxane bond formation. Several studies using single pulse techniques have been used to

quantitate the specific ratios of condensed nuclei and to correlate results with structural and physical characteristics.⁷⁸⁻⁸⁰ Using peak deconvolution methods, the extent of condensation has been used to determine overall siloxane connectivity as a function of sol-gel processing conditions.^{20,49,68,74} One disadvantage of this technique is its inability to differentiate between nonbridging end groups (e.g., silanol versus alkoxide). In liquids ²⁹Si NMR, frequency shifts between hydroxy and alkoxy silane species are readily distinguishable; however, in the case of solid state NMR it is found that peak broadening (associated with anisotropic chemical shifts) limits sensitivity. Thus, only the relative degree of siloxane bond formation may be determined for silica gels. Complementary single pulse ²⁹Si NMR experiments, however, can be used to quantify percentile distribution of the condensed silicon nuclei in a silica-based network. Both methods have been employed in this research to develop a more complete chemical assessment of the sol-gel process.

The term “conversion efficiency” has been used in various reports to express the degree of condensation in a silica gel network.⁷⁸⁻⁸⁰ By definition, the conversion efficiency is a percentage value based on the ratio between observed and theoretical connectivity, as given in Equation 4.1. Since each Q_n species contains a specific number of siloxane bridges, the observed connectivity can be determined based on the overall deconvoluted compositional percentages found from SP spectra. Equation 4.2 represents the conversion equation for a silica system with a theoretical connectivity of 4. The degree of conversion can be calculated for any silica gel by inserting compositional percentages for each Q species. Based on the conversion efficiency, the total silanol content can be referenced and correlated with condensation and reaction efficiencies.^{48, 62}

$$\% \text{ Conversion Efficiency} = \frac{\text{Observed Functionality}}{\text{Theoretical Functionality}} \quad \text{Equation 4.1}$$

$$\% \text{ Conversion Efficiency} = \frac{2 * Q_2 + 3 * Q_3 + 4 * Q_4}{4} \quad \text{Equation 4.2}$$

4.2.3 ^1H - ^{29}Si Cross Polarization Experiments

Use of the CP technique, in combination with SP/MAS NMR, provides a method to assess the siloxane bridging vs. nonbridging formations. Single pulse experiments provide relative measures of the Q_0 , Q_1 , Q_2 , Q_3 , and Q_4 content. In gels with similar Q_0 - Q_4 population distributions as determined by SP experiments, differences arising in CP Q_4 intensities provide structural information related to silanol distribution in the silica network. Random distribution of the silanol content in the gel network lead to an increase in the observed CP Q_4 intensity. Conversely, gels with more localized concentrations of silanol or condensed clusters of Q_4 nuclei result in a decreased CP Q_4 intensity. The inherent differences between CP/SPE Q_4 intensities provide a qualitative means of determining silanol distributions, which can be used to correlate variations in the gel microstructure as a function of processing conditions.

4.2.4 ^1H - ^{13}C Solid State NMR

Solid State ^1H - ^{13}C CP/MAS NMR has been used as a complementary technique to identify the presence of unhydrolyzed alkoxide silanes. In solid state media, ^{29}Si NMR techniques are limited to the detection of condensation silicon nuclei. Such experiments cannot be used to differentiate between silanol (-OH) and alkoxide end groups (-OR). Identifying the presence of alkoxy end groups is quite useful, however, because results

can be used to differentiate between hydrolyzed silanol and unreacted alkoxide functionalities. Distinctions between an alkoxide group and a chemisorbed alcohol species are widely described in the literature. Assignments are reported on the basis of frequency shifts and resonance profiles.^{44,63,70} Residual alcohol molecules, which have free molecular mobility, tend to develop very sharp peak profiles. Alkoxysilanes, on the other hand, have limited mobility due to covalent bond formation with the siloxane network. The restriction of molecular movement results in substantially broadened peak profiles (attributed to chemical shift anisotropy).^{44,63,70} An example of the use of this technique was presented by Klemperer and co-workers in which unhydrolyzed methoxide end groups and methanol were differentiated in a silica gel based on a 2 ppm chemical shift with line broadening.⁶³ Blumel and co-workers made similar distinctions between chemisorbed and physisorbed ethanol, based on similar degrees of peak shift and line broadening.⁷⁰ By confirming the presence or absence of alkoxide end groups, the structural assignments for Q₂ and Q₃ species may be referenced to (1) geminal and silanol formations or (2) unhydrolyzed precursor species.

One shortcoming of ¹H-¹³C CP/MAS NMR methods in regard to the present work is the limited ability to quantify the relative carbon to silicon ratio. A quantitative distinction between alcohol and alkoxide may be made through comparisons of deconvoluted peak intensities. Comparisons between the silica and alkoxide content are limited to qualitative assessments in identifying the presence or absence of alkoxide content. Quantitative comparisons can be made, but require special experiments and standardized samples. The ¹H-¹³C CP/MAS NMR technique is used in this research to identify the presence of alkoxide peaks, and to provide qualitative information concerning the degree of hydrolysis in the silica gels.

4.3 Results and Discussion

4.3.1 ^{29}Si SP/MAS and ^1H - ^{13}C CP/MAS Solid State NMR

Figure 4.2 represents a typical ^{29}Si single pulse magic angle spinning (SP/MAS) spectrum for TMOS and TEOS gels. The broad peaks observed at shifts of -94 ppm, -103 ppm, and -112 ppm are those attributed to Q_2 , Q_3 , and Q_4 species in the condensed gel network. Quantified peak percentages, frequency shifts, and conversion efficiencies for each silica gel spectrum are presented in Tables 4.2 and 4.3. Peaks attributed to nuclei present in the 3M surfactants (reference the preceding chapter section indicating the presence and rationale for surfactant presence) have been subtracted out.

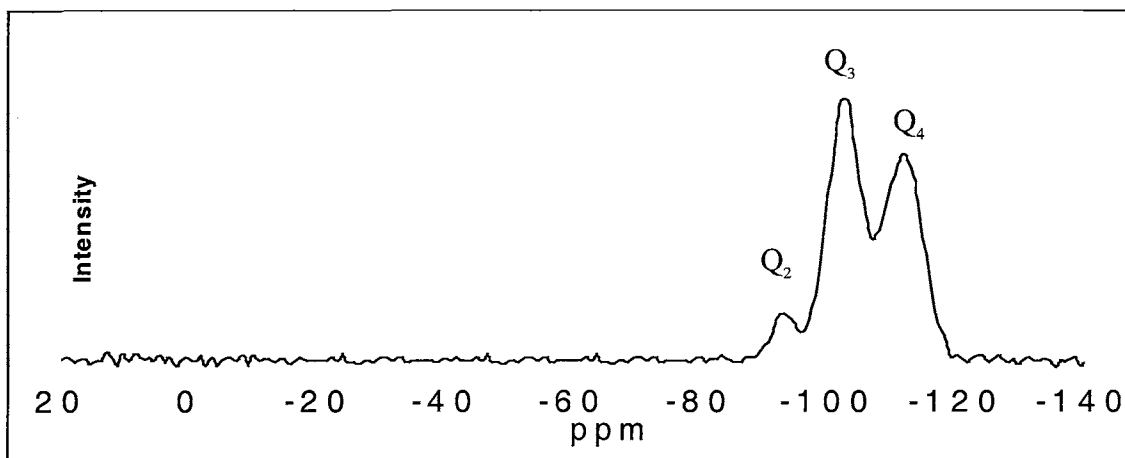


Figure 4.2: ^{29}Si SP/MAS NMR spectrum of silica gel prepared using TMOS and an R value of 4.

Table 4.2: ^{29}Si SP/MAS NMR peak positions and assignments for TMOS prepared silicate with R values of 4, 8, 16, and 24. The values in parenthesis correspond to the designated peak percentages.

TMOS R Value	^{29}Si Single Pulse MAS/NMR Results			Conversion Efficiency
	Q_2	Q_3	Q_4	
4	-93.77 ppm (9 %)	-103.07 ppm (48 %)	-112.10 ppm (43 %)	83 %
8	-94.10 ppm (8 %)	-103.73 ppm (45 %)	-112.98 ppm (47 %)	85 %
16	-94.31 ppm (6 %)	-103.90 ppm (44 %)	-113.00 ppm (50 %)	86 %
24	-93.91 ppm (4 %)	-103.63 ppm (46 %)	-113.08 ppm (50 %)	86 %

Table 4.3: ^{29}Si MAS/NMR peak positions and assignments for TEOS prepared silicate with R values of 4, 8, 16, and 24. The values in parenthesis correspond to the designated peak percentages.

TEOS R Value	^{29}Si Single Pulse MAS/NMR Results			Conversion Efficiency
	Q_2	Q_3	Q_4	
4	-94.07 ppm (9 %)	-103.80 ppm (50 %)	-113.22 ppm (41 %)	82 %
8	-93.97 ppm (8 %)	-103.63 ppm (44 %)	-112.88 ppm (48 %)	85 %
16	-94.46 ppm (6 %)	-103.85 ppm (45 %)	-112.99 ppm (49 %)	86 %
24	-94.36 ppm (5 %)	-103.61 ppm (47 %)	-112.77 ppm (49 %)	86 %

^{29}Si SP/MAS NMR experiments results are presented in Table 4.2 and 4.3 for gels prepared using TMOS and TEOS precursors, respectively. Comparisons between the TMOS and TEOS single pulse NMR results revealed subtle differences in the conversion efficiencies and Q_4 percentages in the R = 4 gels. In both cases the conversion efficiency and Q_4 population density is measurably lower for the R = 4 (limited water) preparation than for preparation conditions that had higher initial water activities. The difference was attributed to less complete precursor hydrolysis. Figures 4.3(a) and 4.4(a) represent ^1H - ^{13}C CP/MAS NMR acquired for the R = 4 TMOS and TEOS gels. In the TEOS spectrum, the broad peak at 17.4 ppm was assigned to a methyl end group from ethanol and ethoxide. The peaks at 58.7 ppm and 60.0 ppm were identified as the $\text{CH}_3\text{-CH}_2\text{-O-X}$ (X= Si or H) carbon, from residual ethanol and unhydrolyzed ethoxide functionalities (from the TEOS precursor), respectively. The R = 4 specimens derived from TEOS had a Q_4 population substantially lower than any other specimens examined. The low Q_4 value is consistent with a large residual population of unhydrolyzed ethoxide precursor. Deconvolution of the 58.7 ppm and 60.0 ppm peaks yielded calculated relative ratios of 1 equivalent of unhydrolyzed TEOS per equivalent of residual ethanol.

In the TMOS R = 4 gel (Figure 4.3(a)), an extremely weak peak was observed at 50.3 ppm, consistent with the presence of residual chemisorbed methanol. Results

presented by Brinker and co-workers showed that unhydrolyzed alkoxide end groups limit the degree of connectivity in xerogels.^{5,11} They also demonstrated that unhydrolyzed ethoxide end groups were poor siloxane bond formers, and that the degree of condensation in such gels was lowered due to steric hindrance which inhibited crosslinking at adjacent silanol sites.

The increase in conversion efficiency and Q_4 intensity as a function of water addition (increased R value) was attributed to changes in the resultant gel structure. The ^1H - ^{13}C CP/MAS NMR spectra illustrated in Figures 4.3(b) and 4.4(b), indicated the R = 8 gels were completely hydrolyzed, as evidenced by the lack of an ethoxide or methoxide peak, and that the residual alcohol content in the xerogels were below detectable limits. Since it is assumed that gels made using the TMOS precursor were completely hydrolyzed, the loss in Q_4 intensity must be attributed to something other than incomplete hydrolysis. It is postulated that the variation in Q_4 intensity could only be accounted for based on fundamental changes in the gel microstructure, such as a change from linear to cyclic structures.

In work published by Li Voon Ng and co-workers, high conversion efficiencies (e.g., efficiencies >83%) in TEOS-derived gels were characteristic of materials composed of cyclic substructures.⁸¹ Subsequent work reported by Li Voon Ng revealed that ring formations were favored with increasing water content.⁸² Under conditions of low water content, the bimolecular reaction competed equally with cyclization, leading to more linear or branched structures (Figure 4.5). Thus, the variations in Q_4 intensity found in going from R = 4 to R = 8, and the concomitant increase in conversion efficiency marks a transition in the gel polymerization mechanism, which arises as a result of more complete hydrolysis and increased ring development.

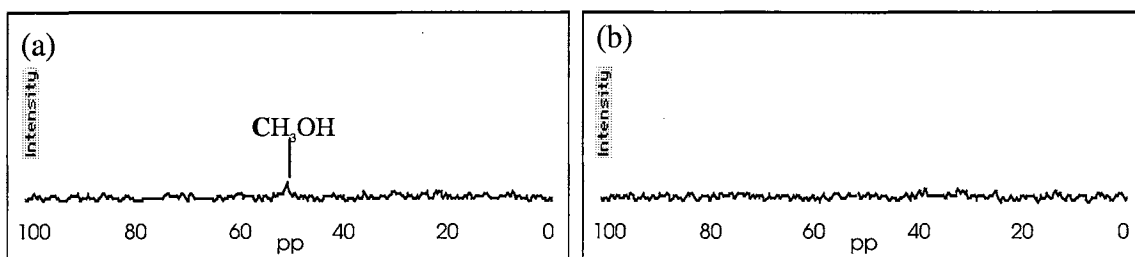


Figure 4.3: ^1H - ^{13}C CP/MAS NMR spectrum of TMOS gels (a) $R = 4$ (b) $R = 8$.

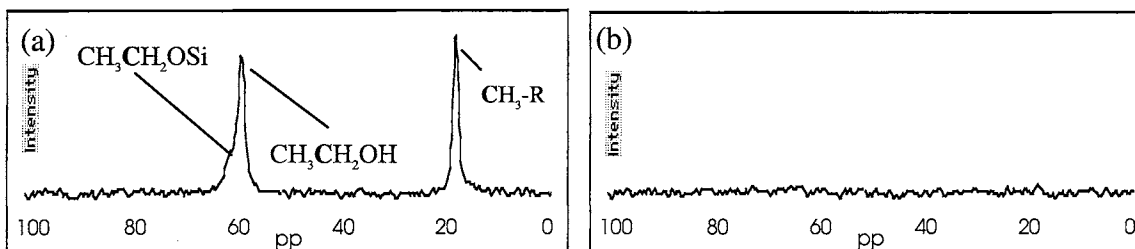


Figure 4.4: ^1H - ^{13}C CP/MAS NMR spectrum of TEOS gels (a) $R = 4$ (b) $R = 8$.

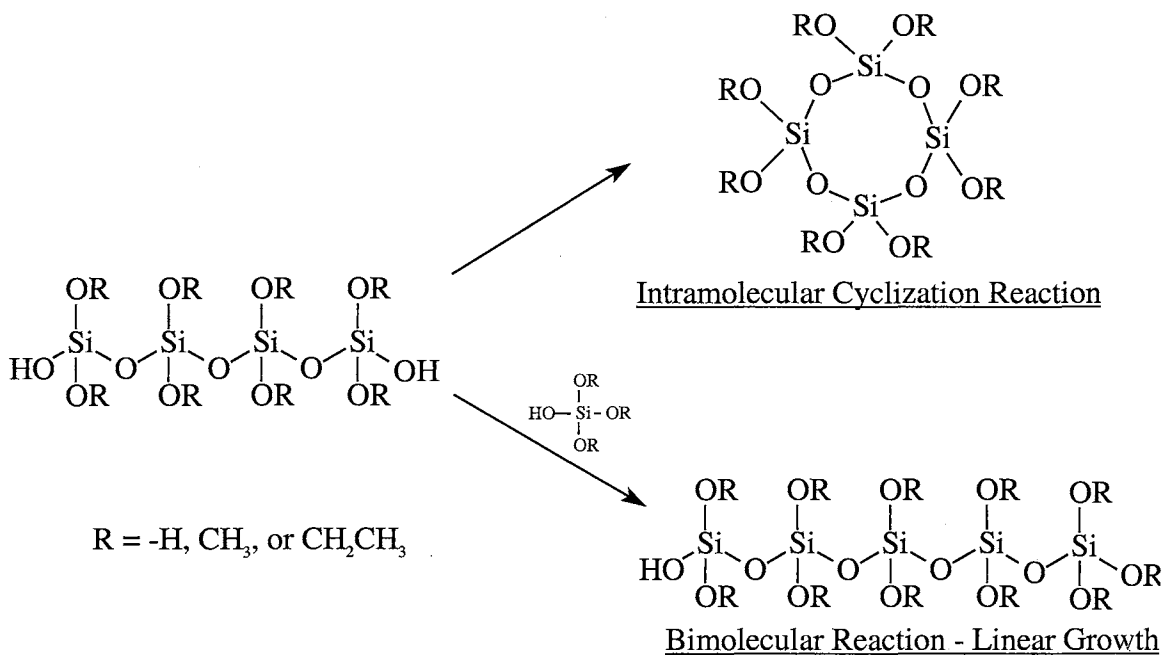


Figure 4.5: Bimolecular and Intramolecular reactions.

4.3.2 ^1H - ^{29}Si CP/MAS Solid State NMR

Figure 4.6 represents a typical ^1H - ^{29}Si CP/MAS spectrum acquired for the TMOS silica gel. CP spectra exhibited peaks at -94 ppm, -103 ppm, and -112 ppm, for Q_2 , Q_3 , and Q_4 species, respectively. Deconvoluted peak percentages, and frequency shifts for the TMOS silica gels are presented in Table 4.5. Comparable spectra were observed for the TEOS-derived gels. Spectra for each gel are located in Appendix A. Deconvoluted peak percentages, and frequency shifts for the TEOS silica gels are presented in Tables 4.6.

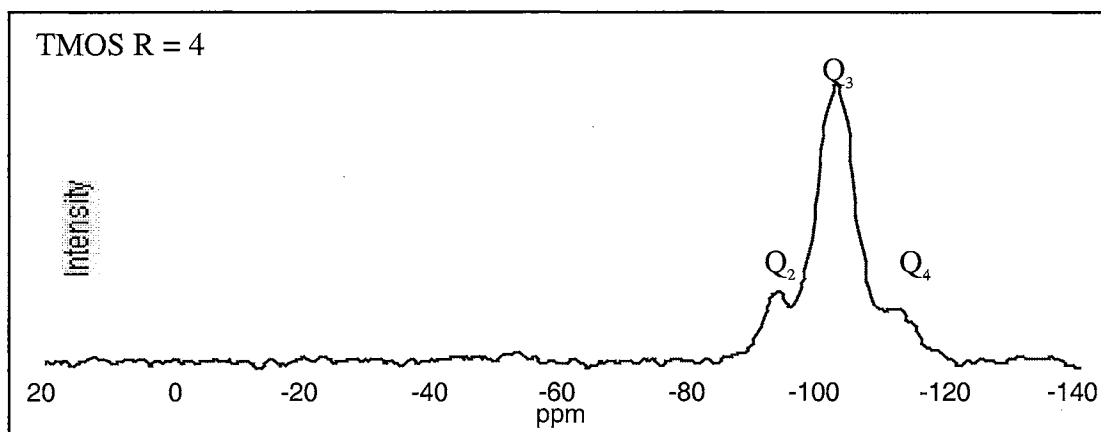


Figure 4.6: ^1H - ^{29}Si CP/MAS NMR spectrum of TMOS gels prepared from R = 4 gel.

Table 4.5: ^{29}Si CP/MAS NMR peak positions and assignments for TMOS prepared silicates with R values of 4, 8, 16, and 24. The values in parentheses correspond to deconvoluted peak percentages.

^1H - ^{29}Si Cross Polarization MAS/NMR Results			
R Value	Q_2	Q_3	Q_4
4	-93.6 ppm (12 %)	-102.8 ppm (77 %)	-112.5 ppm (11 %)
8	-94.1 ppm (10 %)	-103.2 ppm (66 %)	-112.7 ppm (24 %)
16	-93.7 ppm (11 %)	-102.8 ppm (64 %)	-112.4 ppm (25 %)
24	-94.0 ppm (7 %)	-102.8 ppm (74 %)	-112.8 ppm (19 %)

Table 4.6: ^{29}Si CP/MAS NMR peak positions and assignments for TEOS prepared silicates with R values of 4, 8, 16, and 24. The values in parentheses correspond to deconvoluted peak percentages.

^1H - ^{29}Si Cross Polarization MAS/NMR Results			
R Value	Q_2	Q_3	Q_4
4	-93.78 ppm (8 %)	-103.04 ppm (70 %)	-112.80 ppm (21 %)
8	-93.66 ppm (8 %)	-102.78 ppm (70 %)	-112.40 ppm (23 %)
16	-94.04 ppm (6 %)	-102.71 ppm (68 %)	-112.12 ppm (26 %)
24	-93.50 ppm (10 %)	-102.79 ppm (75 %)	-112.51 ppm (17 %)

In comparing SP and CP Q_4 percentages in both TMOS and TEOS derived gels, the variation in Q_4 intensities showed that the local environment surrounding the fully condensed nuclei clearly changes as function of R value. Variations in CP Q_4 intensities revealed signs of three different types of structures. In the lower water content gels (R = 4), the gels were characterized by lower conversion efficiencies (Table 4.2 and 4.3) and low CP Q_4 intensities (Tables 4.4 and 4.5). As the water content increased into moderate value range (R = 8 and 16), the gels were identified with higher conversion efficiencies and higher CP intensities. The highest water content gels (R = 24) were found to have high conversion efficiencies, but anomalously low CP Q_4 intensities. Based on these results, three different gel substructures have been postulated with polymeric growth mechanisms that are based on low, medium, and high R values. These mechanisms are detailed in sections 4.3.3, 4.3.4., and 4.3.5, respectively.

4.3.3 Low water content gels

NMR studies of low water content (R = 4) aqueous-phase gels evidence a microstructure derived from the entanglement of linear or lightly branched chains. In the R = 4 TMOS gel, the low CP Q_4 percentage indicated the Q_2 and Q_3 silanol species were highly localized and isolated from the fully condensed Q_4 nuclei. Such characteristics are

consistent with a gel microstructure containing small micropores with high concentrations of neighboring silanol species at the pore surface. In Table 4.7, the density of 2.00 g/cm^3 observed for the TMOS $R = 4$ gel was also consistent with a prediction made by Brinker, that gel structures derived from linear chain entanglement tend to yield denser microporous networks.^{5,11,16} Similar results presented by Strawbridge, et. al., on a low R -valued alcohol-based gel indicated that it was composed of a microporous network derived from cross-linked linear chains. Their model system had a reported matrix density of 1.99 g/cm^3 in good agreement with the 2.00 g/cm^3 value observed for the TEOS $R = 4$ specimen.²⁷

The $R = 4$ TEOS gel results were significantly different from those observed in the TMOS gel. The TEOS $R = 4$ gel had a low CP Q_4 density attributed to the effects of unhydrolyzed ethoxide groups found to exist in the silica matrix. Comparatively high densities of isolated silanol groups in the TEOS network accounts for the additional coupling of Q_4 nuclei to a proton source. The low 1.88 g/cm^3 density of the TEOS $R = 4$ (Table 4.7) was attributed to the large quantity of residual ethanol and unreacted ethoxide groups trapped in the network, and the influence of unreacted ethoxide groups on crosslinking and packing efficiency. The development of lower density gels through entrapment of organic solvents and/or residual alkoxide is described in the literature in good agreement with the results of this experiment.^{16,23}

Overall, it was found that gels derived using small water ratios yielded xerogels which give evidence of formation through linear chain. The close resemblance of aqueous phase-derived gels and literature reports of alcohol based sol-gel preparations imply that only relatively minor differences occur in processes without added alcohol solvent when R values are low. The similarities between alcohol and water based gels at

R = 4 were attributed to the presence of alcohol by-products. Hydrolysis of each mole of alkoxide results in the consumption of one mole of water with the production of one mole of alcohol. With systems having an equal number of water and alkoxide species (R = 4), the reaction caused the sol to progressively change from an aqueous-based to an alcohol-based solvent system. Brinker has shown that in low R valued sols, precursors tend to react in a manner which is based on simple steric arguments wherein monomers are more readily hydrolyzed than dimers or end chain groups. Also, oligomer groups are more readily hydrolyzed than alkoxides in the middle of a chain.^{5,16} The postulated mechanism of linear or lightly branched network growth for TEOS and TMOS gels agrees with the NMR findings (i.e. hydrolysis extent and conversion efficiency, etc) and with trends reported elsewhere in the literature.

Table 4.7: Density Measurements for TMOS and TEOS prepared silicate gels with R values of 4, 8, 16, and 24. Standard deviation was less than 0.001 g/cm³.

Density Results		
R Value	TMOS	TEOS
4	2.00 g/cm ³	1.88 g/cm ³
8	1.92 g/cm ³	1.95 g/cm ³
16	1.90 g/cm ³	1.91 g/cm ³
24	2.00 g/cm ³	1.96 g/cm ³

4.3.4 Intermediate water content gels

The intermediate water content gels (R = 8 and R = 16) give indications of having microstructure derived from branched cyclic particulate rather than the linear chains seen in the case of low water content gels. SP NMR results indicated the increase in condensed species was associated with cyclic ring formations. In the TMOS R = 8 and 16 gels, the increased CP Q₄ intensity pointed to an increase in the silanol distribution,

characteristic of less efficient packing and the formation of more highly branched network.

The suggestion of branching in the TMOS-derived gel microstructure was also supported by a subsequent decrease in density, from 2.00 g/cm^3 ($R=4$) to 1.92 g/cm^3 ($R = 8$) and 1.90 g/cm^3 ($R = 16$). The reduction in density with increasing R implied there was an increase in branching as initiation by water activity increased. Lower measured density in the TMOS gel was attributed to a loss of packing efficiency, due to the branching, and disruption in the siloxane network. This trend was also consistent with the increased CP Q_4 intensity reported for TMOS gels in section 4.3.4.

The effects of increase water content for the TEOS gels appear on the surface to run counter to those observed in the case of the TMOS gels. The CP Q_4 intensity was slightly lower for the TEOS $R = 8$ gel, signifying a lower degree of branching with improved packing efficiency than for the comparable TMOS-derived gel. The salient difference between the TEOS-derived $R = 4$ and $R = 8$ gels lies in the extent of hydrolysis while the $R = 4$ gels were found to have much residual ethoxy functionality, the $R = 8$ gel had no measurable alkoxy residue. Since they also had only limited branching, they are much more similar to a TMOS-derived $R = 4$ gel (2.00 g/cm^3) than to a TEOS $R = 4$ gel (1.88 g/cm^3). As the R value increased to 16 for the TEOS specimen, the CP Q_4 intensity was similar to values observed for the TMOS-derived gel, as was the measured density.

The variations in branching observed between the TMOS and TEOS gels were attributed to the lower reactivity of the TEOS precursor. Unlike TMOS, the TEOS gel did not exhibit complete hydrolysis until an R value of 8 was used. The lower reactivity would account for the lower degree of branching and increased density in the $R=8$ TEOS gel. In the $R=16$ value gels, the effects of reactivity were not as influenced by the elevated water content, development of more extensive branching, and alcohol dilution effects.

4.3.5 High water content valued gels

Gel densities were maximized in this study for the highest water activity used, corresponding to $R = 24$. The literature contains several papers dealing with gelation mechanisms in water-rich media. In a study by Strawbridge and co-workers, it was concluded that the high water ratios have the effect of producing what is virtually an aqueous system that encourages intramolecular reactions and small, dense colloidal particle formation.²⁷ Once the particles reach a critical size, a gel is formed through particle coalescence. Gelation under this mechanism yields a 3-dimensional network composed of dense particles and small voids. In essence, gels prepared under high water conditions become micro-heterogeneous systems, composed of dense fractal particles which form a micro-porous network at the macro level.

The growth mechanism proposed for the $R = 24$ gels is very similar to those reported for silicic acid ($\text{Si}(\text{OH})_4$). Mechanisms proposed by Iler suggest that polymerization in silicic acid solutions occurs via (1) polymerization of monomers to form particles, (2) growth of the particle, and (3) linking of particles into chains which subsequently form a network. According to Iler, in silicic acid solutions having a pH of 2 (similar to conditions used in this research), initial particle growth occurs through preferential condensation reactions between large more highly condensed species and smaller, less condensed species. For example, dimerization occurs slowly, but once dimers form they rapidly react with monomers to form trimers, which then quickly react with a fourth monomeric unit. In this model, tetramers tend to undergo rapid cyclization. Growth of the cyclic tetramer continues through addition of lower-molecular weight species, such as monomers, dimers, and trimers. Sequential condensation reactions occur between these species such that the number of $\equiv\text{Si}-\text{O}-\text{Si}\equiv$ bond formations are maximized and the concentration of non-bridging silanol end groups is minimized. Colloidal particle growth continues until the particle reaches a size of 2-4 nm at which point growth

becomes negligible. Colloids coalesce, with the formation of a linked network, composed of small highly condensed particles.

In this study, sols prepared with elevated R values behave in a manner very similar to the Iler's silicic acid systems. Conditions with elevated water activity essentially resulted in complete hydrolysis of the monomer species prior to any condensation reactions. Since the relative amount of residual alcohol, formed as a result of hydrolysis, is small in comparison to the amount of excess water, the effects of esterification reactions were minimal. Without esterification, the sol is essentially composed of $\text{Si}(\text{OH})_4$. Polymerization and growth proceeds via a silicic acid mechanism, resulting in small particles. Coalescing of small particles is consistent with NMR, conversion efficiency and density results, especially those indicating cyclization reactions in elevated water preparations.

4.4 Conclusion

Results from both systems indicate a progressive development from linear chain to aggregate particle formation. Figure 4.7 represents the three postulated silica gel network growth mechanisms as identified by NMR and density results taken in the context of literature assessments. The low R value gels developed through the entanglement of linear chains to form dense microporous silica networks. As the R value increased to intermediate values, the alkoxide precursor was completely hydrolyzed, which increased cyclization of the polymeric siloxane chains. Without a solvent medium to distribute the hydrolyzed species, the coalescence between cyclic fragments was inefficient and a randomly branched network formed with a loss in density and higher distribution of silanol. Further increases in the R values led to a greater dispersion of the hydrolyzed species, which provided conditions suitable for particle development. Packing of particles into a three-dimensional silica network resulted in a dense microporous network. Based on NMR results, the sol gel process was clearly altered by variations in

the R value. The structural variations were similar with those observed in alcohol derived sol gels with similar R values.

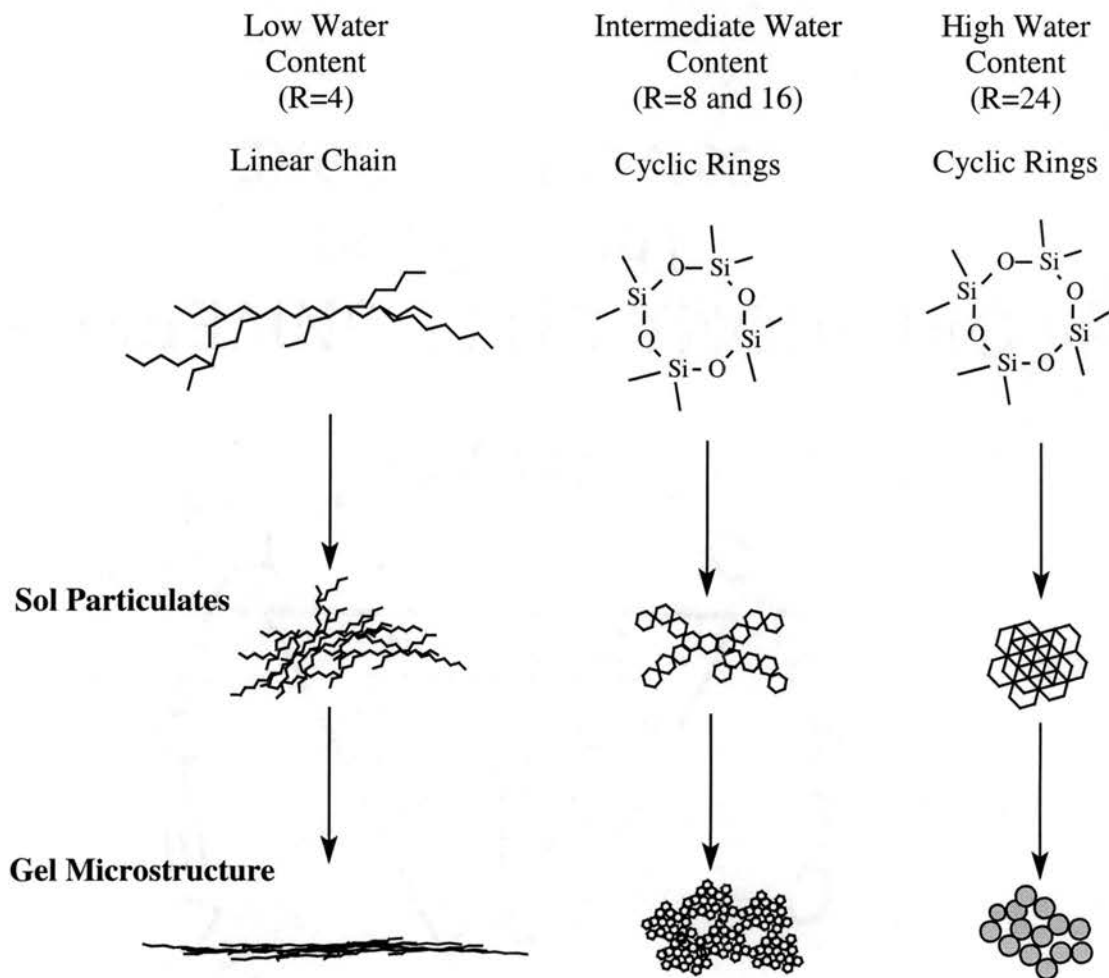


Figure 4.7: Sol particulates and gel microstructures observed in water based gels.

CHAPTER 5

RAMAN INVESTIGATION OF WATER-BASED SOL-GELS AS A FUNCTION OF CURING TEMPERATURE

5.1 Introduction

Raman spectroscopy is a method well suited for studying gels on a molecular level. The technique provides a direct and non-destructive method of probing information concerning the chemical composition and structure of constituent species. This enables information pertaining to gel microstructure and chemical content to be identified and monitored as a function of processing parameters such as curing temperature. In Raman studies conducted on silica glasses and gels, characteristic vibrational bands have been used to identify the presence of unhydrolyzed precursors, residual alcohol by-products, distinctions in surface and bulk silanol, and variations in the siloxane network during densification. Monitoring of many of the vibrational bands enables the chemical content to be identified and correlated with gel compositions and microstructures previously identified in Chapter 4. The densification process in silica gels can be correlated with identifying gel structures derived from variations in the processing conditions by monitoring spectral losses and developments in the silanol and siloxane vibrations.

Over the past 40 years, a significant amount of Raman studies have been conducted on various types of SiO₂ glasses and sol-gel systems. Studies have included

crystalline SiO₂, thermal silicate glasses, sol-gel glasses (acid and base), sol-gel to glass evolution, and modeling of vibrational modes.^{59-61,82-100} The impact of unhydrolyzed precursors, silanol content, and structural formations have been monitored to identify structural evolution in sol solution and in gelled structures.^{83,95,100} Studies conducted over incremental curing ranges have used intensity variations in the silanol and siloxane peaks to monitor the densification process and identify structural compositions as a function of curing temperature.^{59,83,96} In other studies, distinctions between surface and bulk silanols have provided an ideal method of characterizing surface compositions with physical attributes, such as surface area.^{89,94} Raman spectroscopy is used in the present work to identify specific silanol and siloxane bond formations during densification. Complementary chemical characterization methods, such as Raman spectroscopy, may be used to elucidate structural features in the sol-gel microstructure and correlated to essential gel growth mechanisms.

Silicate gels derived from linear chains, branched chains/clusters, and particle formations are reported to have very different densification mechanisms. In a study by P.F. James, it was noted that the smaller micropores (≤ 2 nm) collapsed gradually with increased temperature up to 600 °C, whereas the larger pore (≥ 7 nm) did not collapse until temperatures of 700 °C or more were reached.³¹ In a related study, Yamane and co-workers identified that the smaller pores collapsed between 400-500 °C and the large pores collapsed between 700-900 °C.¹⁰¹⁻¹⁰² The variations in densification temperatures are based on the increase in surface energy with respect to pore size. As the pores become smaller, the surface energy increases, resulting in forces which drive network collapse at much lower temperatures.⁸³ In gels derived from linear chain entanglement,

densification tends to occur at the lowest temperatures, a characteristic which is attributed to a higher concentration of small micropores.

The specific densification temperature for a given gel is dependent on pore density, pore size, and pore size distribution. In gels derived from highly branched chains or clusters, entanglement and coalescence between branched particles result in a network characterized by a combination of small and large pores. During densification, the smaller pores collapse at lower temperatures, while the larger pores require elevated temperatures. In gels derived from the coalescence of small colloids, the interstitial voids create a “pore microstructure” that is primarily composed of large pores. Structural densification at low temperature may lead to some improvements in the packing efficiency and/or connectivity of such gels, but the large pores created by the interstices will require elevated temperatures in order to initiate more widespread pore collapse. The structural peculiarities associated with each gel type may be identifiable through spectral variations in the silanol and siloxane peak intensities. By monitoring silanol peak losses and specific siloxane peak developments, densification mechanisms can be identified and used to elucidate the starting and final gel microstructure.

In this chapter, the vibrational structure of water-based silica systems were investigated and monitored as a function of curing temperature and water/silane ratios (R value). Gels prepared from TMOS and TEOS precursors having R values of 4, 8, 16, and 24 were cured in ambient air at room temperature (RT), 60 °C, 150 °C, 300 °C, and 450 °C. Raman spectra were used to identify products of incomplete hydrolysis, overall bulk silanol content, surface silanol content, bulk and surface densification features. Based on spectral results, chemical and structural information was assessed and correlated to chemical processing parameters (e.g., R value or precursor type).

5.2 Background

5.2.1 Raman Active Vibrational Bands in Silica

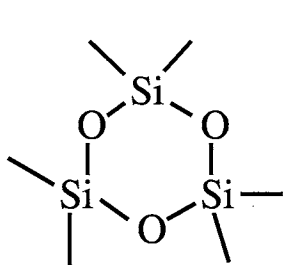
Raman studies and theoretical modeling of silica glasses and sol-gels have identified several vibrational bands for SiO_2 and alkoxide precursors used in sol-gel processes. Silica vibrational bands located in the region between 300 and 1200 cm^{-1} have provided information concerning siloxane connectivity, surface hydroxyl content, bulk silanol content, and structural stability of strained systems.^{83-5,87,96-100} Most of the original peak assignments were derived from studies conducted on fused silica and vitreous glass. From those studies, six Raman active vibration modes have been identified and categorized as originating from cyclic ring formations, surface silanol, bulk silanol, and structural defects. More recent studies conducted on sols and gels have identified several additional vibrational bands, corresponding to specific, precursor species, reaction intermediates, and reaction by-products. These data have been used to monitor reaction rates and to identify the formation of condensed species.⁹⁵⁻⁹⁸ A compilation of Raman vibrational assignments applicable to this research is present in Table 5.1.

Table 5.1: Representative vibrational frequencies and assignments for observed bands in TMOS and TEOS derived sol-gels.

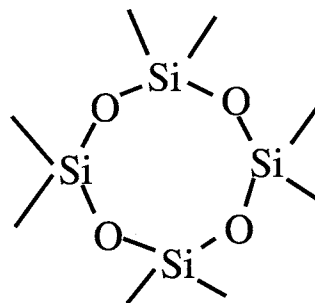
Frequency (cm ⁻¹)	Vibrational Assignment	References
430-470	Symmetric Stretch SiO ₂	59-61,82-100
490	Stretch ≡Si-OH	59-61,82-100
606	Cyclic three member siloxane ring	59-61,82-100
800	Bending SiO ₂	59-61,82-100
875	In phase ≡C-C-O stretch (Ethanol)	83,100
910	Stretching ≡Si(OH) ₂	84
980	Stretching ≡SiOH	59-61,82-100
1047	N-O stretching (NO ₃ ⁻)	59-61,103
1075	≡C-O Stretching (Ethanol or TEOS)	59-61,83,100
1454	-CH ₃ Asymmetric Deformation (Ethanol and TEOS)	59-61,83,100
1485	=CH ₂ bend (TEOS)	59-61,83,100
2880	=CH ₂ Symmetric stretch	59-61,83,100
2900	-CH ₃ Symmetric stretch	59-61,83,100
2930	=CH ₂ Anti-symmetric stretch	59-61,83,100
2980	-CH ₃ Anti-symmetric stretch	59-61,83,100
3100	-O-H Stretch	59-61,83,100

5.2.2 Terminology

The silica networks observed in quartz and vitreous glass have been characterized with a number of different sized siloxane rings. In order to simplify references to specific siloxane ring vibrations, a numerical nomenclature has been adopted. Ring size is identified on the basis of the number of silicon atoms located in the ring structure. Figure 1 represents the chemical structures for the 3- and 4-member siloxane rings. The actual number of nuclei in each heterocycle is actually twice that reference by this convention. The discussion presented in this chapter will follow those cited in the literature and used to address vibrational modes for the 3- and 4- member siloxane rings.



3-Member Siloxane Ring



4-Member Siloxane Ring

Figure 5.1: Numerical notation for siloxane ring structures.

5.3 Results and Discussion

Figures 5.2 through 5.5 represent general spectra acquired for silica gels derived using TMOS and TEOS precursors. Figures 5.2 and 5.3 represent gels made using low ($R = 4$) water content. Figures 5.4 and 5.5 represent gels made using elevated ($R = 24$) water content.

5.3.1 TMOS $R = 4$ Value Silica Gel

The Raman spectra associated with $R = 4$ gels prepared using TMOS as a precursor are shown in Figure 5.2 as a function of curing temperature. The broad vibrational band at 430 cm^{-1} was identified as a $\equiv\text{Si-O-Si}\equiv$ stretching mode arising from cyclic silicate rings.^{85,99} This band is described as a symmetric oxygen stretching vibration of the bent $\equiv\text{Si-O-Si}\equiv$ linkages and/or vibrational modes involved in five, six, and higher member rings of SiO_4 tetrahedra.⁹⁹ The asymmetry and width of the band has been reported to be a function of the $\equiv\text{Si-O-Si}\equiv$ bond angles distribution within the siloxane network.¹⁰¹ Consequently, the broad nature observed in the spectra at $450 \text{ }^\circ\text{C}$ indicated the presence of a wide distribution in bond angles, characteristic of a highly amorphous

network. The increase in the intensity of the 430 cm^{-1} band at elevated curing temperatures was attributed to reductions in the silanol content (seen as a decrease in the 490 cm^{-1} peak intensity) with resultant siloxane bond formations. The intense siloxane vibrations and broad nature of the 430 cm^{-1} peak indicated that the $R = 4$ TMOS gel structure consisted of a well formed and highly amorphous siloxane network.

A second siloxane vibration at 800 cm^{-1} band was identified as a $\equiv\text{Si-O-Si}\equiv$ bonding vibration parallel to the bisector of the $\equiv\text{Si-O-Si}\equiv$ angle.⁹⁴ The broad band was observed to increase gradually as a function of curing temperature.

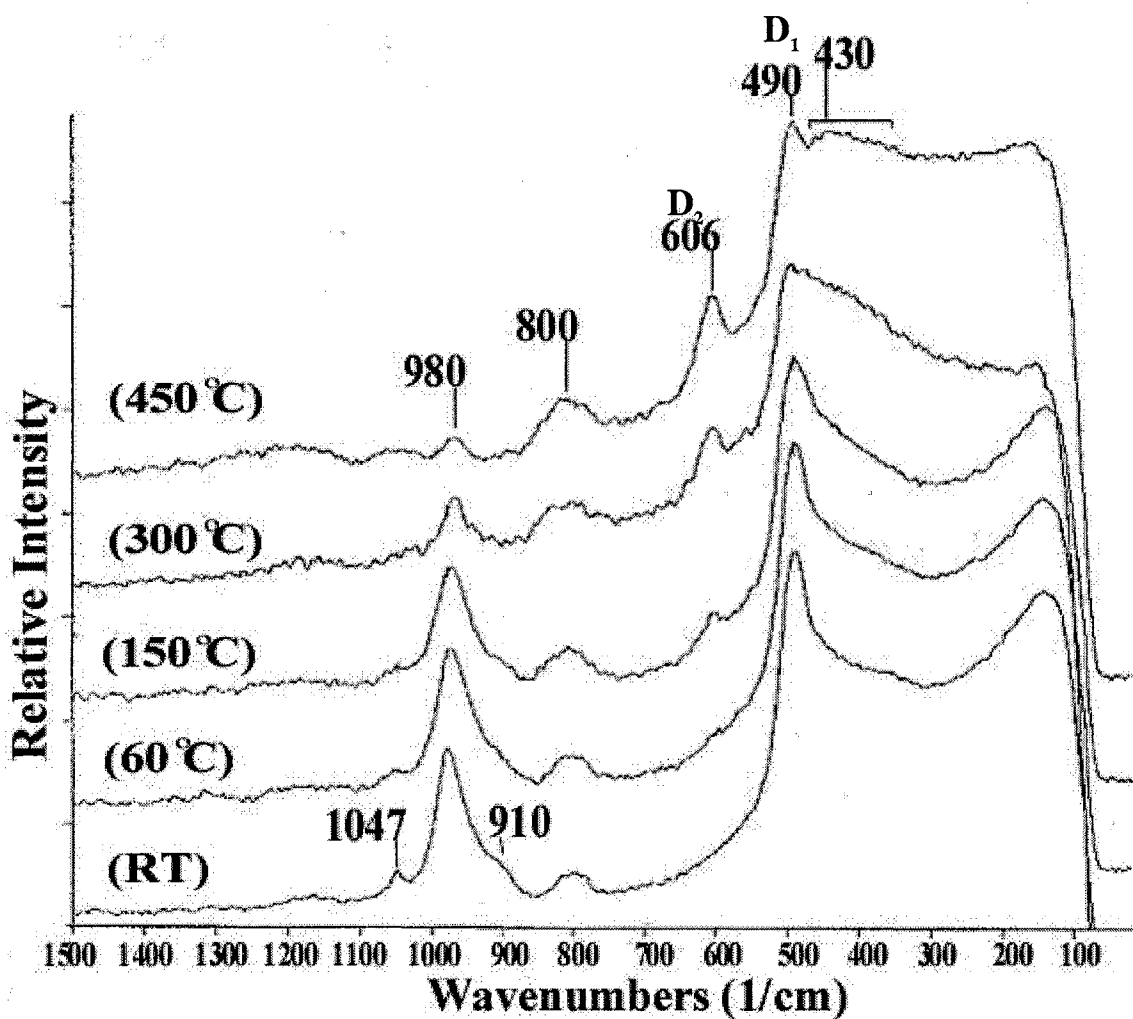


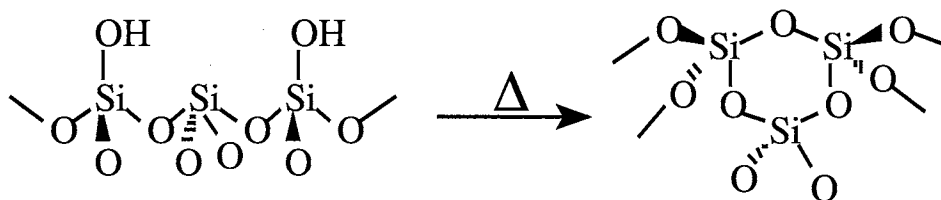
Figure 5.2: Overlaid Raman Spectra of SiO₂ gels prepared using a TMOS solution with an R value of 4 cured at room temperature (RT), 60 °C, 150 °C, 300 °C, and 450 °C. Spectral intensities have been adjusted in reference to the 800 cm^{-1} siloxane peak.

The 490 cm^{-1} band, commonly referred to in the literature as the “D₁” band, was identified as a symmetrical breathing mode of a cyclic 4-member siloxane ring containing exposed $\equiv\text{Si-OH}$ side groups. Experiments conducted by Brinker and co-workers using ^{18}O -enriched water concluded that the 490 cm^{-1} $\equiv\text{Si-OH}$ vibration was due motion of the O atom normal to a surface plane and is phenomenon which only occurs for surface silanols.⁹³ The sharp nature of this peak has been attributed to periodically repeating units over a distance of at least 25 \AA , as explained by Phillips.⁸⁷ The relatively strong intensity of this peak in the Figure 5.2 room temperature spectrum, considered in light of the progressive loss of this peak with increasing curing temperature, indicated that the densification process involved condensation between surface silanols. Since essentially all of the densification which occurs in a silica gel at $450\text{ }^\circ\text{C}$ is pore collapse, it is postulated that these silanol species reside at pore surfaces.

The 910 cm^{-1} shoulder and 980 cm^{-1} peaks were identified as symmetric stretch vibrations of silanol species. The 980 cm^{-1} peak is reported to be composed of two different silanol vibration modes. The dominate 980 cm^{-1} peak arises from surface silanol vibrations, while a second peak at 970 cm^{-1} develops from internal silanol vibrations. A single sharp peak at 980 cm^{-1} was referenced only as a bulk silanol vibration. The vibration at 910 cm^{-1} , observed as a shoulder to the 980 cm^{-1} , is attributed to a geminal ($\text{OSi}(\text{OH})_2$) vibration. The gradual loss in the silanol vibrations indicated the densification process was initiated at temperatures as low as $60\text{ }^\circ\text{C}$ and occurred over a wide temperature range and involved both surface and bulk silanol species. The low concentration of silanol after curing to $450\text{ }^\circ\text{C}$ correlated to a high degree of densification, a characteristic found in a microporous networks.

The 606 cm^{-1} band, referred to in the literature as the “D₂ band”, was identified as a $\equiv\text{Si-O-Si}\equiv$ vibration developing from oxygen breathing modes found in highly strained 3-member rings located at the SiO_2 surface, illustrated in Reaction 5.1. Onset of the peak

is observed after curing at 150 °C, becoming more rapidly observed at a curing temperature of 450 °C. Onset of the 3-member ring formation is attributed to an endothermic condensation reaction which occurs between neighboring surface silanols.^{82,93} The intensity of the band is correlated with a surface densification rather than a bulk densification process.^{82-3,103} Raman studies conducted on high surface area gels and colloidal particle systems exhibit extremely intense D₂ vibrations upon densification.^{89,92} The rise of a intense 606 cm⁻¹ band is attributed in the literature to the formation of high concentrations of surface condensed species rather than densification through pore collapse.^{82,104} In the presently studied TMOS R = 4 gel, the loss of a large silanol peak was found to give rise to a comparatively weak peak, indicating the densification process developed as a result of pore collapse with the formation of larger unstrained rings, rather than condensation between surface silanols.



Reaction 5.1: Formation of 3-member siloxane ring defect (D₂) through surface silanol condensation.

The 1047 cm⁻¹ band was the only vibration not identified as a silica or carbon vibration. The peak was assigned to an ≡N-O- stretching vibration in a nitrate ion. The nitrate assignment was based on the presence of nitric acid, which is used as a catalyst in the hydrolysis reaction. A 1047 cm⁻¹ vibrational peak assignment was previously reported by J.F. Staden and co-workers.¹⁰³ After curing to 60 °C the nitrate peak was lost, presumably due to volatilization.

5.3.2 TEOS R = 4 Value Silica Gel

In Figure 5.3, the R = 4 TEOS gel revealed similar peak trends seen in the TMOS gel, along with signs of the type of incomplete hydrolysis. The 430 cm^{-1} , 490 cm^{-1} , 600 cm^{-1} , 800 cm^{-1} , 910 cm^{-1} , 980 cm^{-1} , and 1047 cm^{-1} were all present and corresponded with similar peak intensities and evolution as those found in the TMOS gel. Additional peaks observed at 1075 cm^{-1} , 1454 cm^{-1} , 1485 cm^{-1} , 2880 cm^{-1} , 2900 cm^{-1} , 2930 cm^{-1} , and 2980 cm^{-1} were identified as $\equiv\text{C}-\text{C}\equiv$, $\equiv\text{C}-\text{O}-$, or $\equiv\text{C}-\text{H}$ vibrations, substantiating earlier evidence of incomplete hydrolysis and entrapment of residual ethanol (Section 4.8). The vibration at 875 cm^{-1} , attributed to the presence of absorbed ethanol was observed only after room temperature and $60\text{ }^{\circ}\text{C}$ curing.^{83,100} After curing to $150\text{ }^{\circ}\text{C}$, the 875 cm^{-1} peak loss and general reduction in other organic vibrations was indicative of ethanol loss via evaporations. The remaining peaks at 1095 cm^{-1} , 1294 cm^{-1} , 1454 cm^{-1} and 1485 cm^{-1} were attributed to unreacted ethoxide. Loss of all peaks associated with organic compounds at curing temperature greater than $150\text{ }^{\circ}\text{C}$ was attributed to thermal decomposition of the ethoxide group, consistent with reported losses of unreacted alkoxides in the literature.^{82,105} The comparatively high temperature stability of the ethoxide groups suggests there are two possibilities for deriving silica gels free of residual ethoxide functionalities: (1) complete silane hydrolysis through the use of excess water prior to gelation; or (2) use of curing temperatures of $300\text{ }^{\circ}\text{C}$ or more. Comparison of the TEOS and TMOS R = 4 gels cured at $450\text{ }^{\circ}\text{C}$ indicates very little difference between the chemical bond types in these two gel systems (Figure 5.2 and 5.3).

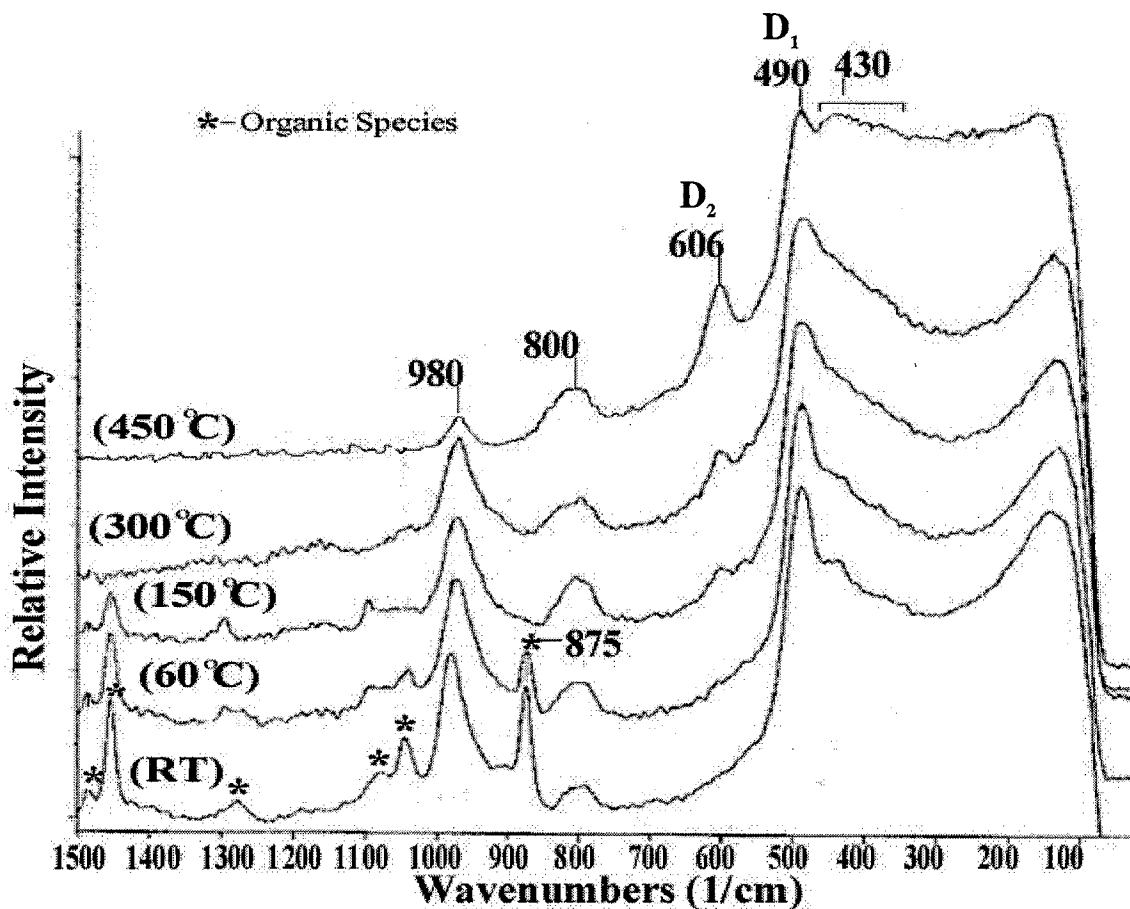


Figure 5.3: Overlaid Raman Spectra of SiO_2 gels prepared using a TEOS solution with an R value of 4 cured at room temperature, 60 °C, 150 °C, 300 °C, and 450 °C. Spectral intensities have been adjusted in reference to the 800 cm^{-1} siloxane peak.

5.3.3 TMOS and TEOS Intermediate to High R Value Gels ($R = 8, 16, \text{ and } 24$)

Spectra for gels prepared with R values of 8, 16, and 24 resulted in very similar vibrational frequencies and peak development for both TMOS and TEOS-derived gels. Figures 5.4 and 5.5 represent typical spectra acquired for TMOS and TEOS gels prepared with an R value greater than 4. Additional spectra and intensity tables for gels prepared with R values of 8 and 16, not shown, are presented in Appendix B.

In Figures 5.4 and 5.5, peaks similar to those observed in the $R = 4$ valued gels were observed at 430 cm^{-1} , 490 cm^{-1} , 606 cm^{-1} , 800 cm^{-1} , 910 cm^{-1} , 980 cm^{-1} , and 1047 cm^{-1} . In both the TMOS and TEOS systems, all of the silanol peaks decreased as a

function of increased curing temperatures. There appeared to be a more substantial loss in the surface silanol (490 cm^{-1}) than for the bulk silanol species (980 cm^{-1}). Comparing the $R = 4$ spectra after curing to $450\text{ }^{\circ}\text{C}$ (Figure 5.2 and 5.3), final silanol content (evidenced by the peak at 980 cm^{-1}) was substantially more intense for gels prepared with excess water. The 606 cm^{-1} peak showed similar growth during the $150\text{ }^{\circ}\text{C}$ to $450\text{ }^{\circ}\text{C}$ curing temperature transition. The intensity of the 606 cm^{-1} peak after curing to $450\text{ }^{\circ}\text{C}$ is much more pronounced in Figures 5.4 and 5.5 than for the compared spectra in Figures 5.2 and 5.3. The concurrent silanol losses and substantial 3-member ring formations found at elevated curing temperature indicated that silanol loss occurred as a result of condensation between surface silanols rather than bulk densification. Further spectral comparisons revealed that increased R values resulted in subtle yet distinctive narrowing of the 430 cm^{-1} peak width as curing temperature increased. Since peak narrowing is known to be indicative of a bond angle distribution reduction, increase in R value was found to contribute to the development of a somewhat more ordered network structure. To summaries, the gels prepared with R values of greater than 4 indicated fewer signs of structural densification, lower distribution in bond angles, higher concentration of surface condensed siloxane, and higher concentrations of uncondensed silanol.

The 1047 cm^{-1} nitrate band was observed to be relatively intense in Figure 5.4 and 5.5 at room temperature, but underwent a rapid intensity loss after curing to $60\text{ }^{\circ}\text{C}$. In addition, a new peak, centered at 1310 cm^{-1} , was observed in the RT and $60\text{ }^{\circ}\text{C}$ spectra. Both the 1047 cm^{-1} and 1310 cm^{-1} peaks were lost after curing to $150\text{ }^{\circ}\text{C}$. The relevant literature is absent of any reference to a 1310 cm^{-1} peak. Nitrate loss accompanied by the development of a 1310 cm^{-1} peak was attributed to either the decomposition of nitrate to form nitrogen dioxide, or some type of vibrational coupling interaction occurring between the nitrate and silica matrix. Recorded intensities for each vibrational band are presented in Appendix B.

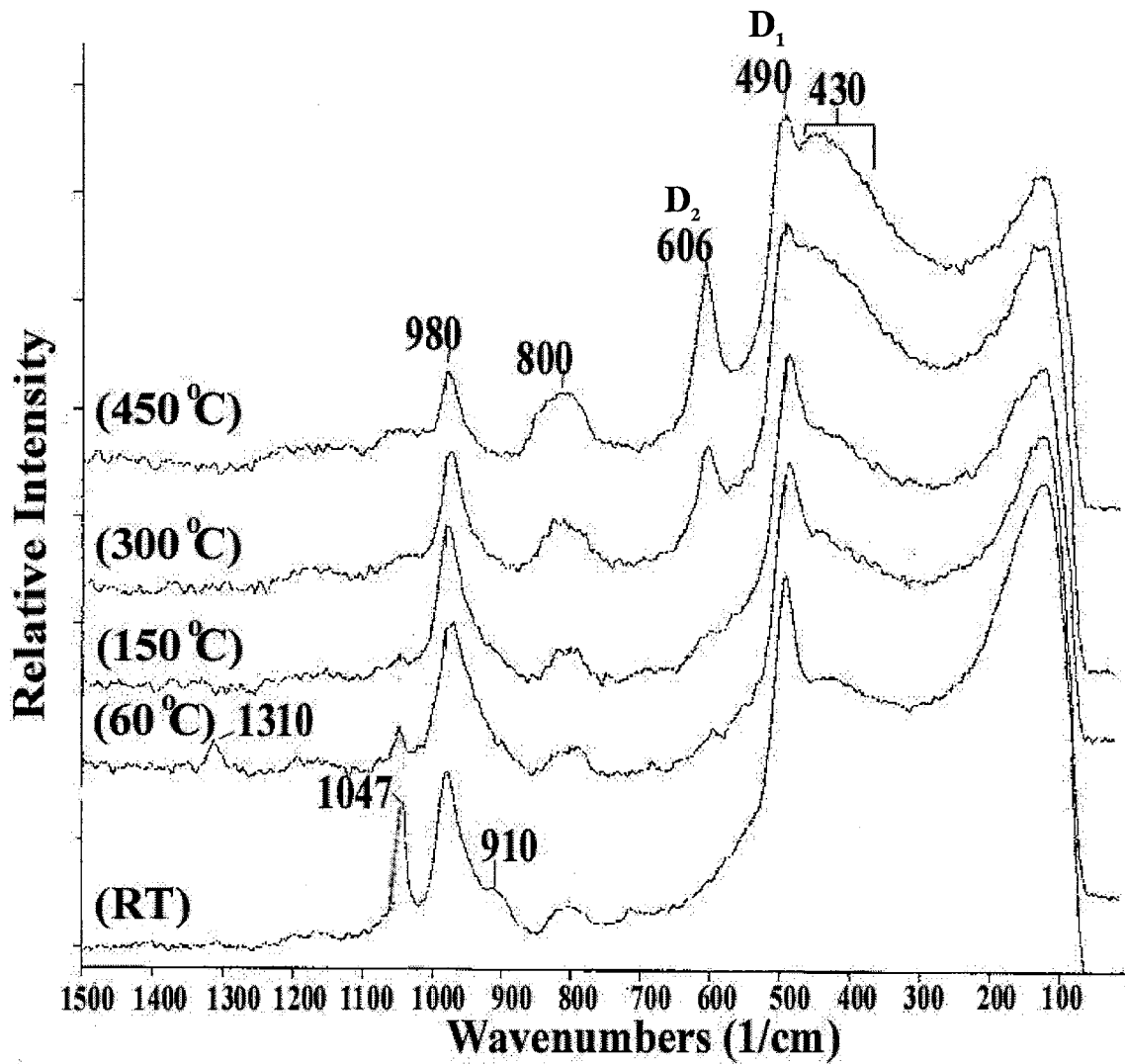


Figure 5.4: Overlaid Raman Spectra of SiO₂ gels prepared using a TMOS solution with an R value of 24 cured at room temperature, 60 °C, 150 °C, 300 °C, and 450 °C. Spectral intensities have been adjusted in reference to the 800 cm⁻¹ siloxane peak.

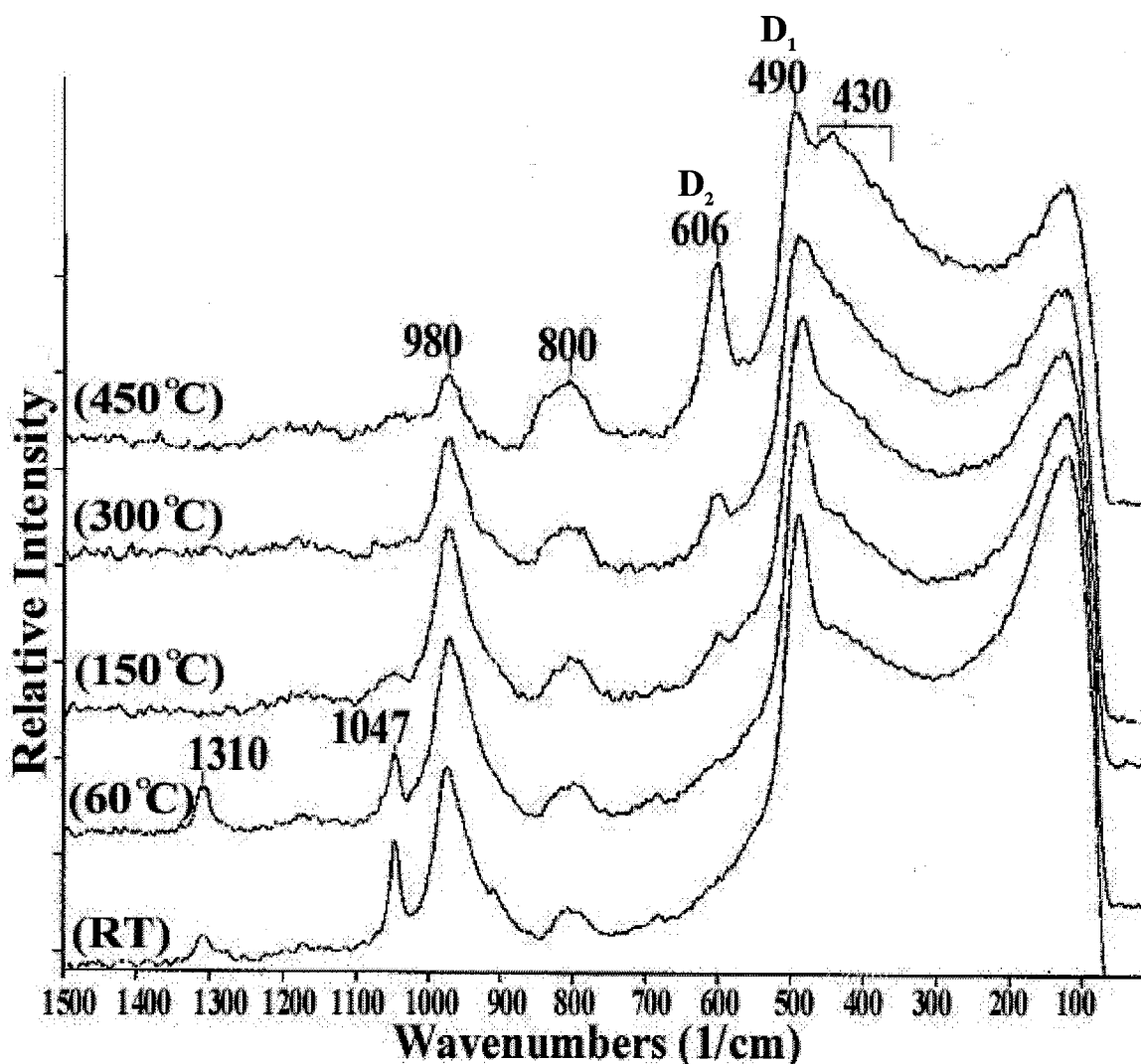


Figure 5.5: Overlaid Raman Spectra of SiO₂ gels prepared using a TEOS solution with an R value of 24 cured at room temperature, 60 °C, 150 °C, 300 °C, and 450 °C. Spectral intensities have been adjusted in reference to the 800 cm⁻¹ siloxane peak.

5.3.3.a Silanol Loss and Densification

Figure 5.6 represents a comparison between the TMOS R = 4 and R = 24 gels at room temperature and 450 °C. After curing to 450 °C, the R = 4 gels were observed to have a lower bulk silanol content. The low concentration implied that the network resulted in a higher degree of condensation and densification. The more proficient loss also implied the silanol species were in close proximity with one another and structurally

free to react, consistent with densification of small micropores. In the higher R valued gels, a similar loss in silanol content was observed, but the final silanol content was notably higher, indicative of a lesser degree of densification. The contrasting differences in the final silanol content indicated that an increased R value lead to a gel microstructure composed of a more open structure with larger pores, consistent with gels derived from branched clusters and/or particulate formations.

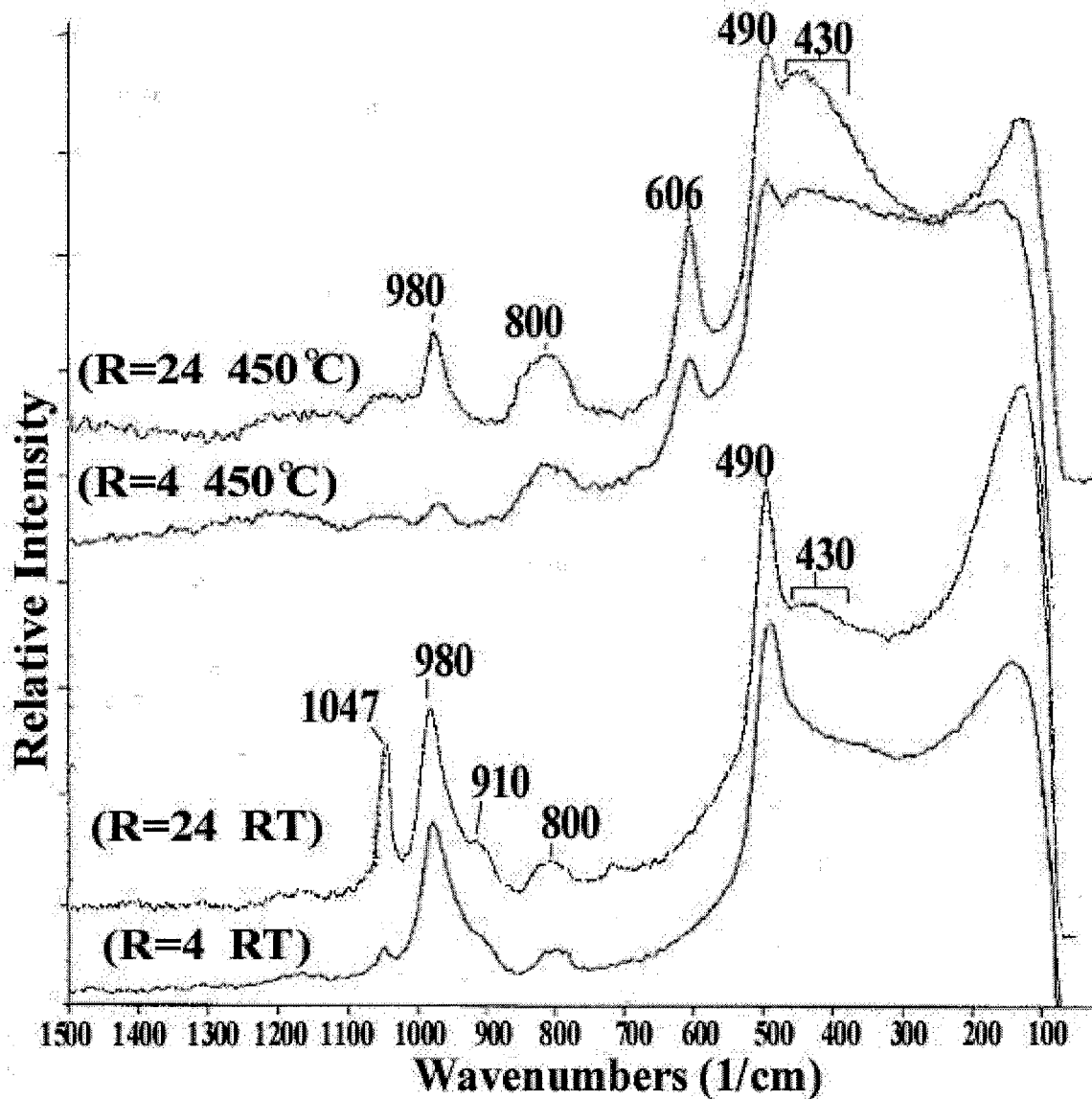


Figure 5.6: Raman spectral comparison of low and high R valued gels for TMOS at room temperature and 450 °C.

5.3.3.b 3-Member Siloxane Ring Formation

Figure 5.7 compares the development of the 606 cm^{-1} “D₂ defect” peak as function of curing temperature. Relative intensity comparison between in the $450\text{ }^{\circ}\text{C}$ peak intensities revealed a progressive increase in ring formation with increased R value. When assessing silanol losses with 3-ring formation, thermal curing below $150\text{ }^{\circ}\text{C}$ was correlated with the pore collapse and condensation between particles, while densification at higher temperatures was attributed to additional pore collapse in the low R value gels and more surface condensation in the higher R value gels. After curing $450\text{ }^{\circ}\text{C}$, the 3-member siloxane ring formations were notably smaller for the lower R=4 valued gels, consistent with a microstructure having high concentrations of small micropores and an increase in structural densification upon curing. The gradual increase in 3-member ring peak intensity with increased R value was attributed to a microstructure with larger pores and a more rigid structure, which underwent preferential surface densification rather than pore collapse. In conclusion, the densification products observed in the low R=4 gel were consistent with linear chain entanglement, while the gradual increase in ring formation with higher R values was more consistent with branched or particle-like microstructures.

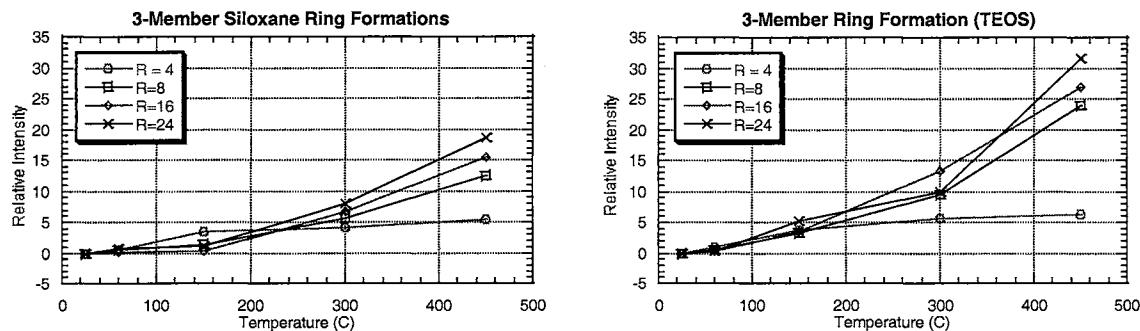


Figure 5.7: Relative intensities ratios between the 606 cm^{-1} and 800 cm^{-1} siloxane peaks observed in the TMOS and TEOS gels prepared with R values of 4, 8, 16, and 24. Results are shown as a function of curing at RT, $60\text{ }^{\circ}\text{C}$, $150\text{ }^{\circ}\text{C}$, $300\text{ }^{\circ}\text{C}$, and $450\text{ }^{\circ}\text{C}$. The lines are only present to guide the eyes.

5.3.3.c Bond Angle Distributions

Evaluation of the 430 cm^{-1} peak profile indicated the distribution in siloxane bond angles was notably different between the low and high R valued gels. In a comparison between the $450\text{ }^{\circ}\text{C}$ spectra (TMOS spectra illustrated in Figure 5.6), the lower R=4 gels revealed much broader peak profiles, indicative of a wide distribution in bond angles. In the higher R valued gels, the sharper peak profile revealed a lower distribution in bond angles, indicative of a gel with fewer variations in ring structures. The significant variations in bond angle distributions for the R = 4 gel were attributed to the random nature of ring formations occurring during gel formation and densification. In the higher R valued gels, the ring structures were formed in the sol prior to gelation. As a result, higher concentrations of small, unstrained ring structures were formed. After gelation, the distribution in bond angle decreased based on a higher concentration of ring structures and fewer variations in the bond angles during densification. In conclusion, the narrowing observed in the 430 cm^{-1} siloxane peak with increased R value was in agreement with a transformation in gel structure from linear to cyclic ring formations, consistent with results in Chapter 4 and 6.

5.3.4 Nitrate Loss

In Figure 5.8, the relative intensity of the nitrate peak with respect to the 800 cm^{-1} siloxane peak revealed that the dried gels contained increasing amounts of nitric acid with increased R values. The apparent increase in the nitrate peak was attributed to the relative increase in the amount of 0.05 M nitric acid water with respect to the total silica content. The presence of the 1310 cm^{-1} peak at room temperature and $60\text{ }^{\circ}\text{C}$ was

attributed to nitrogen dioxide, a product of nitric acid decomposition.¹⁰⁶ The loss of both peaks after curing to 150 °C indicated the catalyst was lost through evaporation or decomposition to NO₂. Confirmation of nitrate presence and loss with heat does not provide any structural information, but may prove to be detrimental to certain gel structures types.

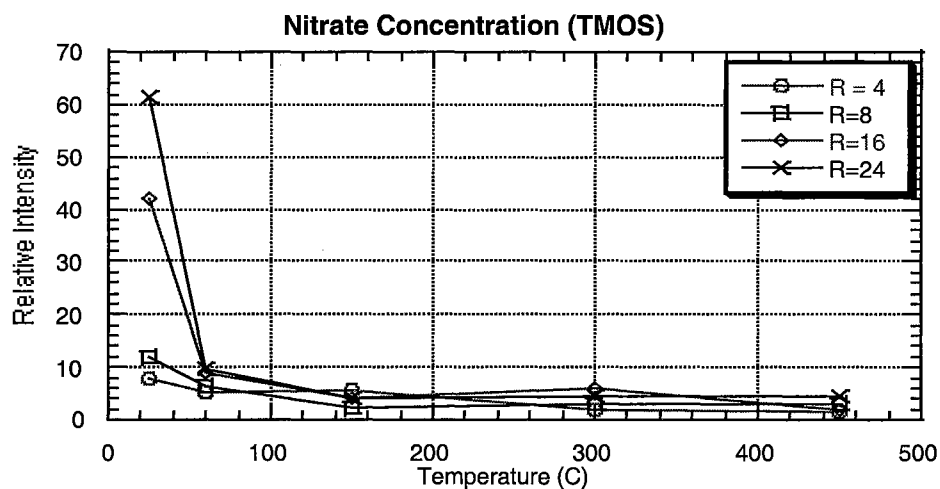


Figure 5.8: Relative intensities for the 1047 cm⁻¹ nitrate peak observed in the TMOS gels prepared with a R value of 4, 8, 16, and 24. Results are shown as a function of curing at RT, 60 °C, 150 °C, 300 °C, and 450 °C. The lines are only present to guide the eyes. Relative intensity was based on ratios against the 800 cm⁻¹ peak.

5.4 Conclusions

5.4.1 Low R Value Gels

Evolution in the R = 4 gels lead to the conclusion that the system was derived from the entanglement of linear or lightly branched fragments. During the curing process, the R = 4 gels revealed two characteristic trends, indicating the siloxane network formed as a result of linear chain entanglement. First, the significant loss of silanol accompanied by limited surface condensed species indicated that the densification process occurred as a result of structural densification by the mechanism of pore collapse,

rather than surface condensation. Second, the broad 430 cm^{-1} siloxane peak profile revealed a wide distribution in bond angles. The distribution was consistent with the densification of a gel derived from linear chain entanglement. Based on the Raman results during densification, the $R = 4$ gels support a growth mechanism derived from linear chain entanglement.

In support of these conclusions, Brinker and many others, have reported that the gelation occurring through the entanglement of linear species gives very small overlapping clusters, which aggregate and lead to gels with high densities and microporous networks.^{5,16} It has also been recognized that the extended degree of flexibility provided by the linear chains enable the network to bend, rotate, and plastically deform into a denser gel characterized by a microporous network. During densification, the small micropores collapse at a lower temperature based on high surface energy in the pores and flexibility provided by the network. Thus, gels derived from linear chains will result in much lower densification temperatures, lower degrees of residual silanol after curing, and a lower concentrations of 3-member ring formations, similar to observation in the Raman spectra for gels prepared with R values of 4.

5.4.2 Intermediate and High R Value Gels

In the intermediate ($R = 8$ and 16) and high R ($R = 24$) valued gels, the Raman results indicated the gel networks were derived from gel structures consistent with cyclic clusters and/or particle type microstructures. First, the limited silanol loss and extensive 3-ring formations were consistent with a rigid gel containing an increasing amount of larger pores and less structural densification. Second, the decrease in bond angle distributions with increasing R value supports a network with a more ordered structure,

namely cyclic cluster or particle formation. The progressive increases in silanol content, 3-ring formation, and lower bond angle distributions also indicate a progressive move to a more particle-like structure composed of cyclic rings.

Unlike the linear chained structure, cyclic clusters and particles are more structurally hindered, limiting the degree of structural mobility during densification. In a highly branched or cyclic network, the microstructure would be composed of interconnected cluster, resulting in a microporous network characterized by large and small pores. The size and distribution of the pores would be based on the degree of branching and inter-connectivity between cyclic rings and particles. In either case, the densification process was limited because of the ability of the network to resist pore collapse.

CHAPTER 6

FT-IR INVESTIGATION OF SILICA THIN FILM COATINGS DERIVED FROM A WATER-BASED SOL-GEL SYSTEM

6.1 Introduction

In this study, Fourier transform infrared reflectance spectroscopy was used as a complementary IR method to elucidate structural formations found in the initial stages of polymeric growth and to monitor transformations in the siloxane network as function of curing temperature. Films deposited shortly after hydrolysis are essentially composed of small siloxane fragments formed during the early stages of polymeric growth. The rapid coalescence which takes place between sol particulates result in films with characteristic species found primarily in the early stages of gel growth. Structural features, such as linear and cyclic siloxane formations can be identified through characteristic IR absorbencies and spectral variations. Chemical and processing effects, such as precursor type, water activity, and curing temperature can be identified as a function of changes in the species which develop in the film.

Monitoring the siloxane development in solution has its limitations due to inherent problems associated with using water as a solvent, such as absorption, stability of a suitable transmission cell (KBr), and sample concentration. By using thin film applied on to a reflective surface, inherent problems with aqueous processing can be minimized. By investigating thin films deposited in the early stages of hydrolysis,

reflectance IR spectroscopy can be used to identify initial siloxane fragments and monitor developments in the densification process as a function of curing temperature.

In the literature, it is difficult to locate any publications, which have specifically addressed films derived from water-based sol-gels. Surfactants have been used to provide high quality coatings on aluminum substrates, permitting the use of FT-IR reflectance methods to study sol-gel film chemistry. In this chapter, the vibrational structure of water-based silica films were investigated and monitored as a function of curing temperature and water/silane ratios (R value). Silica thin films coated onto aluminum substrates were prepared from sols using TMOS and TEOS precursors with R values of 4, 8, 16, and 24 and cured in air at room temperature (RT), 60 °C, 150 °C, 300 °C, and 450 °C. Single reflectance FT-IR spectra were used to identify the silanol content, ring formations, and structural densification. Spectral variations were used to correlate the effects of water/silane ratios on precursor development and mechanisms in sol-gel growth.

6.2 Background

Infrared spectroscopy has been used extensively to identify the effects of processing with respect to siloxane connectivity and silanol content. The fingerprint spectral region between 350 cm^{-1} and 1300 cm^{-1} can provided detailed information concerning silanol content, structural formations, and gel densification. The region between 2500 cm^{-1} and 3400 cm^{-1} is also used, but tends to be limited to the identification of hydroxyl and residual organic species. The assessment of qualitative information concerning the siloxane connectivity using reflectance FT-IR makes it an ideal method

for monitoring chemical and structural alterations in silica thin films. A general review of the IR vibrational assignments applicable to this study have been compiled in Table 6.1.

Table 6.1: Representative vibrational frequencies and assignments for observed bands in TMOS and TEOS derived sol-gels.

Frequency	Vibrational Assignment	References
420 cm ⁻¹	Bending (in plane) ≡Si-O-Si≡	59-61, 90, 100, 105, 107-115
800 cm ⁻¹	Symmetric stretch ≡Si-O-Si≡	59-61, 90, 100, 105, 107-115
940 cm ⁻¹	Stretching ≡Si-O-H	59-61, 90, 100, 105, 107-115
1040 cm ⁻¹	Anti-symmetric stretch ≡Si-O-Si≡ (T.O)	59-61, 90, 100, 105, 107-115
1200 cm ⁻¹	Anti-symmetric stretch ≡Si-O-Si≡ (L.O)	59-61, 90, 100, 105, 107-115
3200 cm ⁻¹	-O-H Stretching	59-61, 90, 100, 105, 107-115

The detection of alkoxide and residual organic species by IR spectroscopy is limited based on the strong absorption characteristics of the ≡Si-O-R vibrations (R = -Si≡, -H, -CH₃). Organic vibrations, such as ≡C-C≡, ≡C-H, and ≡C-O-, are generally obscured by the dominating presence of the much more intense ≡Si-O- vibrations. IR spectra of silica based material with small amounts of organic species generally do not exhibit resolvable vibrations characteristic of such materials unless the organic content is excessively high. In a study by Capozzi, et. al., the intensity of ≡Si-O- vibrations was well illustrated with an investigation of inorganic/organic gels containing variable concentrations of organically modified silicate precursors.¹¹⁶ Comparisons between spectra with different organic concentrations revealed the ≡C-O- vibrations were clearly masked by the stronger ≡Si-O vibrations. It was not until the organic content exceeded 25% that ≡C-H and ≡C-C≡ vibrations at 2964 cm⁻¹ and 1262 cm⁻¹ were observed. As the

organic content reached 50%, the organic vibrations became discernable, but still remained several times less intense than the $\equiv\text{Si-O-Si}\equiv$ vibration.

6.3 Results and Discussion

Figures 6.1 through 6.4 represent general spectra acquired for silica films derived using TMOS and TEOS precursors. Figures 6.1 and 6.2 represent films made using low ($R = 4$) water content. Figures 6.3 and 6.4 represent films made using elevated ($R = 24$) water content. The two sets of spectra represent low and high water content gels. Peak assignments follow those in the published literature (shown in Table 6.1).

6.3.1 Low R value systems

In Figures 6.1 and 6.2, the low $R = 4$ TMOS and TEOS gel spectra exhibited broad peaks identified as siloxane and silanol vibrations. At room temperature, the vibrational band at 940 cm^{-1} , identified as the $\equiv\text{Si-O}$ stretch occurring in silanol, was the most prominent feature in both spectra.¹¹⁷ The strong intensity with respect to other vibrations indicated the films contained elevated concentrations of uncondensed silanol end groups. As the film was cured, the 940 cm^{-1} peak intensity progressively decreased, indicating a clear loss in silanol content.¹⁰⁷⁻¹⁰ The concurrent development in the siloxane vibrations at 430 cm^{-1} , 800 cm^{-1} , 1040 cm^{-1} , and 1200 cm^{-1} with silanol loss with respect to temperature was attributed with siloxane development via silanol condensation.

The 1040 cm^{-1} and 1200 cm^{-1} bands were identified as the transverse optic (TO) and longitudinal-optic (LO) component of the $\equiv\text{Si-O-Si}\equiv$ asymmetric stretch with the oxygen atoms moving along a direction parallel to $\equiv\text{Si-O-Si}\equiv$ plane, respectively. The

strong presence and evolution in both peaks with respect to curing temperature was indicative of a linear or more open chained siloxane network formation.⁵⁹⁻⁶¹ In consideration to the strong silanol and weak siloxane intensities at room temperature, the film was characterized as a broken network of short chained siloxane fragments with numerous silanol end groups. With the increase in temperature, condensation between silanol groups lead to an extension in the siloxane network and siloxane peak growth with corresponding decreases in the silanol peak intensity. The broad peak width observed in the 1040 cm^{-1} band at $450\text{ }^{\circ}\text{C}$ was attributed with a wide distribution in bond angles and overall amorphous structure. The final spectrum at $450\text{ }^{\circ}\text{C}$ was very similar to low R values silica films, crystalline quartz, and vitreous glass.

The apparent lack of organic vibrations in the spectra did not eliminate the possible presence of unreacted alkoxide, but did imply only a small fraction if any could have been present. The 1200 cm^{-1} peak, identified as the $\equiv\text{Si-O-Si}\equiv$ stretch vibration, could have also contained an overlapping $\equiv\text{Si-O-R}$ vibration at temperatures below $300\text{ }^{\circ}\text{C}$. Detection of purely organic vibrations such as $\equiv\text{C-H}$ and $\equiv\text{C-C}\equiv$ are limited, but $\equiv\text{Si-O-C-}$, which contain the $\equiv\text{Si-O-}$ character, exhibit a strong stretch vibrations. The potential alkoxide assignment at 1200 cm^{-1} was eliminated based on the peak's continual growth and intense presence after curing to $450\text{ }^{\circ}\text{C}$. As demonstrated in Chapter 5, the $\equiv\text{Si-O-C-}$ alkoxide bond thermally decomposed after curing above $300\text{ }^{\circ}\text{C}$. The continual presence after curing to $450\text{ }^{\circ}\text{C}$, would support the hypothesis that the concentration of alkoxide groups was minimal.

The vibrational band at 430 cm^{-1} , identified as the rocking motion of a bridging oxygen atom perpendicular to the $\equiv\text{Si-O-Si}\equiv$ plane or bending mode of $-\text{O-Si-O-}$, and the

800 cm^{-1} , identified as the bending motion of the oxygen atom along the bisector of the $\equiv\text{Si-O-Si}\equiv$ bridges group, grew rapidly after initial heating to 60 $^{\circ}\text{C}$.^{105,112-3,118} Work by Kamitsos and co-workers, have identified the intensity of these vibrations were dependent on the L.O.-T.O. splitting of the rocking vibration and strengthened through long-range Coulombic interactions associated with network cross-linking through the formation of $\equiv\text{Si-O-Si}\equiv$ bridges.^{107,110} Subsequently, the increases in the long range ordering resulted in an increase in the $\equiv\text{Si-O-Si}\equiv$ peak intensities. The strong vibrational presence of both peaks was attributed with linear polymeric siloxane having long range ordering.

Comparisons between the TMOS and TEOS films revealed some subtle differences between the two systems. The TMOS film revealed a more through loss in the silanol peak and growth in the 440 cm^{-1} and 800 cm^{-1} vibration. Stronger development in the 800 cm^{-1} and 440 cm^{-1} peaks implied the TMOS film may have contained higher concentrations of linear chained fragments. The lack of silanol loss in the TEOS gel may have been associated with the potential presence of unhydrolyzed ethoxide. Previous NMR and Raman results indicated the bulk gels did contain residual traces of ethoxide groups and remained in the gel until temperatures in excess of 300 $^{\circ}\text{C}$ were applied. Decomposition of the ethoxide group would account for an increase in silanol content and be consistent with previous confirmations of ethoxide presence.

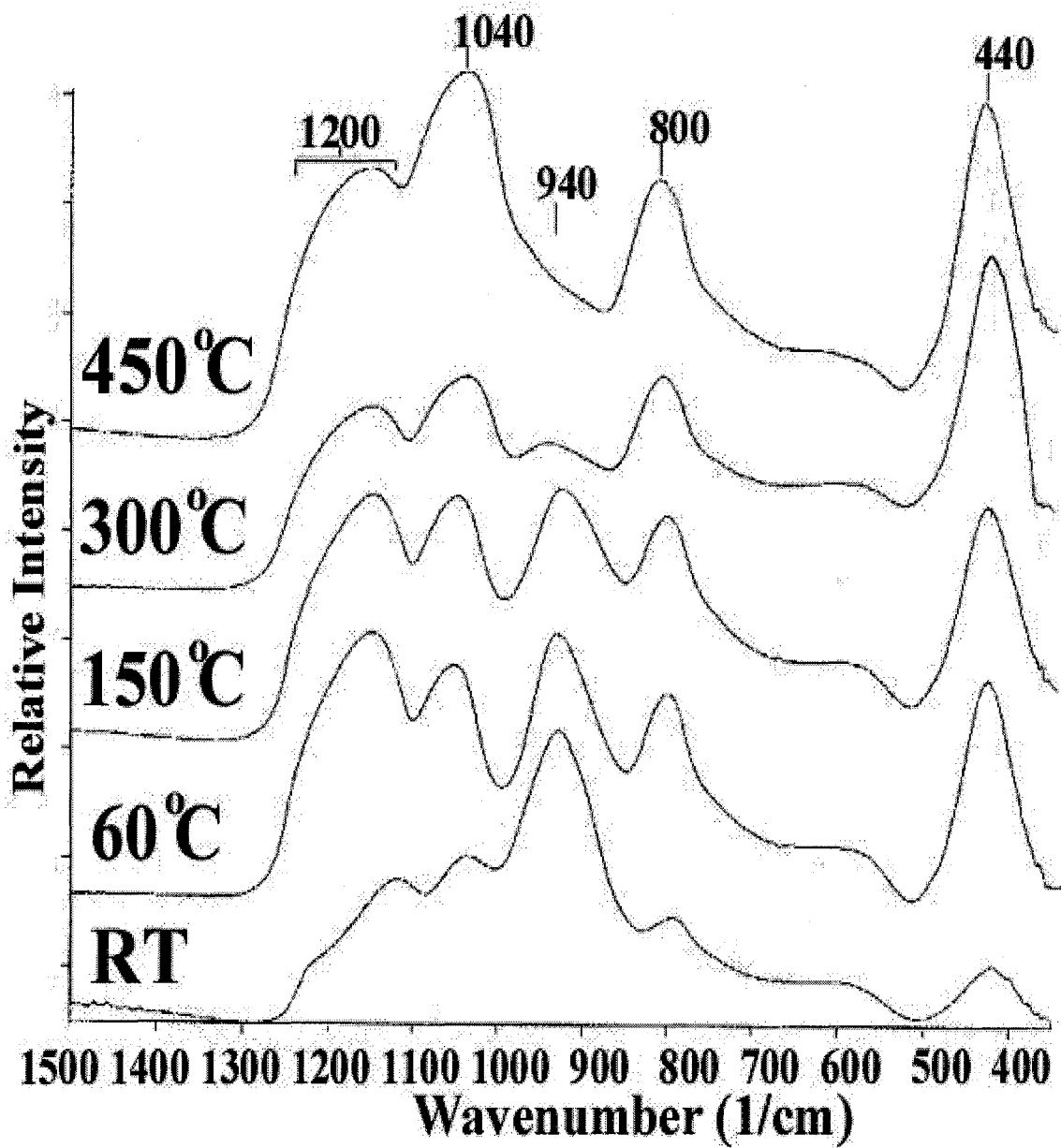


Figure 6.1: Overlaid IR reflectance spectra of SiO₂ thin film prepared with a TMOS solution using a R value of 4. Spectra presented are from films cured at room temperature, 60 °C, 150 °C, 300 °C, and 450 °C.

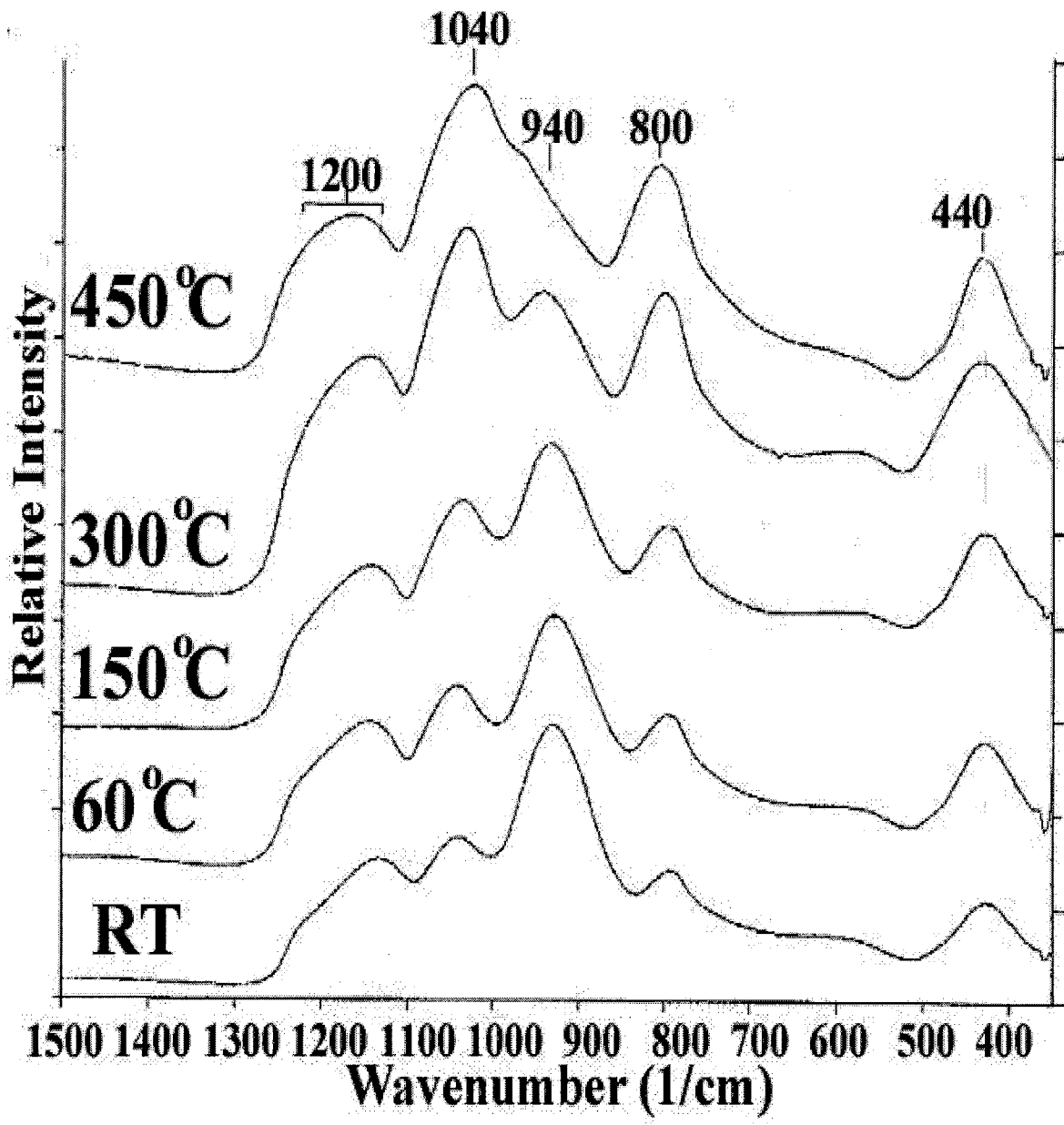


Figure 6.2: Overlaid IR reflectance spectra of SiO₂ thin film prepared with a TEOS solution using a R value of 4. Spectra presented are from films cured at room temperature (RT), 60 °C, 150 °C, 300 °C, and 450 °C.

6.3.2 Intermediate and High R value systems

Reflectance spectra for coatings prepared with R values of 8, 16, and 24 resulted with very similar vibrational frequencies and general peak developments. Figures 6.3 and

6.4 represent general spectra acquired for both TMOS and TEOS coatings prepared with an R value of 24. The spectra for gels prepared with R values of 8 and 16 are presented in Appendix C.

In contrast to the lower R valued films, the 1040 cm^{-1} siloxane peak was the prominent feature in each spectrum. The frequency and profile of the peak indicated the system was no longer linear, but more of a cyclic network. In a comparison between the T.O. (1040 cm^{-1}) and L.O. (1200 cm^{-1}) vibrations, the stronger intensity in the T.O vibration was attributed to the elevated presence of cyclic structures. Cyclic siloxane ringed structures have been identified with the strong vibrational band occurring between 1000 cm^{-1} and 1100 cm^{-1} .^{59-61, 119} The frequency of the peak has also been shown to be depending on ring size. The $\equiv\text{Si-O-Si}\equiv$ stretching frequencies for cyclotrisiloxanes rings have been identified at 1020 cm^{-1} , while larger cyclotetrasiloxanes have frequencies near 1080 cm^{-1} .⁵⁹⁻⁶¹ Frequencies for cyclopenta and higher ringed systems range have frequency ranges between 1050 cm^{-1} to 1100 cm^{-1} . The position of the 1040 cm^{-1} indicated the system was composed of a mix of 3, 4, and higher member siloxane ring structures. In contrast to the $R = 4$ gels, the narrow width of the peak indicated the average distribution in bond angles was much smaller, consistent with a more ordered ring-like structure. The reduction in the 440 cm^{-1} and 800 cm^{-1} intensity was interpreted as loss of long range interactions, consistent with random connectivity between cyclic clusters or fragments. Overall, the films prepared with R values greater than 4 resulted in very similar spectral profiles, but with slight variations in frequency shifts and intensities.

Spectral comparisons between the TMOS and TEOS films did not reveal any significant difference. Both films showed similar losses in the silanol band and growth in the siloxane peaks.

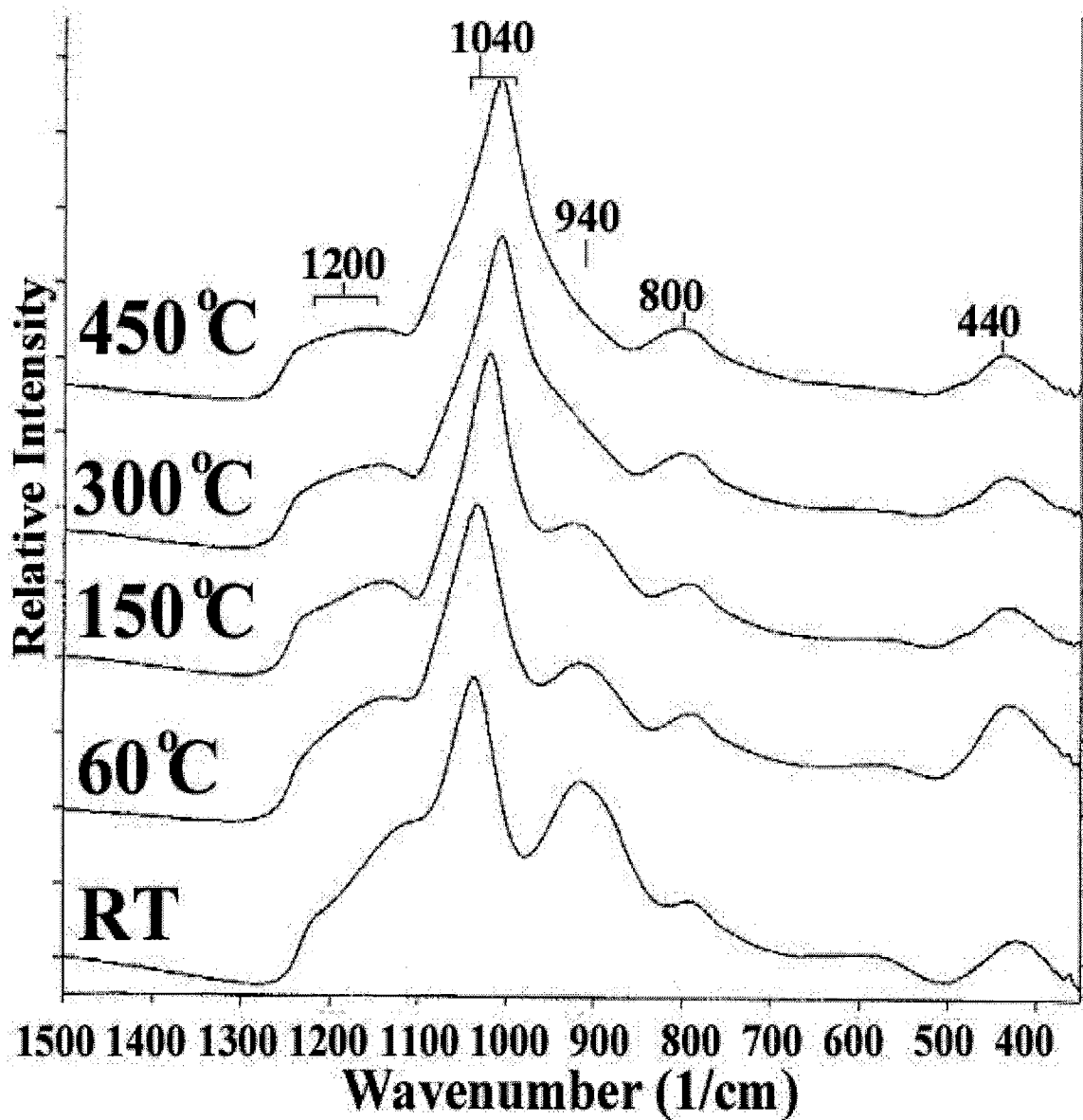


Figure 6.3: Overlaid IR reflectance spectra of SiO₂ thin film prepared with a TMOS solution using an R value of 24. Spectra presented are from films cured at room temperature (RT), 60 °C, 150 °C, 300 °C, and 450 °C.

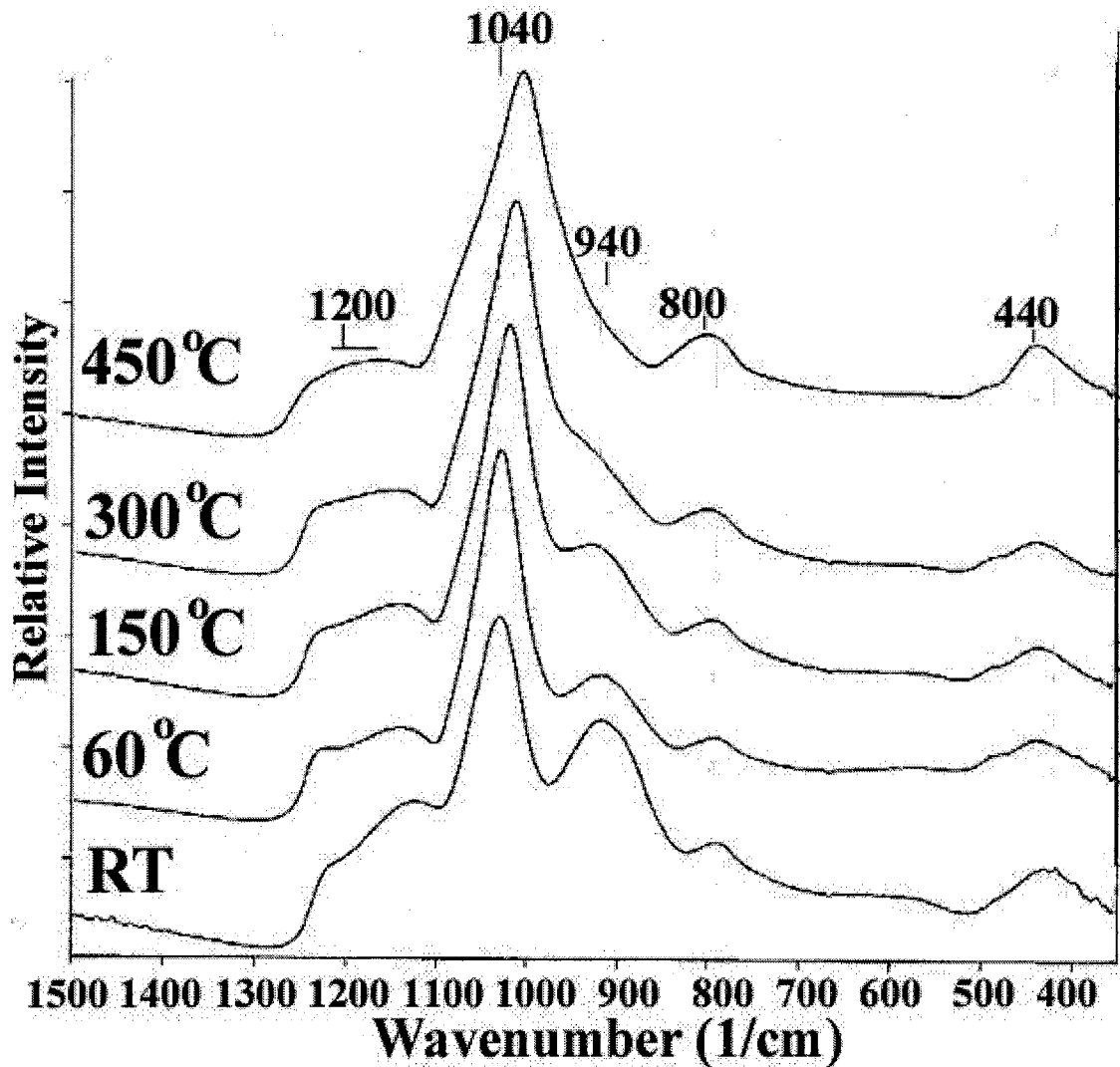


Figure 6.4: Overlaid IR reflectance spectra of SiO₂ thin film prepared with a TEOS solution using an R value of 24. Spectra presented are from films cured at room temperature (RT), 60 °C, 150 °C, 300 °C, and 450 °C.

6.3.3 Silanol and Hydroxyl Content

Figure 6.5, 6.6, and 6.7 depict relative intensity ratios between the silanol (940 cm⁻¹) and the siloxane (440 cm⁻¹ and 800 cm⁻¹) peaks standardized against the 1040 cm⁻¹ siloxane vibrations as function of curing temperature. Since all of the peak intensities

changed as a function of curing temperature, a method using peak intensity ratios was considered as the best alternative to illustrate spectral changes as a function of curing temperature. In Figure 6.5, the intensity ratios between the 940 cm^{-1} silanol and 1040 cm^{-1} siloxane peaks were used to show the progressive losses in silanol content and to depict film densification. In Figures 6.6 and 6.7, the intensity ratios between the 440 cm^{-1} and 800 cm^{-1} peaks against the 1040 cm^{-1} siloxane peaks were used to reveal variations in network connectivity (ring vs. linear chained networks). The intensity ratios do not represent actual concentrations, but do provide an effective method of revealing spectral trends in a simple graphical manner.

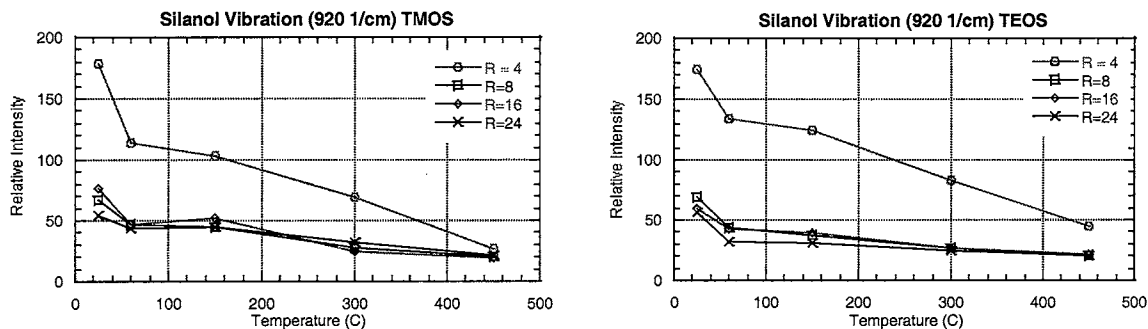


Figure 6.5: Relative intensities for the 940 cm^{-1} silanol peak observed in the TMOS and TEOS thin films prepared with R values of 4, 8, 16, and 24. Results are shown as a function of curing temperature. Line is only present to guide the eyes.

Figure 6.5 graphs depict the relative silanol content in each film as function of R value and curing temperature. The consistent slopes observed in each system revealed that all of the films underwent densification with increased curing temperatures. Since the relative intensities reported in each graph are based on ratios against the 1040 cm^{-1} siloxane peak, the intensity losses can be correlated with reductions in the silanol content and further development in the siloxane networks. At room temperature, the elevated

intensity ratios reported for the $R = 4$ films implied the initially deposited siloxane networks were not thoroughly formed during thin film application. The apparent low siloxane and high silanol peak intensities indicated the networks were composed primarily of small hydrolyzed fragments with limited siloxane connectivity. The gradual intensity losses with respect to temperature revealed the coatings progressively evolved into highly condensed siloxane networks. The incremental and thorough loss of silanol end groups suggested that the deposited silanol fragments or chains were closely spaced and structurally mobile to react. For the higher R value coatings, the lower initial silanol intensity implied there was a more developed siloxane network formed at or prior to thin film deposition. The relatively weak silanol intensities indicated the films were composed primarily of siloxane networks with little silanol content. The moderate decreases in intensities at $60\text{ }^{\circ}\text{C}$ were attributed to silanol condensation reactions occurring as a result of improved packing between particulates. The lower intensity losses up to $450\text{ }^{\circ}\text{C}$ were attributed to minimal losses in the silanol content and limited siloxane development in the way of silanol condensation. The stronger initial siloxane development indicated the higher R valued films were deposited from more highly condensed siloxane fragments able to coalesce in much more efficient method. The dramatic intensity variations between the R valued films clearly indicate that the $R = 4$ and higher R valued gels were derived from different types of sol particulates.

Figure 6.6 and 6.7 represent intensity comparisons between the 440 cm^{-1} and 800 cm^{-1} peaks ratioed against the 1040 cm^{-1} siloxane peak. Comparisons in the two graphs revealed the $R = 4$ films exhibited elevated 440 cm^{-1} and 800 cm^{-1} peak intensities in contrast to the $R = 8, 16,$ and 24 coatings. The elevated intensity ratios were correlated with a higher degree of long range order in the $R = 4$ film, which was identified with

linear or weakly branched chain formations. In a linear chained network, the rocking of the oxygen atom perpendicular to the $\equiv\text{Si-O-Si}\equiv$ plane (linear network) was considered to be enhanced, due to the presence of longer extension in the siloxane network and to the lesser degree of structural rigidity associated with cyclic ringed structures. The stronger intensities in the TMOS system implied that the linear content may have been more prevalent than in the TEOS film, which may have contained shorter chain fragments and/or increased cyclic formations. The inconsistent intensity ratio in the TMOS R = 4 film at room temperature was identified with the limited siloxane development and elevated silanol content, rather than a loss in 440 cm^{-1} and 880 cm^{-1} peak intensity. In reference to the spectra in Figure 1, the silanol peak was very intense with severe overlap onto the siloxane peak. The overlap resulted in an elevated intensity for the siloxane peak, which in effect lowered the intensity ratios for the 440 cm^{-1} and 800 cm^{-1} peaks. As the silanol peak decreased and the siloxane peak developed, the overlapping effect was minimized resulting in more consistent results. In the higher R valued films, the relative peak intensities were extremely weak, which was more consistent with cyclic ring formations. High concentrations of small inner-connected siloxane rings were considered to limit the rocking motion of the oxygen atom and decrease the overall vibrational activity. In light of the variations in 440 cm^{-1} and 800 cm^{-1} peak intensities, the R = 4 films were identified with a network derived from linear chain fragments, whereas higher R valued coatings were identified with more cyclic particulates.

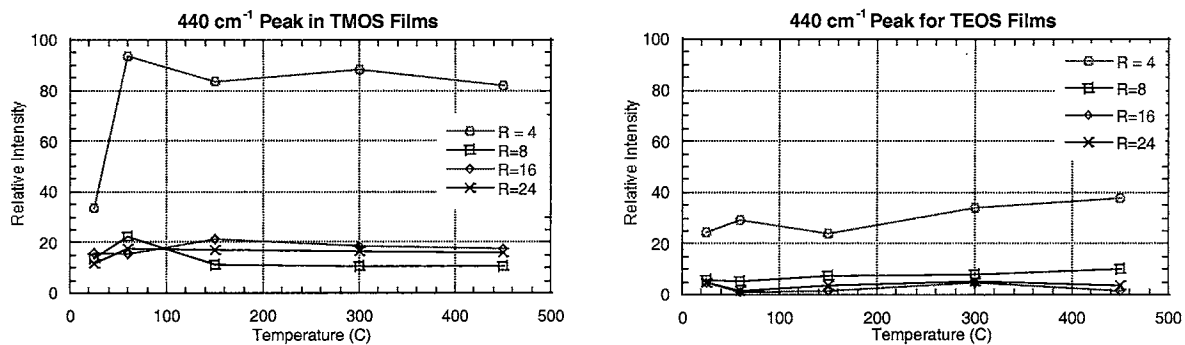


Figure 6.6: Relative intensities for the 440 cm^{-1} $\equiv\text{Si-O-Si}\equiv$ peak observed in the TMOS and TEOS thin films prepared with R values of 4, 8, 16, and 24. Results are shown as a function of curing temperature. Line is only present to guide the eyes.

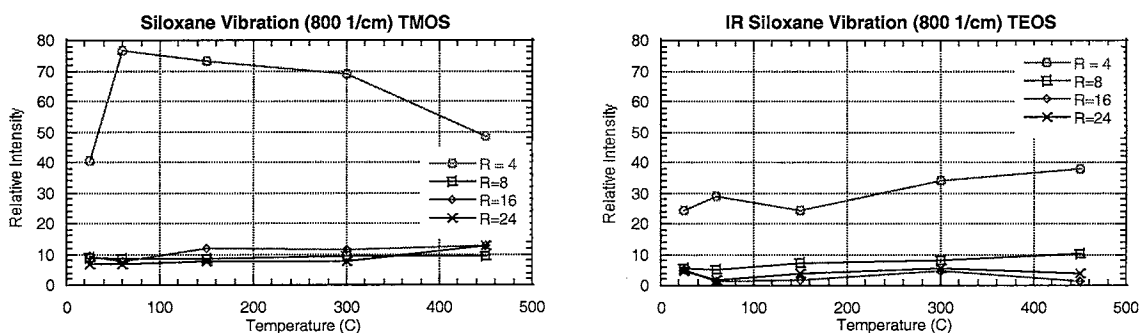


Figure 6.7: Relative intensities for the 800 cm^{-1} $\equiv\text{Si-O-Si}\equiv$ peak observed in the TMOS and TEOS thin films prepared with R values of 4, 8, 16, and 24. Results are shown as a function of curing temperature. Line is only present to guide the eyes.

6.3.4 Frequency Shifts in “ 1040 cm^{-1} ”(T.O.) Si-O-Si Vibration

Table 6.2 shows frequency shifts for the T.O. Si-O-Si vibrations centered near 1040 cm^{-1} . The average frequency shift during the temperature transition from RT to $450\text{ }^{\circ}\text{C}$ ranged between 15 and 30 cm^{-1} . For the $R = 4$ gel, the shifts were attributed more to silanol loss and peak formations, while peak shifts in the higher R valued films were identified with structural densification via condensation reactions.

The frequency shift in higher R valued films was identified with trimer ring formation through silanol condensation reactions. Initial frequencies between 1039 cm^{-1} and 1046 cm^{-1} at room temperature were identified with distributions of 3, 4, and 5 member siloxane ringed networks. As the films were cured, the shift to lower frequencies revealed an increase in the cyclic trimer formations. A shifts to lower frequencies can only be attributed to trimer formations since all other ring vibrations occur above 1050 cm^{-1} . Similar densification shifts have been reported by other researchers.¹¹⁵ In addition, comparisons between silanol losses and frequency shifts correlate well with the form of 3-member rings via silanol condensation.

Table 6.2: Relative frequency shifts for the $\equiv\text{Si-O-Si}\equiv$ (L.O) peak in the TMOS and TEOS thin films prepared with R values of 4, 8, 16, and 24. Results are shown as a function of curing temperature.

TMOS		Frequency (cm^{-1})			
Temperature	R = 4	R = 8	R = 16	R = 24	
Rm	1036.2	1039.3	1038.0	1046.2	
60°C	1051.2	1035.6	1035.4	1040.8	
150°C	1046.9	1022.0	1027.9	1035.4	
300°C	1036.9	1008.9	1014.2	1023.9	
450°C	1014.9	1009.5	1012.0	1014.9	
TEOS		Frequency (cm^{-1})			
Temperature	R = 4	R = 8	R = 16	R = 24	
Rm	1040.7	1031.8	1038.7	1040.7	
60°C	1030.6	1030.6	1046.1	1051.5	
150°C	1025.2	1021.2	1040.0	1043.1	
300°C	1024.8	1012.8	1023.5	1021.0	
450°C	1024.0	1006.6	1022.2	1029.2	

6.3.5 Structural Assignment of the $R = 4$ Film

During the transition from room temperature to 450 °C, the $R = 4$ system revealed several characteristic trends indicating the siloxane network formed as a result of linear chain entanglement. First, the initially deposited siloxane film was composed of short chain fragments with a high concentration of silanol end groups. The limited degree of siloxane content prior to film deposition would be consistent with a controlled mechanism of hydrolysis and condensation reactions. Further more, the rapid loss of solvent and random coalescing between linear fragments would account for the weak siloxane connectivity and elevated silanol content in the film network. The incremental and thorough loss of silanol end groups with increased temperature was also considered to be consistent with gradual condensation between silanol end groups and inner-connectivity between fragments or chains. Secondly, the strong peak intensities at 440 cm^{-1} and 800 cm^{-1} were identified and correlated with linear polymeric chain formations. Thirdly, the broad vibrational frequencies at 1040 cm^{-1} and 1100 cm^{-1} coincide to a wide distributed of bond angles and connectivity, characteristic of a highly amorphous silica network. Forth, the strong peak presence at both 1040 cm^{-1} and 1200 cm^{-1} was characteristic of an open chained siloxane network. Based on these observations, the low $R = 4$ coatings were recognized to be composed primarily of linear and branched chain fragments entangled into a dense silica film.

6.3.6 Structural Assignment of the $R = 8, 16, \text{and } 24$ Films

The $R = 8, 16, \text{and } 24$ films were identified to have developed from more cyclic siloxane linkages based on three characteristic trends. First, the stronger initial siloxane network formation at room temperature indicated the films were deposited from more highly condensed siloxane fragments and able to coalesce in much more efficient method. Highly localized or weakly branched ring formations in solution would lead to condensed

particulates able to coalesce in a more efficient method. Second, the strong dominance of a single vibration at 1040 cm^{-1} was identified with characteristic of cyclic ring formations. Third, the weak 440 cm^{-1} and 800 cm^{-1} peak intensities indicated there was a loss in long range ordering and preferential ring formation. Forth, the lower distribution in bond angles was consistent with a more ordered structure, characteristic of ring formations. Based on these observations, the higher R valued gels of 8, 16, and 24 were identified with cyclic ring structures connected into a condensed siloxane film.

6.4 Conclusions

The IR vibrational structure of water-based silica films were investigated and monitored as a function of temperature. The transition from room temperature to $450\text{ }^{\circ}\text{C}$ resulted in silanol loss, siloxane bond formations, and frequency shifts in the asymmetric $\equiv\text{Si-O-Si}\equiv$ stretch vibrations. Variations in silanol and siloxane peak intensities revealed two different types of siloxane microstructures. For the low R valued films ($R = 4$), strong peak intensities at 440 cm^{-1} , 800 cm^{-1} , 1020 cm^{-1} , and 1100 cm^{-1} were identified with a linear-type microstructure, consistent with previous low R value polymeric growth mechanisms. In the higher R value films, the strong dominance of 1040 cm^{-1} siloxane peak with small intensities at 440 cm^{-1} , 800 cm^{-1} , and 1200 cm^{-1} were identified with a microstructure derived from cyclic-ringed formations. The apparent division between R valued films was consistent with previous NMR and Raman conclusion.

CHAPTER 7

SOLID STATE ^{13}C AND ^{29}Si NMR INVESTIGATION OF AN EPOXIDE ORMOSIL SYSTEM AS A FUNCTION OF ORGANIC AND WATER CONTENT

7.1 Introduction

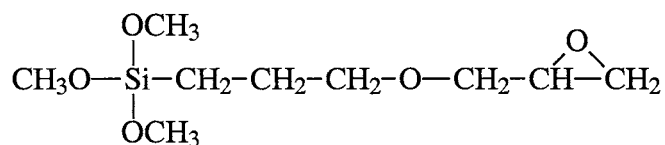
In the previous three chapters, the effects of a water-based sol-gel process were shown to influence the development of an inorganic network. Such network effects are also investigated in hybrid systems. The complexity of hybrid systems can give rise to large number of chemical modifications. Hybrid gels prepared using organically modified silicates and tetraalkoxide silicate precursors introduce additional parameters in the processing of sol-gel systems, such as the immiscibility of the organic group in the solution, stability of the organic functional group, steric influence on the siloxane network, and incorporation into the hybrid matrix. Even hybrid gel systems with only two different silane precursors prove to have significant complexity and can result in many different types of gel microstructures depending on processing conditions (i.e. organic content, water content, and curing temperature). In this and the following two chapters, ^{13}C and ^{29}Si NMR, Raman spectroscopy, and IR spectroscopy will be used to characterize and address the influence of organic content and water concentration in the preparation of a water-based epoxide ormosil sol-gels.

In the development of organically modified ceramic (ormocer) materials, a great deal of interest has been focused on the identification of chemical and structural changes as a result of variations in the organic content and gel processing conditions. Modifications in organic content and processing conditions have been shown in several of studies to change the physical attributes of the resulting gels and influence the physical characteristics, such as flexibility, density, phase domains, hardness, hydrophobicity, and optical properties.^{6-8,45,133,150-158} Most of the alterations in ormocer properties have been identified with variations in siloxane connectivity, organic/inorganic phasic composition, and the chemical intrinsic characteristics of the modifying organic group(s). Investigations using ¹³C and ²⁹Si NMR techniques have been focused on compositional and structural changes in a variety of hybrid gel systems.^{47,78-9,112,120-3} Chemical information pertaining to the organic and inorganic networks has been used to address effects associated with gel preparation. Solid state NMR techniques are used in this network to elucidate structural and chemical alterations in epoxide-modified silicate gels. The influences of preparative conditions are correlated to fundamental changes in the resulting hybrid gel networks.

Organic functionality of the silane precursor has been shown to influence structural formations and gel properties. Organic groups chemically linked to the alkoxide silane can act as a network modifier or as a network former, depending on the chemical functionality. When acting as a network modifier, the organic group can limit the degree of crosslinking or polysiloxane network. By reducing the number of coordination sites, a hybrid film or gel is able to relieve stresses developed during gelation. Relaxation of the network, through the introduction of non-rigid organic modifiers, provides a substantial increase in the flexibility of the siloxane network and, as

a result, lowers gel densification temperature when compared to pure inorganic gels. When organic modifiers act as network formers, the organic moiety becomes an intimate component of the overall network structure. Cross-linking between organic groups in such gels can lead to further densification, resulting in additional alteration of the macroscopic physical properties. By controlling the concentration of organic content, the structural and physical properties of the ormosil can be tailored to provide blended characteristics derived from the unique attributes associated with inorganic network, such as silica, and the organic network, such as an epoxide modifier.

The elevated water content used in a water-based sol-gel process can introduce concerns on the stability of the functional group in an epoxide ormosil system. Historically, epoxide ormosils have been prepared using low water concentrations, between 2 and 4 moles of water per mole of silane, to limit the side reactions between water and epoxide end groups. Under such conditions, the alkoxide silane hydrolysis reaction preferentially consumes a large portion of the added water, rendering the epoxy functional group largely unaffected. Stability studies on the glycidoxypropyltrimethoxy silane have shown that the epoxide group can undergo ring-opening reactions with both water and alcohol to form diol and non-polymeric ether formations.¹²⁴⁻⁶ The rates of epoxide decomposition are also dependent on acid type.¹²⁷⁻⁸ In a study by H. Schmidt and B. Seiferling, acids, such as HClO_4 , H_2SO_4 , and H_3PO_4 , lead to the decomposition of the epoxide ring, whereas acetic acid, HCl , and CO_2 tend to leave the epoxide group intact.⁴⁴ Thus, stability of the epoxide functional group under the preparation conditions of interest (e.g. acidic aqueous) is expected to be an important feature of the chemistry of epoxide ormosils.



Glycidoxypropyltrimethoxysilane

Figure 7.1 Glycidoxypropyltrimethoxysilane precursors use in epoxide ormosil preparations.

Decomposition of the epoxide group under acidic aqueous conditions, can lead to the formation of diol, a chemical species which can potentially be an influential factor in the development of the gel microstructure. Diol end groups in a silica-based sol-gel process are expected to lead to esterification reactions between silanol and alcohol end groups (Reaction 7.3). Under conditions where the new $\equiv\text{Si}-\text{O}-\text{C}\equiv$ carbosiloxane bonds are not hydrolyzed prior to gelation, the organic-inorganic linkages become an integral part of the hybrid ormosil matrix. Linkages of this type have been addressed in epoxide ormosil gels and in similar hybrid gel systems, but the carbosiloxane bond formation has never been specifically identified by any spectroscopic technique.⁴⁴⁻⁵ Under conditions where the carbosiloxane linkages are hydrolyzed (Reaction 7.4), the diol group acts only as a network modifier. With the potential of a large number of side-reactions occurring in ormosil sols, the stability of constituent functional group and products formed upon decomposition of the ring becomes a critical aspect of understanding and controlling the chemical content and structural connectivity of an ormosil network.

Nuclear magnetic resonance has been a fundamental technique used in the characterization and analysis of epoxide containing materials for many years.

41,63,123,129,130-3

Carbon-13 NMR studies on epoxide based materials and epoxide ormosils have identified characteristic peaks associated with the epoxide functional group and unreacted

silane precursors.^{123-5,129-32} In studies conducted with the epoxide functionalized silane precursor (GPTMS), peak assignments have been made identifying the unreacted alkoxides, epoxide groups, polymerization products, and diol formations.^{41-3,123,130,133-4} Studies conducted on epoxide based polymers have made similar peaks assignments and have used diol and epoxide peak intensities to assess the extent of network polymerization and epoxide decomposition reactions.^{129,131-2} Using the collective body of literature in the field, it is possible to make comprehensive peak assignments from ¹³C NMR spectra, and to elucidate the local chemistry of the epoxide-modified silicate network.

In this chapter, epoxide ormosil gels prepared from water-based sols using TEOS and GPTMS precursors were investigated to determine the influence of water on the silica network and epoxide reactivity. Hybrid epoxide based ormosil gels containing 10%, 20%, 40%, 60%, and 80% organic content were prepared with D values of 1, 2, 4, and 6. Solid state ¹³C and ²⁹Si NMR methods were used to identify organic and inorganic structural modifications. Single pulse ²⁹Si NMR experiments were used to quantify siloxane species and determine local environments surrounding silicon nuclei. Cross-polarization ¹H-¹³C NMR experiments were used to identify and monitor epoxide stability, diol formation, epoxide-epoxide polymerization, and organic-inorganic cross-linking. Observed chemical and structural modifications were correlated as a function of D value and organic content.

7.2 Background

7.2.1 ^{29}Si NMR Background

Solid State ^{29}Si NMR spectroscopy of hybrid ormosils have been extensively investigated over in the past 10 years. In early studies on silica materials, authors developed a “Q” notation to label the various types of silicate structures observed, as described in Chapter 4. This notation was later extended to include modified trialkoxy silicate systems. This notation was later extended to include silicate systems with functionalized (or non-functionalized) organic groups covalently attached to the silicon-oxide based systems through the use of “T” notation.¹³⁵ “T” indicates a trialkoxysilane capable of forming 3 siloxane bonds when fully condensed. Subscript designations are added to indicate the number of siloxane bond formations surrounding the T nucleus. For example “T₁” indicates a silicate species with one $\equiv\text{Si-O-Si}\equiv$ linkage, two uncondensed sites, and one covalent $\equiv\text{Si-C}$ linkage. As the subscript number increases, so does the number of siloxane linkages. A full representation of both “Q” and “T” notation are illustrated in Figure 7.2. These notations provided a clear and flexible method by which to identify various silicate species.

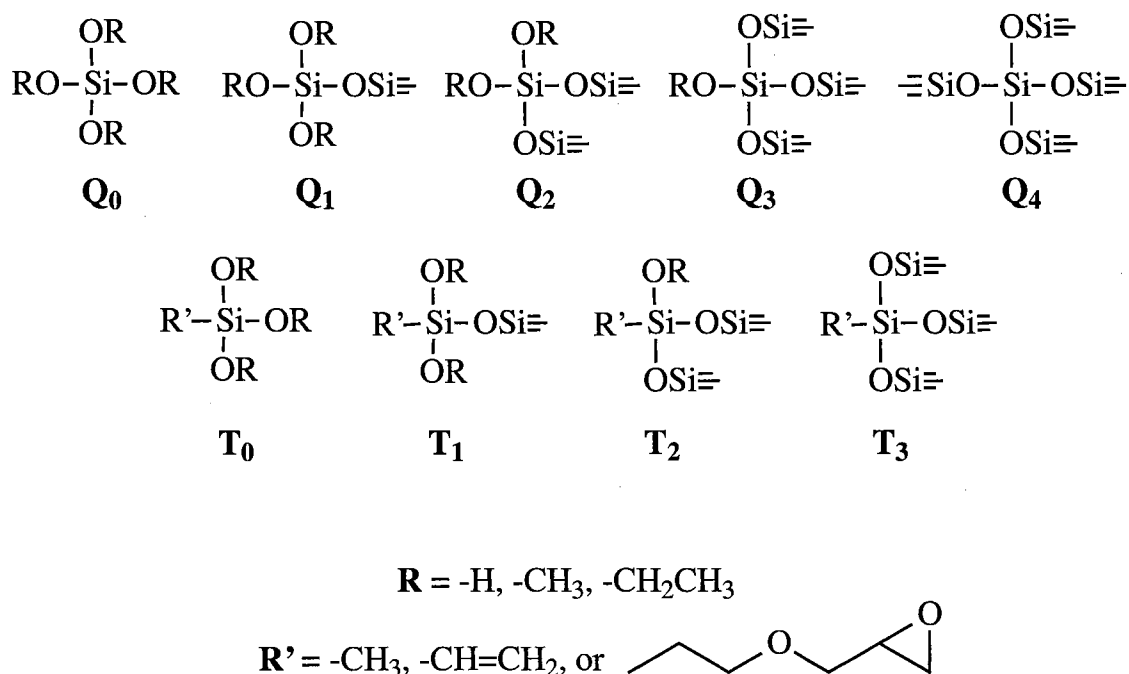


Figure 7.2: Siloxane species represented by “Q” and “T” notation.

7.2.2 Conversion Efficiency

The term “conversion efficiency” has been used in many studies to express the degree of condensation in a silica gel network.⁷⁸⁻⁸⁰ By definition, the conversion efficiency is a percentile value based on the ratio between observed and theoretical polysiloxane connectivity, as given in Equation 7.1. Since each T_n and Q_n species contains a specific number of siloxane bond formations, the observed connectivity can be determined based on the overall deconvoluted compositional percentages found from single pulse spectra. Equation 7.2 represents the conversion equation for a hybrid system prepared with both T and Q species. The theoretical functionality value for the T and Q species is 3 and 4, respectively. The degree of conversion can be calculated for any hybrid gel by inserting compositional percentages and mole fraction (X) for each T and Q

species. Based on the conversion efficiency, the total silanol content can be referenced and correlated with condensation and reaction efficiencies.^{65,68}

$$\% \text{Conversion Efficiency} = \left(\frac{\text{Observed Functionality}}{\text{Theoretical Functionality}} \right) \quad \text{Equation 7.1}$$

$$\% \text{Conversion} = \left(\left(\frac{Q_1 + 2Q_2 + 3Q_3 + 4Q_4}{4} \right) (1-X) + \left(\frac{1T_1 + 2T_2 + 3T_3}{3} \right) (X) \right) \times 100\% \quad \text{Equation 7.2}$$

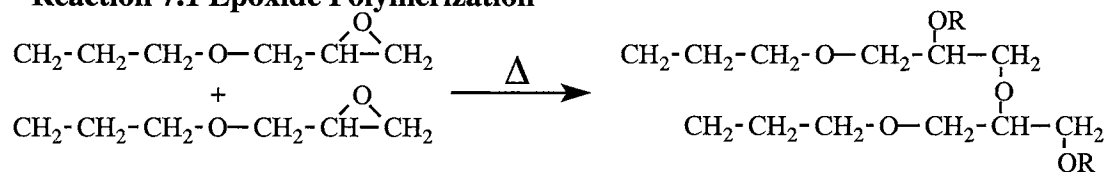
X = mole fraction of T precursor

7.2.2 Products derived from epoxide reactions

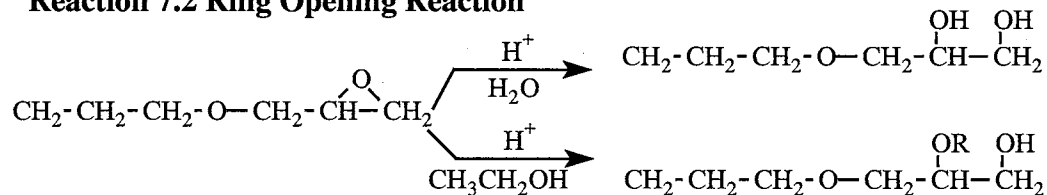
Four reactions have been reported to occur with the ethylene oxide ring in epoxide ormosil gels. Reaction 7.1 consists of epoxide end groups undergoing a polymerization reaction and resulting in the formation of ether linkages. The polymeric product has been identified in comparable systems, through the use of ¹³C NMR methods, by the presence of peaks at 74 and 77 ppm.¹²⁴⁻²⁵ Polymerization in such systems normally occurs at elevated temperatures between 100 °C and 150 °C, but has been reported in other systems at much lower temperatures.^{82,113} Reaction 7.2(a) and 7.2(b) represent a ring opening reaction under acidic condition, involving either water or alcohol with the ethylene oxide ring. These reactions result in the formation of a terminal diol and/or a non-polymeric ether group.^{124,134} Reactions of this type are favored in acidic conditions with excess concentrations of water or alcohol.^{124,146} Distinctions between the terminal and polymeric ether formations have been made using the chemical shift of the alkyl carbon on the non-polymeric ether group. The methyl and ethyl ether groups have been identified in comparable systems with peaks at 58 ppm and 68 ppm, respectively. Diol

formations are generally distinguished from the other products through the development of terminal (63 ppm) and secondary (70 ppm) alcohol peaks.¹³¹⁻² Reaction 7.3 represents a carbosiloxane linkage formed between a diol end group and an uncondensed silanol species. The NMR peak assignments for the carbon nuclei will appear very similar to those observed for the diol end group except that the peak profiles will be severely broadened. Carbosiloxane bond formation covalently links the formerly free organic group into the growing polysiloxane network, thereby limiting the molecular mobility. In the absence of molecular mobility, anisotropic chemical shifts increase and become apparent through line broadening. Similar variations in line resonance characteristics have been used in prior NMR studies of silica sol gel materials to distinguish between absorbed alcohol and chemisorbed alkoxide species.^{44-5,63,70,136} Reaction 7.4 represents the hydrolysis reaction of the carbosiloxane bond and reformation of terminal free diol and silanol species. Reaction 7.5 represents thermal decompositions reactions of the epoxide (forming an aldehyde and ketone)¹⁴⁵⁻⁶ and of the diol (forming a aldehyde).¹⁴⁵⁻⁶ Thermal decomposition reactions will be addressed in thermal studies in Chapter 8 and 9. By monitoring epoxide losses and subsequent peak formations, the effects of processing conditions can be correlated with specific reaction mechanisms and products in the hybrid epoxide gels.

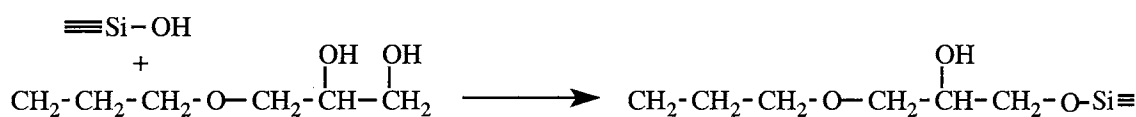
Reaction 7.1 Epoxide Polymerization



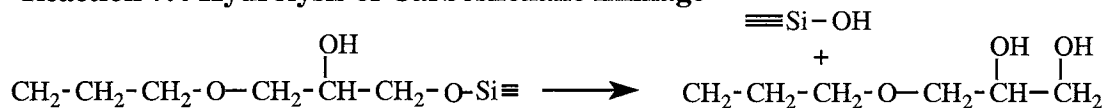
Reaction 7.2 Ring Opening Reaction



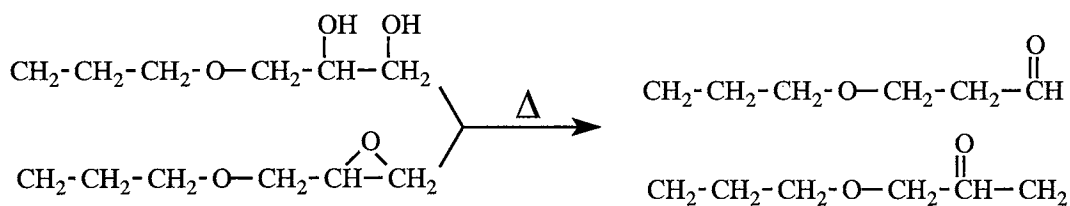
Reaction 7.3 Carbosiloxane Linkage



Reaction 7.4 Hydrolysis of Carbosiloxane Linkage



Reaction 7.5 Epoxide Decomposition



7.2.3 ¹³C NMR Background

Solid State ¹³C NMR spectroscopy is a very useful tool in monitoring the effects of experimental conditions and correlating structural modifications with secondary

species. In epoxide based materials, ^{13}C NMR has been used quite extensively to monitor the reactivity of the epoxide functional side group. Under conditions where the chemical functionality of constituent groups has been modified, the reaction products formed were monitored as a function of the processing conditions.^{125,133-4} ^{29}Si NMR has limited sensitivity regarding the detection of $\equiv\text{Si-O-Si}\equiv$ bonds or linkages; therefore, ^{13}C NMR studies were used to differentiate between polysiloxane and/or uncondensed sites containing -OH or -OR end groups. In regard to specific chemical shifts and peak broadening, ^{13}C NMR has been used to differentiate between the presence of unreacted alkoxide precursors and residual alcohol by-products. Thus, ^{13}C NMR methods have been used to characterize variations in chemical shifts and peak resonance has been used to qualitatively assess the epoxide ring stability and hydrolysis activities in the silica network. A compilation of the relevant peak assignments found in the literature is given in Table 7.1.

Table 7.1: Carbon-13 NMR assignments for hybrid epoxide ormosils.

Chemical Shift	Carbon Peak Assignment	Reference
9 ppm	$\equiv\text{Si}-\underline{\text{C}}\text{H}_2\text{CH}_2\text{CH}_2\text{O}-\text{CH}_2\text{CH}^{\text{O}}-\text{CH}_2$	41,123,130,133
15 ppm	$\equiv\text{Si}-\text{CH}_2\text{CH}_2-\text{CH}_2-\text{OCH}_2\text{CH}_2(\text{OH})-\text{CH}_2\text{O}-\text{CH}_2\underline{\text{C}}\text{H}_3$	70,133
17 ppm	$\equiv\text{Si}-\text{OCH}_2-\underline{\text{C}}\text{H}_3$	70,123,136
22 ppm	$\equiv\text{Si}-\text{CH}_2\underline{\text{C}}\text{H}_2\text{CH}_2\text{O}-\text{CH}_2\text{CH}^{\text{O}}-\text{CH}_2$	42,123,130
44 ppm	$\equiv\text{Si}-\text{CH}_2\text{CH}_2\text{CH}_2\text{O}-\text{CH}_2\text{CH}^{\text{O}}-\underline{\text{C}}\text{H}_2$	41,63,123,129,130-3
49 ppm	$\equiv\text{Si}-\text{O}\underline{\text{C}}\text{H}_3$	63,123,130
51 ppm	$\equiv\text{Si}-\text{CH}_2\text{CH}_2\text{CH}_2\text{O}-\text{CH}_2\underline{\text{C}}\text{H}^{\text{O}}-\text{CH}_2$	41,63,123,129,130-3
58 ppm	$\equiv\text{Si}-\underline{\text{C}}\text{H}_2\text{CH}_2-\text{CH}_2-\text{OCH}_2\text{CH}^{(\text{OH})}-\text{CH}_2\text{O}-\underline{\text{C}}\text{H}_3$	124
58/59 ppm	$\text{H}-\text{O}\underline{\text{C}}\text{H}_2-\text{CH}_3$	70,123,136
60 ppm	$\equiv\text{Si}-\text{O}\underline{\text{C}}\text{H}_2-\text{CH}_3$	70,123,136
63 ppm	$\equiv\text{Si}-\text{CH}_2\text{CH}_2-\text{CH}_2-\text{OCH}_2\text{CH}^{(\text{OH})}-\underline{\text{C}}\text{H}_2(\text{OH})$	123,129,132
63 ppm	$\equiv\text{Si}-\text{CH}_2\text{CH}_2-\text{CH}_2-\text{OCH}_2\text{CH}^{(\text{OH})}-\underline{\text{C}}\text{H}_2-\text{O}-\text{Si}-$	45
68 ppm	$\equiv\text{Si}-\text{CH}_2\text{CH}_2-\text{CH}_2-\text{OCH}_2\text{CH}^{(\text{OH})}-\text{CH}_2\text{O}-\underline{\text{C}}\text{H}_2\text{CH}_3$	124-5,129,131
70 ppm	$\equiv\text{Si}-\text{CH}_2\text{CH}_2-\text{CH}_2-\text{OCH}_2\text{CH}^{(\text{OH})}-\underline{\text{C}}\text{H}_2\text{O}-\text{CH}_2\text{CH}_3$	-
70 ppm	$\equiv\text{Si}-\text{CH}_2\text{CH}_2-\text{CH}_2-\text{OCH}_2\underline{\text{C}}\text{H}^{(\text{OH})}-\text{CH}_2(\text{OH})$	43,123-4,129,132
71 ppm	$\equiv\text{Si}-\text{CH}_2\text{CH}_2\text{CH}_2\text{O}-\underline{\text{C}}\text{H}_2\text{CH}^{\text{O}}-\text{CH}_2$	123,125,130,133-4,41-3
72 ppm	$\equiv\text{Si}-\text{CH}_2\text{CH}_2-\text{CH}_2-\text{O}\underline{\text{C}}\text{H}_2\text{CH}_2^{(\text{OH})}-\text{CH}_2-(\text{OH})$	123,125,130,133-4,41-3
73 ppm	$\equiv\text{Si}-\text{CH}_2\text{CH}_2\underline{\text{C}}\text{H}_2\text{O}-\text{CH}_2\text{CH}^{\text{O}}-\text{CH}_2$	123,125,130,133-4,41-3
73 ppm	$\equiv\text{Si}-\text{CH}_2\text{CH}_2-\underline{\text{C}}\text{H}_2-\text{OCH}_2\text{CH}^{(\text{OH})}-\text{CH}_2-(\text{OH})$	123,125,130,133-4,41-3
72-77 ppm	$\equiv\text{Si}-\underline{\text{C}}\text{H}_2\text{CH}_2-\text{CH}_2-\text{O}\underline{\text{C}}\text{H}_2\text{CH}^{(\text{OH})}-\underline{\text{C}}\text{H}_2\text{O}-\text{R}$	125,128,131

7.2.4 C^{13} NMR Structure Assignments:

In Figure 7.3, the NMR peak assignments have been correlated with products identified in this study. The structure assignments are a subset of those listed in Table 7.1.

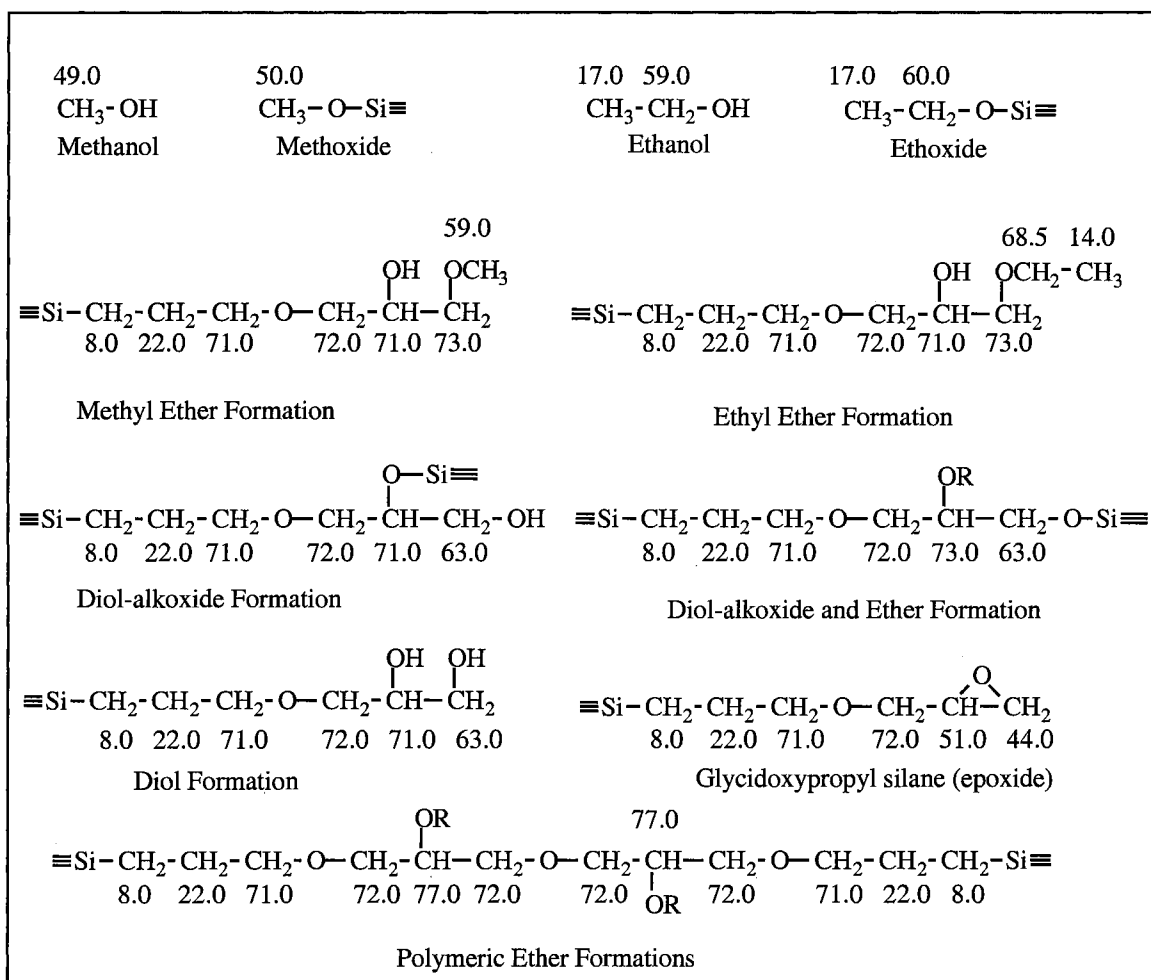


Figure 7.3: Reference to carbon nuclei with end group formations observed in the hybrid gels.

7.2.5 ^{29}Si NMR Chemical Shifts

In high resolution ^{29}Si NMR, the chemical shifts typically observed for hybrid systems fall into two regions depending on the precursor used. The tetraalkoxysilane derived species (Q) are observed between the range of -72.3 ppm and -110.0 ppm. The

trialkoxysilane (T) are shifted upfield and found in a broader spectral range between – 38.5 ppm and –73.7 ppm. The chemical shifts observed for the modified systems are highly dependent on organic functional group attachment. In each region there are well-defined peak areas which correspond directly to specific condensed species. The reported chemical shifts observed for Q_n and T_n silicate nuclei are presented in Table 7.2.

Table 7.2: Typical ²⁹Si chemical shifts observed for tetra-oxide and tri-oxide silicate species. Peak shifts are referenced against a tetramethyl silane (TMS) standard

Peak Type	Chemical Shifts	References	Peak Type	Chemical Shifts	References
Q ₀	-72 to -82	62-80	T ₀	-39 to -44	5,47, 78-9,120, 123,125, 133-4,135
Q ₁	-82 to -89		T ₁	-48 to -52	
Q ₂	-91 to -97		T ₂	-56 to -60	
Q ₃	-100 to -104		T ₃	-64 to -68	
Q ₄	-108 to -110		-	-	

7.3 Results and Discussion

The results have been divided into two sections. Section 7.3.1 focuses on identifying structural variations in the organic network as a function of organic content and D value using ¹H-¹³C NMR. Section 7.3.2 focuses on variations in the siloxane network as a function of organic content and D value using ²⁹Si NMR. Conclusions drawn from each section were used to identify the chemical structure of hybrid gels prepared under different experimental conditions.

7.3.1: ^1H - ^{13}C Cross Polarization Solid State NMR

7.3.1.(a) General Characterization

In Figures 7.4(a)-7.4(d), the 10% hybrid gel spectra exhibited peaks identified with propyl side chain, ethyl ether, unhydrolyzed ethoxide, and diol formations. All peak assignments have been made by referral to the literature assignments shown in Table 7.1. Specific chemical shift frequencies for each resonance band can be found in Appendix D.

In Figure 7.4(a), the peaks at 17 ppm and 59/60 ppm were identified with unhydrolyzed ethoxide silanes and absorbed ethanol. The intense nature of the 17 ppm peak was attributed to a relatively high concentration of $-\text{CH}_3$, and the narrow peak shape with the molecular mobility of the methyl group in this gel. The sharp peak at 59 ppm and broad peak at 60 ppm were identified with the ethanol and ethoxy alkoxide group, respectively. The intense broad width of the 59/60ppm peak indicated the ethyl groups present were primarily associated with unhydrolyzed ethoxide, rather than ethanol. (If the peaks were associated with absorbed or residual ethanol, the 59 ppm peak would have appeared with equal intensity and sharpness to the 17 ppm peak.^{63,136}) The relative intensity of the 17 and 60 ppm peaks with respect to other hybrid peaks implied a small percentage of the unreacted ethoxide silane was present in hybrid gels formed under these conditions and the hydrolysis reaction was not complete in the D=1 gel.

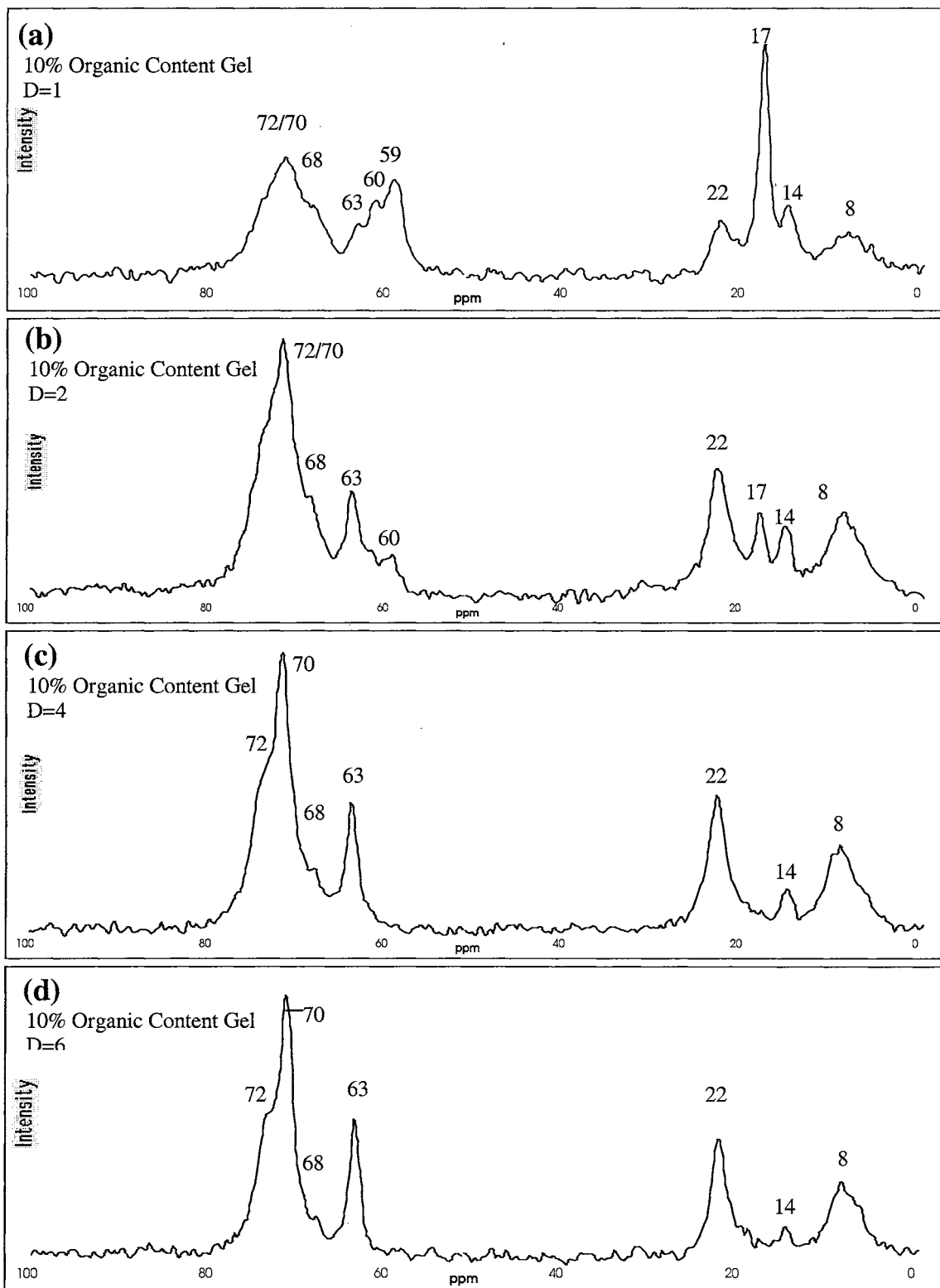


Figure 7.4: ^1H - ^{13}C CP/MAS/NMR spectrum of 10% epoxide ormosil gels prepared with D values of 1, 2, 4, and 6.

Observation of the 17 and 59/60 ppm ethoxide peaks in Figures 7.4(a)-7.4(d) reveals a rapid decrease in intensity of these peaks with increased water content. The rapid loss of an ethoxide peak was consistent with improved hydrolysis generally observed for higher D valued systems. In comparison with the TEOS-derived gels, presented in Chapter 4, the 10% organic content gel required a slightly higher water concentration in order to reach a state of complete hydrolysis. The apparent reduction in hydrolysis efficiency for the hybrid gels was not consistent with reported trends seen in other hybrid systems. Kinetic studies have shown the rate of hydrolysis is clearly faster for modified silicates than for comparable tetraalkoxysilanes.¹²⁰ In particular, the GPTMS precursor contains methoxy rather than ethoxy side chains. Methoxy substitution naturally tends to increase the hydrolysis rate, an effect which is consistent with the more complete degree of hydrolysis in this reaction mixture. Since the hydrolysis rate was not the limiting factor in degree of hydrolysis, the reduction in hydrolysis efficiency was attributed to influences associated with epoxide decomposition. Therefore, the presence of substantial amounts of unreacted ethoxide silane in the low D value gels was attributed to conditions of low water content and influence of the epoxide group, while the complete hydrolysis of the ethoxy silane in the elevated D values was attributed to conditions of elevated concentration of water.

Evidence of epoxide decomposition is a key aspect of the study of chemical structures in gels derived from epoxide-modified ormosil precursors. In Figures 7.4(a) through 7.4(d), the peaks located at 14 ppm, 68 ppm, and 70/72 ppm were identified with an ether product formed by an epoxide ring opening reaction. This product is the result of attack by ethanol, as shown in Reaction 7.2(b). Ethanol, a by-product of TEOS hydrolysis, reacts with the epoxide ring under acidic conditions, resulting in an ethyl ether

formation. The 14 ppm peak and shoulder at 68 ppm were identified as the terminal $-CH_3$ and $-CH_2-O-$ carbons on an ethyl ether chain, respectively. The decrease in the intensity of the 14 ppm and 68 ppm (ethyl ether) peaks as a function of increasing D value was consistent with lower probability of a ring opening as ethanol activity in the sol is lowered. The results indicate that the epoxide ring tends to be more susceptible to attack by ethanol under conditions of low D value.

The hybrid systems showed substantial sensitivity to water activity, especially at elevated D values where the epoxide ring could be induced to decompose into a terminal diol. Diol formation in the gel was identified by the peaks at 63.0 ppm and 70.0 ppm, identified as the terminal and secondary alcohols, respectively. Comparisons between the spectra in Figure 7.4 revealed that the line resonance observation in the diol peaks slowly sharpened with an increase in D value. The substantial line broadening at 63 ppm and 70 ppm indicated the terminal end of the diol functional group had become progressively more immobilized, presumably through gel densification or crosslinking bond formation.

The broad peak profiles observed in the lower D valued peak profiles lead to the assignment of a new carbosiloxane bond formation. Bonding of the functional group to the matrix could only have occurred as a result of either epoxide polymerization or diol esterification. The absence of epoxide peaks (44 and 51 ppm) and broadening in the 70/72 ppm doublet peaks in Figure 7.4 is consistent with both reaction mechanisms. In fact, Schmidt and co-workers have previously reported that the loss of the epoxide peaks and broadening in the 70/72 doublet were signs of epoxide polymerization.¹³³ In their assignments, however, they neglected to consider the broadened 63 ppm terminal diol and 68 ppm non-terminal ethyl ether peaks seen in D = 1 and, to a lesser extent for the D = 2 specimens. These peaks have been used in other epoxide polymerization studies to

quantify the degree of end group hydrolysis and an overall reduction in epoxide polymerization.¹³¹⁻³² More recent studies by Templin, et. al., indicated polymerization between the glycidoxypropyl end groups in an epoxide ormosil were identified by peaks at 77 ppm.¹²⁵ Evidence gathered in this research indicated that the chance of epoxide polymerization at room temperature, in the presence of water, and at such low hybrid concentration is highly improbable. The exclusion of epoxide polymerization as a significant contributor to the hybrid network implies that the line broadening observed in Figure 7.4 must be attributed to some other crosslinking mechanism arising from diol esterification.

7.3.1(b) Confirmation of Carbosiloxane Formation:

Evidence supporting carbosiloxane linkage formation comes from three different sets of observations. First, the broadened 63 ppm and 70 ppm peaks ($D = 1$), consistent with immobilization of the functional group. Second, the presence of unreacted ethoxide silane in lower D value gels indicated reaction conditions were such that the hybrid gels were incompletely hydrolyzed. Since the carbosiloxane linkage and ethoxysilane side groups are both derived from the same type of $\equiv\text{Si-O-C}\equiv$ bond, the formation of an inorganic-organic carbosiloxane crosslink product would be expected to be hydrolytically stable in systems with lower D values. Third, the 63 ppm and 71 ppm diol peaks became increasingly intense and sharpened with increasing D value. The sharp resonance was consistent with more extensive hydrolysis of the carbosiloxane bond and formation of a non-terminated diol end group (as in Reaction 7.4). Similar carbosiloxane type bond formations have been reported for hybrid gels prepared using ethylene glycol.⁴⁵ The variations in the C^{13} NMR line width was explained through structural mobility and bond

formations.⁴⁵ The results and evidence presented suggest that the effects of line broadening with characteristic diol peak formations are consistent with the assignment of carbosiloxane bond formation and inconsistent with the epoxide polymerization attributed to such systems in previous articles.

Results found in Chapters 8 and 9 will provide additional evidence supporting the formation, under selected conditions, of the carbosiloxane linkages.

7.3.1.(c) Epoxide Stability in an 80% Organic Gel as a Function of D Value

Unlike the 10% organic content gel, the 80% organic content gel showed very little loss of the epoxide group in the $D = 1$ gel. In Figure 7.5(a), the two intense peaks at 44 ppm and 51 ppm were identified with the alpha and beta carbons of the epoxide ring. Comparison of the spectrum in Figure 7.5(a), $D = 1$, with elevated D valued Figures 7.5(b)-(d) shows that a rapid decrease in the intensity of the epoxide peaks occurred as water activity was increased. Loss of the epoxide group with increasing D value was attributed to instability of the ethylene ring under acidic aqueous sol conditions. Comparisons between the 10% and 80% organic content gels indicated there was greater degree of epoxide stability in the low $D = 1$ 80% hybrid gel, but with an increase in D value the epoxide stability afforded to the 80% organic gels was lost with an increase in water content.

The epoxide peak losses in Figures 7.5(b) through 7.5(d) were identified with the decomposition of the ethylene oxide ring and subsequent diol formation as evidenced by the increasing peak intensity at 63 ppm. Figure 7.4(c) and (d) demonstrated that the epoxide group was completely lost under conditions of elevated water activity (e.g. $D = 4$,

6). The epoxide loss was also accompanied by rapid development of the 63 ppm peak, indicating conversion to diol.

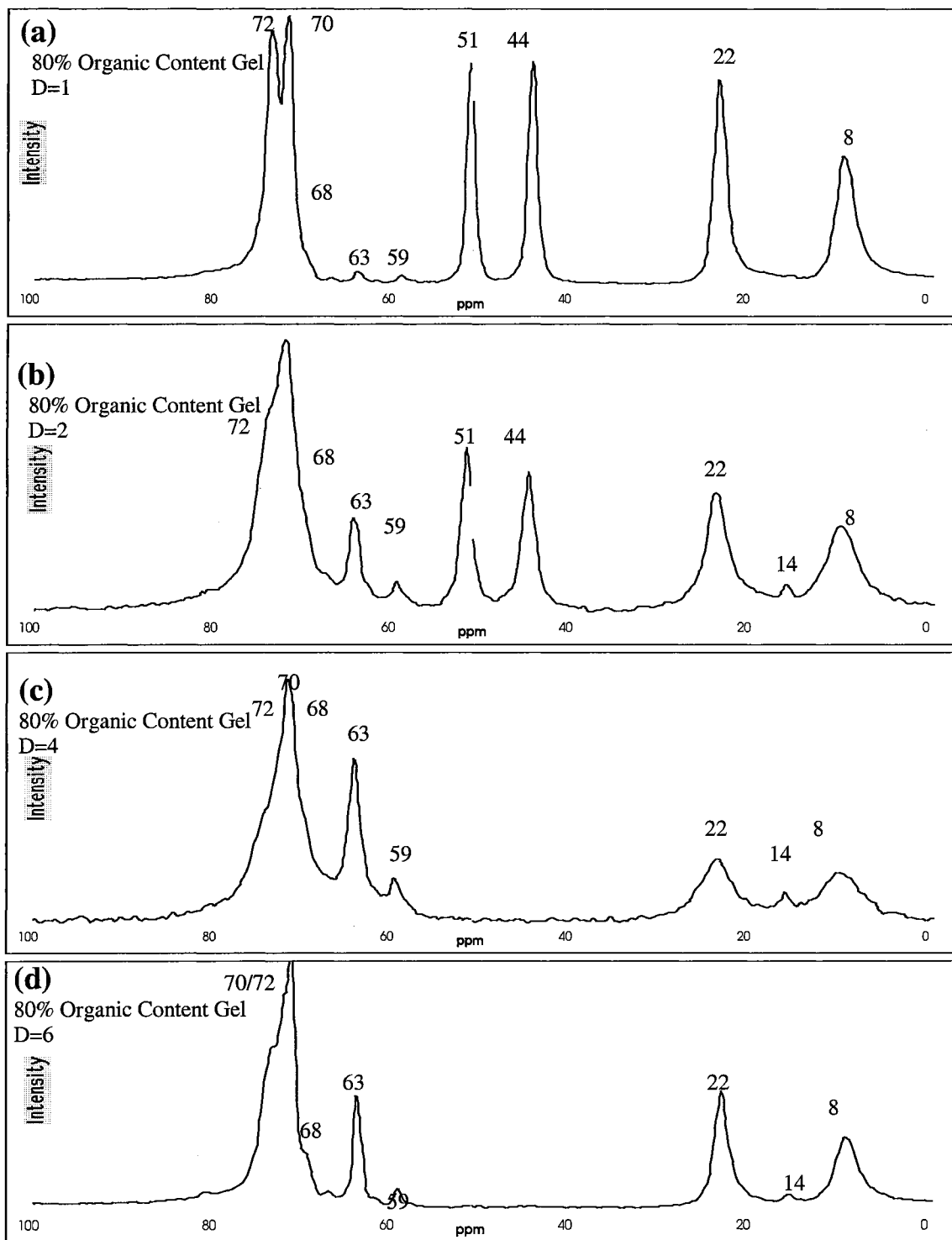


Figure 7.5: ^1H - ^{13}C CP/MAS/NMR spectrum of 80% epoxide ormosil gels prepared with D values of 1, 2, 4, and 6.

7.3.1.(d) Stability of Epoxide Group as a Function of Organic content

The epoxide peak intensity was observed as a function of organic composition for systems having low water content ($D = 1$). This was done in order to ascertain the dependence of organic content and the resultant influence of water activity. Figure 7.6 represents spectra for the $D = 1$ gels prepared at each organic concentration. The gradual loss of the epoxide peaks at 44 and 51 ppm indicated the epoxide group decomposed as a function of organic content. When comparing the relative molar ratios between the epoxide and water content, the stability observed in the elevated organic content gels was attributed to relative reduction in the overall water content.

Loss of the epoxide functionality in the low D value gels was characterized as a function of system water content. Comparison between the $D = 1$ organic content gels in Figure 7.6, revealed a progressive increase in the epoxide peaks with as a function of organic content. In the lower organic content gels, the concentrations of water with respect to alkoxide content were identical, however, the relative concentrations between the epoxide and water content were greatly reduced. In the 10% organic content $D = 1$ gel, the mole ratio of water to epoxide was approximately 40 times higher than in the 80% organic content gel. In such conditions, the higher relative water content increased the probability of epoxide decomposition. As the mole ratio between water and epoxide was reduced through an increase in organic content, the overall loss of epoxide group was lowered. The strong correlation between water concentration and epoxide loss implied the stability of the epoxide group was primarily affected based on the relative mole ratio between water and the epoxide functional group.

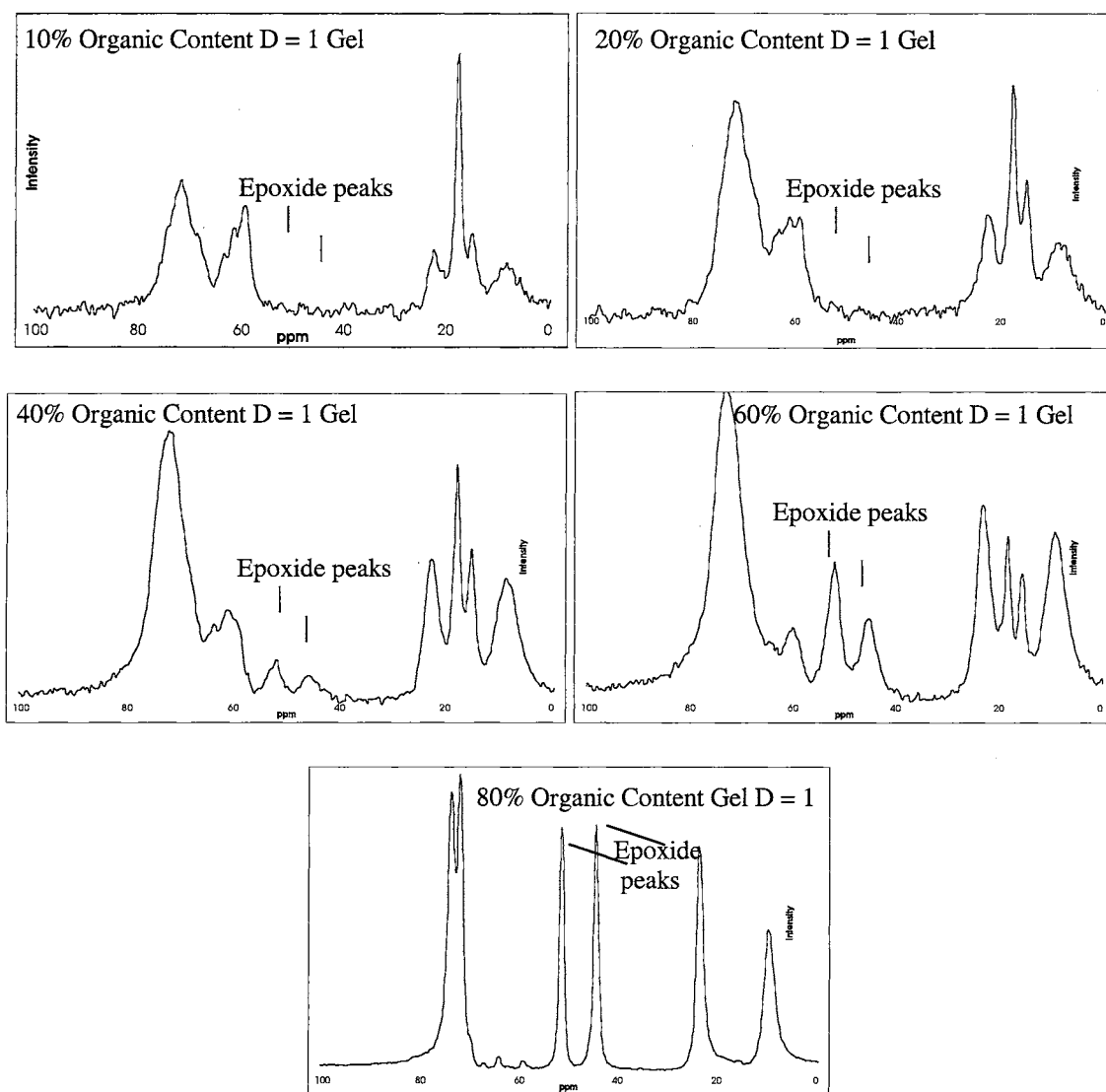


Figure 7.6: ^1H - ^{13}C CP/MAS/NMR spectrum of 10%, 20%, 40%, 60%, and 80% epoxide ormosil gels prepared with D values of 1.

7.3.1.(e) Carbosiloxane Stability as a Function of D Value

A qualitative assessment of the carbosiloxane formation was made using peak profiles in the diol peaks at 63 and 72 ppm given in Figure 7.7. The 60% organic content spectra series reveals signs of carbosiloxane formation at low D values, with evidence of some hydrolysis at moderate D values, and substantial carbosiloxane hydrolysis at the highest D value studied. The D = 1 spectrum revealed signs of broadening in the 63 ppm

and 72 ppm peaks with a small loss in the epoxide peak. Complete loss of the epoxide peaks in the $D = 2$ spectrum was accompanied by the development of a broad, poorly-defined diol peak at 63 ppm. The poorly-defined nature of the peak implied that the diol group was rigidly held most probably by carbosiloxane bond formation. The increase in D value to 4 resulted in a sharp intense peak profile in the 63 ppm and less broadening in the 72 ppm peaks. The sharper peak profile indicated a large portion of the carbosiloxane formation had been hydrolyzed to a free diol end group. Increasing further the D value to 6 resulted in sharp well-defined diol peaks at 63 ppm and 70 ppm. These were attributed to complete hydrolysis of the carbosiloxane formation, as suggested under highly water activity conditions (Reaction 7.4). Thus, the effects of line broadening in the 63 and 71 ppm diol peaks indicated the carbosiloxane bond formation was the primary product at low D value and was hydrolyzed to a non-terminated diol formation at elevated D values.

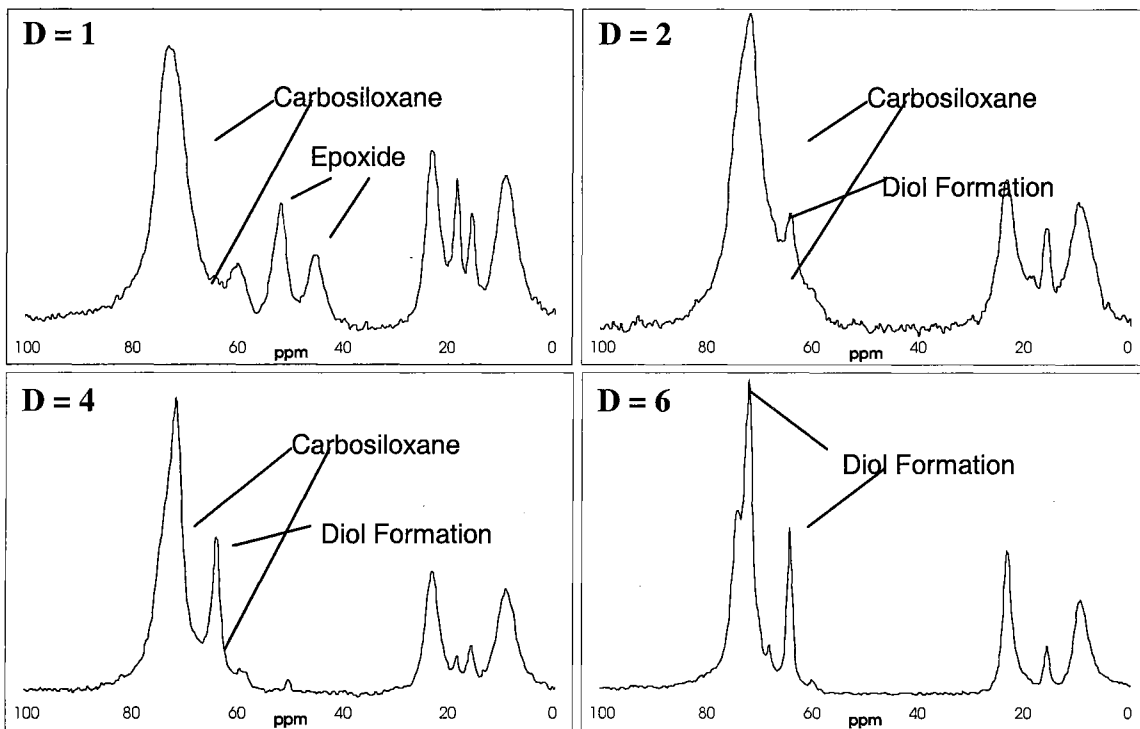


Figure 7.7: ^1H - ^{13}C CP/MAS/NMR spectrum of 60% epoxide ormosil gel prepared with D values of 1, 2, 4, and 6.

7.3.1(f) Review of ^{13}C NMR Results

In summary, the stability of the epoxide group was demonstrated to be directly dependent on the relative concentration of water and alcoholic by-products. Epoxide decomposition resulted primarily in diol formation, which at low D values tended to react with silanol to yield a crosslinked carbosiloxane linkage. At elevated D values, the carbosiloxane formation was hydrolyzed and the functional group was found to have the attributes of a free diol end group. The effects of epoxide decomposition and influence of the carbosiloxane bond formation have a profound effect on the chemical and structural features of the hybrid gel systems. Depending on D value, the final hybrid gel structures result in either a copolymer network characterized by a mixture of carbosiloxane and

siloxane linkages or a network entirely composed of siloxane linkages with non-terminated diol end groups.

7.3.2 ^{29}Si - Single Pulse Solid State NMR

^{29}Si NMR spectroscopy was used to identify the structural influences on the siloxane network as a function of organic content and carbosiloxane bond formation. In the previous section, ^{13}C NMR resulted in the identification of water content effects on epoxide group stability, as well as the postulated existence of carbosiloxane bond formations. Carbosiloxane bond formations in the hybrid gel are highly significant, as their presence can significantly alter the overall polymer network development. Since ^{29}Si SP/MAS NMR experiments provide quantitative results concerning siloxane development, correlation between siloxane connectivity and carbosiloxane formations can be used to assess organic/inorganic phasic composition and overall structural developments in hybrid networks.

Figure 7.8 represents typical ^{29}Si single pulse/MAS spectra for epoxide hybrid ormosil gels prepared with low and high D values. The broad peaks observed at shifts of -51 ppm, -60 ppm, -68 ppm, -94 ppm, -103 ppm, and -112 ppm were identified as T_1 , T_2 , T_3 , Q_2 , Q_3 , and Q_4 species, respectively. Quantified peak percentages and frequency shifts for each of the hybrid gel spectra are presented in Appendix D. Integrated peak areas were used to quantitatively identify the relative species population for those present in each specimen. The population numbers were used to calculate polysiloxane network conversion efficiencies (Equation 7.2).

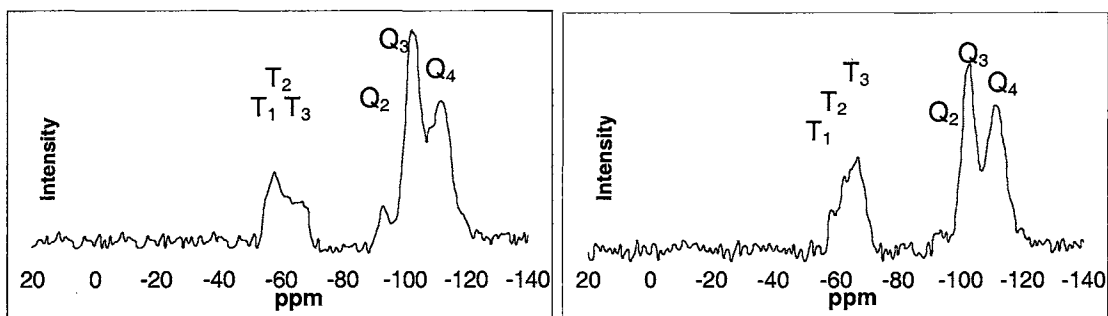


Figure 7.8: Representative ^{29}Si Single pulse/MAS NMR spectrum of a 60% organic hybrid ormosil gel prepared with D values of 1 and 6.

7.3.2(a) Effects of Incomplete Hydrolysis on the Siloxane Network

Figure 7.9 represents computed polysiloxane conversion efficiency plots for each of the hybrid systems studied (from equation 7.2). Conversion efficiency plots for the 80% hybrid system were not available due to poor spectral quality and insufficient signal to noise ratios for this composition using ^{29}Si SP/MAS NMR methods. In general, the highest conversion efficiencies for the hybrid gels were found for specimens containing the smallest amount of organic modifier content prepared under conditions with greatest water activity.

In the 10% and 20% organic content gels, the lower conversion efficiencies for the D = 1 gels were associated with (a) unreacted ethoxide and (b) carbosiloxane formations. The C^{13} NMR spectrum for the 10% and 20% D = 1 hybrid gels (Figure 7.4 and 7.6) were found to correlate with extensive residual ethoxide group and carbosiloxane bond formation, respectively. With an increase in D value to 2 the peak intensity and spectral features were identified, using ^{13}C NMR methods, with substantially reduced populations of unreacted ethoxide groups and carbosiloxane crosslinks. These observations are confirmed by the ^{29}Si SP NMR measurements, which indicated a substantial increase in polysiloxane conversion efficiency for D = 2 compared to D = 1 specimens, as seen in

Figure 7.9. Since the hydrolysis of the ethoxide groups and carbosiloxane formations was near completion in the $D = 2$ hybrid gel, additional increases in the D value did not lead to any significant improvements in the conversion efficiency. The correlation between improved conversion efficiency and hydrolysis implied that the presence of the unreacted ethoxide groups and carbosiloxane formations in the 10% and 20% organic content gels limited the condensation reaction and lead to gels with a substantial portion of the gel comprised of uncondensed sites.

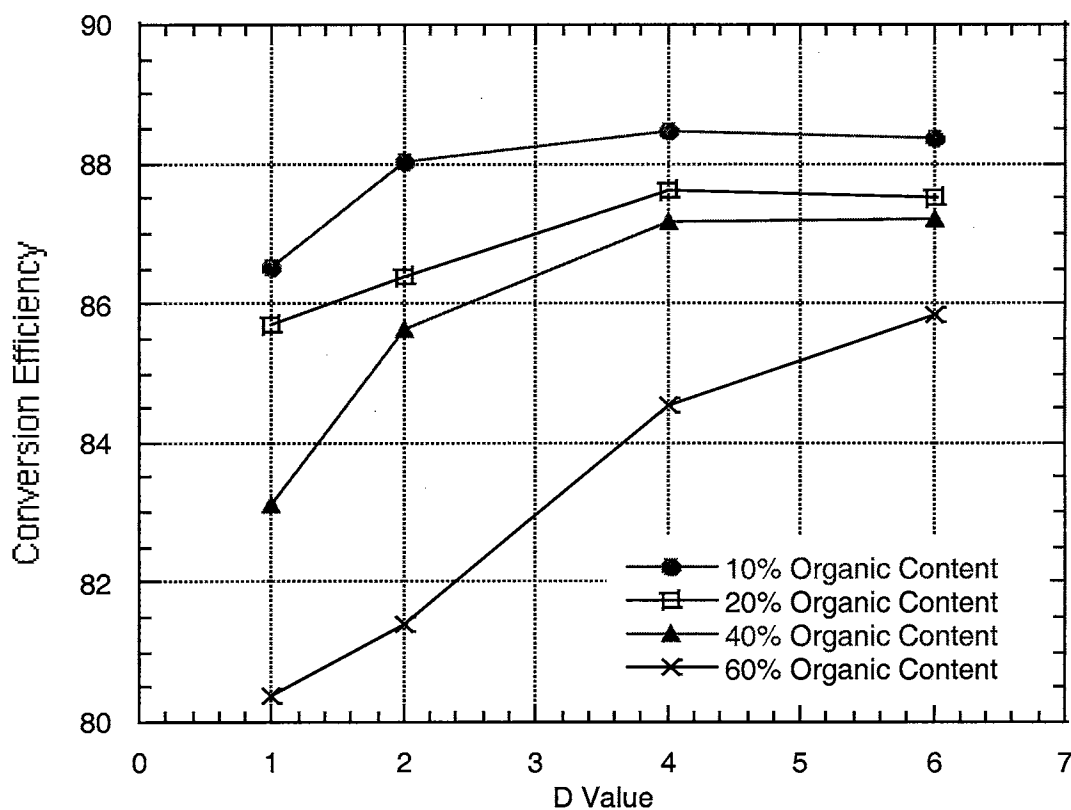


Figure 7.9. Conversion efficiency in 10%, 20%, 40%, and 60% organic content gels prepared with D values of 1, 2, 4, and 6.

The comparatively low polysiloxane conversion efficiency for the 60% organic content gel was attributed to the elevated carbosiloxane bond formation. Previously in

Figure 7.7, the ^{13}C NMR spectra for the $D = 2$ specimen was shown to have broad 63 ppm and 70/72 ppm diol peaks, which corresponded to carbosiloxane formation. The $D = 4$ gel on the other hand, exhibited a much sharper diol peak profile. This is consistent with carbosiloxane bond hydrolysis. When comparing the qualitative trends discussed in Figure 7.7 to the quantitative data shown in Figure 7.9, it can be seen that increases in polysiloxane conversion efficiency may be directly attributed to carbosiloxane hydrolysis followed by silanol condensation.

Lower polysiloxane conversion efficiencies were generally associated with higher organic content. This effect is attributed to steric hindrance induced by the bulky glycidoxypropyl side chain, and by carbosiloxane bond formations. Steric influences exerted by the functional group was largest in the case of carbosiloxane crosslinking due to the formation of an intimately mixed hybrid organic-inorganic co-polymer network composed of a mixture of carbosiloxane and siloxane linkages. Incorporating the organic chain segments into the inorganic network disrupts normal development of the siloxane network. Since carbosiloxane bond formation and local chemical steric effects are intimately coupled, the reduced conversion efficiency in the low D value systems was attributed to a combination of these effects.

In the elevated (40% and 60%) organic content gels, evidence of phase segregation is seen. In the absence of stable carbosiloxane bond formation, the organic functional groups are postulated to act as network modifiers. The relatively large size of the glycidoxypropyl tail and the elevated concentration found in 40% and 60% organic gel specimens tends to make incorporation into the hybrid network take place in an inhomogeneous fashion. Homogenous distribution of the organic modifier tends to essentially disrupt the siloxane network, resulting in a very high number of uncondensed

sites. Such a mechanism is problematic in the sense that overall system energy remains high compared to a fully condensed network. It is possible, however, for the system to achieve lower energy through preferential phase segregation. Phase segregation can be accomplished in a variety of ways, including preferential orientation of the minor phase toward the surface, or by the formation of a minor phase "dispersion" within a matrix composed of the major phase(s).

Phase segregated systems have been reported for elevated organic content gels. In a study by Peeters, et. al., epoxide ormosils with elevated organic content were identified as being phase segregated.⁷⁹ The mechanism of phase segregation was found to involve preferential orientation of the organic functional group to surface sites. Similarly, in a study on the distribution of methyl modified ormosil gels, De Witte, et. al., concluded that at elevated organic concentrations the organic functional groups tend to occupy micropore surfaces, whereas at low organic loading levels the organic group tends to be homogeneously incorporated into the network.⁴⁷ For the work presented herein, the 40% and 60% organic content gels with elevated D values were found to have the spectroscopic signatures of phase segregated gels, while the lower D value gels were found to have spectroscopic signatures consistent with homogeneously distributed carbosiloxane linkages and an intimately mixed organic-inorganic hybrid material.

7.3.3 Proposed Chemical Structures for Hybrid Ormosil Gels

7.3.3.(a) Proposed Chemical Structure for Low D Valued Hybrid Ormosils:

Figure 7.10(a) represents the proposed gel structure identified for a 10% organic content gel prepared using a low D value. Conclusions drawn from ¹³C NMR results indicated that these hybrid gels contained unreacted ethoxysilane and carbosiloxane bond

formations. ^{29}Si NMR conversion efficiencies indicated the number of condensed sites was lower than the elevated D value hybrid gels, due to steric influence of the carbosiloxane formation and alkoxide occupation of a silica coordination site. The combination of carbosiloxane formation and lower siloxane connectivity indicated the hybrid network was a co-polymer matrix consisting of both carbosiloxane and siloxane linkages.

7.3.3(b) Proposed Chemical Structure for Elevated D Valued Hybrid Ormosils

Figure 7.10(b) represents the proposed structure identified in the 10% and 20% hybrid gels with elevated water content. Conclusions drawn from ^{13}C NMR results indicated that these hybrid gels were completely hydrolyzed, with extensive diol end group formations. Conversion efficiencies from ^{29}Si NMR results indicated that these networks were composed of a highly condensed siloxane network. The greater molecular mobility attributed to the diols in this system implied that the functional groups were preferentially oriented towards sites that were less confining to molecular mobility, thus leading to narrow ^{13}C NMR peaks widths. Since the gel structure is known to be microporous, it is postulated that these diol groups were preferentially oriented toward pores rather than into the bulk matrix as free species. Elevated water activity in these gels resulted in the formation of a highly condensed siloxane network with non-terminated diol formations. There was no indication of a bonding interaction between the organic functional group and siloxane network in these specimens.

Results, which are supportive of these conclusions, are presented in Chapter 9.

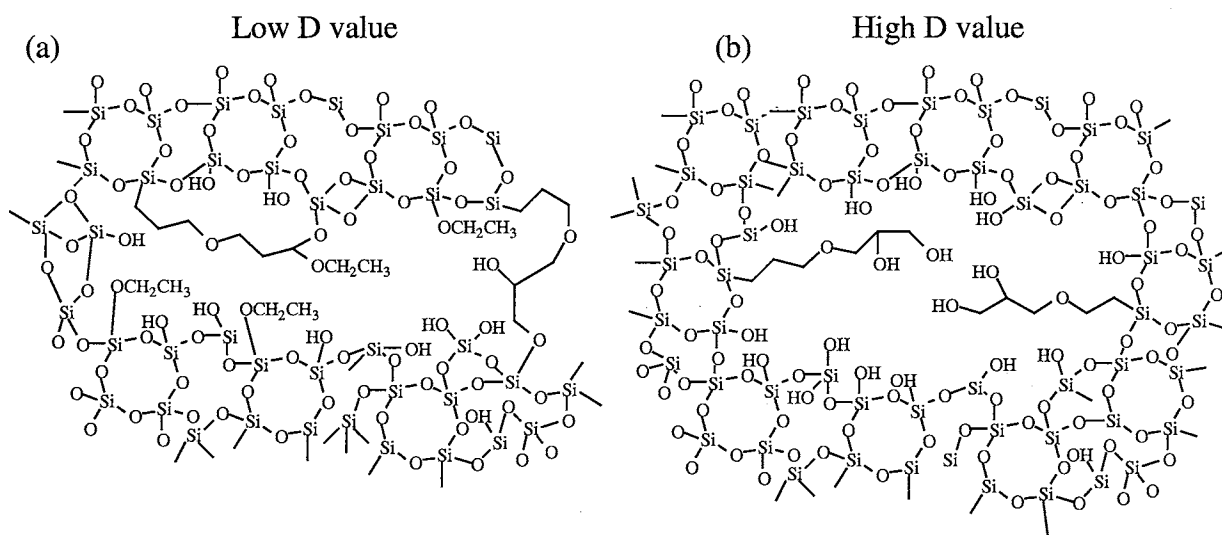


Figure 7.10: Chemical structural of the organic networks formed in lower organic content gels with low and high D values.

7.3.4 Proposed Structure for 80% Hybrid Ormosils:

The 80% organic content gel at low D values was found to exhibit minimal epoxide decomposition via ^{13}C NMR spectroscopy. In the absence of diol formation, the influence of esterification and carbosiloxane bond formations are minimized. In these specimens, a siloxane network develops such that with the glycidoxypopyl groups act only in the role of network modifiers. The elevated concentration of the organic side chains and the large steric hindrance generated by these groups and evidence of the complete nature of siloxane network development all support formation of a phase segregated system composed of siloxane clusters surrounded by surface-oriented epoxide functional groups. The surface-orientated epoxide groups are stable under low D preparative conditions for the 80% organic content gels, as previously discussed (Section 7.3.1(c)) towards the surface. This assignment, which is consistent with assignments

made by other authors in high organic content materials is also supported by complementary IR and Raman spectroscopic methods in Chapters 8 and 9.

At elevated D values, the microstructure of the 80% organic content gels was characterized as a co-polymer matrix dominated by carbosiloxane linkages rather than being characteristic of a polysiloxane network. ^{13}C NMR spectra indicated that the epoxide decomposition was accompanied by diol end group formations. Broadening of the peaks associated with carbosiloxane formation was less substantial than the broadening found for the lower organic content gels. The lesser degree of peak broadening was attributed to an overall reduction in the local rigidity of the gel matrix. Unlike lower organic content gels, the 80% organic content ormosil is composed largely of organic chains. The ratio between silicon nuclei and epoxide functional groups was 2 to 1. Theoretically, the entire network could be connected through carbosiloxane linkages. It is postulated that a network comprised of flexible organic fragments result in greater localized molecular mobility, which in turn is evidenced by sharper peaks. Based on preliminary NMR results, interpreted in light of similar studies by other researchers, it is postulated that the network for these gels formed through carbosiloxane linkages rather than siloxane bond formations as shown in Figure 7.11(b). This characterization is tested using Raman and IR studies described in Chapter 8 and 9.

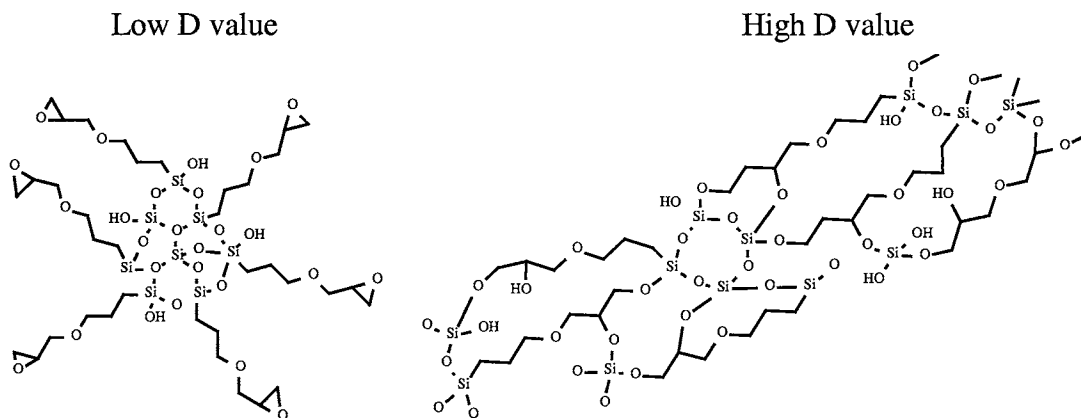


Figure 7.11: Chemical structural of the organic networks formed in the elevated organic content gels with low and high D values.

7.4 Conclusions

The effects of using a water-based process for the epoxide ormosil gels was shown to directly affect both the chemical and structural nature of the hybrid gels. The stability of the epoxide functional group in an aqueous environment (acidic), identified to be primarily dependent on water/epoxide ratios, was the single most important contributor to the final characterized hybrid network.

The hydrolysis of the epoxide group and esterification of the diol-end group formation were found to be the most influential factors in the development of the hybrid gel microstructures. Conclusions drawn from ^{13}C NMR indicated the epoxide ring was hydrolyzed under conditions with elevated water:epoxide molar ratios. The hydrolysis of the epoxide group to a diol end group formations resulted in the development of two different types of networks. At low D values, the diol group was esterified with silanol end groups resulting in the development of a carbosiloxane bond formation. With organic group acting as a network former, the carbosiloxane linkage in the lower D valued gels was considered to tie the function group into silica network with further siloxane bond formations continuing in the surrounding network. At elevated D values, the

carbosiloxane formation was hydrolyzed resulting in non-terminated diol end groups. Acting only as a network modifier, the functional group was incorporated into the hybrid network with preferential orientation toward surface sites. Thus, future work conducted on epoxide based ormosils must address the epoxide stability and subsequent stability of the carbosiloxane formation.

CHAPTER 8

RAMAN INVESTIGATION OF AN EPOXIDE ORMOSIL SYSTEM AS A FUNCTION OF CURING TEMPERATURE AND ORGANIC CONTENT

8.1 Introduction

Despite the widespread use of hybrid materials and the enormous amount of Raman spectroscopy, very few Raman studies have been conducted to investigate the basic chemical reactions in epoxide-based ormosil material. In the past twenty years, a wealth of information concerning densification, reaction kinetics, and structural formations has been reported independently for both silica and epoxide based materials.^{59-61,116,138-143} In each system, vibrational frequencies of chemical species have been well characterized. Silica gels have been monitored from the initial stage of hydrolysis all the way thru gel formation and the glass transition.^{83-4,90,100} Characteristic vibrations reported for silica-based materials have preceded peak assignments of silanol, siloxane, and assorted microstructural features. In epoxide-based resins and polymers, changes to the characteristic ethylene oxide ring vibrations have been used to assess epoxide content and monitor the progress of polymerization reactions.¹⁴¹ The present work seeks to integrate previously reported mechanisms and peak assignments with the goal of understanding the underlying chemical processes in epoxide-modified ormosils. Parametric variables of interest include organic content, D value, and curing temperature.

Raman studies conducted on ormosil and epoxide containing material have provided a basic reference for distinguishing and identifying characteristic vibrations in a hybrid gel network. Silica networks, which have been well characterized in studies of quartz, vitreous glass, and unmodified sol gel materials, tend to have a limited number of vibrations occurring below 1200 cm^{-1} . In the case of silica sol-gel media, information concerning silanol content, degree of siloxane network formation, and overall densification have been previously reported in the literature. Similarly, a wide variety of epoxide containing materials, such as resins, polymers, and ormosil systems, have been the focus of literature reporting peaks associated with epoxy ring vibrations. One problematic issue associated with peak assignments in several of these published epoxide studies is the presence of intense overlapping organic vibrations. Organic side chains, which may be connected with the epoxide group, can produce a wide distribution of Raman-active vibrations. Peak overlap can limit the ability of Raman methods to detect subtle spectroscopic differences associated with the selection of certain processing conditions such as temperature or organic content. However, in a controlled system with known compositions, the vibrational spectra can be used to identify new bond formations, polymerization products, and structural alterations occurring in epoxide based ormosil gels.

In this study, Raman analysis was used to complement the NMR studies reported in Chapter 7 and to test the chemical species assignments made. Experiments targeted the affirmation of post-curing epoxide polymerization reactions. Raman spectra were acquired for hybrid gels composed of 10%, 20%, 40%, 60%, and 80% organic content. Specimens were prepared with D value of 1, 2, 4, and 6 and three curing temperatures (room temperature, $60\text{ }^{\circ}\text{C}$, and $150\text{ }^{\circ}\text{C}$). Spectra were assessed with a focus on

identifying epoxide content, organic polymerization, organic-inorganic cross-linking, epoxide decomposition, degree of hydrolysis, and silanol densification.

8.2 Background

8.2.1 Raman Active Vibrational Bands of Epoxide-based Ormosil System

Previously reported Raman studies conducted on silica- and epoxide-based polymeric materials will be used to make peak assignments and to help identify new bond formations. Silica vibrational bands located in the region between 300 cm^{-1} and 1200 cm^{-1} have provide vast information concerning siloxane connectivity, surface hydroxyl content, bulk silanol content, and the structural development of siloxane ring systems.^{83-4,90,100} In studies conducted on epoxide based material, characteristic ethylene oxide ring vibrations have been used to identify specific vibrational frequencies, generally over a region lying between 600 cm^{-1} and 3500 cm^{-1} . With a large body of knowledge pertaining to related materials systems, numerous vibrational assignments are catalogued for organic polymers and inorganic silane groups. A compilation of the Raman vibrational assignments, which are applicable to this work, is given in Table 8.1.

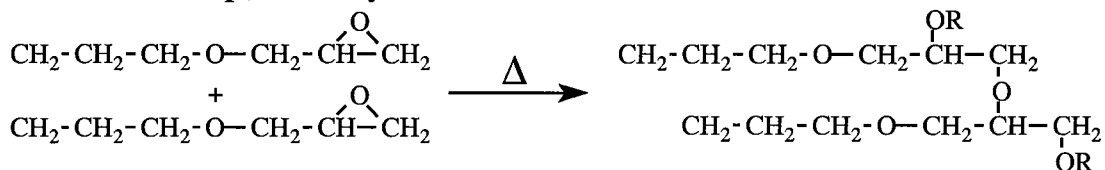
Table 8.1: Representative vibrational frequencies and assignments for observed bands in epoxide- and silica-based materials.

Frequency	Vibrational Assignment	References
350	$\equiv\text{C}-\text{O}-\text{C}\equiv$ Stretching	59-61,124
430	Symmetric Stretch SiO_2	59-61,82-100
490	Stretch $\equiv\text{Si}-\text{OH}$	59-61,82-100
606	Cyclic three member siloxane ring	59-61,82-100
800	Bending SiO_2	59-61,82-100
750-880	Epoxy ring deformation (symmetric)	59
800-900	$\equiv\text{C}-\text{C}-\text{O}$ In phase stretch primary and sec. alcohol	59-61
800-850	$\equiv\text{Si}-\text{C}$ stretch (symmetric)	59-61,116,140,144
855	$\equiv\text{C}-\text{O}-\text{C}\equiv$ stretch (symmetric)	59-61,124
875	In phase $\equiv\text{C}-\text{C}-\text{O}-$ stretch (alcohol)	12,2
908	Epoxy ring deformation (anti-symmetric)	59-61,141,144
980	Stretching $\equiv\text{SiOH}$	59-61,82-100
1047	$=\text{N}-\text{O}$ stretching (NO_3^-)	59-61,103
1075	$\equiv\text{C}-\text{O}$ Stretching (Ethanol or TEOS)	59-61,83,100
1060-1150	$\equiv\text{C}-\text{O}-\text{C}\equiv$ Anti-symmetric stretch	59-61,141,144
1000-1075	$\equiv\text{C}-\text{C}-\text{O}-$ out of phase stretch primary alcohol	59-61,124
1075-1150	$\equiv\text{C}-\text{C}-\text{O}-$ out of phase stretch secondary alcohol	59-61
1075	$\equiv\text{Si}-\text{O}-\text{C}\equiv$ stretch	59-61,82,105
1130-1120	$=\text{CH}_2$ Oxirane Wag (epoxide)	59-61
1256	Epoxy ring breathing	59-61,141,144
1295	$=\text{CH}_2$ in phase twisting	59-61, 144
1342	$=\text{CH}_2$ wag	59-61, 144
1417	$-\text{CH}_3$ or $=\text{CH}_2$ Anti-symmetric Deformation	59-61
1454	$-\text{CH}_3$ or $=\text{CH}_2$ Symmetric Deformation	59-61,83,100,143-4
1485	$=\text{CH}_2$ Scissors	59-61,83,100,143-4
1695	Absorbed H_2O	59-61
1710	$\text{C}=\text{O}$ Anti-symmetric stretch	59-61
2843	$-\text{CH}_2$ Symmetric stretch	59-61,83,100,143-4
2884	$-\text{CH}_3$ Symmetric stretch	59-61,83,100,143-4
2929	$=\text{CH}_2$ Anti-symmetric stretch	59-61,83,100,144
2944	$-\text{CH}_3$ Anti-symmetric stretch	59-61,83,100,143-4
3005	Epoxy ring ($=\text{CH}_2$) Symmetric stretch	59-61, 154
3055	Epoxy ring ($=\text{CH}_2$) Anti-symmetric stretch	59-61, 154

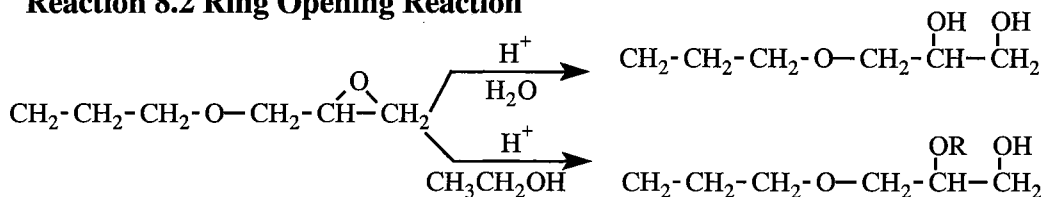
8.2.2 Products from Epoxide Reactions

In the preparation and curing of epoxide based ormosil gels, the ethylene ring can undergo reactions previously described in Chapter 7 and repeated here for convenience. Reaction 8.1, involving epoxide group polymerization through the formation of ether linkages, gives rise to a Raman peak at 855 cm^{-1} (ether vibrations).^{59,125,146} In reaction 7.2(a), epoxide ring decomposition under aqueous acidic conditions results in the generation of a pair of diol peaks ($1000\text{-}1075\text{ cm}^{-1}$ for the primary, $1075\text{-}1150\text{ cm}^{-1}$ for the secondary alcohol).⁵⁹⁻⁶¹ Decomposition of alcoholic conditions, shown in Reaction 8.2(b), gives rise to a Raman peak at 2944 cm^{-1} (alkyl carbon on the ethyl ether).^{59-61,83,100,143} Reaction 8.3 yielding the carbosiloxane linkage, gives rise to Raman peaks in the $950\text{-}1100\text{ cm}^{-1}$ region.⁵⁹ Reaction 8.5 represents thermal decomposition reactions of the epoxide (forming an aldehyde and ketone) and of the diol (forming a ketone).¹⁴⁴⁻⁶ Aldehyde and ketone formations are readily identified by the characteristic C=O stretching vibration at 1730 cm^{-1} . Since the C=O stretch peak occurs in a spectral region which is comparatively free of overlapping vibrations, the development of a peak at this energy value provides quick and unambiguous indication of thermal decomposition leading to carbonyl groups. By monitoring epoxide losses and subsequent peak formations, the effects of preparation and curing conditions can be correlated with specific reaction mechanisms and products in the epoxide hybrid gels.

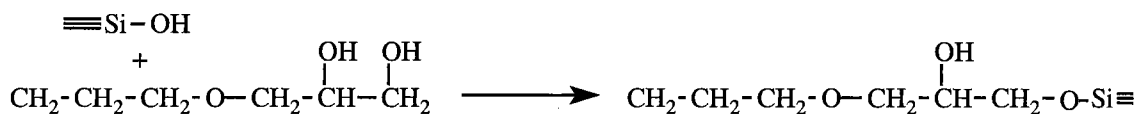
Reaction 8.1 Epoxide Polymerization



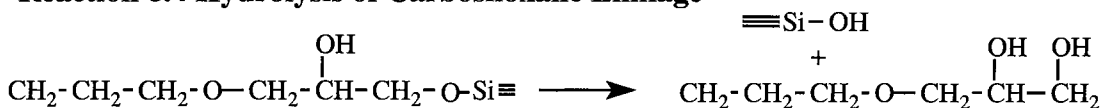
Reaction 8.2 Ring Opening Reaction



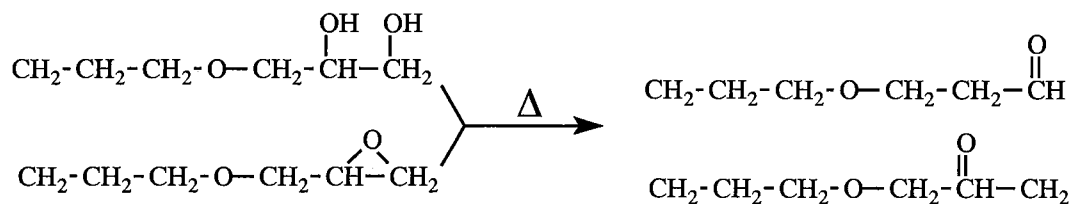
Reaction 8.3 Carbosiloxane Linkage



Reaction 8.4 Hydrolysis of Carbosiloxane Linkage



Reaction 8.5 Diol and Epoxide Decomposition



8.2.3 Qualitative Determinations of Epoxide Content

Raman spectroscopy is recognized as an analytical technique capable of providing quantitative results.⁶¹ Using Raman analysis in a quantitative manner to obtain analytical results requires significant details to instrumental parameters such as laser power, excitation frequency, detector response, and sample volume and alignment in order to

achieve the necessary reproducibility of peak intensities and frequency positions.¹³⁵ One effective method of correcting such inconsistencies is to use reference vibrations in order to calibrate unknown peak intensities relative to one or more known peaks. Reference peaks may either be derived from a known standard internal vibration or from an externally added material with a known vibration and concentration. By referencing against a known standard, the relative concentration of a functional group or compound can be quantifiably determined.

Qualitative measurements of epoxide content has been used quite extensively in epoxy resins and organic polymer systems.^{61,146} In such systems, characteristic ring vibrations are determined with respect to a set of standardized vibrations. In many instances, the multitude of vibrations arising from various organic compounds, such as fillers, catalyst, and organic side chains, creates difficulties in making quantitative comparisons between vibrations. In such cases, a qualitative or semi-quantitative assessment of epoxide content can be made by simple comparisons between specific peak intensities. This simplified technique enables Raman analysis to provide a simple and fast method to characterize epoxide content as function of preparation conditions and/or curing temperatures.

In a system composed of GPTMS and TEOS, the limited number of possible organic vibrations improves the utility of standardized internal reference peaks. In a study by U. Posset and co-workers, the vibrational bands of GPTMS were reported; assignments were made based on the known features of silica, epoxides, and other organic vibrational bands.¹⁴⁴ The glycidoxypropyl side chain is largely composed of CH₂ groups; thus, the characteristic vibrations associated with this group would provide an ideal internal reference standard. The CH₂ twists, reported at 1296 cm⁻¹, is a relatively

weak peak relative to some of the stronger CH₂ vibrations, but is less susceptible to interference and peak overlap from methoxide and/or ethoxide CH₃ vibrations. Several epoxide ring vibrations have been previously identified. These peaks, which exhibit varying intensities, are found over a wide frequency range between 700 cm⁻¹ and 3055 cm⁻¹. The strongest epoxide vibration, located at 1256 cm⁻¹, is located immediately adjacent to the CH₂ twist peak, but the two peaks have minimal overlap. Since these peaks are closely paired, baseline drifts have little or no effect on their relative peak intensities. Thus, it is possible to use simple intensity comparisons between the 1296 cm⁻¹ CH₂ twist and 1256 cm⁻¹ epoxy breathing vibrations in order to make a qualitative determination of epoxide content as a function of the overall organic content. This approach was used to observe the relative amount of epoxide content in the hybrid gels as a function of processing conditions.

8.2.4 Silica Network

Studies on fused silica and vitreous glasses have identified 6 Raman vibrations at 430 cm⁻¹ (SiO₂ symmetric stretch), 490 cm⁻¹ (≡Si-OH stretch), 606 cm⁻¹ (3-member siloxane ring), 800 cm⁻¹ (SiO₂ bending), 910 cm⁻¹ (=Si(OH)₂ stretch), and 980 cm⁻¹ (≡Si-OH stretch). These bands are a subset of those compiled in Table 5.1. It is important to note that not all of the peaks are observed in every silica system, and intensities vary as a function of the nature of the siloxane network. The unique relationship that exists between peak frequency and intensity lends valuable insights structural information and chemical content.

8.3 Results and Discussion

Figures 8.1 through 8.3 represent low ($D = 1$) and high ($D = 6$) D valued gels prepared with 10%, 20%, 40%, 60%, and 80% organic content. Spectra have been interpreted and correlated with NMR results and proposed structures in Chapter 7.

8.3.1 Low D Valued Gels

In Figures 8.1 and 8.2, $D = 1$ hybrid gel spectra are shown for specimen having 10%, 20%, 40%, 60%, and 80% organic content. Figure 8.1 represents compositional overlap of the full spectra from 0 cm^{-1} to 4000 cm^{-1} , while Figure 8.2 represents an overlay enlargement of the fingerprint region between 0 cm^{-1} and 1800 cm^{-1} .

Using the internal standard ($=\text{CH}_2$ peak centered at 1295 cm^{-1}), it is possible to see that by inspection of Figure 8.2 the epoxide peaks (760 cm^{-1} , 908 cm^{-1} , and 1256 cm^{-1}) decrease in intensity compared to the 1295 cm^{-1} peak. The apparent trend, which indicates greater epoxide decomposition for hybrids having the lowest organic content, is consistent with findings detailed in Chapter 7 for comparable systems. The 10% and 20% organic content gels were found to have complete loss of the epoxide peaks, while the 40% and 60% organic content gels exhibited moderate intensity losses. The loss of intensity implied the epoxide group had decomposed.

Epoxide decomposition in the 10% and 60% organic content gels was blamed for the reduced peak resolvability over the 700 cm^{-1} and 1135 cm^{-1} region in Figure 8.2. Epoxide decomposition to a diol results in the formation of both primary and secondary alcohol groups. The decomposed epoxides give rise to multiple $\equiv\text{C}-\text{C}-\text{O}-$ vibrations, stemming from the $-\text{CH}_2-\text{CH}_2-\text{O}-\text{CH}_2-\overset{\text{OH}}{\text{C}}-\text{CH}-\text{OH}$ diol formation. In addition, the $\equiv\text{C}-\text{C}-\text{O}-$ in and out of phase stretching vibrations, which occur between $1000-1150\text{ cm}^{-1}$

and 800-900 cm^{-1} , were substantially broadened due to internal hydrogen bonding interactions.¹³³ The combination of multiple vibrational modes for primary and secondary alcohol groups, in addition to broadening from hydrogen bonding gave rise to very broad overlapping peaks, and overall decrease in peak resolvability. Nonetheless, background broadening is secondary and confirming evidence of epoxide decomposition.

The 80% organic content gel exhibited a Raman spectrum that indicated minimal losses in the intensity of the epoxide-indicator peaks, and did not exhibit a loss in peak resolvability seen in the other specimens. In the absence of epoxide decomposition, the only $\equiv\text{C}-\text{C}-\text{O}-$ vibrations that could be generated in the organic network would be due to the ether linkage in the glycidoxypropyl side chain. Absence of the diol formation minimized the number of variable $\equiv\text{C}-\text{C}-\text{O}-$ vibrations, which in turn resulted in greater peak resolvability in the 700 cm^{-1} to 1135 cm^{-1} portion of the spectrum. The presence of the intense 1256 cm^{-1} epoxide peak and minimal background broadening indicated the epoxide groups in the 80% organic content gels were largely left intact under $D = 1$ preparation conditions. This confirms the ^{13}C NMR result reported for such gels in Section 7.3.1.

Evidence of carbosiloxane linkage formation was observed in the 60% and lower organic content gels. The 1075 cm^{-1} peak was attributed to a carbosiloxane $\equiv\text{Si}-\text{O}-\text{C}\equiv$ stretch vibration.¹³³ The progressive increase in 1075 cm^{-1} peak intensity as a function of organic content, up to a maximum at 60%, implied the peak occurred as a direct result of epoxide decomposition in the presence of free silanol group. If the peak were, instead, due to the presence of unreacted ethoxide groups or residual ethanol, the 1075 cm^{-1} peak intensity would have been most intense in the 10% organic content gel (due to the

relatively large amount of unreacted ethoxide functionality in these gels). In addition, the relative intensity of the 2944 cm^{-1} $-\text{CH}_3$ stretch vibration, corresponded to unreacted TEOS and ethyl ether formations, was found to decrease with an increase in organic content. If the alkoxide peak were identified with TEOS precursor, the 2944 cm^{-1} $-\text{CH}_3$ peak intensity would have progressively increased as the 1075 cm^{-1} peak developed. This combination of observations is independent verification of carbosiloxane $\equiv\text{Si}-\text{O}-\text{C}\equiv$ bond formation in the 10%-60% organic content D = 1 gels.

Similarly, the absence of a peak at 1075 cm^{-1} peak in the 80% organic content gel is indicative of a lack of carbosiloxane linkages. Since diol formation is prerequisite to carbosiloxane linkage development, it is clear by inspection of Figure 8.2 that the 80% D = 1 gels could not have appreciable carbosiloxane development due to the stability of the epoxide groups. The lack of diol formation also eliminates the possibility of diol esterification reactions. These results also independently confirm the ^{13}C solid state NMR results reported in Section 7.3.2.

Examination of the 490 cm^{-1} silanol and broad 456 cm^{-1} siloxane vibrations in the 60% and lower organic content gels indicated that there was an increase in silanol content, with respect to the overall siloxane development as a function of decreasing organic content. Using the 490 cm^{-1} peak as a relative indicator of the availability of silanols to form polysiloxane network, the progressive decrease of the 456 cm^{-1} siloxane vibration with increasing organic content is consistent with the suggested polymerization mechanism, in which the development of the siloxane network is disrupted in the 10%-60% organic content gels as organic modifier content increases. The 10%-60% organic content gels were found to have extensive decomposition and carbosiloxane formation. As discussed in Chapter 7, carbosiloxane linkages lead to the formation of a co-polymer

matrix having intimate mixtures of both siloxane and carbosiloxane bonding. The carbosiloxane formation results in a network in which the modified organic group is incorporated in to siloxane network, which disrupts the siloxane network and leads to elevated levels of uncondensed silanol species. Thus, these observations are all consistent with a model in which 10%-60% organic content $D = 1$ gels form mixed siloxane-carbosiloxane hybrid co-polymers.

Disruption of the siloxane network was minimized in the 80% organic content gel (as expected for preparation with minimal unmodified silane). The relative intensities of the 490 cm^{-1} and 456 cm^{-1} peaks were smaller, but the difference in the intensity of the two peaks is the smallest of the specimens observed. The 456 cm^{-1} siloxane peak was found to be quite broad, overlapping the 490 cm^{-1} silanol vibration. When comparing the relative peak heights with those from the 60% organic content spectrum, the reduction in the $490\text{ cm}^{-1}/456\text{ cm}^{-1}$ relative peak height difference indicated that the siloxane network in the 80% organic content gel was substantially less disrupted and contained lower relative number densities of silanol species.

In the $D = 1$ 80% organic content gel, stability of the epoxide functionality coupled with evidence of siloxane development is consistent with a proposed model for phase segregation in this system. In the absence of carbosiloxane linkages, the glycidoxypropyl side chains can act only as a network modifier, precluding intimate copolymer formation. Systems with elevated organic content have been previously reported to tend toward phase-segregation due to the relatively large size of the organic chain. Since the 80% organic content $D = 1$ gel was identified with a siloxane network and showed no signs of epoxide loss, the hybrid gel was consistent with model predictions of

a phase segregated system with the organic groups preferentially oriented towards surface sites.

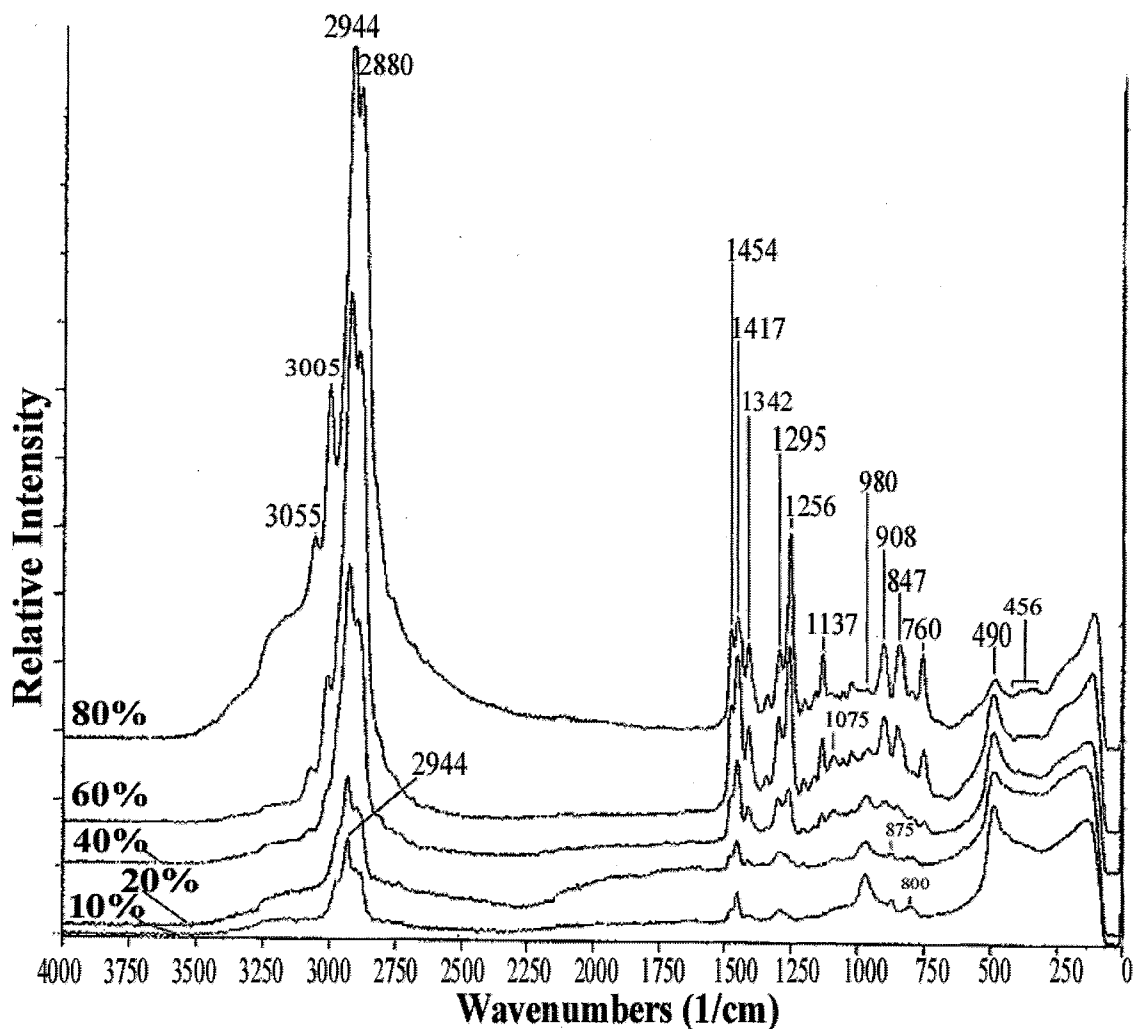


Figure 8.1: Overlaid Raman spectra for the 10%, 20%, 40%, 60%, and 80% epoxide hybrid gels prepared with D values of 1 and cured at room temperature.

Interpretation of the Raman data assignments for the room temperature $D = 1$ gels series were consistent with Chapter 7 NMR results and structures proposed there in. The Raman spectra for the 60% and lower organic content gels identified epoxide decomposition, carbosiloxane formations, and the influence of organic content on the

polysiloxane network development. Interpretations of the Raman data for the D = 1 80% organic content gels indicated there was little or no epoxide loss, and that the repressed carbosiloxane formation left the growing polysiloxane network undisturbed.

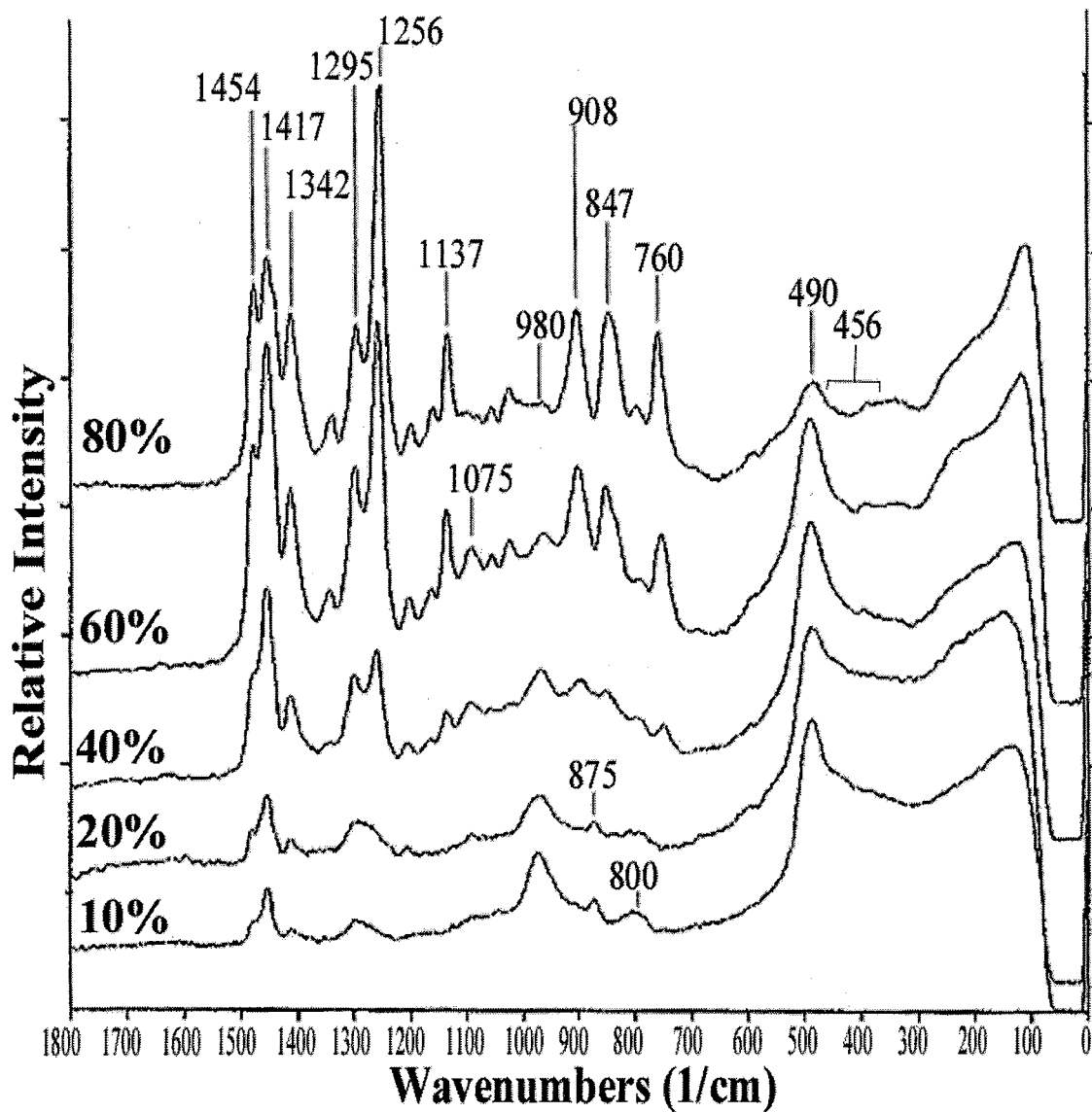


Figure 8.2: Overlaid Raman spectra of the fingerprint region for 10%, 20%, 40%, 60%, and 80% epoxide hybrid gels prepared with an D value of 1 and cured at room temperature.

8.3.2 Epoxide $D = 6$ Value Ormosil Gels

The work in this section focuses on the influence of organic content under comparatively high ($D = 6$) water activity levels. Figure 8.3 represents a full spectra from 0 cm^{-1} to 4000 cm^{-1} , while Figure 8.4 represent an enlargement of the fingerprint region (0 cm^{-1} and 1800 cm^{-1}) for the same spectra.

Spectra for the $D = 6$ ormosil gels exhibited extensive epoxide dissociation with respect to comparable $D = 1$ spectra. The 80% organic content spectrum was the only system to exhibit any residual epoxide, as evidenced by the peaks at 760 cm^{-1} , 908 cm^{-1} , 1256 cm^{-1} , 3005 cm^{-1} , and 3055 cm^{-1} . The substantial reduction of intact epoxide functionality in the 80% gels, and the apparent complete loss of epoxide in the 10%-60% organic content gels indicated that the elevated water activity in these systems lead to essentially decomposition of the epoxide functional group.

As in the 10%-60% $D = 1$ gels, broad background peak development, in areas located between 700 cm^{-1} and 1135 cm^{-1} , indicated the epoxide decomposition resulted in diol formations. The extensive broadening observed in the 700 cm^{-1} to 1135 cm^{-1} region was attributed to elevated diol end group concentrations as well as the influence of hydrogen bonding.

The 1075 cm^{-1} carbosiloxane peak could not be identified in the $D = 6$ spectra due to the broadly overlapping $\equiv\text{C}-\text{C}-\text{O}-$ vibrations. Since the increase in diol formation resulted in additional broadening and loss of peak resolvability, the existence of the carbosiloxane formation could not be conclusively confirmed or rejected. However, the absence of the residual alcohol and $-\text{CH}_3$ alkyl vibrations at 875 cm^{-1} and 2990 cm^{-1} indicated the higher D valued gels were completely free of unreacted alkoxide precursors. This result confirms previous ^{13}C NMR finding.

Comparisons between the 490 cm^{-1} silanol and broad 456 cm^{-1} siloxane peaks in the 10%-60% organic content $D = 6$ gels indicated that there were minimal differences in the degree of siloxane network formation with an increase in the organic content. The only noticeable difference between the spectra was a progressive broadening in the 490 cm^{-1} silanol peak with an increase in organic content. The unchanged characteristic of the broad 456 cm^{-1} siloxane vibration for the specimens implies that the siloxane network was not disrupted by the elevated concentrations of organic content.

The siloxane network is more disrupted, however, in the 80% organic content $D = 6$ gel than it was in the 80% $D = 1$ gel. The 456 cm^{-1} siloxane peak is substantially larger, for this composition, relative to the 490 cm^{-1} silanol peak than for the 10%-60% $D = 6$ spectra. This indicates that the siloxane network was not as well developed and contained relatively high concentrations of silanol end groups.

The stronger development in the siloxane vibration for the 10%-60% $D = 6$ gel specimens, relative to the peaks for comparable $D = 1$ samples, was attributed to the onset of a phase segregated system. As water activity is increased, the carbosiloxane bridges can be hydrolyzed (as suggested in Chapter 7), leading to the formation of a hybrid system composed of a siloxane network with diol end groups. In the absence of carbosiloxane linkages, the organic functional group acts primarily as a network modifier. In these cases, the hybrid gels are predicated to form in a manner such that the siloxane network forms independently, with bound organic groups segregating toward surface sites. Orientation of the organic groups towards the surface tends to yield more complete siloxane network with lower residual numbers of silanol species. Therefore, the developed siloxane networks that formed in the absence of carbosiloxane crosslinking

tends to yield a phase segregated system with organic groups postulated to self-orient towards surfaces (e.g. micropores).

Raman characterization for the 10%-60% organic content gels were consistent with interpretations of data presented in Chapter 7 NMR results. The variations and developments in the Raman spectra identified epoxide losses, diol formations, and siloxane network development even with elevated organic concentrations. Epoxide decomposition and severe spectral broadenings were consistent with hydrolysis of the epoxide group to form diols. Esterification reactions occurring between the diol and silanol end groups were not disproved. The presence of intense 456 cm^{-1} siloxane vibrations in the 40% and 60% organic content gels implied the hybrid systems had some degree of phase segregation.

Raman interpretations of the D = 6 80% organic content spectra indicated there was substantial hydrolysis of epoxide, leading to diol formations and subsequently limited siloxane network development. Carbosiloxane interaction could not be specifically proven; however, the combination of diol formation taken in conjunction with evidence of limited siloxane network formation indicates that the Raman data is consistent with proposed structures in Chapter 7 indicating a co-polymer matrix.

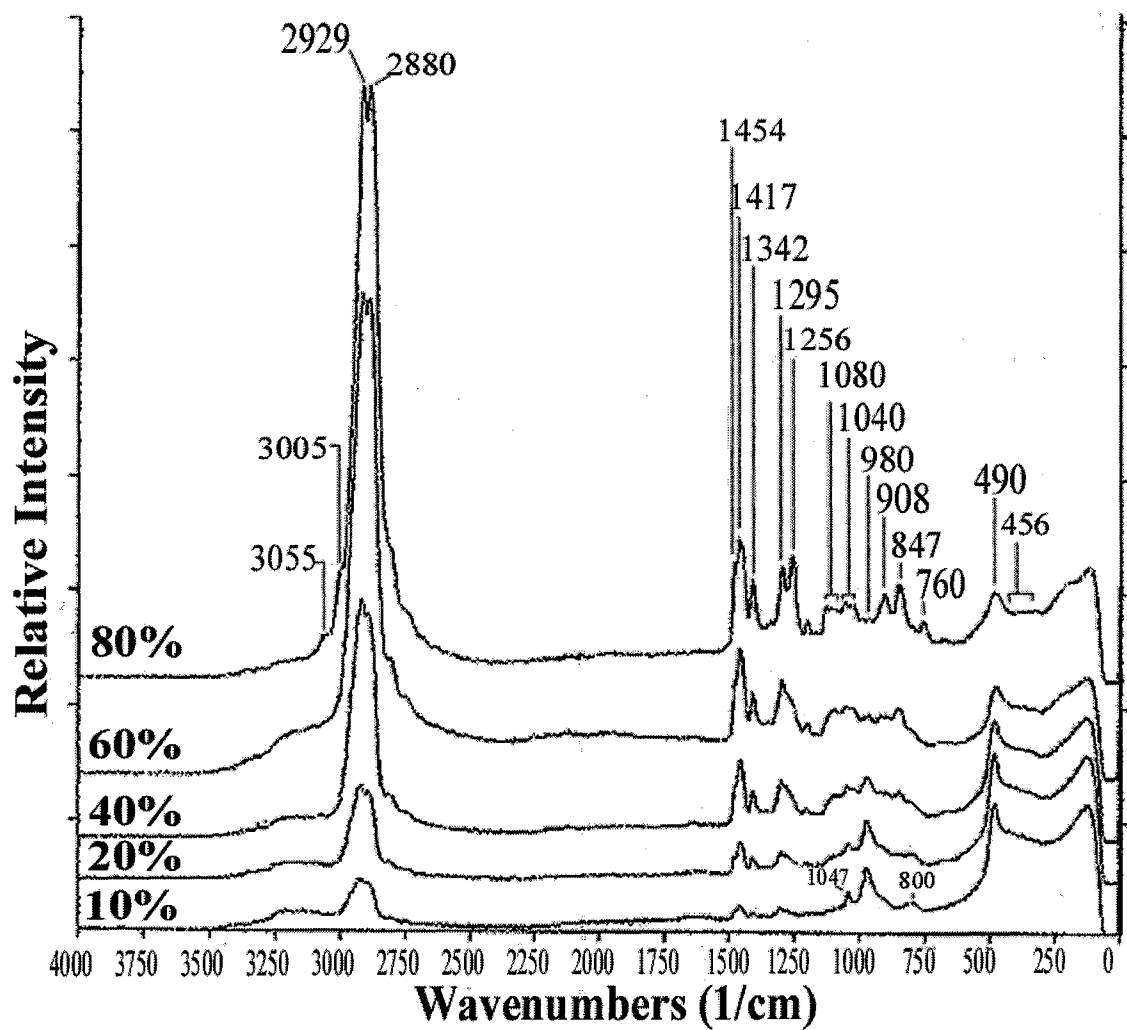


Figure 8.3: Overlaid Raman Spectra for the epoxide hybrid gels prepared with D values of 6 and cured at room temperature.

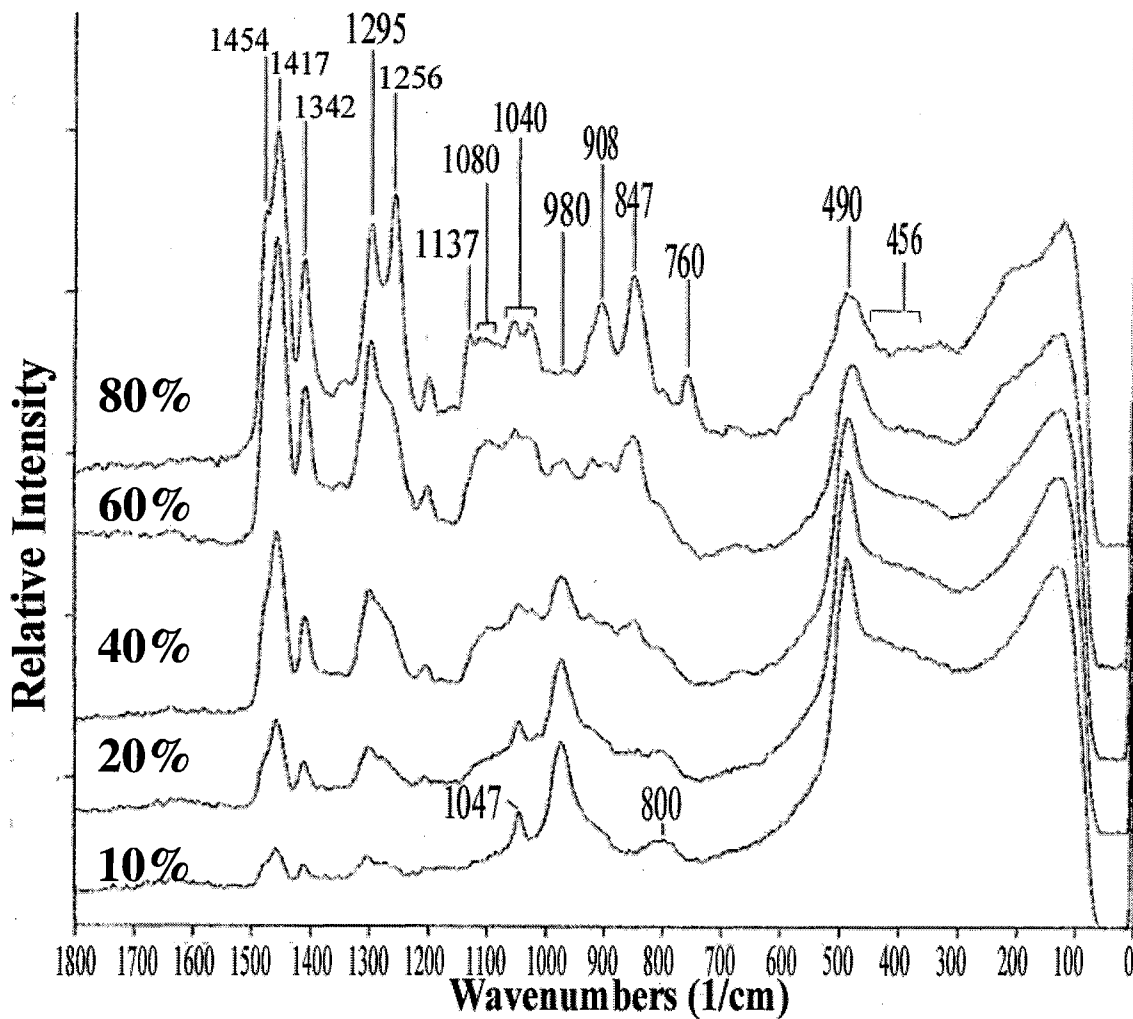


Figure 8.4: Raman Spectra of the fingerprint region for the epoxide hybrid gels prepared with a D value of 6 and cured at room temperature.

8.3.3 Curing of Hybrid Ormosil Gels to 150 °C.

Curing the hybrid gels to 150 °C investigated signs of silanol densification as a function of water content and hybrid composition. Figure 8.5(D = 1) and 8.7(D = 6) represent before and after curing to 150 °C spectra.

Examination of Figure 8.5(a) indicates that the 980 cm^{-1} and 490 cm^{-1} peaks associated with uncondensed silanol species are slightly to moderately diminished in

intensity after curing at 150 °C (Fig 8.5(b)). The change is most obvious in the 60% organic content spectrum. Coincident with silanol disappearance is a slight to modest increase in polysiloxane network formation, evidence by the increased broad bond peaks intensities at 456 cm⁻¹. This increase in Figure 8.5 is again most notable in the 60% specimen. Analogous changes are seen as a function of 150 °C curing in the elevated water content specimens as well (D = 6); Figures 8.6(a) and (b).

The most distinctive difference between the two systems was the formation of a 606 cm⁻¹ siloxane peak and presence of the 1075 cm⁻¹ alkoxide peak, these features were only observed in the D = 1 spectra (Figure 8.5).

The presence of the 1075 cm⁻¹ peak indicated the carbosiloxane bond formation was comparatively stable, remaining in the lower D valued gels after curing. At room temperature, the only clearly identifiable carbosiloxane peaks were in the 40% and 60% organic content gels. If the carbosiloxane peak was present in the 10% and 20% D = 1 gels, the identifying peak, 1075 cm⁻¹ peak was obscured by residual alcohol vibration. After curing, the 1075 cm⁻¹ peak in the 10%, 20%, and 40% organic content spectra were visible confirming the presence and stability of the carbosiloxane bond formation up to 150 °C.

The 606 cm⁻¹ band, referenced in the literature as the D₂ peak, is attributed to the formation of highly strained 3-member rings located at the SiO₂ surface.^{93,104} The development of the 606 cm⁻¹ band is associated in the literature with a densification process involving surface condensation rather than being generated as a product of structural densification.^{110, 35} In the low D value gels, the silanol loss with heating and concomitant D₂ formations indicated that the densification processes involved

condensation between surface silanols. In the elevated water ($D = 6$) gels, the loss of silanol without D_2 formation indicated the densification process involved bulk structural densification rather than a surface phenomenon. This finding is consistent with previously described results indicating that hybrid gels prepared under elevated water concentration ($D = 6$) tend to have orientation of the organic functional groups towards surface sites. Occupation of surface sites by the modified silicates would in principle limit surface densification.

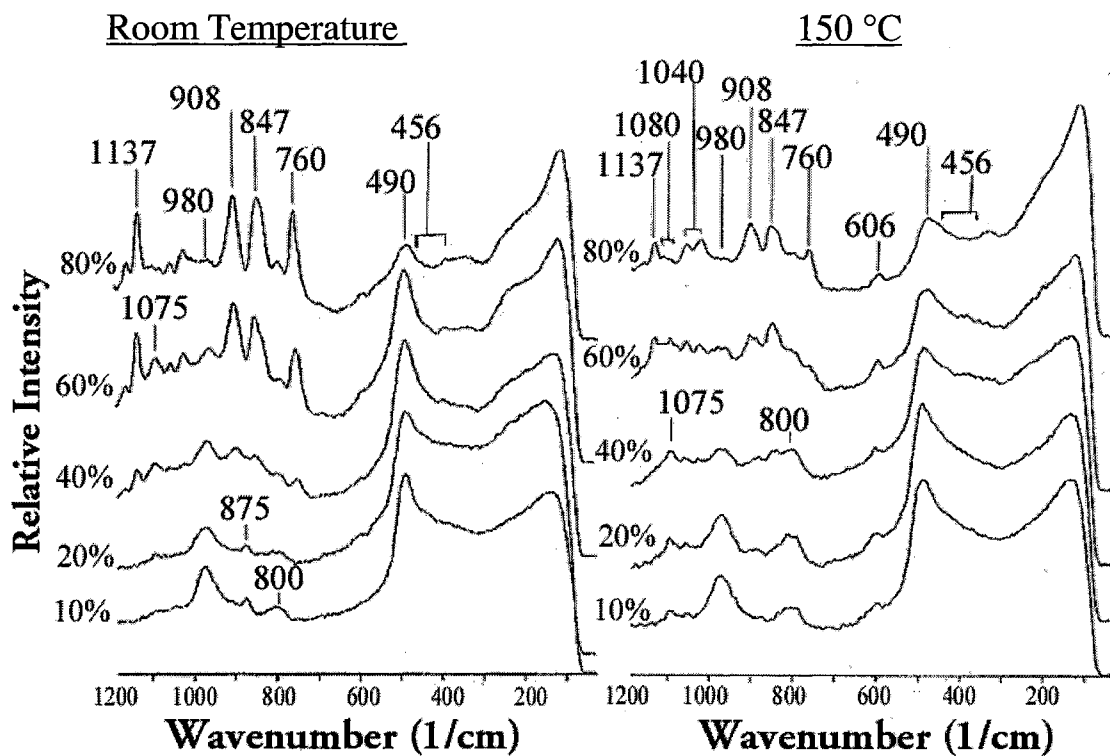


Figure 8.5 Spectral overlay of hybrid ormosil gels prepared with a D value of 1 cured at room temperature and 150 °C.

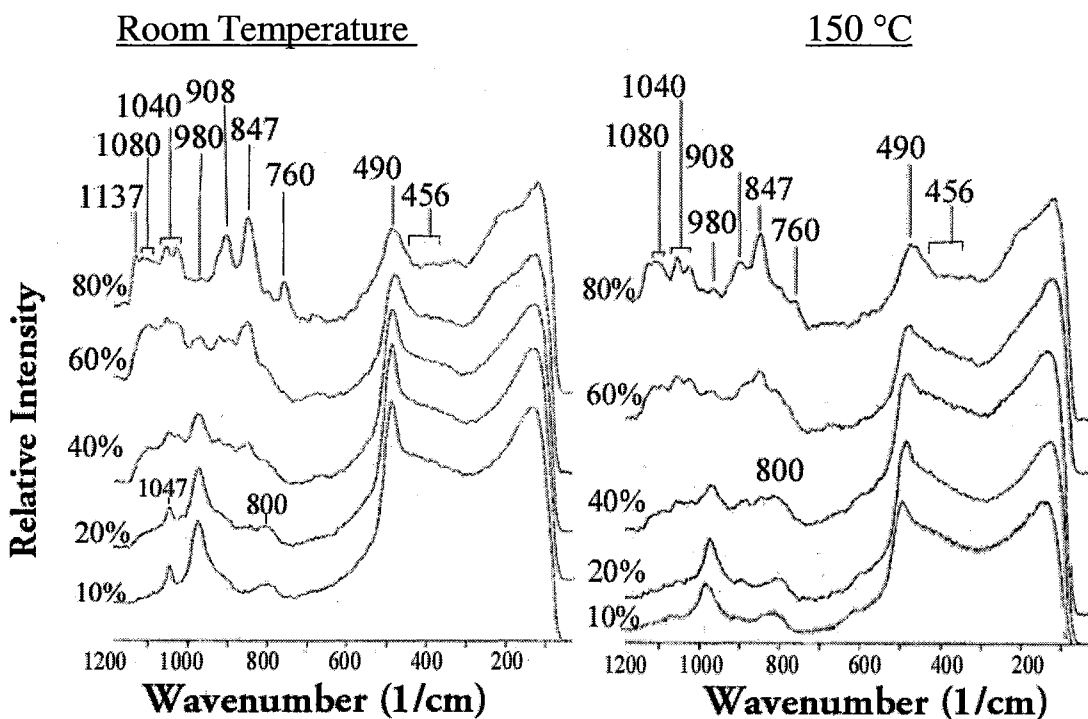


Figure 8.6 Spectral overlay of hybrid ormosil gels prepared with a D value of 6 cured at room temperature and 150 °C.

8.3.6 Monitoring of the Organic Network as a Function of Curing

Figure 8.7 represents the results of studies aimed at assessing chemical and structural differences in the 80% organic content gels as a function of water content ($D = 1, 6$) and as a function of curing temperature (RT and 150 °C). The 80% composition was chosen because it tends to have the highest level of intact epoxide groups, and would thus have the greatest probability of exhibiting signs of epoxide polymerization.

Comparisons between the 80% organic content $D = 1$ spectra (top curve) revealed a large loss in the epoxide content with 150 °C curing, as evidenced by losses in peak intensities at 760 cm^{-1} , 908 cm^{-1} , and 1256 cm^{-1} . However, this dramatic loss in epoxide peak intensity w/elevated curing temperatures occurred without any noticeable development of an 847 cm^{-1} $\equiv\text{C}-\text{O}-\text{C}\equiv$ ether linkage. A new peak did arise at 1735 cm^{-1} , but this peak is attributed to $=\text{C}=\text{O}$ stretch vibration. The intense development of the $=\text{C}=\text{O}$ stretch without development in the 847 cm^{-1} ether vibration indicated that the epoxide group decomposed to form a carbonyl species rather than undergoing polymerization.

Inspection of the $D = 6$ spectra (lower 2 curves) in Figure 8.7 shows that the RT-cured gels have far less intact epoxide than the comparable $D = 1$ gel. The RT-cured gel epoxide content, while minimal, was still identified by the small peaks at 760 cm^{-1} , 908 cm^{-1} , and 1256 cm^{-1} . After curing these gels to 150 °C, the resultant spectrum revealed complete loss of the epoxide peaks without any development of the 847 cm^{-1} ether vibration. A small peak was observed at 1726 cm^{-1} , consistent with carbonyl formation. The relatively weak intensity of the $=\text{C}=\text{O}$ stretch indicated that only minimal amounts of the epoxide or diol had decomposed to form the carbonyl. With essentially complete

epoxide loss and minimal carbonyl formation, the epoxide group was postulated to have been hydrolyzed, forming a diol (with residual water) rather undergoing the necessary rearrangement reactions to form aldehyde or ketone end groups.

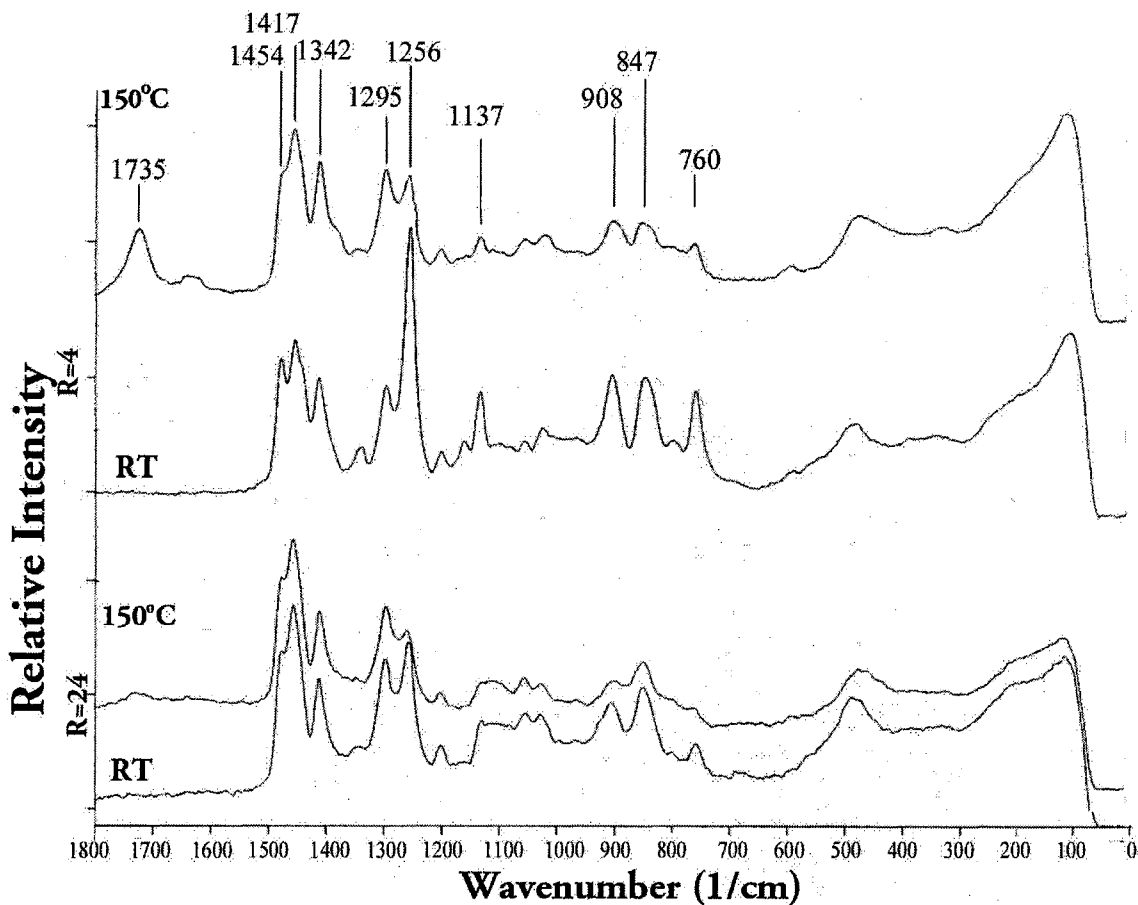


Figure 8.7: Raman spectra of the fingerprint region for the 80% organic content gels cured at room temperature and 150 °C.

8.3.7 Proposed Mechanism of Decomposition

Since epoxide polymerization could not be induced even in the $D = 1$ 80% organic content gel, the aldehyde/ketone formations at elevated curing temperature was attributed to a combination of limited epoxide mobility within the gel matrix and very low concentration of residual water. In the 80% organic content $D = 1$ gel, the silica network

was found to be completely hydrolyzed, giving rise to a well developed siloxane network. Complete hydrolysis at such low D values would imply that effectively all of the water would be tied up in the form of diols and/or siloxane bridges. Thus, very little water would be available in residual form and hydrolysis of the epoxide ring would not occur. The presence of a rigid, developed silica network has the potential to severely limit the mobility of organic functional groups and inhibit the interactions between epoxide groups. Since the epoxide groups were unable to polymerize, due to mobility restrictions, the ethylene oxide ring eventually underwent rearrangement forming an aldehyde or ketone (see Reaction 8.5). Thus, even under conditions when epoxide crosslinking should be favored (e.g., high epoxide content, low water activity), polymerization could not be induced due to the motion-restricting network-inhibiting nature of the intervening polysiloxane network.

Formation of minimal quantities of aldehyde/ketone end groups in the 80% epoxide, D = 6 gel was attributed to the formation of more stable end products, such as diol groups and/or carbosiloxane bonds. The hybrid gels prepared under conditions of excess water had substantial residual water trapped in the pores of the matrix. Exposure to heat in the presence of water resulted in more thorough hydrolysis of the epoxide to form the more stable diol. In addition, low D value gels with carbosiloxane formations were also found to stabilize the end group. Thus, the lower degree of decomposition for the high D valued gels was attributed to a combination of diol formation prior to curing, carbosiloxane formations in the gel, and/or hydrolysis of the epoxide group upon curing.

8.5 Conclusion

The Raman spectra of water-based epoxide ormosil gels were investigated and monitored as a function of D value, organic content, and curing temperature. Raman assignments were consistent with NMR results and proposed structures presented in Chapter 7. Epoxide losses at room temperature were identified with a decrease in organic content and an increase in D value. The decomposition products at room temperature were identified as diol and carbosiloxane formations in the low D = 1 gels, while diol formation was the prominent formation in the higher D valued gels. Variations in the siloxane development indicated the 60% and lower organic content gels prepared with high D values were phase segregated.

Curing of the hybrid gels to 150 °C did not result in epoxide polymerization, but showed signs of decomposition. In the low D value 80% organic content gel, the epoxide group decomposed to an aldehyde/ketone formation. Decomposition was attributed to the absence of water and restricted mobility of the epoxide group. In all other systems, minimal signs of aldehyde/ketone decomposition were observed.

Curing in the silica network was observed to be minimal. Variations in the densification mechanism were correlated with orientation of functional group into the network and at the pore surface. In the low D = 1 gels, the development in surface condensed sites and carbosiloxane linkages was indirectly correlated with incorporation of the functional group into the silica network. In the higher D valued gels, the lack of surface densification and loss of alkoxide type linkages was indirectly correlated with orientation of the organically modified silicates towards surface sites.

CHAPTER 9

INVESTIGATION OF EPOXIDE ORMOSIL THIN FILMS DERIVED FROM A WATER-BASED SOL GEL PROCESS

9.1 Introduction

In this study, the relationships between the epoxide stability, diol formation, and growth of a siloxane network were investigated through the use of IR reflectance spectroscopy. Previous studies (solid state NMR, Chapter 7, and Raman spectroscopy, Chapter 8) focused on epoxide based ormosil gels, and identified evidence correlating chemical reactions in the sol phase, such as epoxide losses, to the evolution of network-modifying species such as diol formation. Direct evidence of a carbosiloxane formation, however, was not conclusively identified. A complementary spectroscopy method, FT-IR is well suited for detection of the strong absorption characteristics found in the $\equiv\text{Si-O-C}\equiv$ vibrations. This approach, then, can serve as a more effective means to identify hybrid $\equiv\text{Si-O-C}\equiv$ linkages and demonstrate a direct coupling between epoxide loss and carbosiloxane formations. Infrared spectra have been collected for epoxide ormosil films prepared using different water/alkoxide ratios and organic content. The formation and structural influences of carbosiloxane formation were investigated and correlated with material processing conditions.

Decomposition of epoxide functional groups has been shown to alter the mechanism in which the organically modified silicate is incorporated into a hybrid

system. In the literature, hybrid films prepared using GPTMS precursor have been investigated in a number of different systems. In most of the reported studies, the influence of the epoxide group has largely been ignored, as it is assumed to be incorporated into the silica network in the same manner as traditional organically modified silicates. Unlike other modified silicate precursors, however, we now know that the epoxide functionalities are susceptible to hydrolysis, especially in aqueous solution, and can result in the conversion of epoxides into diols functionalities. Evidence suggests that diol formation in the sol can significantly alter the mechanism by which the gel network forms and can significantly alter the film composition and microstructure. Hybrid polymers having elevated carbosiloxane bond density, for example, tend to yield a co-polymer system where the organic group is intimately incorporated into the matrix. Conditions in which carbosiloxane bonds are hydrolyzed, on the other hand, cause the organic additives to act as network modifiers with reduced organic-inorganic interaction. Thus, the most influential factors in determining how the organic group is incorporated into epoxide-modified silicate (1) the stability of the epoxide group under the selected preparative conditions, and (2) the chemical nature of the interactions between the diol and silanol functionalities.

In this chapter, water-based epoxide ormosil thin films were investigated using single reflectance FT-IR spectroscopy. Hybrid epoxide-modified silicate films composed of 10%, 20%, 40%, 60%, and 80% organic content were prepared using D values of 1, 2, 4, and 6. Films were coated onto aluminum substrates and cured at room temperature, 60 °C, 150 °C, and 300 °C. Single reflectance FT-IR spectra were acquired and compared as a function of D value, organic content, and curing temperature. Spectral variations were used to identify the effects of water/alkoxide ratios, stability of the epoxide functional

group, formation and influence of the carbosiloxane linkage, influence of organic content on densification, and incorporation of the organic hybrid precursors in the siloxane network.

9.2 Background

In the literature, very few studies have focused on the use of infrared spectroscopy to investigate epoxide-modified silicate materials. The ability to detect organic species in a silica based material by IR spectroscopy is somewhat limited, due to the strong absorption characteristics of the $\equiv\text{Si-O-}$ stretch vibrations (for Si-O-X , where $X = -\text{Si}\equiv$, $-\text{H}$, or $-\text{CH}_3$). In ormosil systems with low organic content, for example, organic vibrations (e.g., $\equiv\text{C-C}\equiv$, $\equiv\text{C-H}$, and $\equiv\text{C-O-}$) are generally obscured by the more intense $\equiv\text{Si-O-}$ vibrations. IR spectra of ormosil materials with small amounts of organic species do not exhibit characteristic organic vibrations unless the organic content is comparatively high. In a paper published by Capozzi and co-workers regarding ormosils with methyl modified silicates, the $\equiv\text{C-H}$ stretch vibrations of the hybrid materials were not observed using IR methods for specimens in which the content was below 33%. The limitations imposed by the relative intensity ratio between $\equiv\text{Si-O-}$ and organic vibrations limits the ability to detect organic functionalities.

Spectral interpretations of ormosils having elevated organic content can also be problematic. Spectral features attributable to $\equiv\text{Si-O-}$, $\equiv\text{C-O-}$, and/or $\equiv\text{C-C}\equiv$, peaks commonly assumed to be present in ormosils with elevated organic content, tend to have substantial overlap. Since the silica vibrations are generally broad vibrations and occur in the region between 800 cm^{-1} and 1200 cm^{-1} , organic vibrations, such as $\equiv\text{C-O-C}\equiv$, $\equiv\text{C-}$

C–O–, and $\equiv\text{C}-\text{C}\equiv$ stretching, can overlap the silica vibrations, thereby reducing peak resolvability.

9.2.1 Vibrational Assignments

A comprehensive review of all the reported FT-IR peak assignments for comparable media is given in Table 9.1. The table references were compiled from studies conducted on collection of several different types of organically modified silicate systems. Organic vibrations, which have not been previously identified in studies on ormosil systems, were taken from comprehensive IR handbooks on inorganic and organic materials.

Table 9.1: Representative vibrational frequencies and assignments for observed bands epoxide based ormosil thin films coated on aluminum substrates.

Frequency	Vibrational Assignment	References
430 cm ⁻¹	Symmetric Stretch SiO ₂ Bending (in plane)	59-61, 90, 100, 105, 107-115
480 cm ⁻¹	≡C-O-C≡ deformation	59-61,109
763 cm ⁻¹	Epoxy ring deformation (symmetric)	54, 59-61
700-830 cm ⁻¹	≡Si-CH ₂ -	59,116,147
800 cm ⁻¹	Bending SiO ₂	59-61, 90, 100, 105, 107-115
847 cm ⁻¹	≡Si-C≡ stretch (symmetric)	59,61116
875 cm ⁻¹	In phase ≡C-C-O stretch	59-61
890 cm ⁻¹	≡C-O-C≡ Stretching	59-61, 141
908 cm ⁻¹	Epoxy ring deformation (anti-symmetric)	59-61, 141
910-970 cm ⁻¹	≡Si-O-H Stretching	59-61, 90, 100, 105, 107-115
1000-1100 cm ⁻¹	Anti-symmetric stretch ≡Si-O-Si≡ (T.O)	59-61, 90, 100, 105, 107-115
1075-1200 cm ⁻¹	≡Si-O-C≡ Stretching TEOS	59-61,109,148
1100-1200 cm ⁻¹	≡C-O-C≡ Anti-stretch	59-61, 109, 141,148
1100-1200 cm ⁻¹	Anti-symmetric stretch ≡Si-O-Si≡ (L.O)	59-61, 90, 100, 105, 107-115
1200-1250	≡Si-CH ₂ - (CH ₂ Wag)	59,116,140,146-8
1256 cm ⁻¹	Epoxy ring breathing	59-61,146
1295 cm ⁻¹	=CH ₂ in phase twisting	59-61
1342 cm ⁻¹	≡C-H wag	59-61
1454 cm ⁻¹	=CH ₂ Symmetric Deformation	59-61
1485 cm ⁻¹	=CH ₂ bend	59-61
1632 cm ⁻¹	Absorbed H ₂ O	59-61,138
2878 cm ⁻¹	=CH ₂ Symmetric stretch	59-61,105,116,140
2938 cm ⁻¹	=CH ₂ Anti-symmetric stretch	59-61,105,116,140
3005 cm ⁻¹	Epoxy ring (CH ₂) Symmetric stretch	59-61,122
3055 cm ⁻¹	Epoxy ring (CH ₂) Anti-symmetric stretch	59-61,122
3200-3400 cm ⁻¹	-O-H Stretching	59-61

9.3 Results and Discussion

The results have been divided into three sections. Section 9.3.1 focuses on variations in the hybrid films as a function of organic content. Section 9.3.2 focuses on variations in the hybrid films as a function of D value. Section 9.3.3. focuses on structural developments in hybrid layers as function of curing temperature. Conclusions drawn from each section were used to identify the chemical structure of hybrid films prepared and processed under different conditions.

9.3.1 Influence of Organic Content on Hybrid Films

9.3.1.a Influence of Organic Content on Films Prepared with Low D values:

Figure 9.1 represents a series of IR reflectance spectra as a function of organic content (curves correspond to 10%, 20%, 40%, 60%, and 80% organic content) for films prepared using a D value of 1. The following peak assignments represented in Table 9.2 have been made based on literature references and trends observed the ormosil specimens under investigation. These eleven peaks serve as the basis for most of the chemical assignments made in this chapter.

Table 9.2 Peak assignments based on literature references.

	Wavenumber	Vibrational Assignment	Structural Group
	940	Si-OH Stretch	Silanol
Extensive Overlap	1040	$\equiv\text{Si-O-Si}\equiv$ Anti-Symmetric Stretch (T.O)	Siloxane
	1180	$\equiv\text{Si-O-Si}\equiv$ Anti-Symmetric Stretch (L.O)	Siloxane
	1180	$\equiv\text{Si-O-C}\equiv$ Stretch	Carbosiloxane
	1200	$\equiv\text{C-C-O-}$ Stretch	Ether
	1400	$=\text{CH}_2$ (twist, bending, wag, deformation)	Methylene Group
	2878	$\equiv\text{C-H}$ Symmetric Stretch	Methylene Group
	2938	$\equiv\text{C-H}$ Anti-symmetric Stretch	Methylene Group
	1256	$=\text{C}^{\text{-O-}}\text{C}=\text{}$ Ring Breathing	Epoxy Ring
	3005	$=\text{C}^{\text{-O-}}\text{C}=\text{(CH)}$ Symmetric Stretch	Epoxy Ring
	3055	$=\text{C}^{\text{-O-}}\text{C}=\text{(CH)}$ Anti-symmetric Stretch	Epoxy Ring

Figures 9.1 (full spectrum) and 9.2 (fingerprint region) show the change that take place in the FT-IR spectra of epoxide ormosils as a function of organic content. In the 10%-60% organic content D = 1 gels, examination of Figure 9.2 indicates that the silanol (940 cm^{-1}) peak decreases as a function of increasing organic content. Similarly, siloxane formation (1040 cm^{-1} , anti-symmetric T.O. bond) decreases with increasing organic content. The overlapping siloxane/carbosiloxane peak (centered at 1180 cm^{-1}) appears to decrease in intensity going from 10% to 20%, and then rapidly increases for the 40% and 60% organic content gels. This is interpreted as an indication that the siloxane network formation is continuously decreasing over the composition range, consistent with the declining 1040 cm^{-1} peak intensity (T.O. bond), while the carbosiloxane peak increases over the same range. Evidence of the presence of methylene groups (1400 cm^{-1} , 2878 cm^{-1} , 2938 cm^{-1}) is observed in the spectra of the 40% and 60% organic content gels.

¹, and 2938 cm⁻¹) from the glycidoxypropyl organic side group increases as a function of organic content. Peaks associated with epoxide groups (1256 cm⁻¹, 3005 cm⁻¹, and 3055 cm⁻¹) are absent in the 10%-60% organic content specimens, indicating decomposition. The transition in gel composition from 10% to 60% organic content, then, is consistent with increasing epoxide hydrolysis, forming diols that can condense with the polysiloxane network to form an intimately mixed organic-inorganic copolymer.

As in previous chapters, a discontinuity appears in the case of the 80% organic content (D = 1) gels with respect to the 10%-60% series. The epoxide peaks (1256 cm⁻¹, 3005 cm⁻¹, and 3055 cm⁻¹) are visible, indicating the presence of intact epoxide rings in this composition. The carbosiloxane peak (1180 cm⁻¹) is substantially reduced in intensity from the 60% specimen, while the ether (1200 cm⁻¹) and silanol (940 cm⁻¹) peaks become dominant features. The most striking trend reversals observed when transitioning from 60% to 80% organic composition are (1) the dramatic increase in silanol, and (2) the evidence of reduced carbosiloxane formation. This data is consistent with an 80% organic content gel that has limited organic-inorganic linkage formation (e.g., undergoes phase separation).

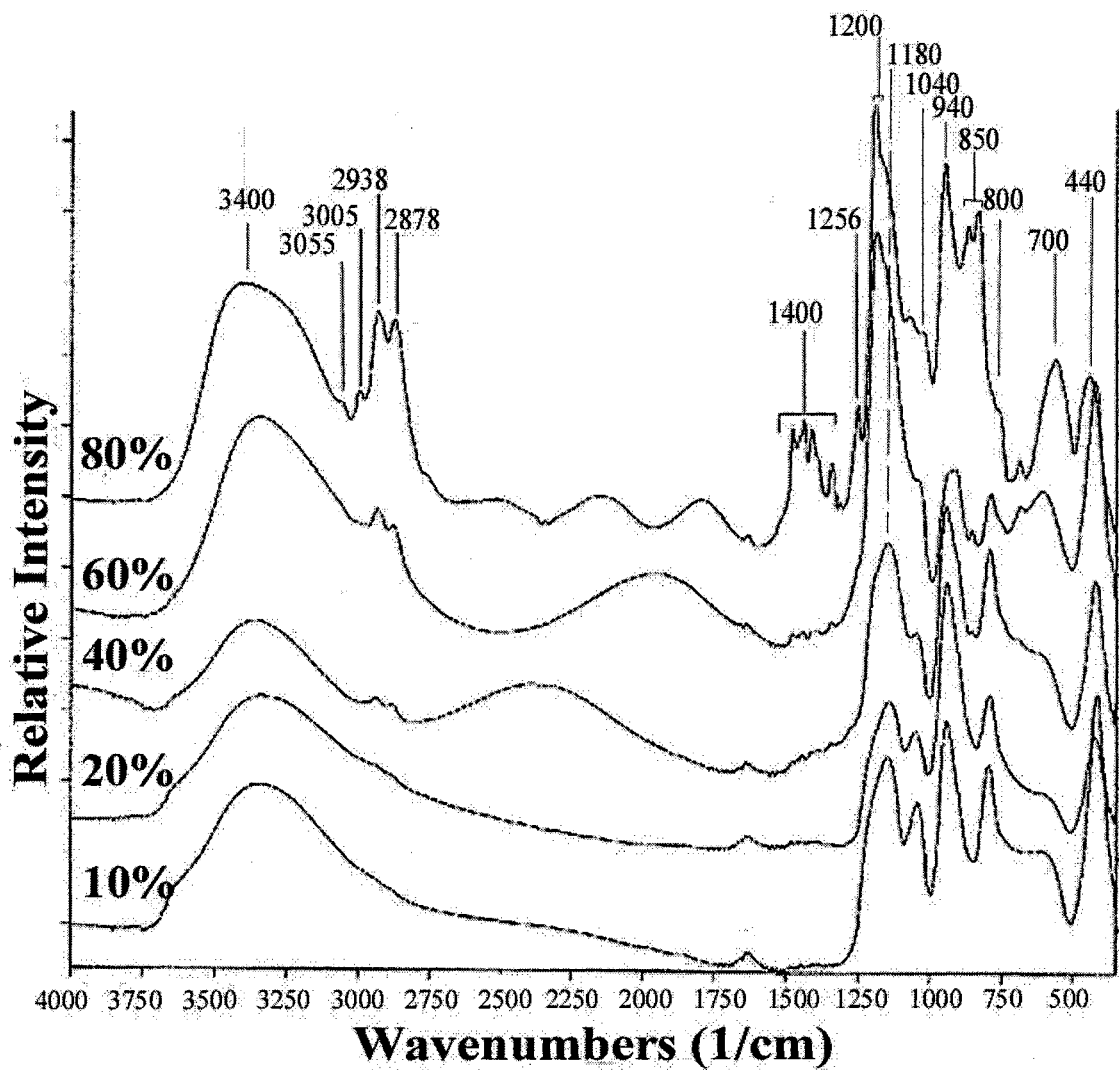


Figure 9.1: Overlaid IR reflectance spectra of epoxide-based ormosil thin film prepared using an D value of 1 and cured at room temperature.

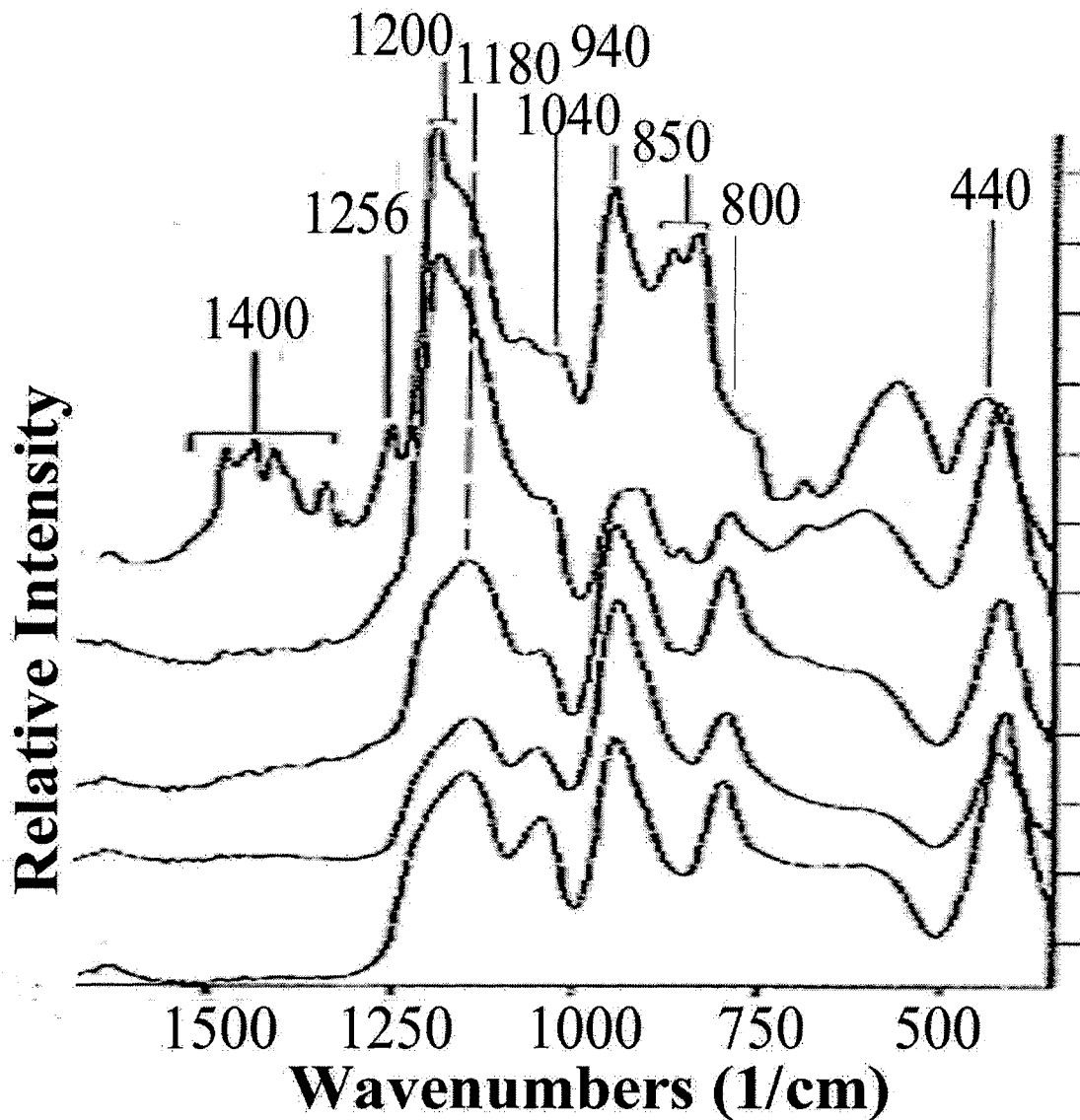


Figure 9.2: Overlaid IR reflectance spectra of epoxide-based ormosil thin film prepared using an D value of 1 and cured at room temperature.

9.3.1.2 Effect of Organic Content on Polymer Chemistry of Higher Water Content (D = 6) Films Cured at Room Temperature

Examination of the spectra in Figures 9.3 and 9.4 show again that (1) water content has a dramatic effect on hybrid film chemistry (e.g., see comparable spectra for comparable D = 1 films in Figure 9.1 and 9.2), and that (2) the 60% and lower organic content films are once again structurally quite different from the 80% organic content

film. For the 10%-60% organic content ($D = 6$) set, a well developed 1040 cm^{-1} siloxane peak become much more intense with increasing organic content. There is little evidence of a carbosiloxane formation (peak centered at 1180 cm^{-1}). The 940 cm^{-1} peak (silanol vibration) was also observed to increase slowly as a function of organic content. There was no evidence of intact epoxide group in any of these specimens. Based on the relative peak intensities associated with siloxane (1040 cm^{-1}), methylene (2878 cm^{-1} and 2938 cm^{-1}), and silanol (940 cm^{-1}) species, the 60% and lower organic film compositions prepared with elevated water activity ($D = 6$) were characterized by well developed siloxane networks with very little hybrid carbosiloxane bridge formation. As previously postulated, increasing silanol population develops as a function of organic content combined with steric effects induced by the comparatively large organic side chain. The steric effects tend to limit the reactivity of adjacent silanol groups, thereby preventing full crosslinking in the hybrid polymers.

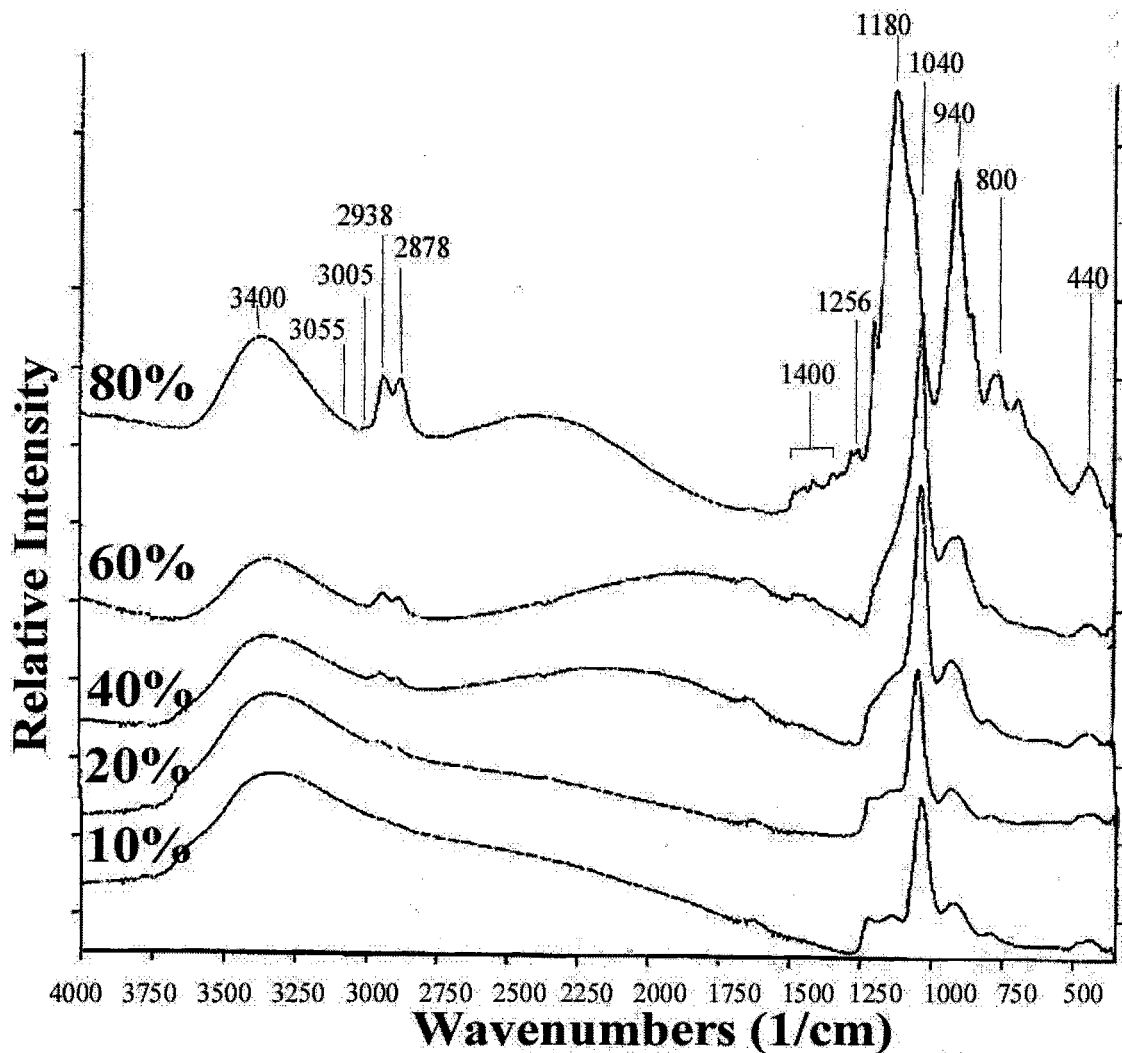


Figure 9.3: Overlaid IR reflectance spectra of epoxide-based ormosil thin film prepared using an D value of 6 and cured at room temperature.

The 80% D = 6 organic content film was significantly different from the 80% D = 1 film (e.g., see 80% spectrum in Figure 9.3 and the spectrum for 80% D = 1 film in Figure 9.1). Unlike the 80% (D = 1) film, the 80% (D = 6) film did not exhibit signs of intact epoxide functionality. This indicated that the increased water activity had caused hydrolysis of most or all of the epoxide groups. The 80% (D = 6) films are also quite different from the 10%-60% organic content series. The 940 cm^{-1} peak indicates substantial silanol content in these films. The intense 1180 cm^{-1} (siloxane

L.O./carbosiloxane) absorption band was noted to be absent the siloxane T.O. companion bond, indicating little polysiloxane network formation, but extensive carbosiloxane crosslinkage. The dominant 1200 cm^{-1} peak corresponds, as in Figure 9.2, to the expected rise in ether linkage density arising from the increased activity of the ormoocer precursor. These results are consistent with earlier findings (Section 8.4.2) that indicate the 80% organic ($D = 6$) films are comprised of a non-bridging silanol-rich network linking the hydrolyzed organic phase to a weakly developed siloxane network through extensive carbosiloxane bond formation.

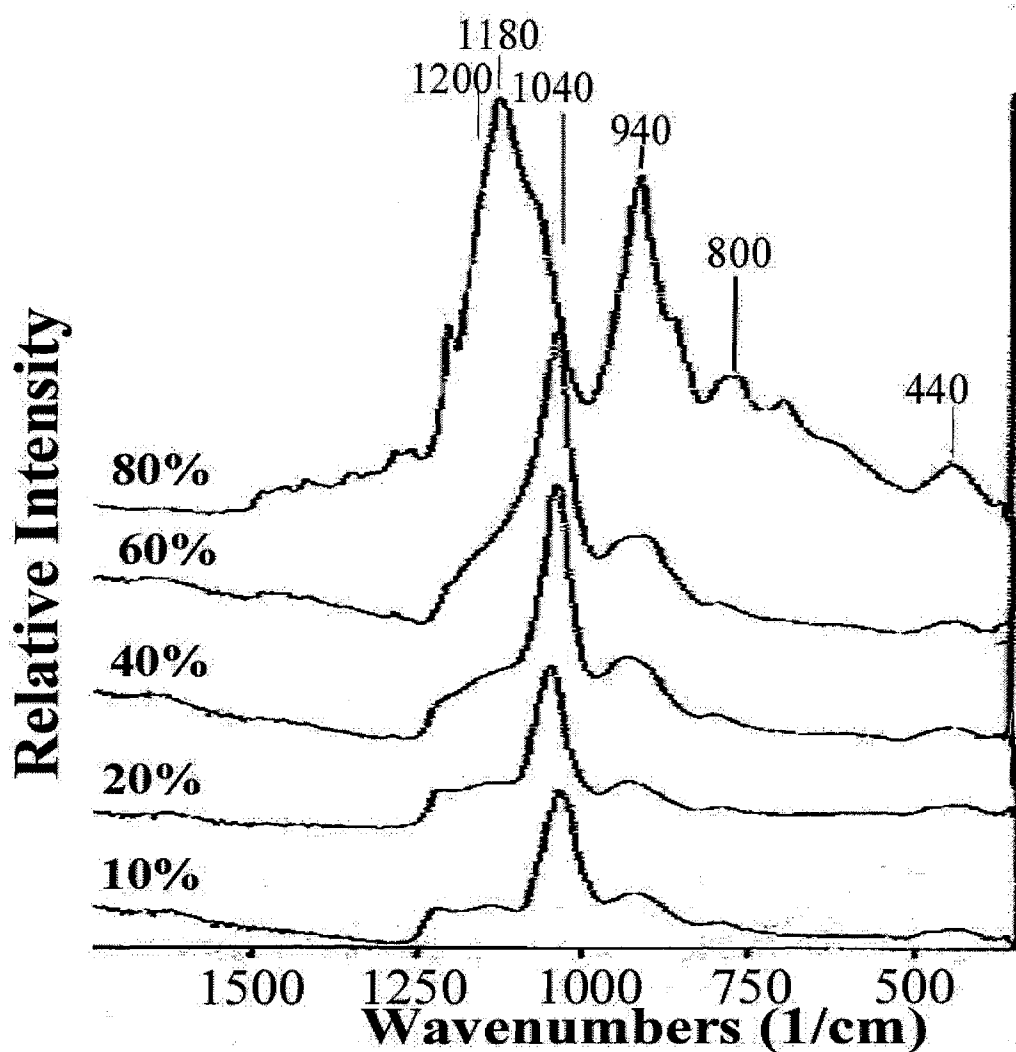


Figure 9.4: Overlaid IR reflectance spectra of epoxide-based ormosil thin film prepared using an D value of 6 and cured at room temperature.

9.3.2 Variations in the Hybrid Films as a Function of D Value

The next set of studies was aimed at elucidating the effects of water activity on gels having 20%, 60%, and 80% organic content. Films were prepared using D values of 1, 2, 4, and 6, and cured at room temperature. Spectral interpretations are used to identify the effects of water content on siloxane development, carbosiloxane formation, and epoxide decomposition for each hybrid composition studied.

9.3.2.1 Effects of Water Content on 20% Organic Content Films

Figure 9.5 represents the spectra acquired for the 20% organic content films prepared using D values of 1, 2, 4, and 6. The D = 1 spectrum is dominated by the intense peak at 940 cm^{-1} , indicating extensive silanol formation. As the amount of water is increased, the intensity of the silanol peak decreases rapidly. The 1040 cm^{-1} peak, on the other hand, has low intensity at D = 1 and rapidly increases as a function of water content. The 1040 cm^{-1} (T.O. siloxane) bond is the most intense peak of the D = 6 spectrum, indicating that the film transition from one with limited polysiloxane network formation, in the case of limited water addition (D = 1), to one with extensive polysiloxane network formation in a system with excess water (D = 6). The comparatively large intensity of the 1180 cm^{-1} band found for the D = 1 spectrum is consistent with a moderate to extensive carbosiloxane formation. The tendency to exhibit substantial carbosiloxane bond densities decreased rapidly, however, as water content was increased from D = 1 to D = 6. It is postulated that the carbosiloxane bonds are hydrolyzed under conditions of elevated water content for 20% organic content gels.

20% Hybrid Content Films

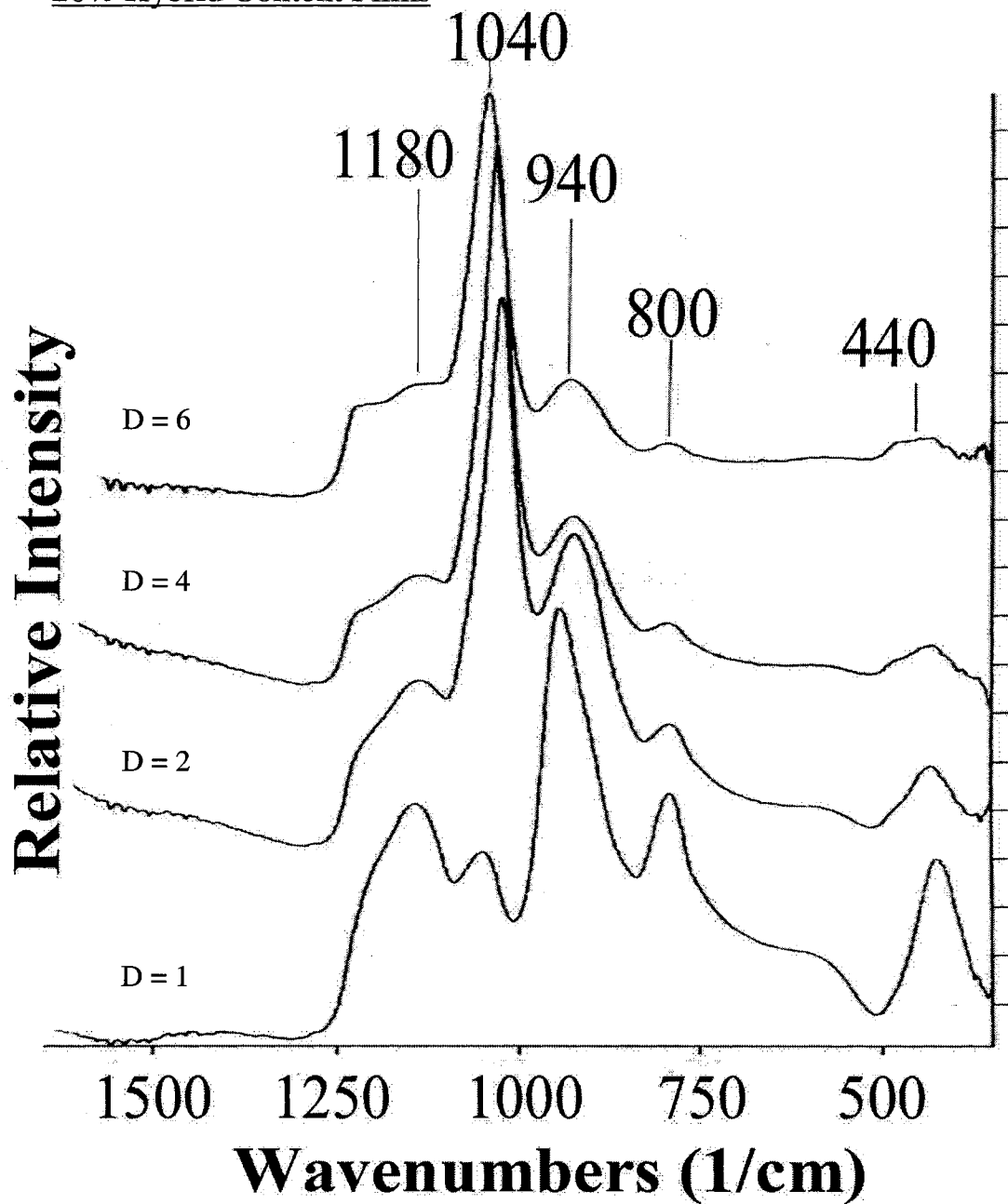


Figure 9.5: Overlaid IR reflectance spectra of 20% organic content ormosil film prepared using a D values of 1, 2, 4, and 6. Films were cured in air at room temperature.

9.3.2.2 Effects of Water Content on 60% Organic Content Films

Figure 9.6 represents the spectra acquired for the 60% organic content films prepared using D values of 1, 2, 4, and 6. The D = 1 and 2 spectra are dominated by the intense peak at 1180 cm^{-1} , indicating extensive carbosiloxane formation. As the amount of water is increased, the intensity of the carbosiloxane peak decreases rapidly in the elevated water content spectra. The 1040 cm^{-1} peak, on the other hand, has low intensities in the D = 1 and 2 and rapidly increases with water addition as observed in the D = 4 and 6 spectra. The intense 1040 cm^{-1} (T.O. siloxane) peak in the D = 6 spectrum indicated that the film contained extensive polysiloxane network formation. In the case of limited water addition (D = 1 and 2), the intense 1180 cm^{-1} (carbosiloxane) peak indicated that the film contained copolymer networks with both carbosiloxane and siloxane linkages. The abrupt intensity loss in the 1180 cm^{-1} and rapid increase in the 1040 cm^{-1} siloxane peak, during the increase in D value from 2 to 4, indicated that extensive carbosiloxane bond densities decreased rapidly. It is postulated that the carbosiloxane bonds are hydrolyzed under conditions of elevated water content for 60% organic content gels and lead to rapid development of the siloxane network.

60% Organic Content Films 1040

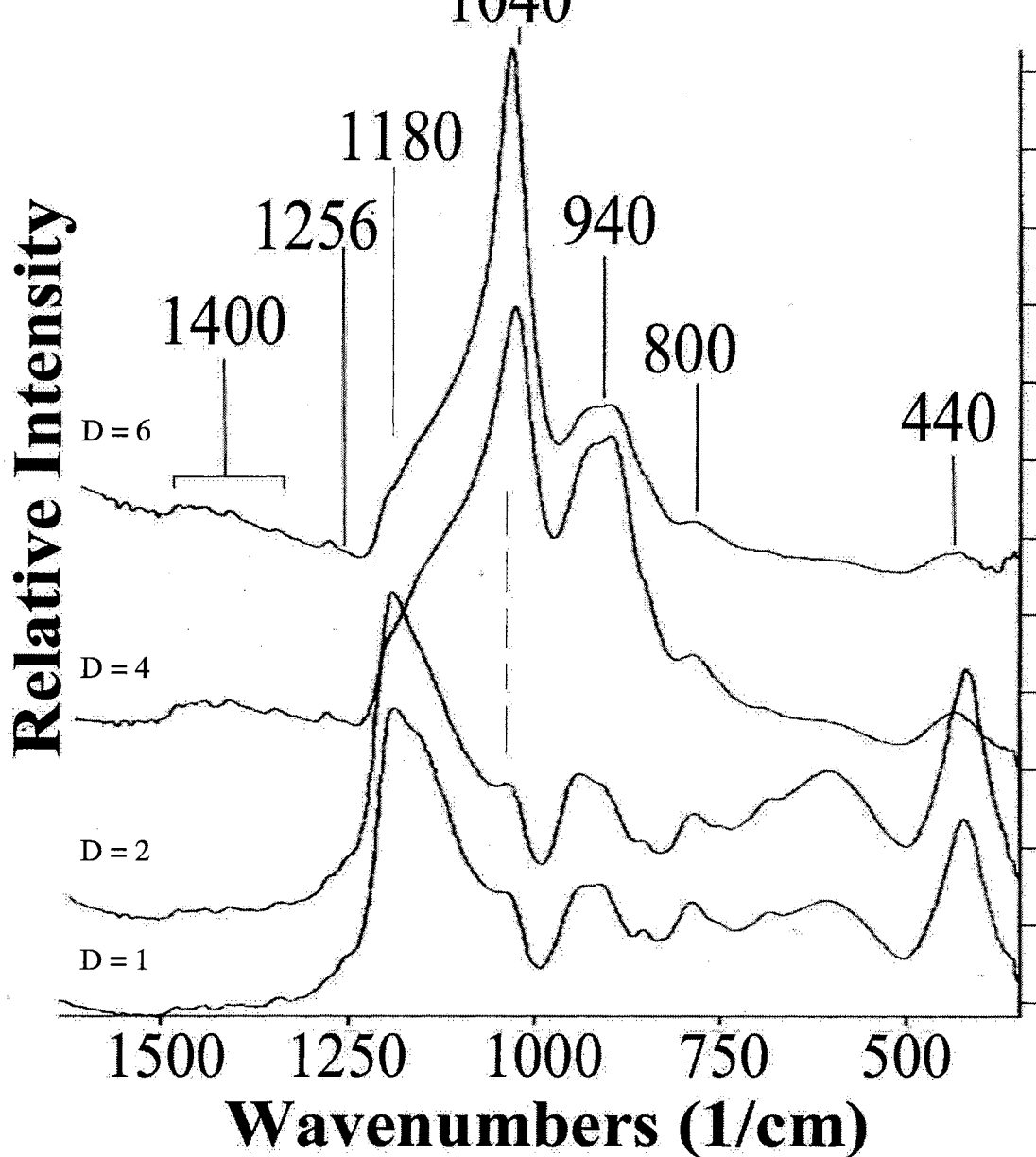


Figure 9.6: Overlaid IR reflectance spectra of 60% organic content ormosil film prepared using a D values of 1, 2, 4, and 6. Films were cured in air at room temperature.

9.3.2.3 Effects of Water Content on 80% Organic Content Films

Spectral differences arising as a function of increasing water content in the 80% organic content films are shown in Figure 9.7. Among the most striking developments are (1) the progressive decomposition of the epoxide functionality as water content increases, and (2) evidence of development of a hybrid co-polymer network. In the $D = 1$ spectrum, epoxide loss was minimal. In the $D = 6$ sample, intensities of the peaks associated with the presence of epoxide had essentially disappeared.

In cases where epoxide groups remained substantially intact (e.g., $D = 1$ or 2), the 80% organic content films were found to be comprised of a minor siloxane network component (as evidenced by the small 1040 cm^{-1} peak) and silanol species (940 cm^{-1}). There was no evidence to support the presence of carbosiloxane species in the 80% organic component films prepared under low D value conditions. In cases where epoxide loss and carbosiloxane formation are prevented, a fully developed siloxane network is formed.

Decomposition of the epoxide group in the $D = 4$ and 6 sols resulted in films composed much more substantially of carbosiloxane, rather than polysiloxane linkages. Examination of the $D = 2$ and 4 spectra reveal a decrease in the intensity of epoxide peaks with a corresponding decrease in the 1040 cm^{-1} siloxane peak and strong increase in the 1200 cm^{-1} carbosiloxane peak. Absence of a siloxane peak in conjunction with substantial development in the carbosiloxane peak, implies that the film microstructure was composed of a co-polymer network with elevated concentrations of silanol and alkoxide precursors inner-connected through carbosiloxane linkages.

The subtle variations in $\equiv\text{Si-O-C}\equiv$ and $\equiv\text{Si-O-H}$ affiliated peak intensities for $D=4$ and 6 spectra indicated the carbosiloxane products were more fully hydrolyzed in the

80% organic content with elevated water activity. Examination of Figure 9.8, D = 4 and 24 spectra, revealed the 1200 cm^{-1} carbosiloxane peak decreased with a concomitant increase in the 940 cm^{-1} silanol vibration. The increase in silanol content parallels the observed carbosiloxane formation.

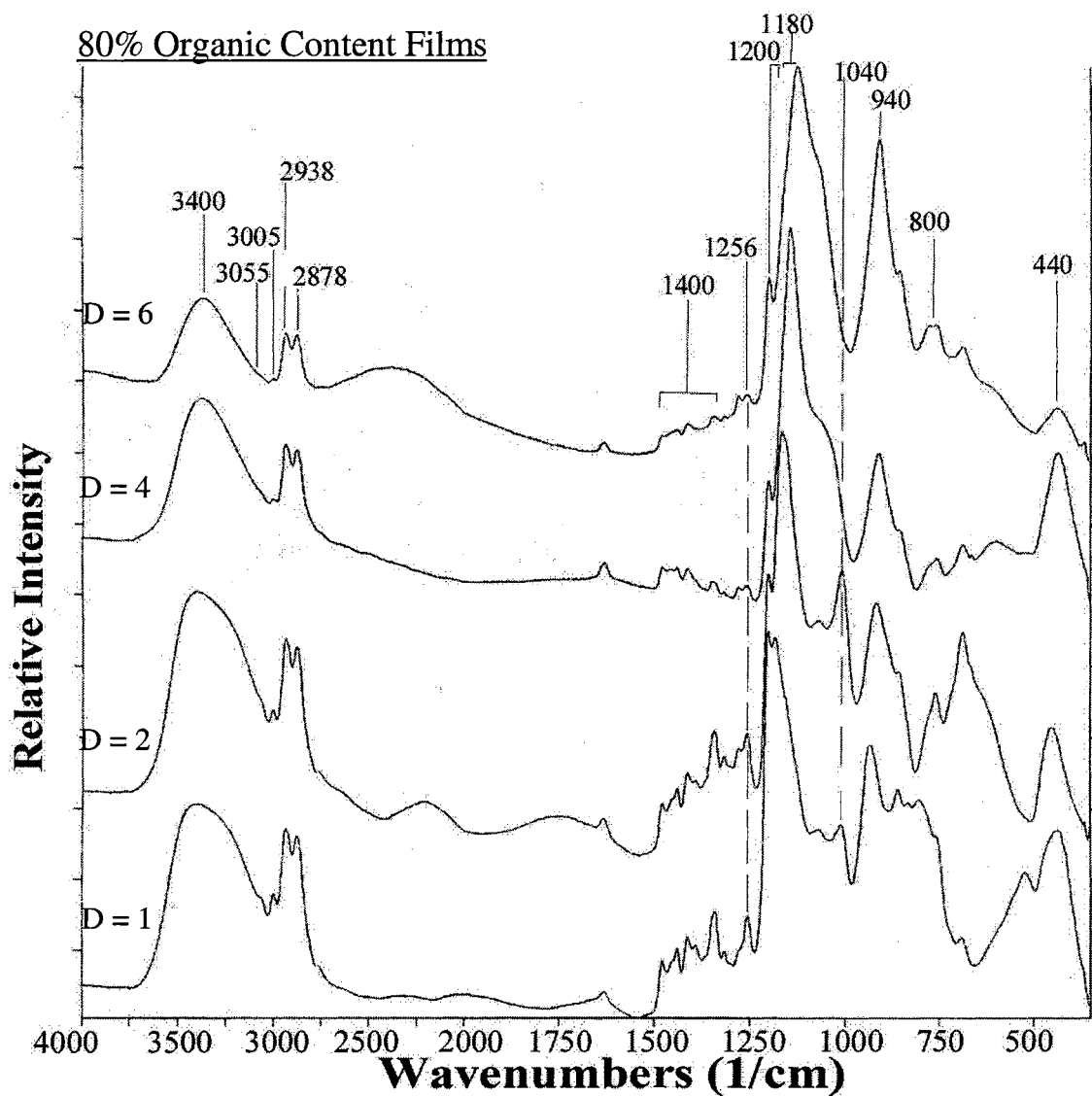


Figure 9.7: Overlaid IR reflectance spectra of 80% organic content ormosil film prepared using a D values of 1, 2, 4, and 6. Films were cured in air at room temperature.

9.3.3 Structural Developments in Hybrid Films as a Function of Curing Temperature

Figures 9.8 through 9.11 represent a series of spectra aimed at developing an understanding of the influence of gel curing temperature for selected epoxide hybrid coatings prepared using D values of 1 and 6. Films were cured at room temperature, 60 °C, 150 °C, and 300 °C. Peak changes were monitored in each spectrum to identify the developments and/or losses in the siloxane network, epoxide content, stability of the carbosiloxane bond formations, and silanol content.

9.3.3.1 Curing of 60% Organic Content ($D = 1$) Films

Spectral differences arising as a function of increasing curing temperature in the 60% organic content $D = 1$ film are shown in Figure 9.8. Among the most striking developments are the (1) densification of silanol species at low temperature and (2) decomposition of the carbosiloxane linkage at elevated temperature.

In the room temperature spectrum, the 60% organic content film was found to be comprised of a copolymer network with carbosiloxane (as evidenced by the large 1180 cm^{-1}) and siloxane network components (as evidenced by the small 1040 cm^{-1} peak) with non-bridging silanol species (940 cm^{-1}) present. In curing the film up to 150 °C, the 940 cm^{-1} silanol peak decreased with respect to the 1040 cm^{-1} siloxane peak, evidence of densification. Condensation between neighboring silanols or diol end groups would lead to development of the 1040 cm^{-1} and 1180 cm^{-1} peaks, as seen in Figure 9.8, and is the postulated condensation mechanism. The loss of the 940 cm^{-1} silanol peak with respect to the 1040 cm^{-1} siloxane peak, for curing temperatures of 150 °C and less, was evidence

of densification. Distinction between carbosiloxane and siloxane bond formations was not confirmed.

Examination of spectral changes between the 150 °C and 300 °C 60% organic content D = 1 spectra gives evidence of substantial decomposition in the carbosiloxane network. The 150 °C spectrum indicated the hybrid film was composed of a co-polymer network with siloxane network formation and carbosiloxane linkage formation. Upon curing to 300 °C, the spectrum revealed substantial losses in the 1180 cm⁻¹ carbosiloxane peak. Loss of the methylene-type organic fragments is evidence by disappearance of the characteristic peaks at 2878 cm⁻¹ and 2939 cm⁻¹. It should be noted that the 300 °C curing was magnified 5-fold in this figure in order to have it appear on the same scale as the other spectra. The 300°C curing was accompanied by substantial material loss, leaving a much lower mass film to characterize. The decomposition of carbosiloxane linkages, was expected to occur at elevated temperatures based on reported decompositions of the ≡Si-O-C≡ bond, and the volatilization of the organic species apparently caused the film network to disintegrate. This result strongly suggests the formation of a highly integrated organic-inorganic network for this particular film composition. Heating to temperatures which cause carbosiloxane dissociation and organic group volatilization results in a widespread breakdown of the chemical bonds which hold the film together, thus leading to the type of disintegration observed.

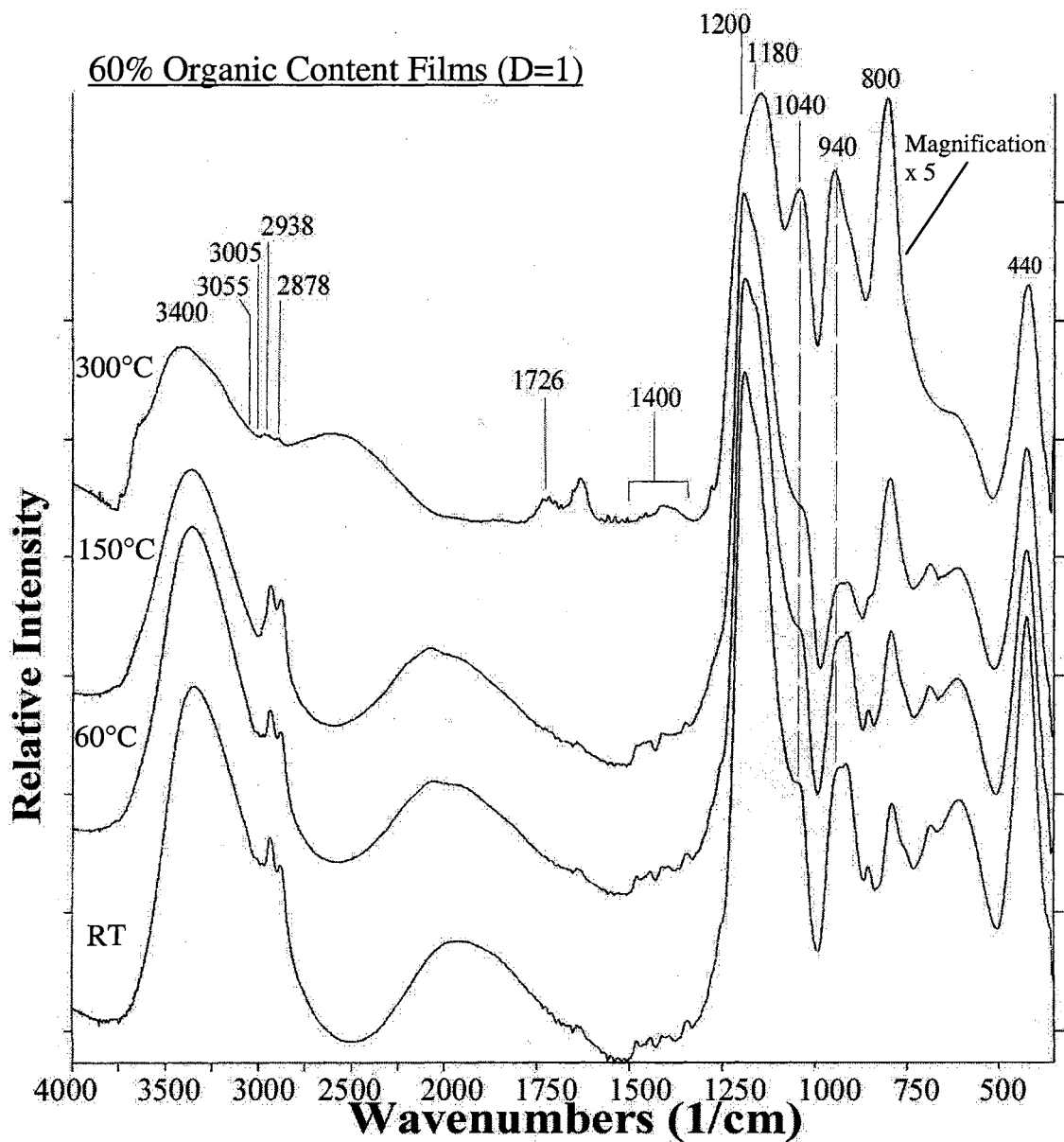


Figure 9.8: Overlaid IR reflectance spectra of 60% organic content ormosil film prepared using a D values of 1 and cured in air at room temperature, 60 °C, 150 °C, and 300 °C.

9.3.3.2 Curing of 60% Organic Content (D = 6) Films

Curing of the 60% organic content film prepared with a D value of 6 provided evidence supportive of the development of a phase segregated system largely composed

of a polysiloxane network, as evidenced by the intense 1040 cm^{-1} peak for all curing temperatures (see Figure 9.9). The room temperature cured specimen was found to exhibit extensive siloxane development with limited silanol species and little or no apparent carbosiloxane formation. It can be that the 940 cm^{-1} silanol peak, which has moderate intensity at RT cure, is substantially eliminated after curing to $150\text{ }^{\circ}\text{C}$. There is little or no change in the silanol peak above $150\text{ }^{\circ}\text{C}$. Peaks associated w/ methylene organic groups (2878 cm^{-1} and 2939 cm^{-1}) are seen to diminish in intensity with curing temperatures above $150\text{ }^{\circ}\text{C}$. The film dried at $300\text{ }^{\circ}\text{C}$ was found to have little or no residual organic content, indicating that the organic species had volatilized. It is interesting to note that there are only minor differences between the inorganic peaks of the $150\text{ }^{\circ}\text{C}$ and $300\text{ }^{\circ}\text{C}$ curing temperature curves. This indicates that the intact inorganic phase is relatively unaffected by the decomposition of the organic phase. This result suggests that the organic and inorganic phases are not intimately mixed for this composition but, rather that they behave somewhat independently. Thus, the findings of high temperature curing studies for 60% organic content ($D = 6$) film are dramatically different from the findings of the 60% ($D = 1$) film.

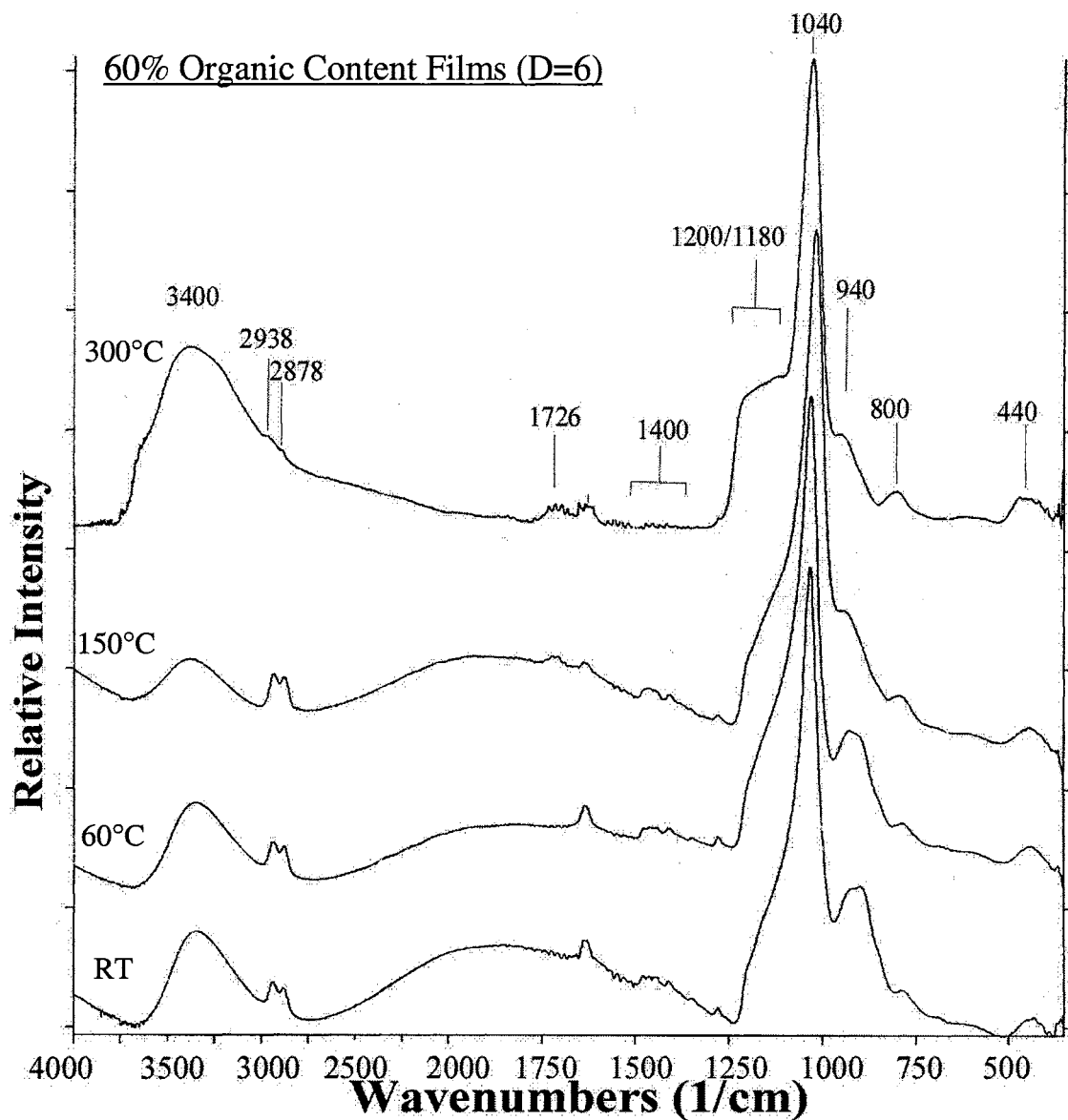


Figure 9.9: Overlaid IR reflectance spectra of 60% organic content ormosil film prepared using a D values of 6 and cured in air at room temperature, 60 °C, 150 °C, and 300 °C.

9.3.3.3 Curing of 80% Organic Content ($D = 1$) Films:

Spectral differences arising as a function of increasing curing temperature in the 80% organic content $D = 1$ film is shown in Figure 9.10. Among the most marked developments are the decomposition of the epoxide groups and loss of the silanol species.

The 80% organic content D = 1 spectra revealed a substantial decrease in the epoxide content with 150 °C curing, as evidenced by losses in peak intensities at 1256 cm^{-1} , 3005 cm^{-1} , and 3055 cm^{-1} . A new peak did arise at 1726 cm^{-1} , and this was attributed to the carbonyl =C=O stretch vibration. The development of an intense carbonyl stretch, with epoxide peak loss, suggested that the epoxide group decompose at elevated temperatures to form a carbonyl species.

Curing of the D = 1 film to 150 °C lead to substantial decrease in the 940 cm^{-1} silanol peak. It can be seen that the 940 cm^{-1} silanol peak, which has a moderate intensity at RT cure, is substantially reduced after curing to 150°C. The silanol peak intensity decrease was attributed to film densification via silanol condensation. Silanol condensation suggests siloxane network development, which is consistent with the further peak development at 1040 cm^{-1} and 1180 cm^{-1} following 150 °C curing. The spectrum indicating 300 °C curing for this composition is quite striking. The film, in effect, has totally decomposed; all that remains is a chemical black residue. This result extends the finding associated with 300 °C curing of a 60% organic content, D = 1 film (Section 9.3.3.1).

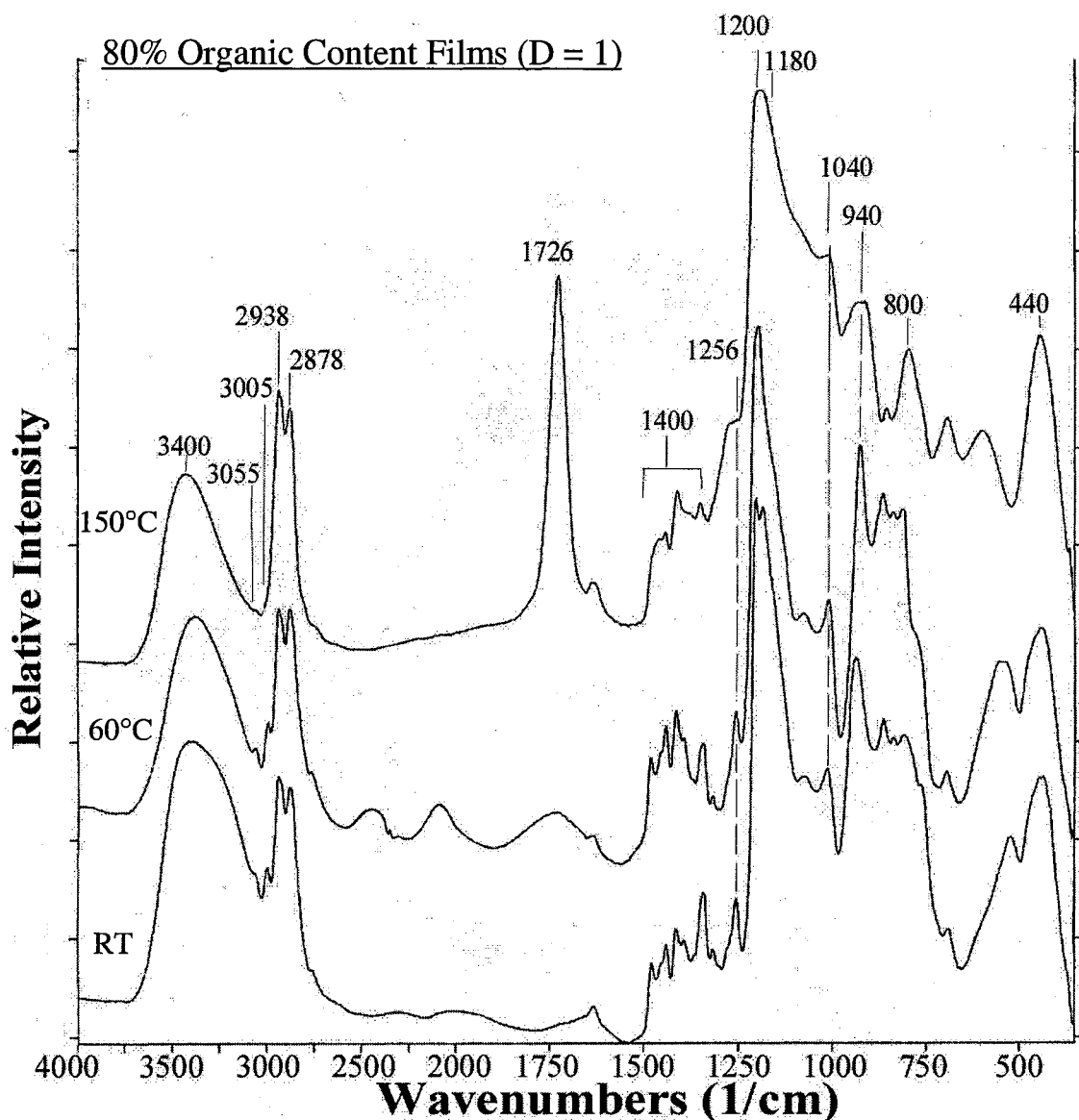


Figure 9.10: Overlaid IR reflectance spectra of 80% organic content ormosil film prepared using an D values of 1 and cured in air at room temperature, 60 °C, 150 °C, and 300 °C.

9.3.3.4 Curing of 80% Organic Content (D = 6) Films

Spectral differences arising as a function of increasing curing temperature in the 80% organic content D = 6 film is shown in Figure 9.10. Among the most striking developments is (1) loss of the residual epoxide content without thermal decomposition to a carbonyl formation and (2) the substantial loss in the silanol content.

Inspection of the D = 6 spectra in Figure 9.11 shows that the RT-cured gels have far less intact epoxide than the comparable D = 1 (Figure 9.8) gel. The RT-cured epoxide content, while minimal was still identified by the small peak at 1256 cm^{-1} . After curing these gels to $150\text{ }^{\circ}\text{C}$, the resultant spectrum revealed complete loss of the epoxide peaks. Absence of the 1726 cm^{-1} carbonyl peak indicated that the epoxide group had decomposed to form the diol in the presence of excess water rather than to decompose to an aldehyde or ketone. These findings are consistent with Raman spectroscopy results presented in Chapter 8.

Densification in the 80% organic content D = 6 film resulted in substantial loss of the silanol content (940 cm^{-1}) with heating to $150\text{ }^{\circ}\text{C}$. There is also evidence of carbosiloxane bond development. In the D = 6 80% organic content room temperature spectrum, the film was previously characterized as a copolymer network with elevated concentration of carbosiloxane formations and silanol species. The siloxane development in the film was limited, as noted by the relative weakness of the 1040 cm^{-1} siloxane peak. The relationship between silanol losses with carbosiloxane and siloxane bond formations implies the 80% organic content D = 6 film underwent further crosslinking with curing to $150\text{ }^{\circ}\text{C}$.

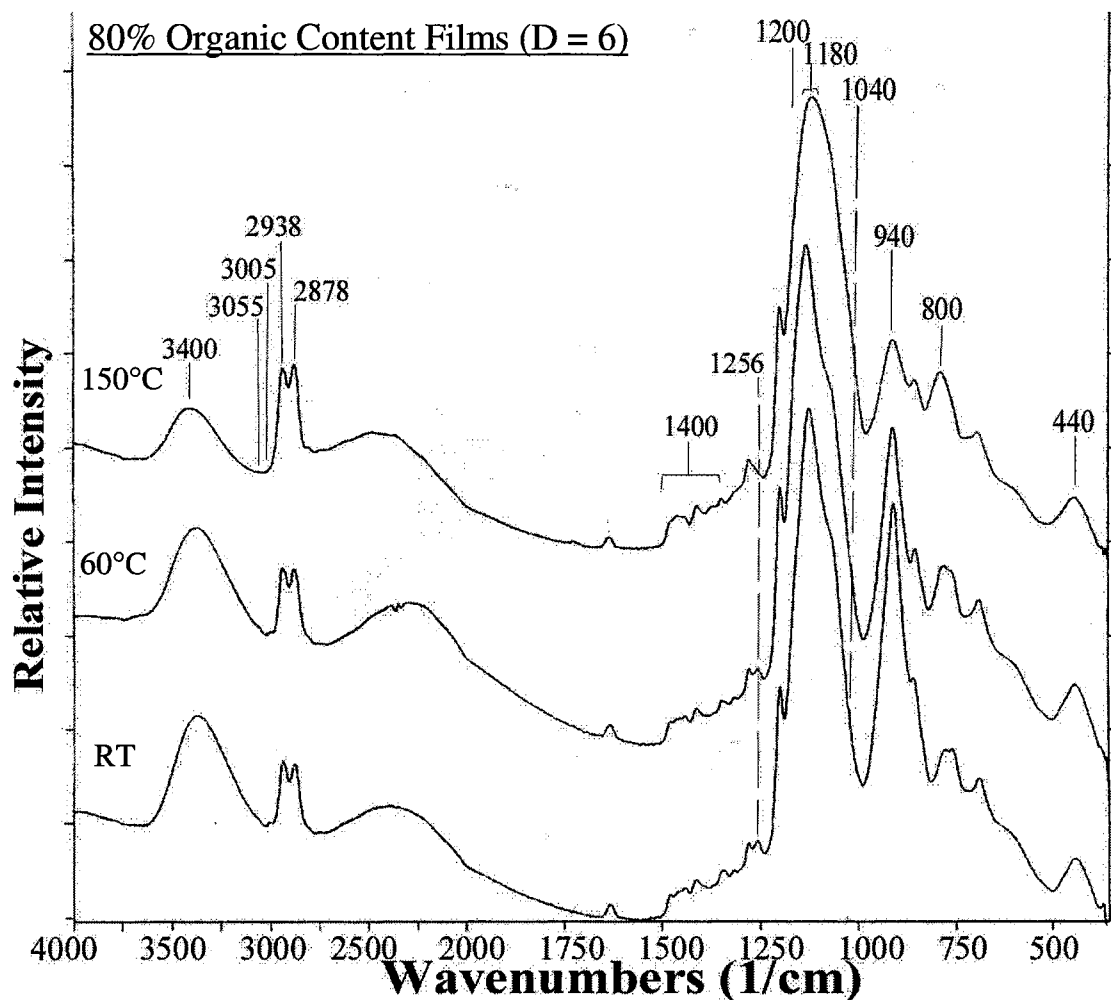


Figure 9.11: Overlaid IR reflectance spectra of 80% organic content ormosil film prepared using a D values of 6 and cured in air at room temperature, 60 °C, 150 °C, and 300 °C.

9.3.4 Summary

Spectral results indicated that the instability of the epoxide group in the water based sol-gel process was the most influential factor in the development of epoxide-based hybrid films. Epoxide decomposition to the diol, and esterification between diol and silanol groups were critical influencing factors in determining hybrid system chemistry and structure. Formation of the carbosiloxane linkages in the lower D valued gels resulted in co-polymers with the organic functional group incorporated into the hybrid

network through carbosiloxane formations. The relative ratio of carbosiloxane to siloxane bond formations was found to increase as a function of organic content. Hydrolysis of the carbosiloxane formation in elevated water content systems resulted in hybrid films with well-developed siloxane networks. The organic phase in the elevated D value hybrid films was postulated to be located in the micropore of siloxane network, in agreement with the findings of previous researchers.

Conditions in which the epoxide group was not hydrolyzed resulted in the films composed of siloxane networks having elevated silanol concentrations. The 80% organic content film prepared using D values of 1 and 2 were the only films identified with elevated intact epoxide functionalities. Absence of carbosiloxane formation in these systems promoted formation of the well-developed siloxane network. Contrary to earlier literature report, there were no spectroscopic evidence of epoxide crosslink formations in any gels, even those containing 80% organic modifier, under any processing conditions. These results strongly suggest that it is worthwhile to reform gelation and network formation models in epoxy-modified ormosil systems.

9.4 Conclusion

Epoxide-based ormosil films with 10%, 20%, 40%, 60%, and 80% organic content were prepared with D values of 1, 2, 4, and 6. The systems were investigated using IR reflectance spectroscopy. Spectral variations were correlated as a function of organic content, D value, and curing temperature. The effects of epoxide decomposition and diol formation were shown to influence the polymerization mechanism and final film microstructure. Epoxide decomposition and esterification between diol and silanol groups was spectroscopically identified and shown to influence the structural

development in the hybrid thin films. Formation of the carbosiloxane linkage in the lower D valued gels resulted in co-polymers with the organic functional group incorporated into the hybrid network. Hydrolysis of the carbosiloxane species in the elevated D valued films resulted in hybrid films with well-developed siloxane networks and the functional groups located in the surface micropores.

Curing of the hybrid films did exhibit silanol losses below 150 °C, but resulted in thermal decomposition upon curing to 300 °C. Hybrid gels cured to 150 °C with elevated concentration of epoxide groups exhibited signs of thermal decomposition rather than epoxide polymerization.

APPENDIX A

NMR SPECTRA AND TABLES OF SILICA GELS

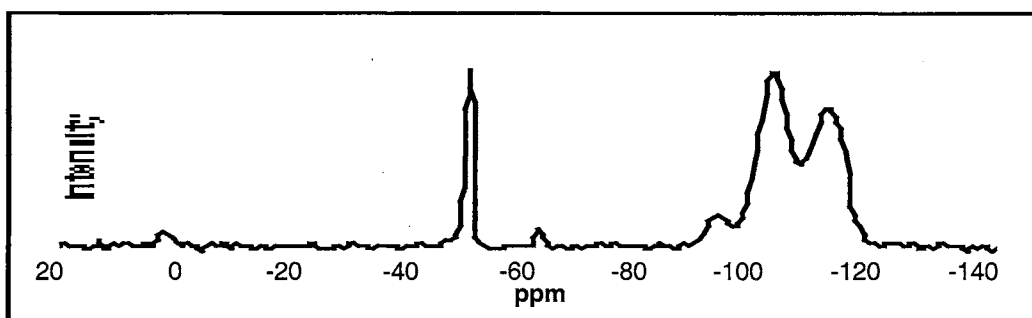


Figure A.1: ^{29}Si SP/MAS NMR spectrum of TMOS gels prepared from $R = 4$.

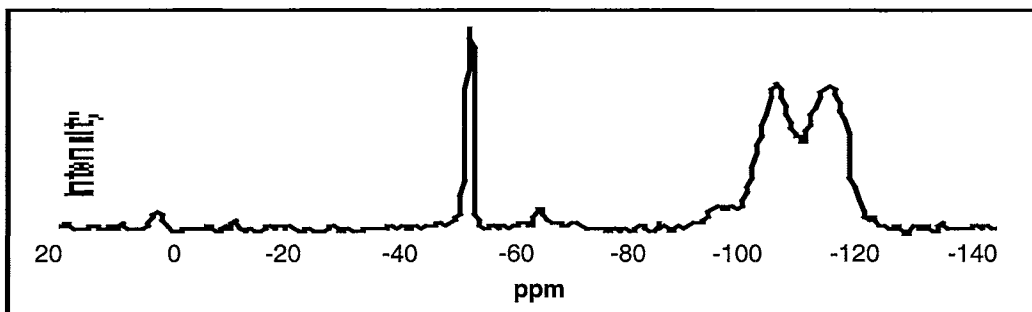


Figure A.2: ^{29}Si SP/MAS NMR spectrum of TMOS gels prepared from $R = 8$.

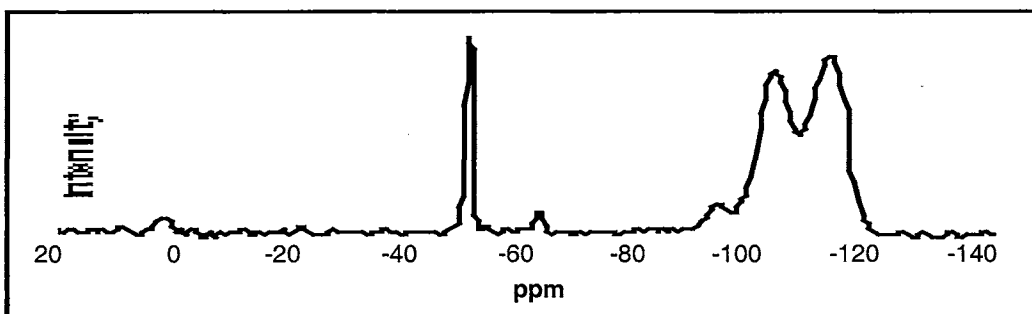


Figure A.3: ^{29}Si SP/MAS NMR spectrum of TMOS gels prepared from $R = 16$.

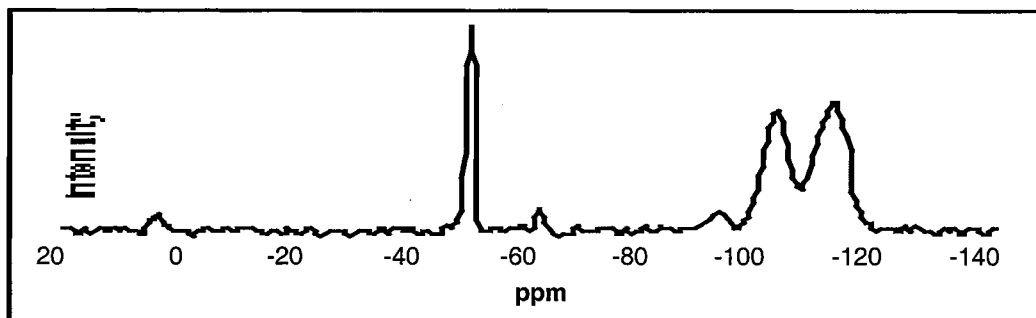


Figure A.4: ^{29}Si SP/MAS NMR spectrum of TMOS gels prepared from $R = 24$.

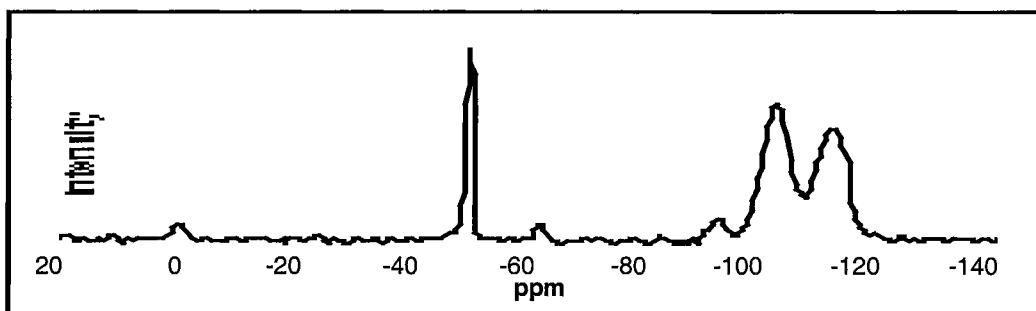


Figure A.5: ^{29}Si SP/MAS NMR spectrum of TEOS gels prepared from $R = 4$.

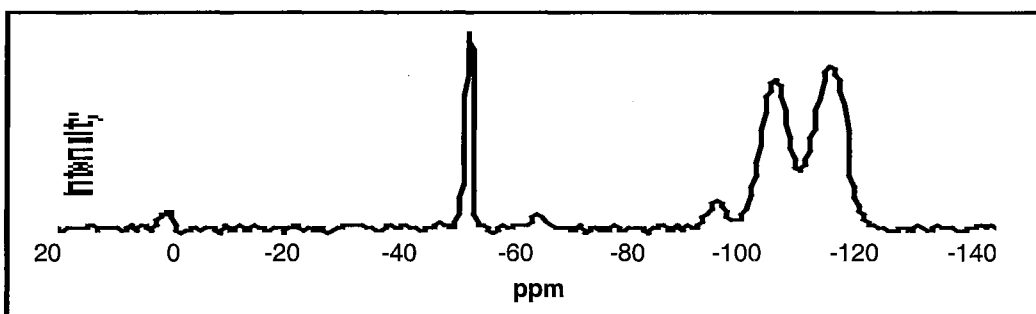


Figure A.6: ^{29}Si SP/MAS NMR spectrum of TEOS gels prepared from $R = 8$.

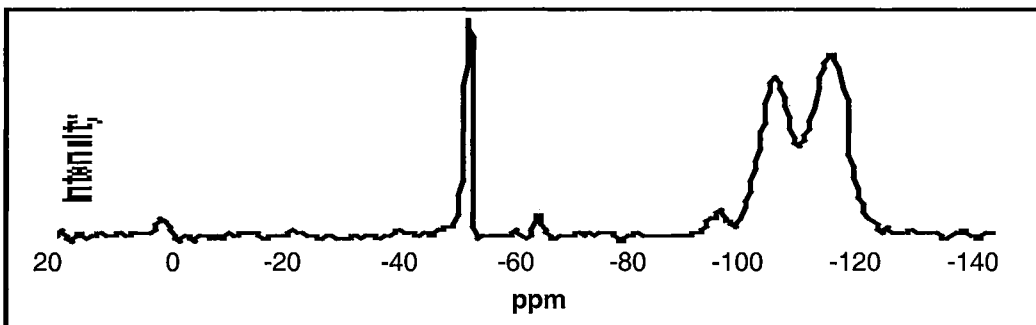


Figure A.7: ^{29}Si SP/MAS NMR spectrum of TEOS gels prepared from $R = 16$.

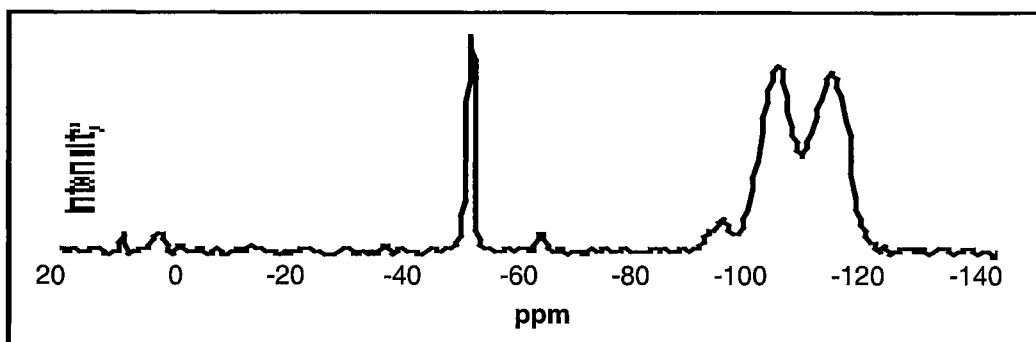


Figure A.8: ^{29}Si SP/MAS NMR spectrum of TEOS gels prepared from $R = 24$.

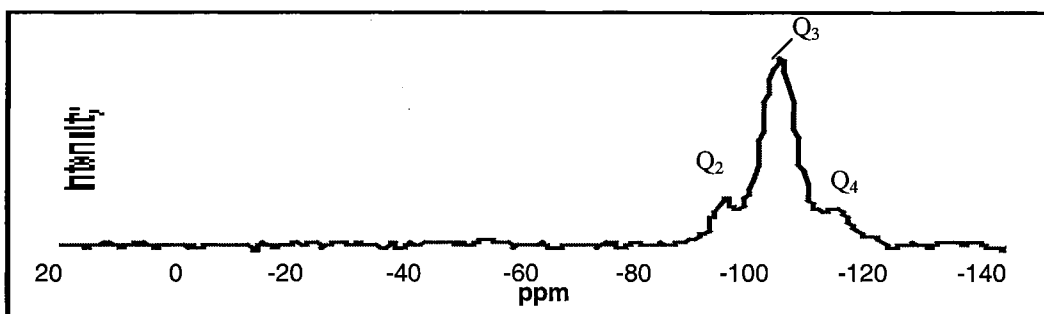


Figure A.9: ^1H - ^{29}Si CP/MAS NMR spectrum of TMOS gels prepared from $R = 4$.

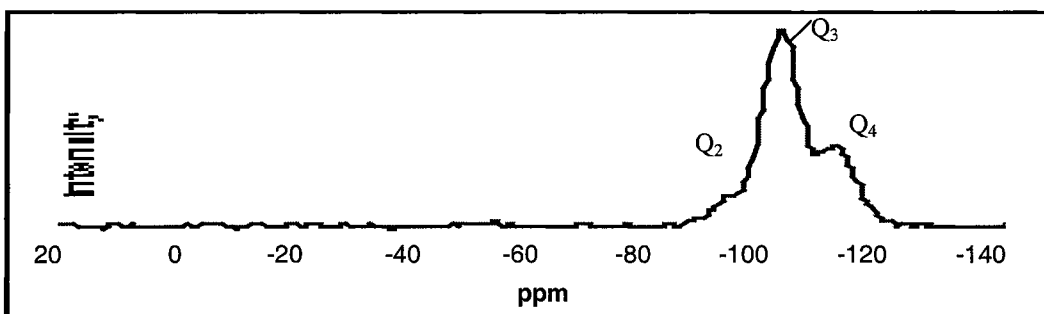


Figure A.10: ^1H - ^{29}Si CP/MAS NMR spectrum of TMOS gels prepared from $R = 8$.

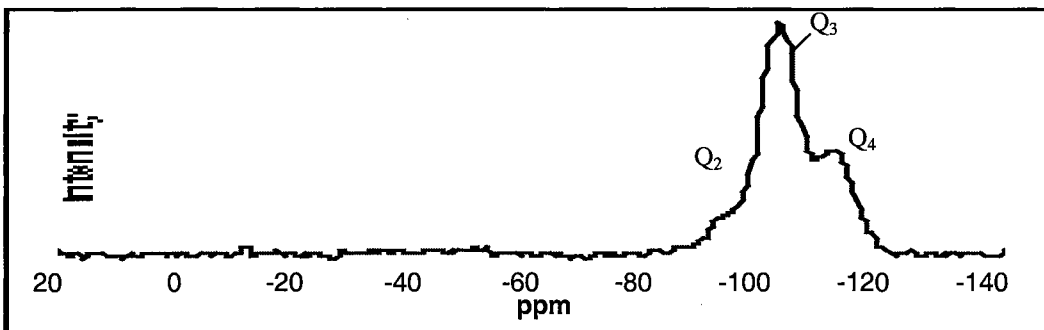


Figure A.11: ^1H - ^{29}Si CP/MAS NMR spectrum of TMOS gels prepared from $R = 16$.

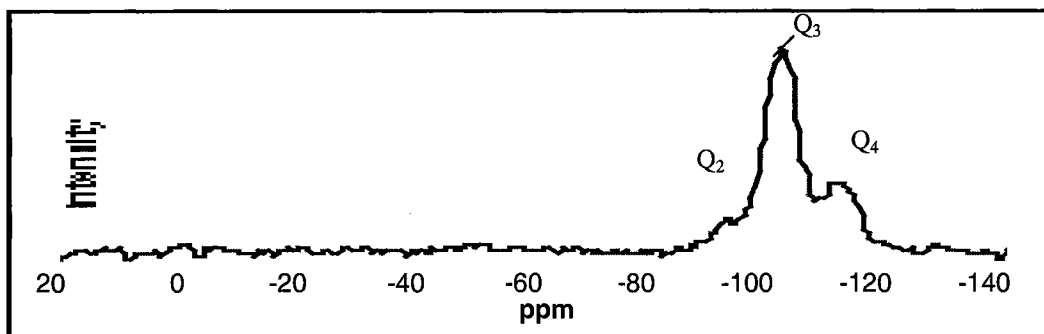


Figure A.12: ^1H - ^{29}Si CP/MAS NMR spectrum of TMOS gels prepared from $R = 24$.

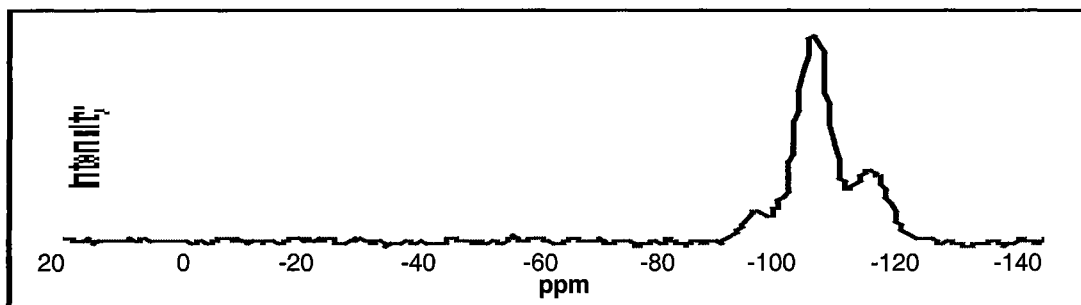


Figure A.13: ^1H - ^{29}Si CP/MAS NMR spectrum of TEOS gels prepared from $R = 4$.

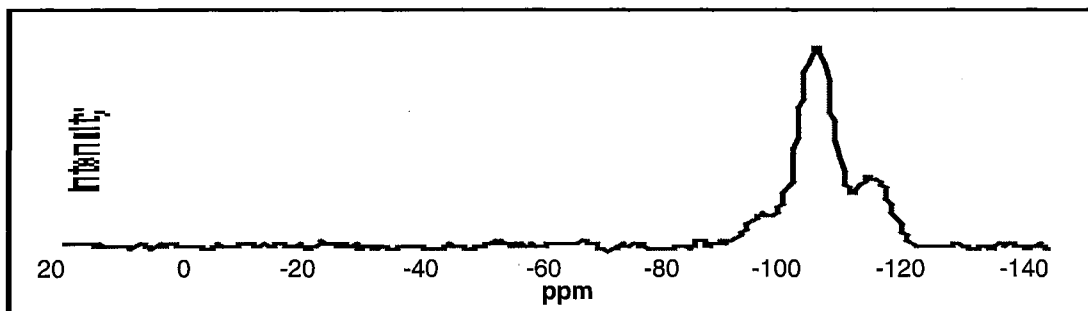


Figure A.14: ^1H - ^{29}Si CP/MAS NMR spectrum of TEOS gels prepared from $R = 8$.

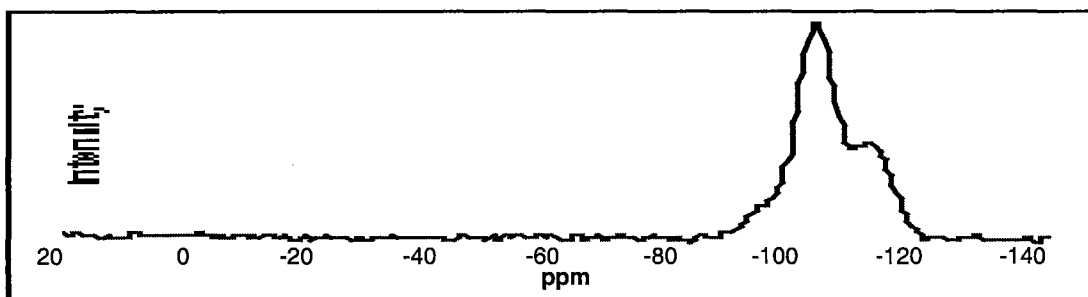


Figure A.15: ^1H - ^{29}Si CP/MAS NMR spectrum of TEOS gels prepared from $R = 16$.

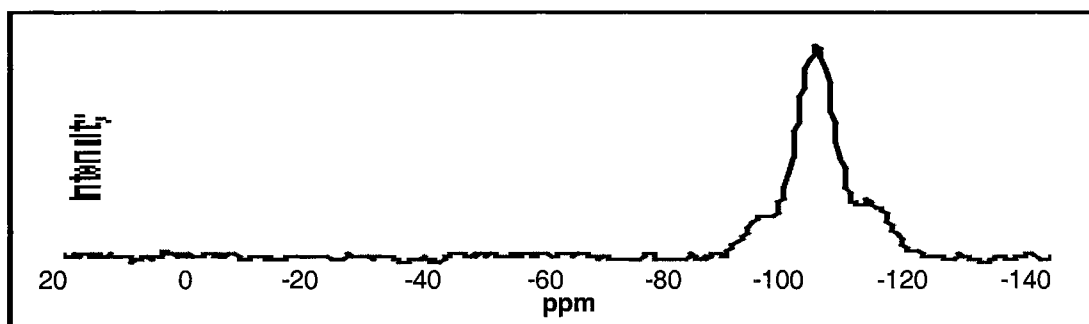


Figure A.16: ^1H - ^{29}Si CP/MAS NMR spectrum of TEOS gels prepared from $R = 24$.

APPENDIX B

RAMAN SPECTRA OF SILICA SOL GELS

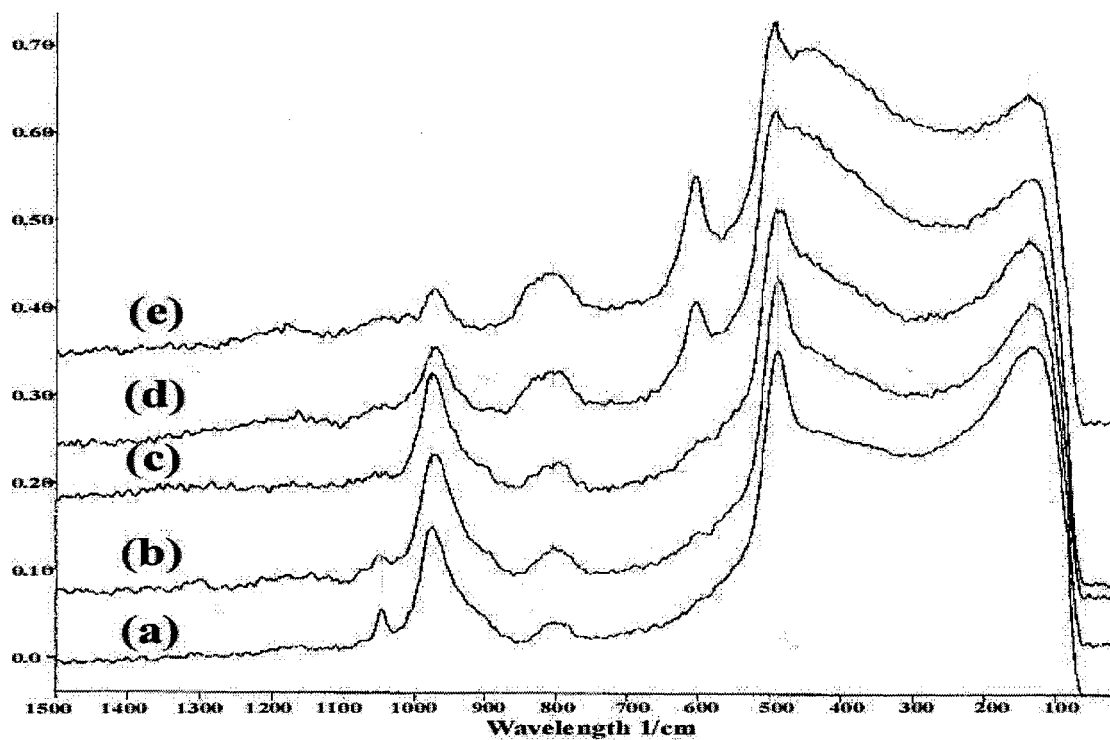


Figure B.1: Overlaid Raman Spectra of SiO₂ gels prepared using a TMOS solution with an R value of 8 cured at room temperature (a), 60 °C (b), 150 °C (c), 300 °C (d), and 450 °C (e).

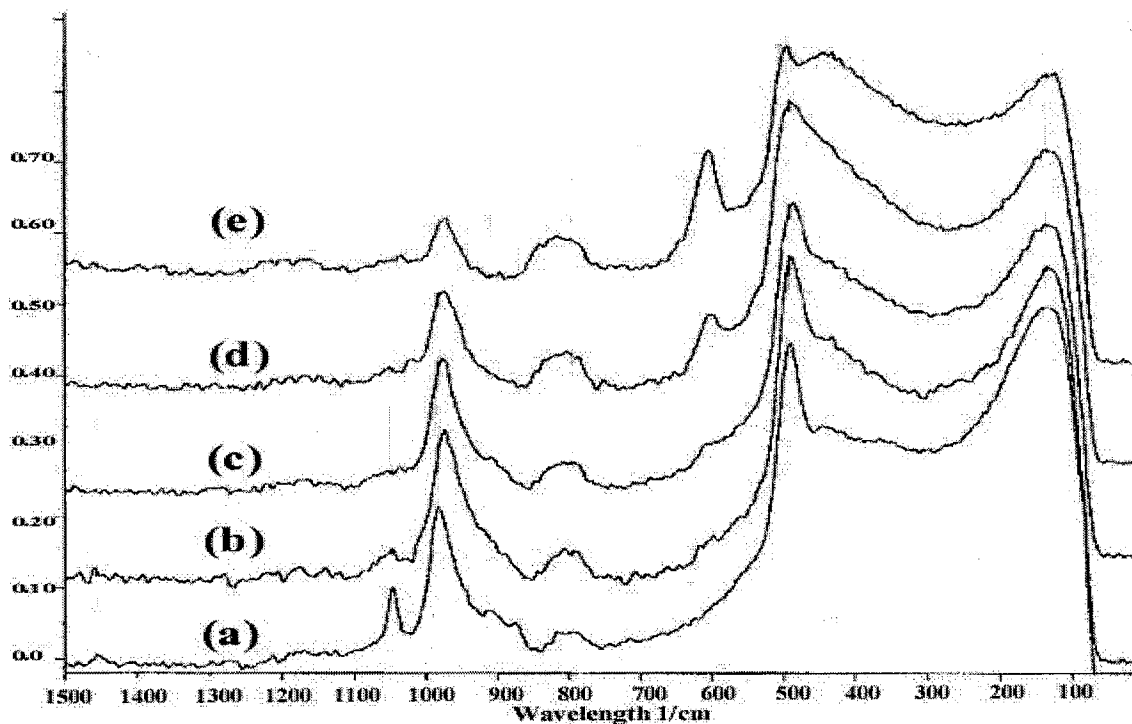


Figure B.2: Overlaid Raman Spectra of SiO₂ gels prepared using a TEOS solution with an R value of 8 cured at room temperature (a), 60 °C (b), 150 °C (c), 300 °C (d), and 450 °C (e).

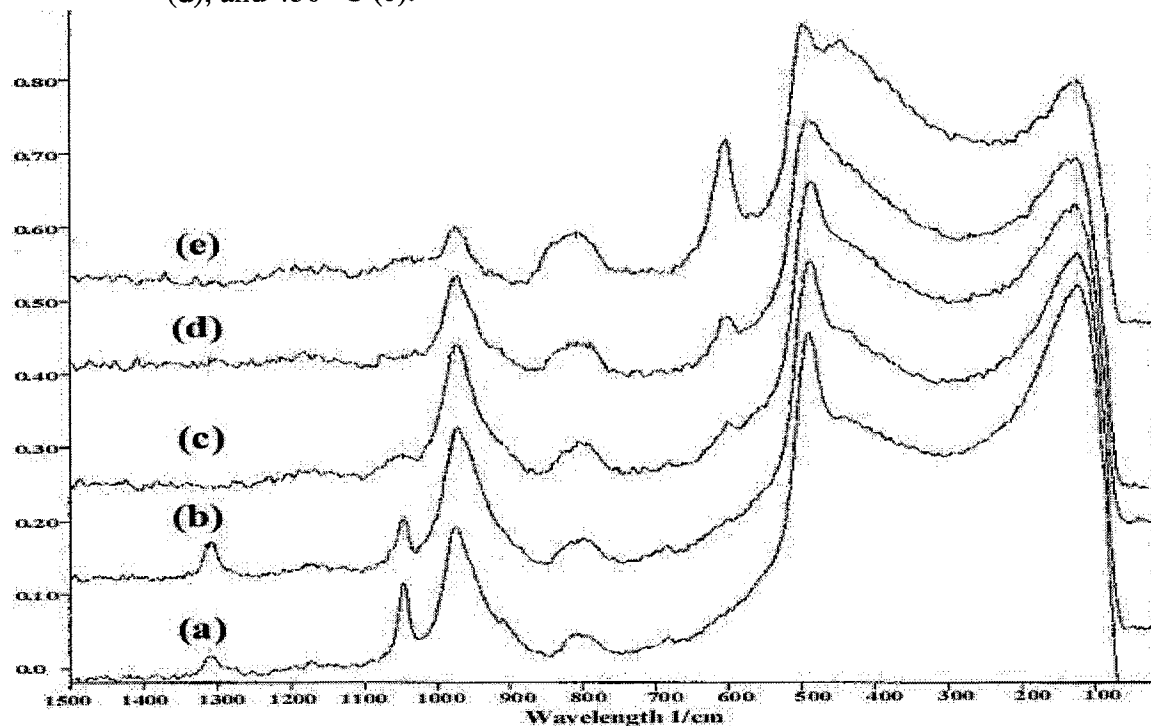


Figure B.3: Overlaid Raman Spectra of SiO₂ gels prepared using a TMOS solution with an R value of 16 cured at room temperature (a), 60 °C (b), 150 °C (c), 300 °C (d), and 450 °C (e).

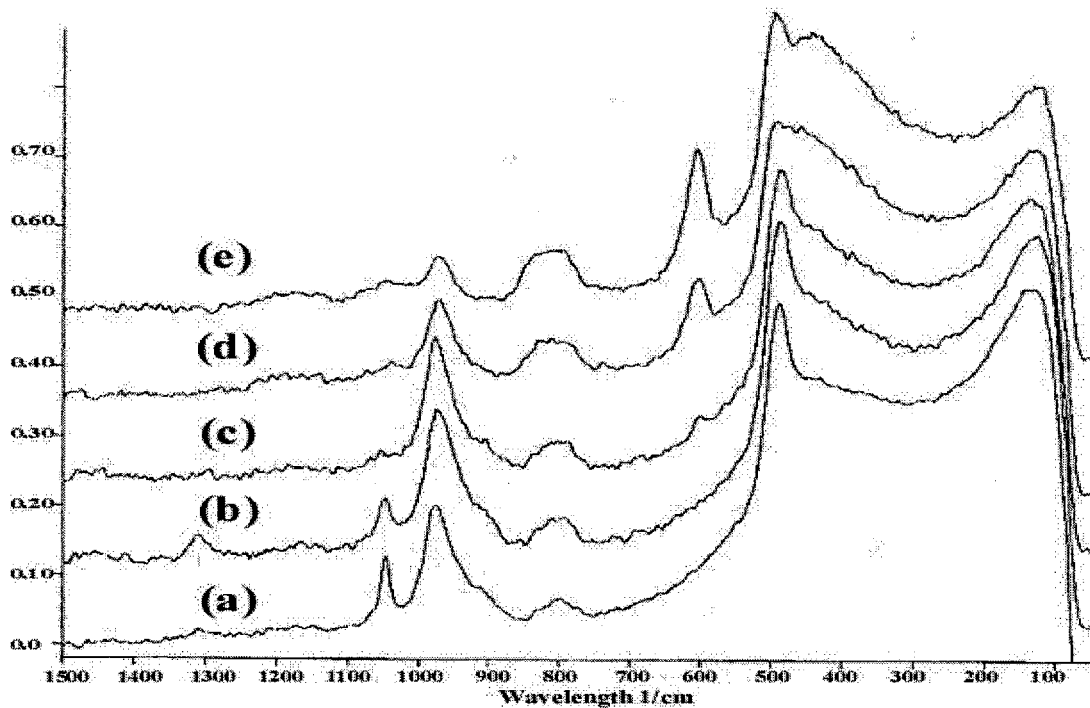


Figure B.4: Overlaid Raman Spectra of SiO₂ gels prepared using a TEOS solution with an R value of 16 cured at room temperature (a), 60 °C (b), 150 °C (c), 300 °C (d), and 450 °C.

Table B.1: Raman intensities found in SiO₂ films prepared from TMOS sols with a R value of 4 and cured at room temperature, 60 °C, 150 °C, 300 °C, and 450 °C.

TMOS		Frequency				
Temp	456 cm ⁻¹	490 cm ⁻¹	606 cm ⁻¹	808 cm ⁻¹	940 cm ⁻¹	1047 cm ⁻¹
Rm	1.507	0.431	0.000	0.100	0.556	0.116
60°C	1.694	0.374	0.0076	0.100	0.531	0.0880
150°C	1.570	0.243	0.0539	0.100	0.384	0.0873
300°C	2.306	0.125	0.180	0.100	0.294	0.0831
450°C	2.349	0.0383	0.128	0.100	0.0647	0.0327

Table B.2: Raman intensities found in SiO₂ films prepared from TMOS sols with a R value of 8 and cured at room temperature, 60 °C, 150 °C, 300 °C, and 450 °C.

TMOS		Frequency				
Temp	456 cm ⁻¹	490 cm ⁻¹	606 cm ⁻¹	808 cm ⁻¹	940 cm ⁻¹	1047 cm ⁻¹
Rm	1.611	0.448	0.000	0.100	0.566	0.194
60°C	1.220	0.265	0.0055	0.100	0.409	0.0779
150°C	1.398	0.194	0.0194	0.100	0.399	0.0292
300°C	1.836	0.951	0.104	0.100	0.221	0.0541
450°C	1.762	0.126	0.220	0.100	0.130	0.0556

Table B.3: Raman intensities found in SiO₂ films prepared from TMOS sols with a R value of 16 and cured at room temperature, 60°C, 150°C, 300°C, and 450°C.

TMOS		Frequency				
Temp	456 cm ⁻¹	490 cm ⁻¹	606 cm ⁻¹	808 cm ⁻¹	940 cm ⁻¹	1047 cm ⁻¹
Rm	1.373	0.430	0.000	0.100	0.597	0.578
60°C	1.262	0.265	0.0015	0.100	0.502	0.111
150°C	1.242	0.269	0.0033	0.100	0.479	0.0526
300°C	1.533	0.101	0.103	0.100	0.329	0.00893
450°C	1.393	0.124	0.214	0.100	0.198	0.00236

Table B.4: Raman intensities found in SiO₂ films prepared from TMOS sols with a R value of 24 and cured at room temperature, 60 °C, 150 °C, 300 °C, and 450 °C.

TMOS		Frequency				
Temp	456 cm ⁻¹	490 cm ⁻¹	606 cm ⁻¹	808 cm ⁻¹	940 cm ⁻¹	1047 cm ⁻¹
Rm	1.406	0.476	0.000	0.100	0.618	0.867
60°C	1.425	0.262	0.0112	0.100	0.573	0.140
150°C	1.061	0.245	0.0113	0.100	0.430	0.0450
300°C	1.626	0.0899	0.132	0.100	0.415	0.0711
450°C	1.110	0.0509	0.206	0.100	0.180	0.0483

Table B.5: Raman intensities found in SiO₂ films prepared from TEOS sols with a R value of 4 and cured at room temperature, 60 °C, 150 °C, 300 °C, and 450 °C.

TEOS		Frequency								
Temp	456 cm ⁻¹	490 cm ⁻¹	606 cm ⁻¹	808 cm ⁻¹	875 cm ⁻¹	940 cm ⁻¹	1047 cm ⁻¹	1454 cm ⁻¹	2934 cm ⁻¹	2978 cm ⁻¹
Rm	1.329	0.331	0.000	0.10	0.519	0.535	0.314	0.518	1.150	0.605
60°C	1.089	0.244	0.0113	0.10	0.377	0.372	0.156	0.309	1.289	0.657
150°C	1.230	0.117	0.0318	0.10	0.368	0.224	0.0425	0.119	0.499	0.251
300°C	1.754	0.151	0.0991	0.10	0.165	0.319	0.0561	0.0177	0.020	0.0184
450°C	2.349	0.0383	0.146	0.10	0.0797	0.0647	0.0594	0.0288	0.046	0.00211

Table B.6: Raman intensities found in SiO₂ films prepared from TEOS sols with a R value of 8 and cured at room temperature, 60 °C, 150 °C, 300 °C, and 450 °C.

TEOS		Frequency				
Temp	456 cm ⁻¹	490 cm ⁻¹	606 cm ⁻¹	808 cm ⁻¹	940 cm ⁻¹	1047 cm ⁻¹
Rm	1.546	0.487	0.000	0.100	0.741	0.312
60°C	1.304	0.321	0.00836	0.100	0.504	0.102
150°C	1.357	0.267	0.0452	0.100	0.489	0.0506
300°C	1.409	0.164	0.132	0.100	0.282	0.0617
450°C	1.524	0.036	0.438	0.100	0.256	0.0484

Table B.7: Raman intensities found in SiO₂ films prepared from TEOS sols with a R value of 16 and cured at room temperature, 60 °C, 150 °C, 300 °C, and 450 °C.

TEOS		Frequency				
Temp	456 cm ⁻¹	490 cm ⁻¹	606 cm ⁻¹	808 cm ⁻¹	940 cm ⁻¹	1047 cm ⁻¹
Rm	1.738	0.367	0.000	0.100	0.588	0.433
60°C	1.447	0.306	0.00439	0.100	0.476	0.189
150°C	1.506	0.2629	0.0516	0.100	0.456	0.0855
300°C	1.673	0.0628	0.222	0.100	0.312	0.0624
450°C	1.578	0.0866	0.343	0.100	0.118	0.050

Table B.8: Raman intensities found in SiO₂ films prepared from TEOS sols with a R value of 24 and cured at room temperature, 60 °C, 150 °C, 300 °C, and 450 °C.

TEOS		Frequency				
Temp	456 cm ⁻¹	490 cm ⁻¹	606 cm ⁻¹	808 cm ⁻¹	940 cm ⁻¹	1047 cm ⁻¹
Rm	1.416	0.397	0.000	0.10	0.525	0.407
60°C	1.312	0.286	0.00350	0.10	0.479	0.217
150°C	1.167	0.228	0.0606	0.10	0.414	0.0667
300°C	1.512	0.195	0.160	0.10	0.368	0.0325
450°C	1.359	0.0669	0.366	0.10	0.131	0.0498

APPENDIX C

FT-IR REFLECTANCE SPECTRA OF SILICA THIN FILMS

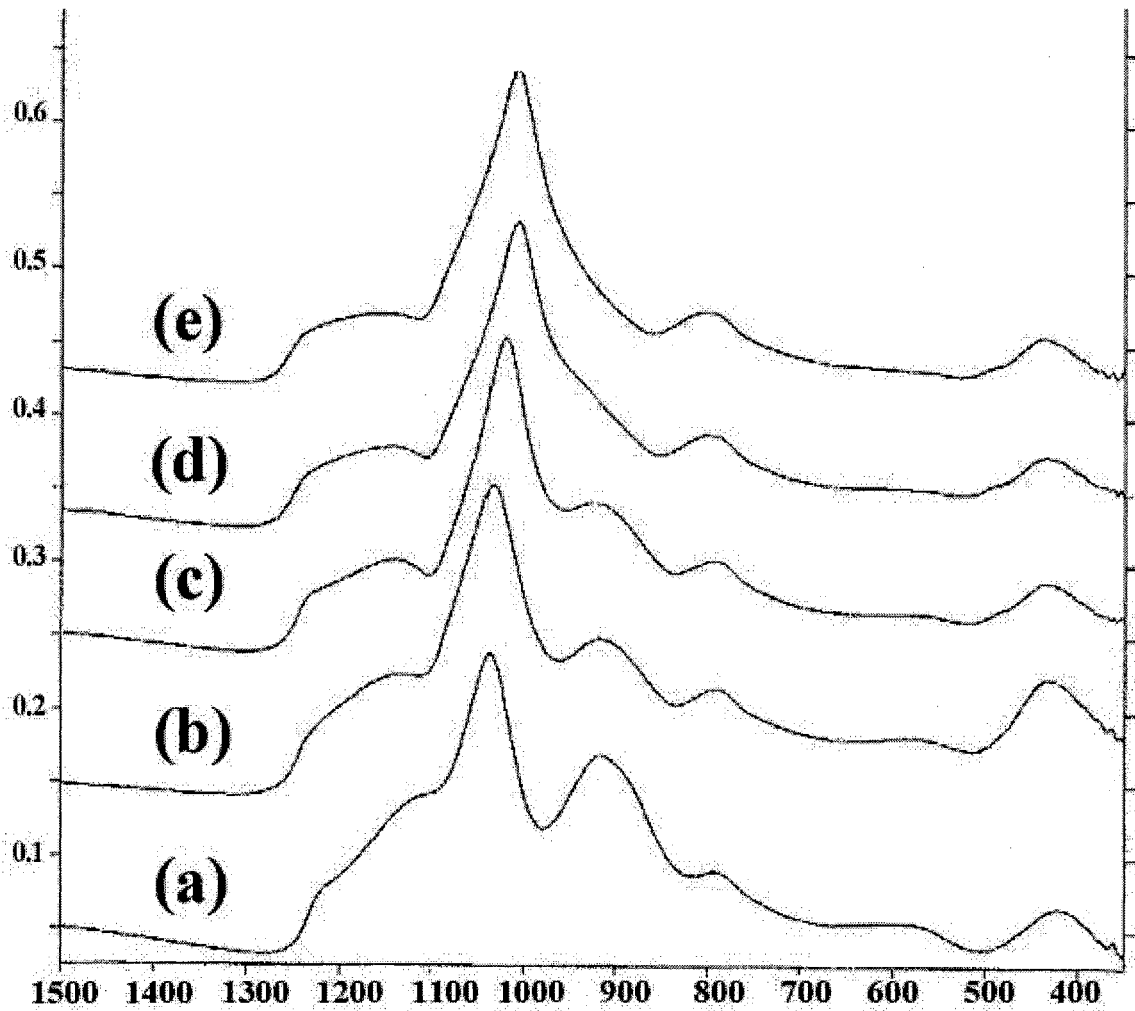


Figure C.1: Overlaid IR Spectra of SiO_2 thin films prepared from a TMOS solution with a R value of 8 and cured at room temperature (a), 60 °C (b), 150 °C (c), 300 °C (d), and 450 °C (e).

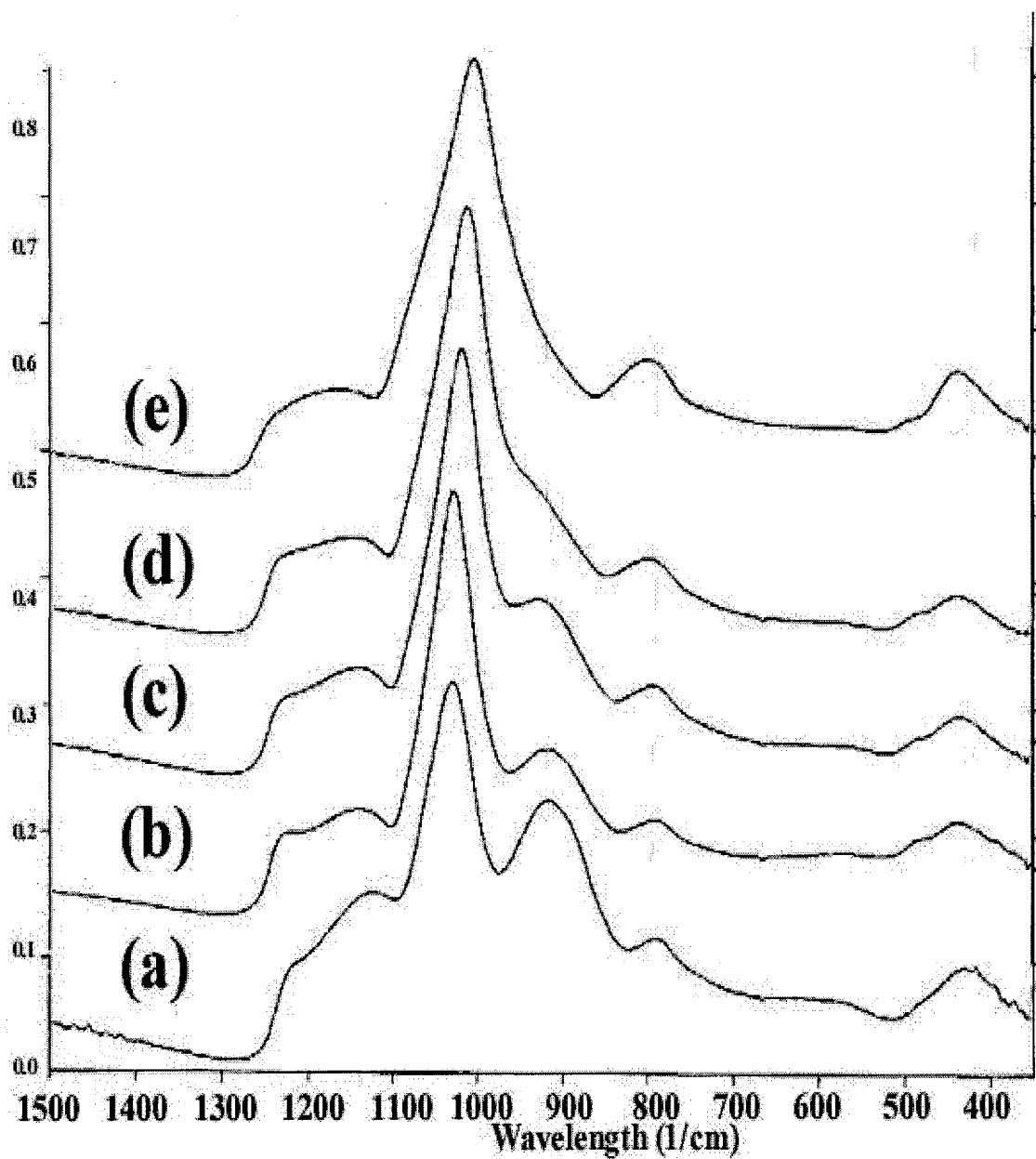


Figure C.2: Overlaid IR Spectra of SiO₂ thin films prepared from a TEOS solution with a R value of 8 and cured at room temperature (a), 60 °C (b), 150 °C (c), 300 °C (d), and 450 °C (e).

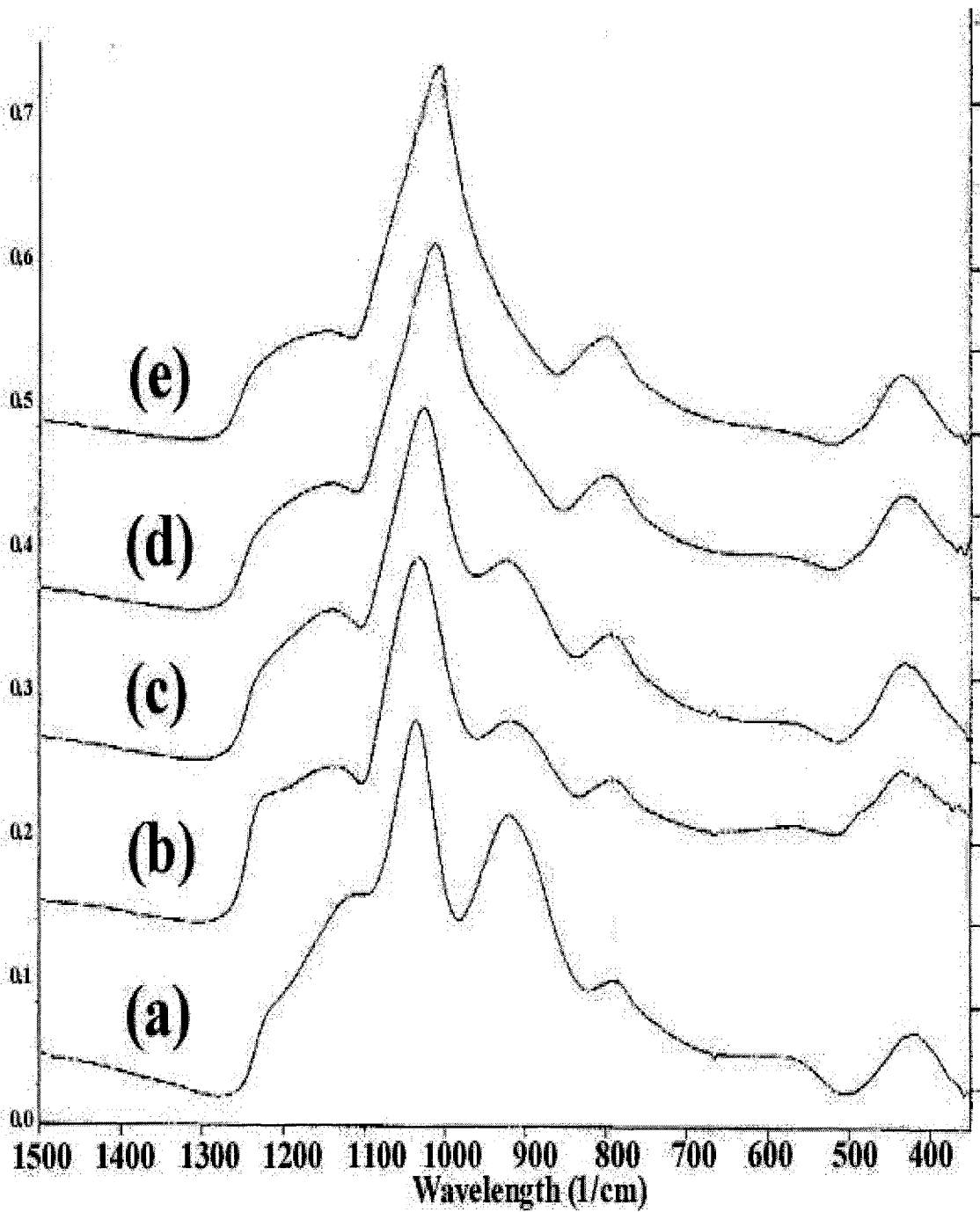


Figure C.3: Overlaid IR Spectra of SiO₂ thin films prepared from a TMOS solution with a R value of 16 and cured at room temperature (a), 60 °C (b), 150 °C (c), 300 °C (d), and 450 °C (e).

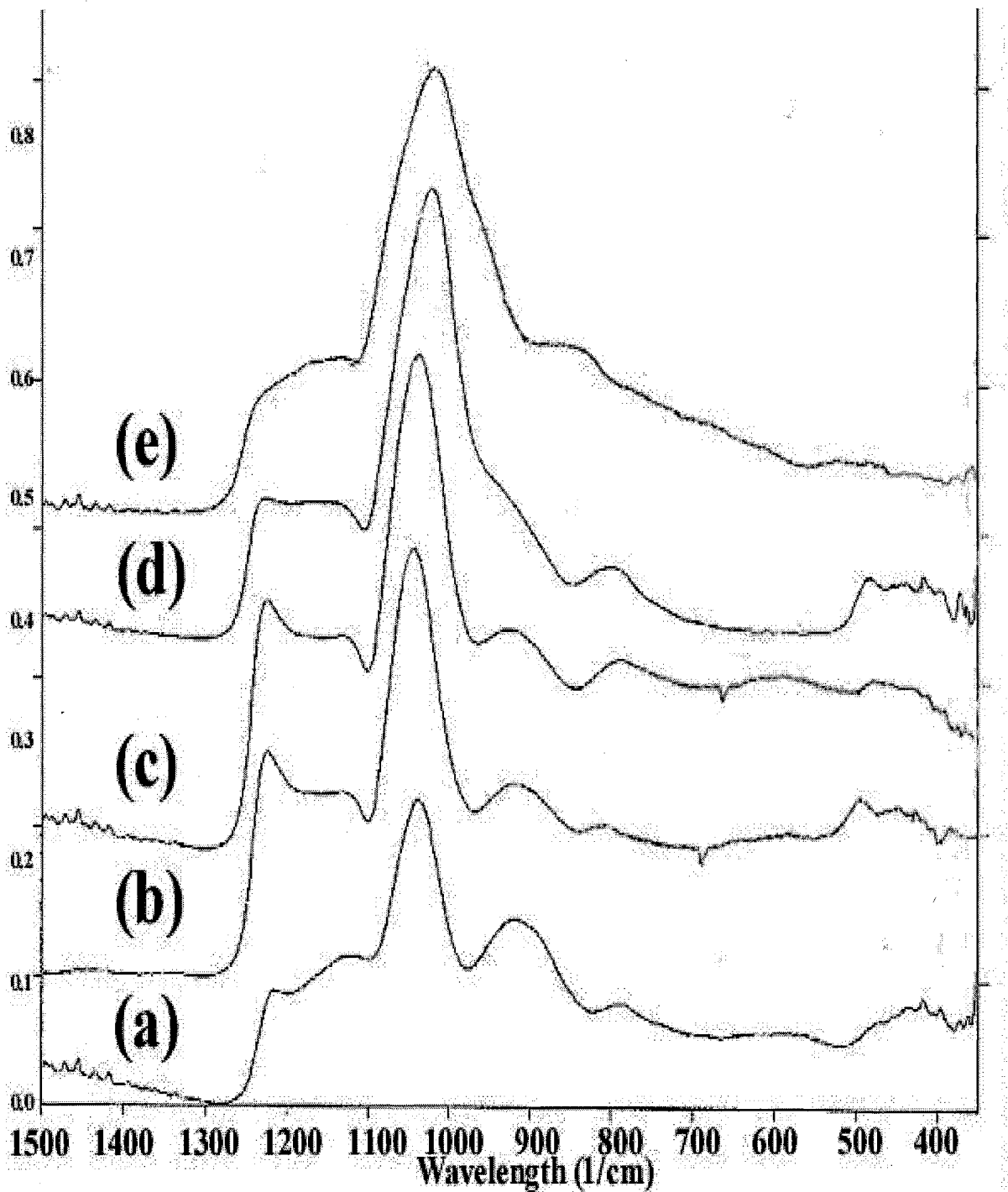


Figure C.4: Overlaid IR Spectra of SiO₂ thin films prepared from a TEOS solution with a R value of 16 and cured at room temperature (a), 60 °C (b), 150 °C (c), 300 °C (d), and 450 °C (e).

Table C.1: IR vibrational frequencies and intensities for SiO₂ films prepared from TMOS sols with a R value of 4 and cured at room temperature, 60 °C, 150 °C, 300 °C, and 450 °C.

TMOS (R=4)		Frequency (Relative Intensity)			
Temp.	(T.O) ≡Si-O-Si≡ (L.O)	≡Si-O-H	≡Si-O-Si≡	≡Si-O-Si≡	≡Si-O-Si≡
RM	1117.2 (86.1)	1036.2 (100.0)	927.6 (178.4)	793.0 (40.6)	419.2 (33.5)
60 °C	1148.5 (113.8)	1051.2 (100.0)	930.1 (113.6)	799.6 (76.5)	424.3 (93.8)
150 °C	1146.9 (100.4)	1046.9 (100.0)	923.7 (103.0)	799.8 (73.3)	424.5 (83.7)
300 °C	1148.0 (85.1)	1036.9 (100.0)	938.5 (69.1)	802.7 (68.8)	416.6 (88.1)
450 °C	1150.2 (74.0)	1035.9 (100.0)	940.6 (26.8)	804.5 (48.4)	425.9 (81.8)

Table C.2 : IR vibrational frequencies and intensities for SiO₂ films prepared from TMOS sols with a R value of 8 and cured at room temperature, 60 °C, 150 °C, 300 °C, and 450 °C.

TMOS (R=8)		Frequency (Relative Intensity)			
Temp.	(T.O) ≡Si-O-Si≡ (L.O)	≡Si-O-H	≡Si-O-Si≡	≡Si-O-Si≡	≡Si-O-Si≡
RM	1140.1 (54.0)	1039.3 (100.0)	918.5 (66.6)	794.4 (8.79)	424.4 (14.00)
60 °C	1139.1 (43.1)	1035.6 (100.0)	919.3 (47.0)	794.7 (8.42)	434.9 (22.17)
150 °C	1143.4 (29.3)	1021.9 (100.0)	925.9 (44.8)	795.3 (8.44)	437.7 (11.33)
300 °C	1146.9 (26.5)	1008.9 (100.0)	934.7 (27.6)	799.1 (9.55)	437.2 (10.90)
450 °C	1154.8 (26.9)	1009.5 (100.0)	939.1 (20.7)	802.6 (9.35)	439.4 (10.83)

Table C.3: IR vibrational frequencies and intensities for SiO₂ films prepared from TMOS sols with a R value of 16 and cured at room temperature, 60°C, 150 °C, 300 °C, and 450 °C.

TMOS (R=16)		Frequency (Relative Intensity)			
Temp.	(T.O) ≡Si-O-Si≡ (L.O)	≡Si-O-H	≡Si-O-Si≡	≡Si-O-Si≡	≡Si-O-Si≡
RM	1141.1 (53.5)	1037.9 (100.0)	922.3 (76.9)	792.4 (9.35)	436.6 (16.22)
60 °C	1138.6 (42.7)	1035.4 (100.0)	920.9 (46.4)	793.7 (7.88)	433.5 (15.67)
150 °C	1142.5 (42.4)	1027.9 (100.0)	926.7 (51.7)	795.1 (12.00)	435.3 (21.29)
300 °C	1141.4 (36.4)	1014.2 (100.0)	935.5 (25.0)	798.8 (11.63)	437.9 (18.44)
450 °C	1150.0 (35.6)	1011.9 (100.0)	937.1 (19.0)	801.8 (12.76)	420.4 (17.43)

Table C.4: IR vibrational frequencies and intensities for SiO₂ films prepared from TMOS sols with a R value of 24 and cured at room temperature, 60 °C, 150 °C, 300 °C, and 450 °C.

TMOS (R=24)		Frequency (Relative Intensity)			
Temp.	(T.O) ≡Si-O-Si≡ (L.O)	≡Si-O-H	≡Si-O-Si≡	≡Si-O-Si≡	≡Si-O-Si≡
RM	1218.5 (56.0)	1046.2 (100.0)	923.2 (54.3)	796.2 (6.74)	422.3 (11.71)
60 °C	1135.6 (50.6)	1040.8 (100.0)	920.2 (43.3)	794.7 (6.92)	438.8 (17.55)
150 °C	1134.4 (47.8)	1035.7 (100.0)	924.5 (44.4)	794.8 (7.50)	438.5 (17.06)
300 °C	1139.0 (49.3)	1023.9 (100.0)	935.1 (32.0)	798.2 (7.68)	438.1 (16.38)
450 °C	1161.2 (45.9)	1014.9 (100.0)	938.3 (21.8)	802.4 (12.61)	439.3 (15.93)

Table C.5: IR vibrational frequencies and intensities for SiO₂ films prepared from TEOS sols with a R value of 4 and cured at room temperature, 60 °C, 150 °C, 300 °C, and 450 °C.

TEOS (R=4)		Frequency (Relative Intensity)			
Temp.	(T.O) ≡Si-O-Si≡ (L.O)	≡Si-O-H	≡Si-O-Si≡	≡Si-O-Si≡	≡Si-O-Si≡
RM	1133.5 (85.0)	1040.7 (100.0)	930.1 (174.7)	796.8 (24.42)	427.9 (58.69)
60 °C	1145.4 (79.6)	1042.3 (100.0)	929.9 (133.6)	795.1 (29.04)	429.8 (55.62)
150 °C	1142.8 (71.4)	1035.8 (100.0)	933.6 (125.0)	795.5 (24.21)	429.8 (53.29)
300 °C	1148.3 (64.5)	1032.8 (100.0)	940.0 (82.7)	801.4 (34.16)	425.2 (49.81)
450 °C	1164.6 (56.0)	1024.0 (100.0)	939.9 (44.2)	805.8 (37.73)	433.1 (46.89)

Table C.6: IR vibrational frequencies and intensities for SiO₂ films prepared from TEOS sols with a R value of 8 and cured at room temperature, 60 °C, 150 °C, 300 °C, and 450 °C.

TEOS (R=8)		Frequency (Relative Intensity)			
Temp.	(T.O) ≡Si-O-Si≡ (L.O)	≡Si-O-H	≡Si-O-Si≡	≡Si-O-Si≡	≡Si-O-Si≡
RM	1139.6 (44.3)	1031.8 (100.0)	919.5 (69.1)	791.8 (5.68)	419.8 (12.89)
60 °C	1140.8 (25.1)	1030.6 (100.0)	921.3 (43.2)	793.9 (5.20)	439.7 (7.44)
150 °C	1143.3 (25.0)	1021.2 (100.0)	931.6 (37.7)	796.1 (7.33)	438.8 (7.00)
300 °C	1148.3 (24.5)	1014.6 (100.0)	939.5 (27.1)	801.4 (7.91)	440.2 (6.21)

Table C.7: IR vibrational frequencies and intensities for SiO₂ films prepared from TEOS sols with a R value of 16 and cured at room temperature, 60 °C, 150 °C, 300 °C, and 450 °C.

TEOS (R=16)		Frequency (Relative Intensity)			
Temp.	(T.O) ≡Si-O-Si≡ (L.O)	≡Si-O-H	≡Si-O-Si≡	≡Si-O-Si≡	≡Si-O-Si≡
RM	1133.5 (43.4)	1038.7 (100.0)	921.9 (60.0)	792.1 (4.95)	419.7 (8.84)
60 °C	1134.2 (52.3)	1046.1 (100.0)	919.4 (42.7)	794.1 (1.18)	439.7 (6.74)
150 °C	1131.2 (50.2)	1039.9 (100.0)	930.5 (39.6)	790.7 (1.84)	450.2 (6.15)
300 °C	1228.7 (32.7)	1023.5 (100.0)	939.5 (26.2)	803.8 (3.02)	452.9 (4.62)
450 °C	1210.5 (49.2)	1022.2 (100.0)	940.0 (21.2)	817.3 (1.50)	456.3 (7.15)

Table C.8: IR vibrational frequencies and intensities for SiO₂ films prepared from TEOS sols with a R value of 24 and cured at room temperature, 60 °C, 150 °C, 300 °C, and 450 °C.

TEOS (R=24)		Frequency (Relative Intensity)			
Temp.	(T.O) ≡Si-O-Si≡ (L.O)	≡Si-O-H	≡Si-O-Si≡	≡Si-O-Si≡	≡Si-O-Si≡
RM	1218.1 (48.5)	1040.7 (100.0)	920.7 (55.9)	792.3 (4.72)	422.1 (13.99)
60 °C	1225.3 (76.3)	1051.5 (100.0)	925.9 (32.4)	798.2 (1.56)	441.5 (8.97)
150 °C	1151.5 (64.3)	1043.1 (100.0)	937.2 (31.1)	796.0 (3.98)	459.1 (7.09)
300 °C	1154.2 (31.6)	1020.9 (100.0)	940.0 (24.8)	802.1 (6.73)	441.5 (6.21)
450 °C	1223.9 (43.1)	1029.2 (100.0)	940.0 (19.7)	804.5 (3.95)	469.7 (6.78)

APPENDIX D

NMR SPECTRA AND TABLES OF ORMOSIL GELS

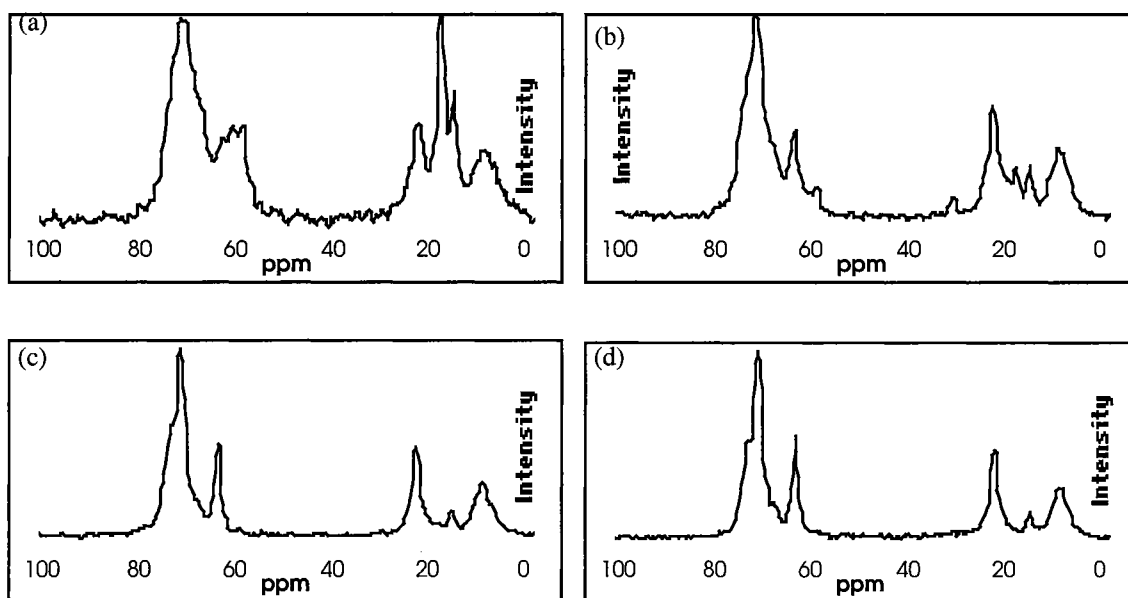


Figure D.1: ^1H - ^{13}C CP/MAS/NMR spectrum of 20% Epoxide Ormosil gels prepared with D values of (a) 1, (b) 2, (c) 4, and (d) 6

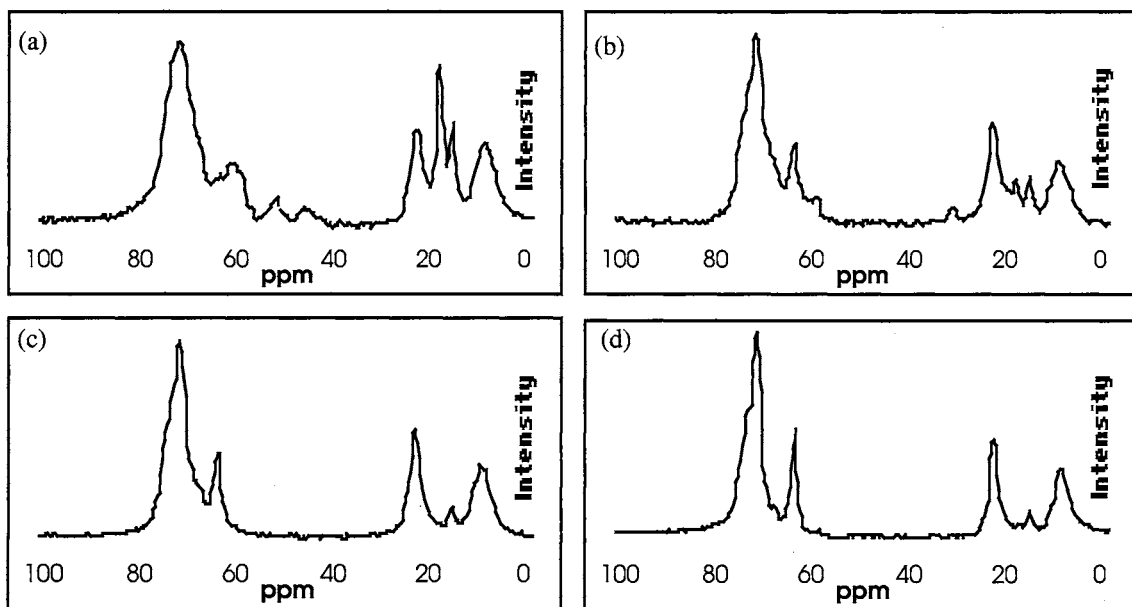


Figure D.2: ^1H - ^{13}C CP/MAS/NMR spectrum of 40% Epoxide Ormosil gels prepared with D values of (a) 1, (b) 2, (c) 4, and (d) 6.

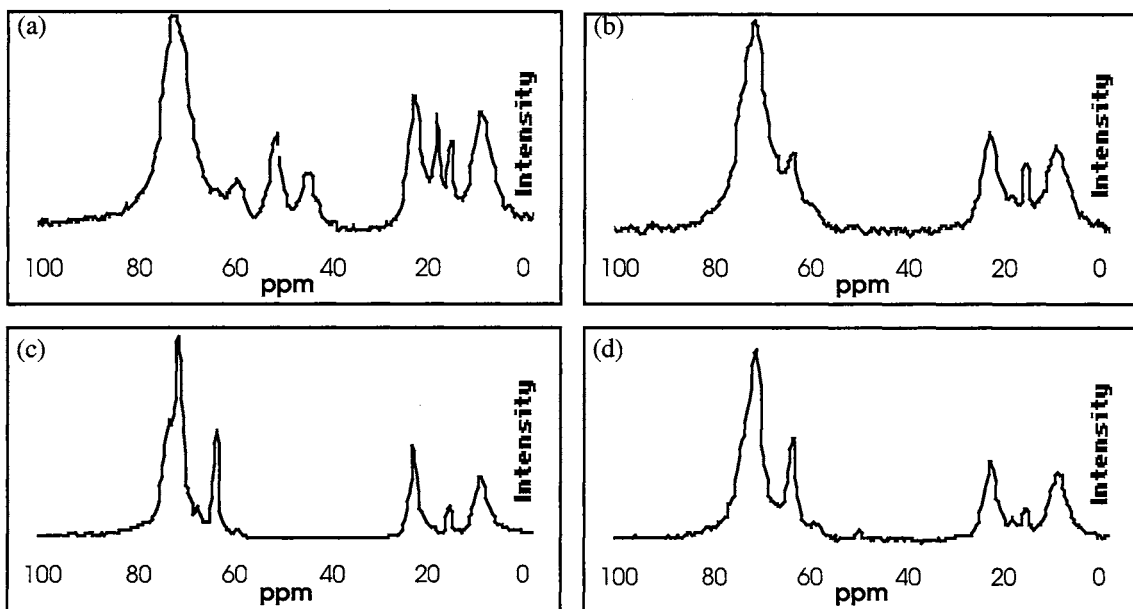


Figure D.3: ^1H - ^{13}C CP/MAS/NMR spectrum of 60% Epoxide Ormosil gels prepared with D values of (a) 1, (b) 2, (c) 4, and (d) 6

Table D.1: ^1H - ^{13}C CP/NMR frequencies and peak assignments for the 10% hybrid ormosil prepared with D values of (a) 1, (b) 2, (c) 4, and (d) 6.

10% Hybrid				
Peak Assignment	D = 1	D = 2	D = 4	D = 6
Si-CH ₂ -R	8.1	8.5	8.9	8.1
R-O-CH ₂ CH ₃	14.7	15.1	14.7	14.7
Si-O-CH ₂ -CH ₃	17.8	17.8	-	-
Si-CH ₂ CH ₂ -R	22.4	22.4	22.8	22.1
-CH ₂ CH ^O -CH ₂	-	-	-	-
-CH ₂ CH ^O -CH ₂	-	-	-	-
R-OCH ₂ -CH ₃	59.2	59.6	-	-
Si-OCH ₂ -CH ₃	61.2	61.2	-	-
R-CH ^(OH) -CH ₂ -OH	63.1	64.3	64.3	63.9
CH ^(OH) -CH ₂ O-CH ₂ CH ₃	68.5	68.5 tr	68.2	68.2
R-CH ₂ -O-CH ₂ -R	71.6	72.0	72.0	71.6

Table D.2: ^1H - ^{13}C CP/NMR frequencies and peak assignments for the 20% hybrid ormosil prepared with D values of (a) 1, (b) 2, (c) 4, and (d) 6.

20% Hybrid				
Peak Assignment	D = 1	D = 2	D = 4	D = 6
Si-CH ₂ -R	7.7	8.9	8.5	8.1
R-O-CH ₂ CH ₃	15.1	15.1	15.1	14.7
Si-O-CH ₂ -CH ₃	17.8	17.8	17.8 tr	-
Si-CH ₂ CH ₂ -R	22.8	22.8	22.8	22.4
-CH ₂ CH ^O -CH ₂	-	-	-	-
-CH ₂ CH ^O -CH ₂	-	-	-	-
R-OCH ₂ -CH ₃	59.2	59.2	59.2	-
Si-OCH ₂ -CH ₃	60.2	-	-	-
R-CH ^(OH) -CH ₂ -OH	63.9	63.9	64.3	63.9
CH ^(OH) -CH ₂ O-CH ₂ CH ₃	-	-	68.5 sh	67.8 sh
R-CH ₂ -O-CH ₂ -R	71.25	72.02	72.0	71.6

Table D.3: ^1H - ^{13}C CP/NMR frequencies and peak assignments for the 40% hybrid ormosil prepared with D values of (a) 1, (b) 2, (c) 4, and (d) 6.

40% Hybrid				
Peak Assignment	D = 1	D = 2	D = 4	D = 6
Si- <u>CH</u> ₂ -R	8.5	8.9	8.8	8.1
R-O-CH ₂ <u>CH</u> ₃	15.1	15.1	15.1	14.7
Si-O-CH ₂ - <u>CH</u> ₃	17.8	17.8	-	17.4
Si-CH ₂ <u>CH</u> ₂ -R	22.4	22.8	22.8	22.4
-CH ₂ <u>CH</u> ^O -CH ₂	45.8	-	-	-
-CH ₂ <u>CH</u> ^O -CH ₂	51.9	-	-	-
R-O <u>CH</u> ₂ -CH ₃	59.2	59.2	-	58.5 t
Si-O <u>CH</u> ₂ -CH ₃	60.8	-	-	-
R-CH ^(OH) - <u>CH</u> ₂ -OH	63.5	63.9	63.9	63.9
CH ^(OH) -CH ₂ O- <u>CH</u> ₂ CH ₃		68.2 sh	68.2 sh	67.7 sh
R- <u>CH</u> ₂ -O- <u>CH</u> ₂ -R	71.6	72.0	72.0	71.6

Table D.4: ^1H - ^{13}C CP/NMR frequencies and peak assignments for the 60% hybrid ormosil prepared with D values of (a) 1, (b) 2, (c) 4, and (d) 6.

60% Hybrid				
Peak Assignment	D = 1	D = 2	D = 4	D = 6
Si- <u>CH</u> ₂ -R	8.9	9.6	8.8	8.8
R-O-CH ₂ <u>CH</u> ₃	15.5	15.5	15.5	15.5
Si-O-CH ₂ - <u>CH</u> ₃	18.2	18.2	-	18.2
Si-CH ₂ <u>CH</u> ₂ -R	22.8	23.2	23.2	22.8
-CH ₂ <u>CH</u> ^O -CH ₂	45.7	-	-	-
-CH ₂ <u>CH</u> ^O -CH ₂	51.8	-	-	-
R-O <u>CH</u> ₂ -CH ₃	59.6	59.6	-	-
Si-O <u>CH</u> ₂ -CH ₃	63.1	-	-	-
R-CH ^(OH) - <u>CH</u> ₂ -OH	64.3	64.3	64.3	63.9
CH ^(OH) -CH ₂ O- <u>CH</u> ₂ CH ₃	-	-	68.2	-
R- <u>CH</u> ₂ -O- <u>CH</u> ₂ -R	73.2	72.0	72.0	71.6

Table D.5: ^1H - ^{13}C CP/NMR frequencies and peak assignments for the 80% hybrid ormosil prepared with D values of (a) 1, (b) 2, (c) 4, and (d) 6.

80% Hybrid Peak Assignment	D = 1	D = 2	D = 4	D = 6
Si- <u>CH</u> ₂ -R	9.3	9.65	9.7	8.9
R-O- <u>CH</u> ₂ CH ₃	-	15.9	16.2	15.5
Si-O- <u>CH</u> ₂ - <u>CH</u> ₃	-	-	-	-
Si- <u>CH</u> ₂ <u>CH</u> ₂ -R	23.6	23.6	23.6	23.2
- <u>CH</u> ₂ <u>CH</u> ^O - <u>CH</u> ₂	44.5	44.9	-	-
- <u>CH</u> ₂ <u>CH</u> ^O - <u>CH</u> ₂	51.5	51.9	-	-
R- <u>CH</u> ^(OH) - <u>CH</u> ₂ <u>OCH</u> ₃	58.9 t	59.6	59.5	59.6
Si- <u>OCH</u> ₂ -CH ₃	-	-	-	-
R- <u>CH</u> ^(OH) - <u>CH</u> ₂ -OH	63.9 t	64.7	64.7	64.3
<u>CH</u> ^(OH) - <u>CH</u> ₂ <u>O-CH</u> ₂ CH ₃	-	68.2	68.6	-
R- <u>CH</u> ₂ - <u>O-CH</u> ₂ -R	72.0 73.96	72.0	72.0	71.6

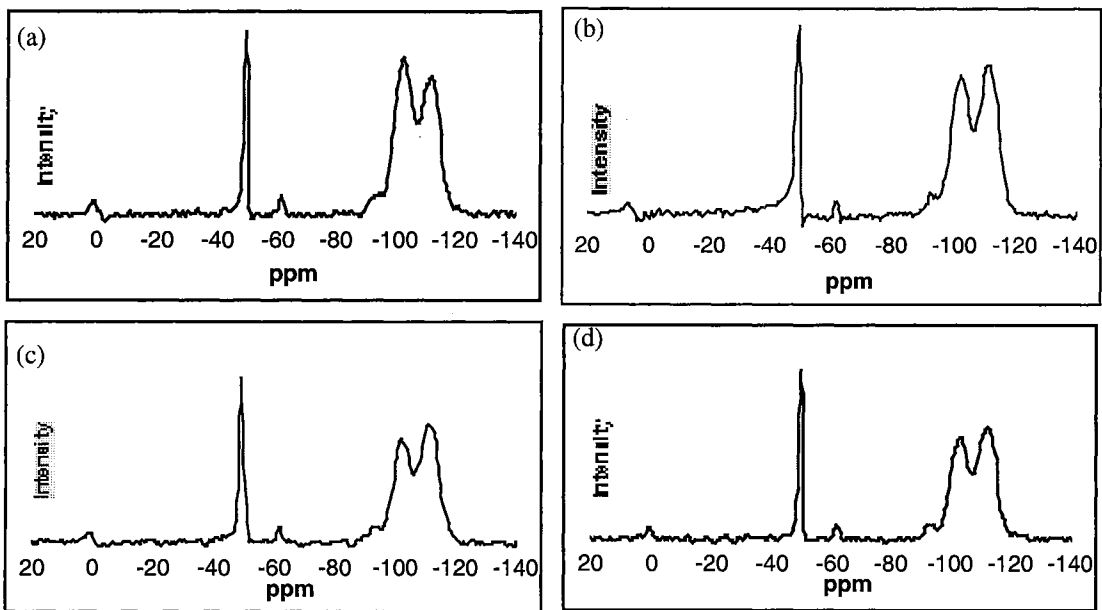


Figure D.4: ^{29}Si Single pulse/MAS NMR spectrum of 10% Epoxide Ormosil gels prepared with D values of (a) 1, (b) 2, (c) 4, and (d) 6

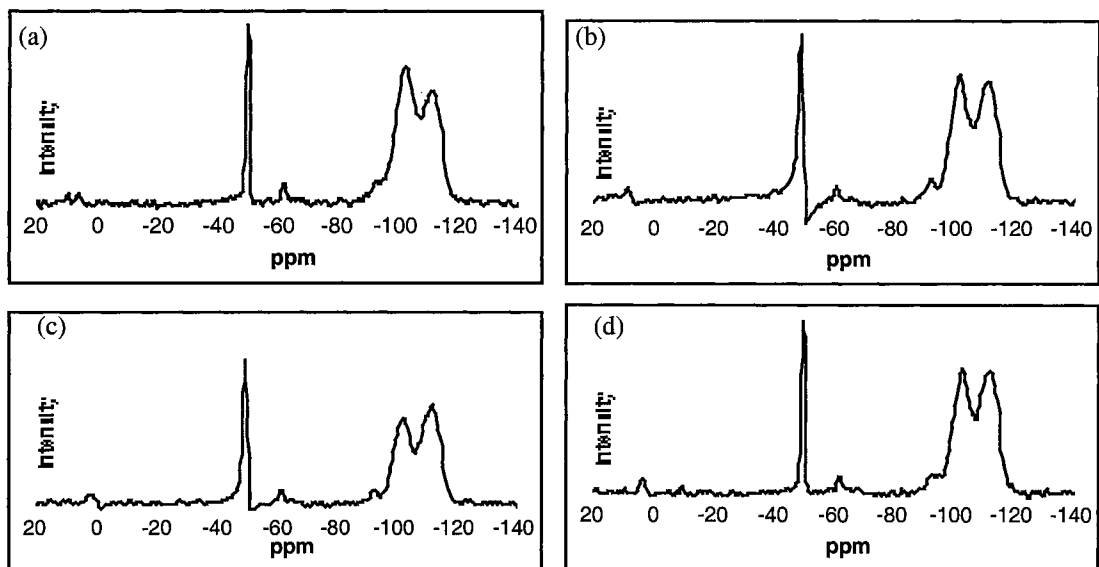


Figure D.5: ^{29}Si Single pulse/MAS NMR spectrum of 20% Epoxide Ormosil gels prepared with with D values of (a) 1, (b) 2, (c) 4, and (d) 6

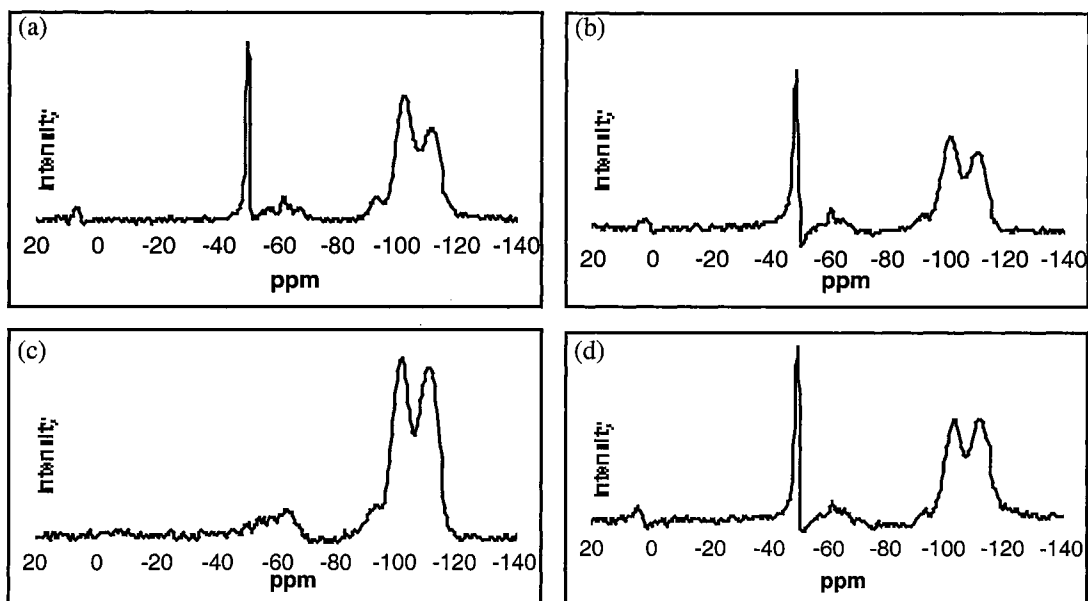


Figure D.6: ^{29}Si Single pulse/MAS NMR spectrum of 40% Epoxide Ormosil gels prepared with D values of (a) 1, (b) 2, (c) 4, and (d) 6.

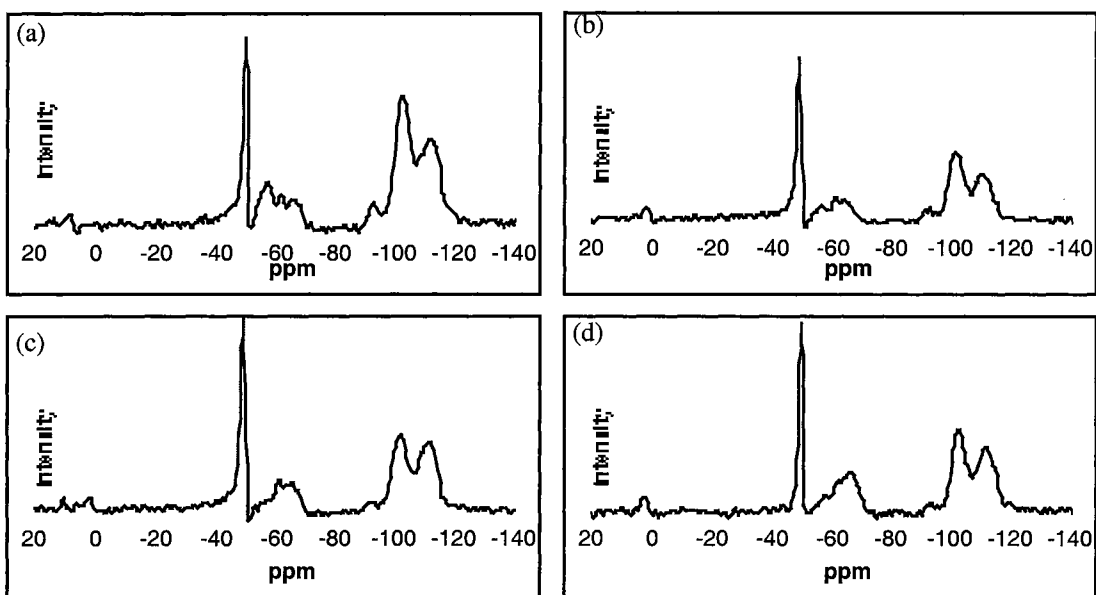


Figure D.7: ^{29}Si Single pulse/MAS NMR spectrum of 60% Epoxide Ormosil gels prepared with D values of (a) 1, (b) 2, (c) 4, and (d) 6.

Table D.5: ^{29}Si SP/MAS NMR frequencies and peak assignments for the 10% hybrid ormosil prepared with D values of (a) 1, (b) 2, (c) 4, and (d) 6. Parentheses values represent quantified peak percentages.

10% Hybrid D value	Frequency Shift (ppm)				
	T ₂	T ₃	Q ₂	Q ₃	Q ₄
1	-	-62.3(-)	-93.2(1.9%)	-103.3(51.0%)	-112.6(47.0%)
2	-	-63.4(-)	-93.4(2.4%)	-103.8(43.6%)	-113.3(54.0%)
4	-	-62.9(-)	-93.3(1.4%)	-103.1(43.3%)	-112.3(55.3%)
6	-	-62.7(-)	-93.4(1.6%)	-103.2(43.4%)	-112.8(55.0%)

Table D.6: ^{29}Si SP/MAS NMR frequencies and peak assignments for the 20% hybrid ormosil prepared with D values of (a) 1, (b) 2, (c) 4, and (d) 6. Parentheses values represent quantified peak percentages.

20% Hybrid D value	Frequency Shift (ppm)				
	T ₂	T ₃	Q ₂	Q ₃	Q ₄
1	-	-63.5(-)	-94.0(1.7%)	-103.7(53.9%)	-112.9(44.5%)
2	-	-63.4(-)	-94.5(3.4%)	-103.8(47.4%)	-113.1(49.2%)
4	-	-63.0(-)	-92.9(2.1%)	-103.0(45.3%)	-112.5(52.5%)
6	-	-63.5(-)	-93.9(2.1%)	-103.9(45.8%)	-113.0(52.1%)

Table D.7: ^{29}Si SP/MAS NMR frequencies and peak assignments for the 40% hybrid ormosil prepared with D values of (a) 1, (b) 2, (c) 4, and (d) 6. Parentheses values represent quantified peak percentages.

40% Hybrid D value	Frequency Shift (ppm)				
	T ₂	T ₃	Q ₂	Q ₃	Q ₄
1	-	-63.5(-)	-94.0(4.1%)	-103.7(54.9%)	-112.6(41.0%)
2	-	-63.5(-)	-86.4(3.0%)	-103.6(49.0%)	-112.7(43.7%)
4	-	-64.5(-)	-93.9(2.2%)	-103.7(44.2%)	-112.9(48.3%)
6	-	-63.3(-)	-93.8(2.2%)	-103.6(45.2%)	-112.5(52.6%)

Table D.8: ^{29}Si SP/MAS NMR frequencies and peak assignments for the 60% hybrid ormosil prepared with D values of (a) 1, (b) 2, (c) 4, and (d) 6. Parentheses values represent quantified peak percentages.

60% Hybrid D value	Frequency Shift (ppm)					
	T ₁	T ₂	T ₃	Q ₂	Q ₃	Q ₄
1	-51.2(32.9%)	-58.1(28.5%)	-67.9(38.6%)	-94.1(4.9%)	-103.0(52.8%)	-112.0(42.3%)
2	-51.3 (24.9%)	-58.1(31.4%)	-66.5(43.7%)	-93.3(4.1%)	-101.4(54.7%)	-111.2(41.1%)
4	-51.0 (14.7%)	-58.8(38.6%)	-66.3(46.7%)	-94.1(1.6%)	-102.2(48.9%)	-112.0(49.5%)
6	-51.4 (13.4%)	-58.5(20.9%)	-67.1(65.7%)	-94.1(2.9%)	-103.0(48.4%)	-112.0(48.6%)

APPENDIX E

RAMAN SPECTRA AND TABLES OF ORMOSIL GELS

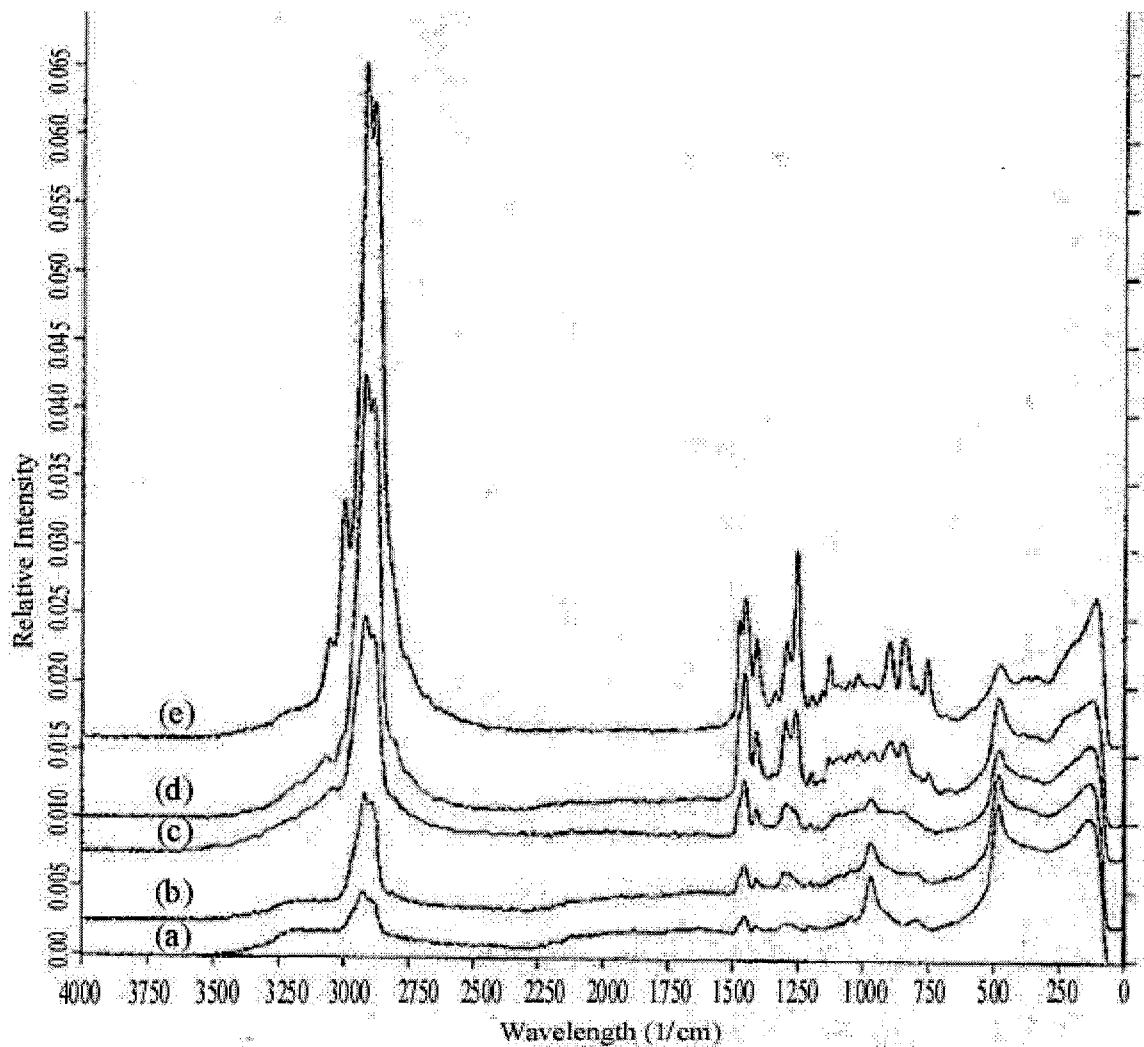


Figure E.1: Overlaid Raman spectra of epoxide hybrid gels prepared with an D value of 2 and incremental concentrations of organic content; (a) 10% hybrid, (b) 20% hybrid, (c) 40% hybrid, (d) 60% hybrid, and (e) 80% hybrid. All gels have been cured at room temperature. Spectral intensities have been adjusted in reference to the siloxane peak.

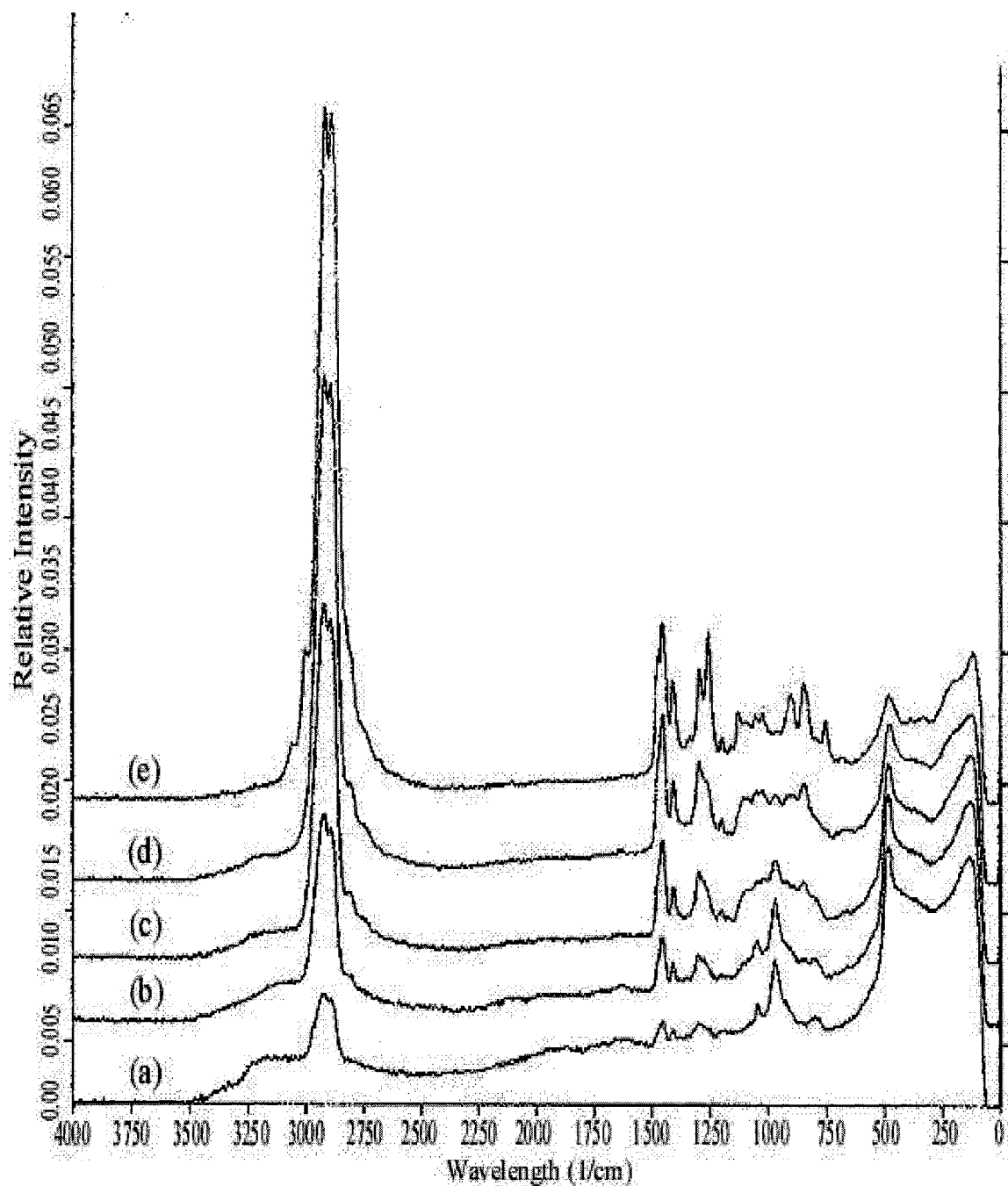


Figure E.2: Overlaid Raman spectra of epoxide hybrid gels prepared with an D value of 4 and incremental concentrations of organic content; (a) 10% hybrid, (b) 20% hybrid, (c) 40% hybrid, (d) 60% hybrid, and (e) 80% hybrid. All gels have been cured at room temperature. Spectral intensities have been adjusted in reference to the siloxane peak.

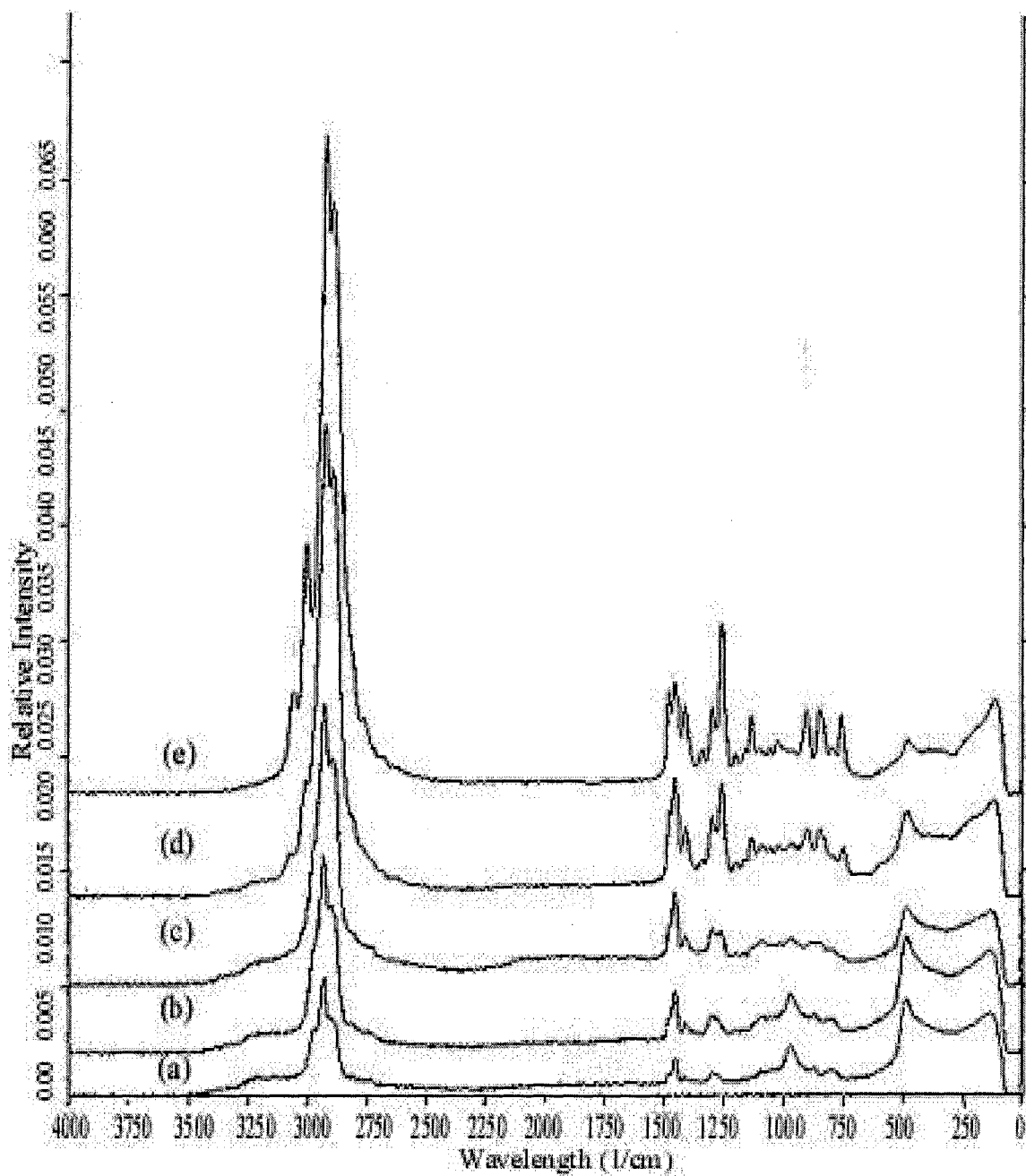


Figure E.3: Overlaid Raman spectra of epoxide hybrid gels prepared with an D value of 1 and incremental concentrations of organic content; (a) 10% hybrid, (b) 20% hybrid, (c) 40% hybrid, (d) 60% hybrid, and (e) 80% hybrid. All gels have been cured at 60 °C. Spectral intensities have been adjusted in reference to the siloxane peak.

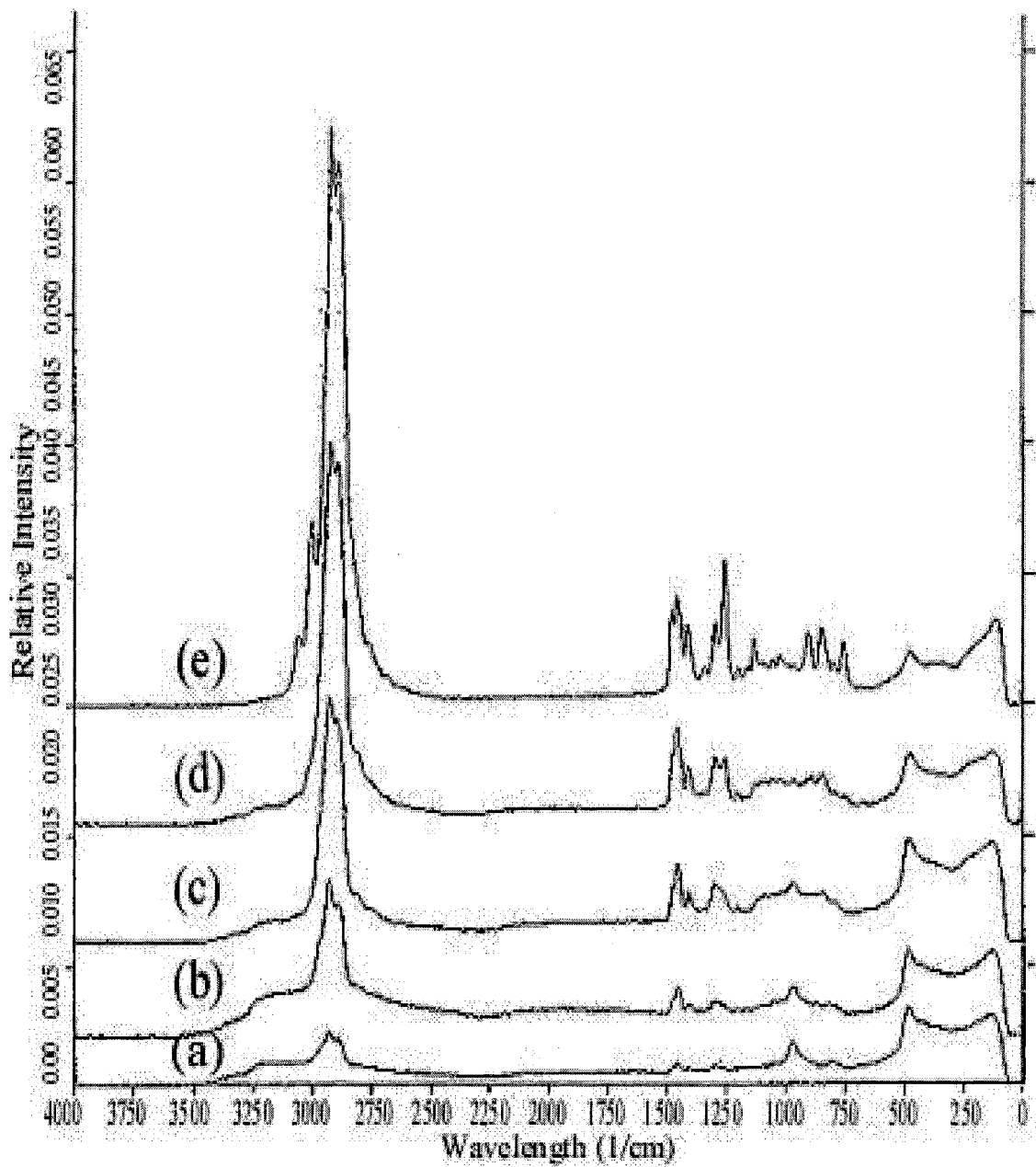


Figure E.4: Overlaid Raman spectra of epoxide hybrid gels prepared with an D value of 2 and incremental concentrations of organic content; (a) 10% hybrid, (b) 20% hybrid, (c) 40% hybrid, (d) 60% hybrid, and (e) 80% hybrid. All gels have been cured at 60 °C. Spectral intensities have been adjusted in reference to the siloxane peak.

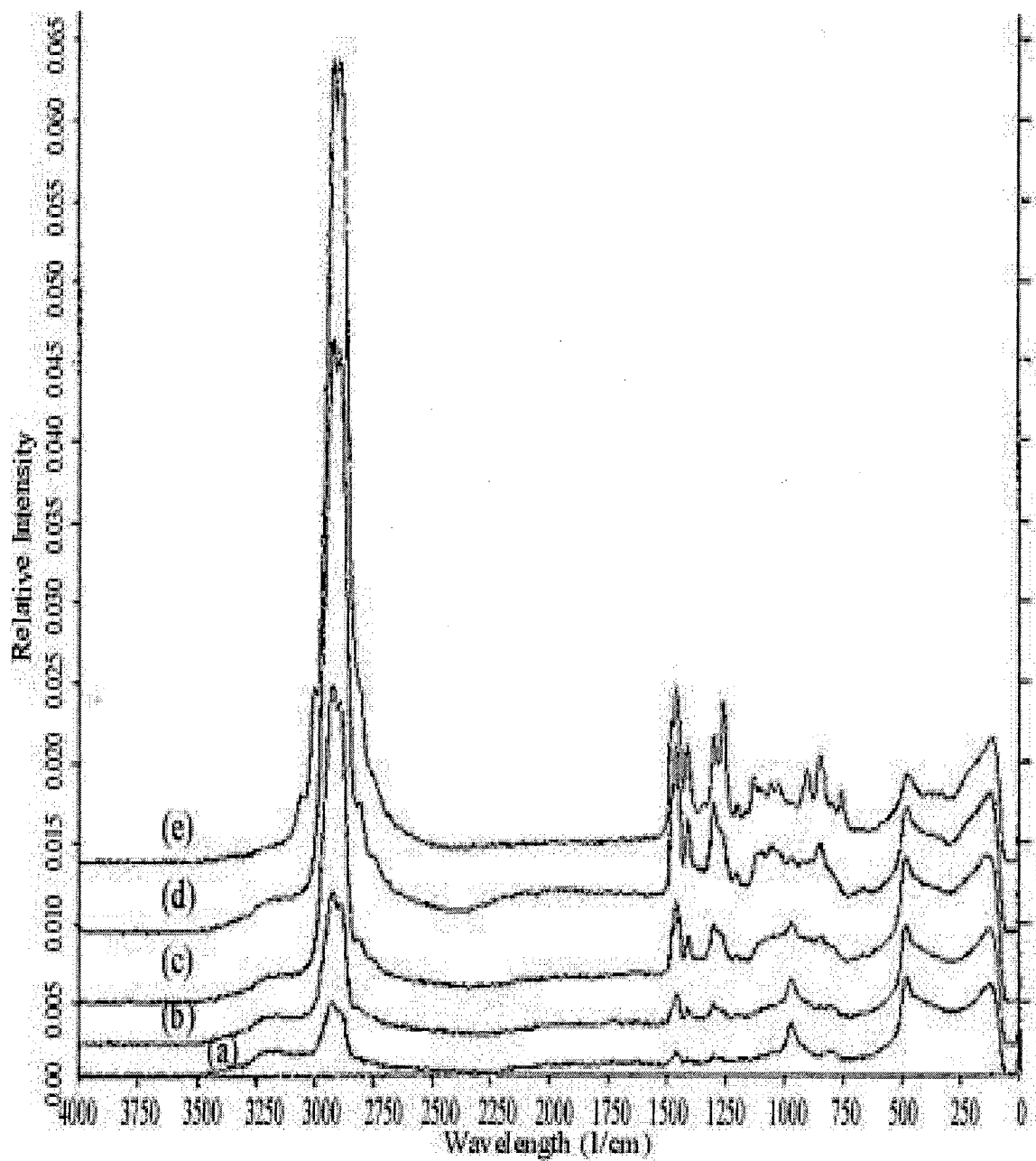


Figure E.5: Overlaid Raman spectra of epoxide hybrid gels prepared with an D value of 4 and incremental concentrations of organic content; (a) 10% hybrid, (b) 20% hybrid, (c) 40% hybrid, (d) 60% hybrid, and (e) 80% hybrid. All gels have been cured at 60 °C. Spectral intensities have been adjusted in reference to the siloxane peak.

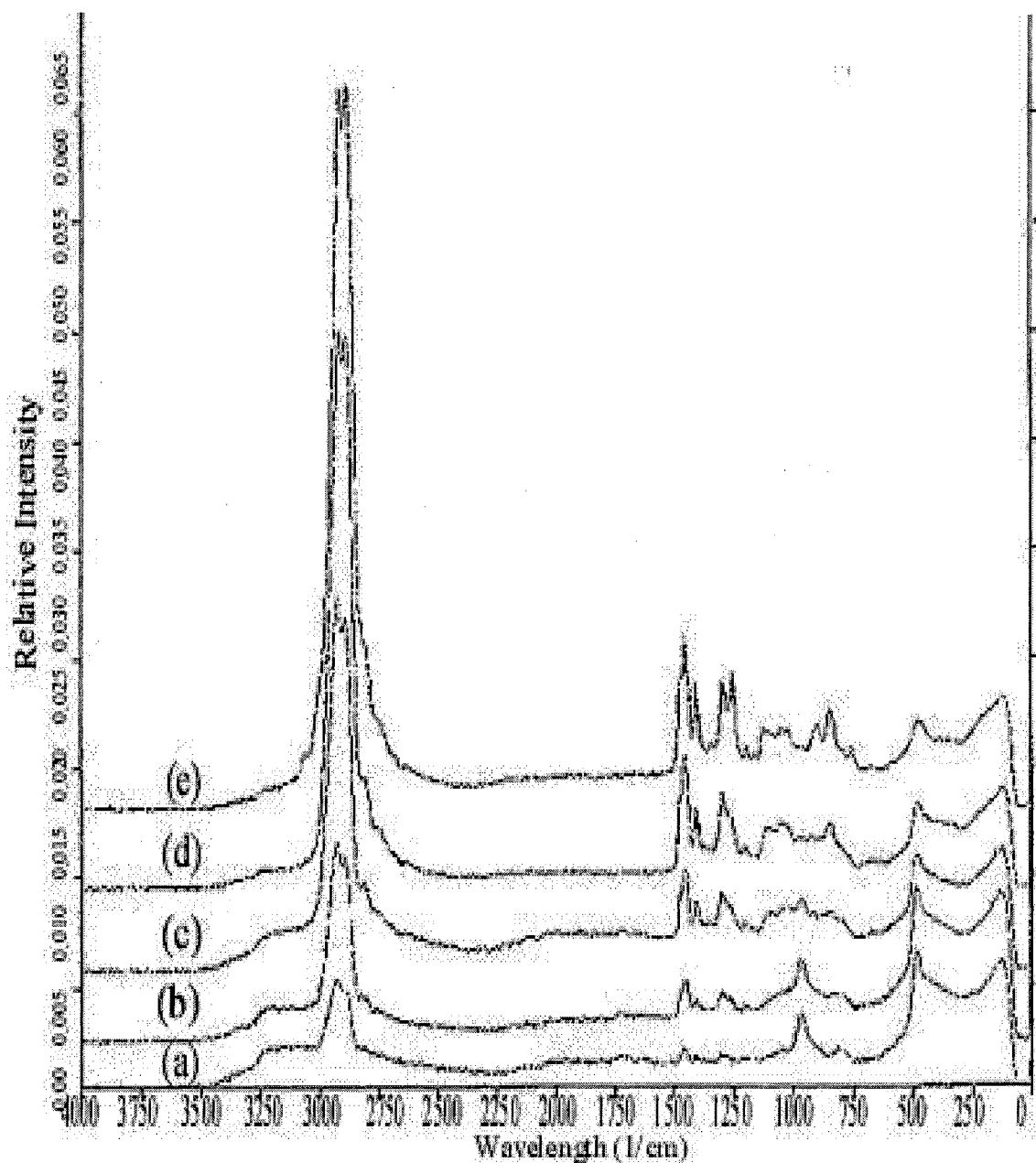


Figure E.6 Overlaid Raman spectra of epoxide hybrid gels prepared with an D value of 6 and incremental concentrations of organic content; (a) 10% hybrid, (b) 20% hybrid, (c) 40% hybrid, (d) 60% hybrid, and (e) 80% hybrid. All gels have been cured at 60 °C. Spectral intensities have been adjusted in reference to the siloxane peak.

R=4 Epoxide Ormosils cured at 150 °C

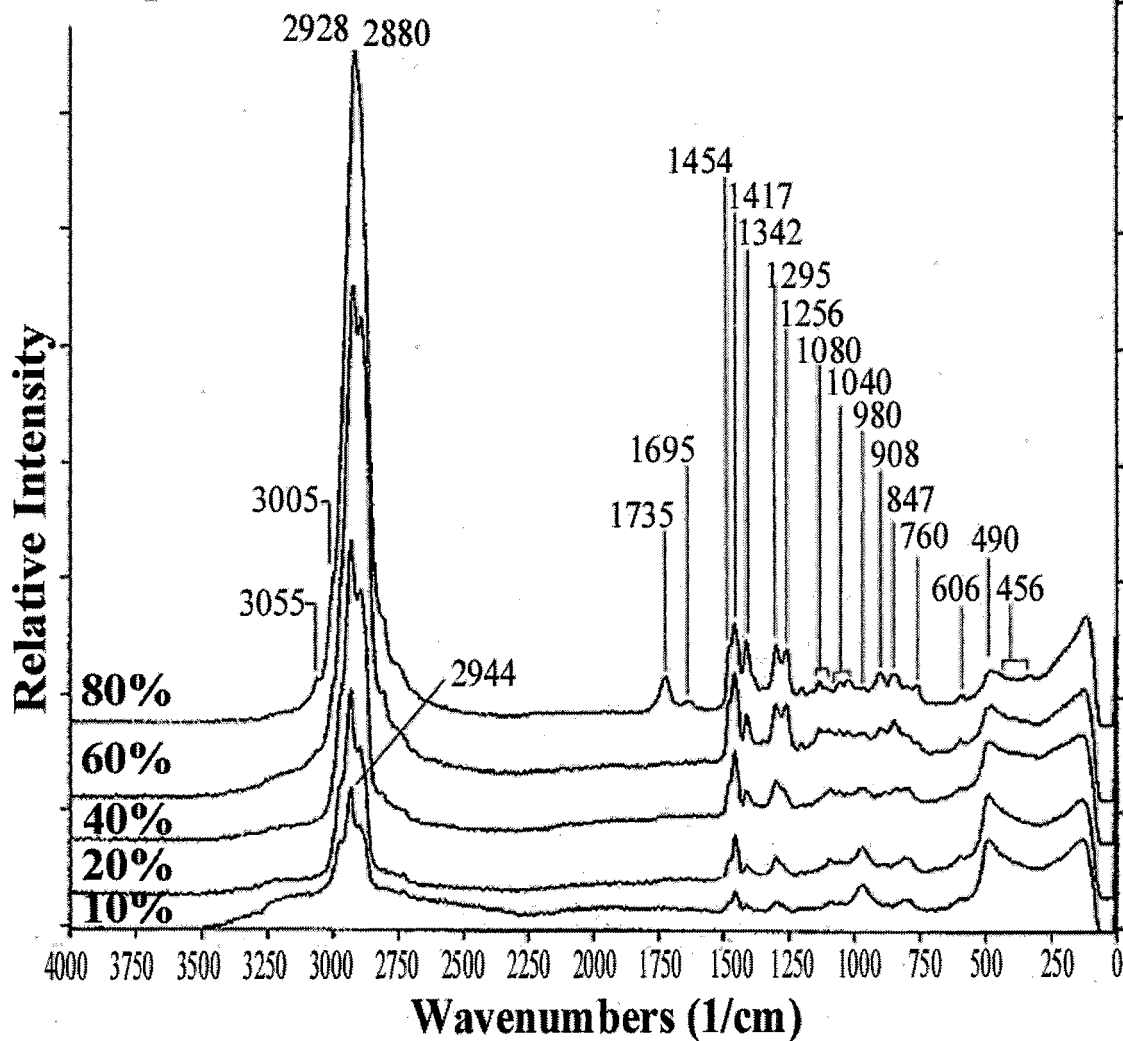


Figure E.7 : Overlaid Raman Spectra for the epoxide hybrid gels prepared with D values of 1 and cured at 150 °C. Spectral intensities have been adjusted in reference to the siloxane peak.

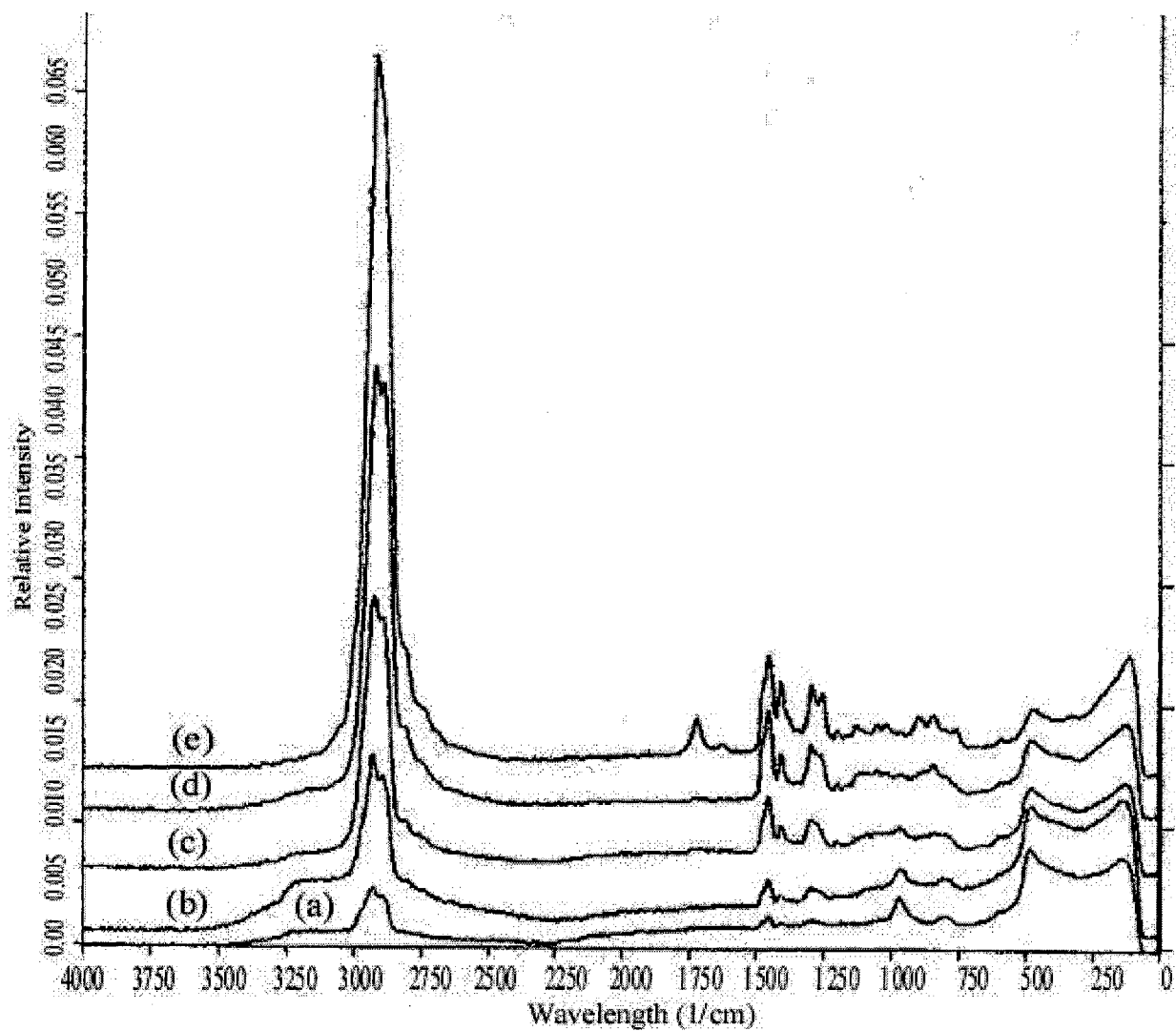


Figure E.8: Overlaid Raman spectra of epoxide hybrid gels prepared with an D value of 2 and incremental concentrations of organic content; (a) 10% hybrid, (b) 20% hybrid, (c) 40% hybrid, (d) 60% hybrid, and (e) 80% hybrid. All gels have been cured at 150°C. Spectral intensities have been adjusted in reference to the siloxane peak.

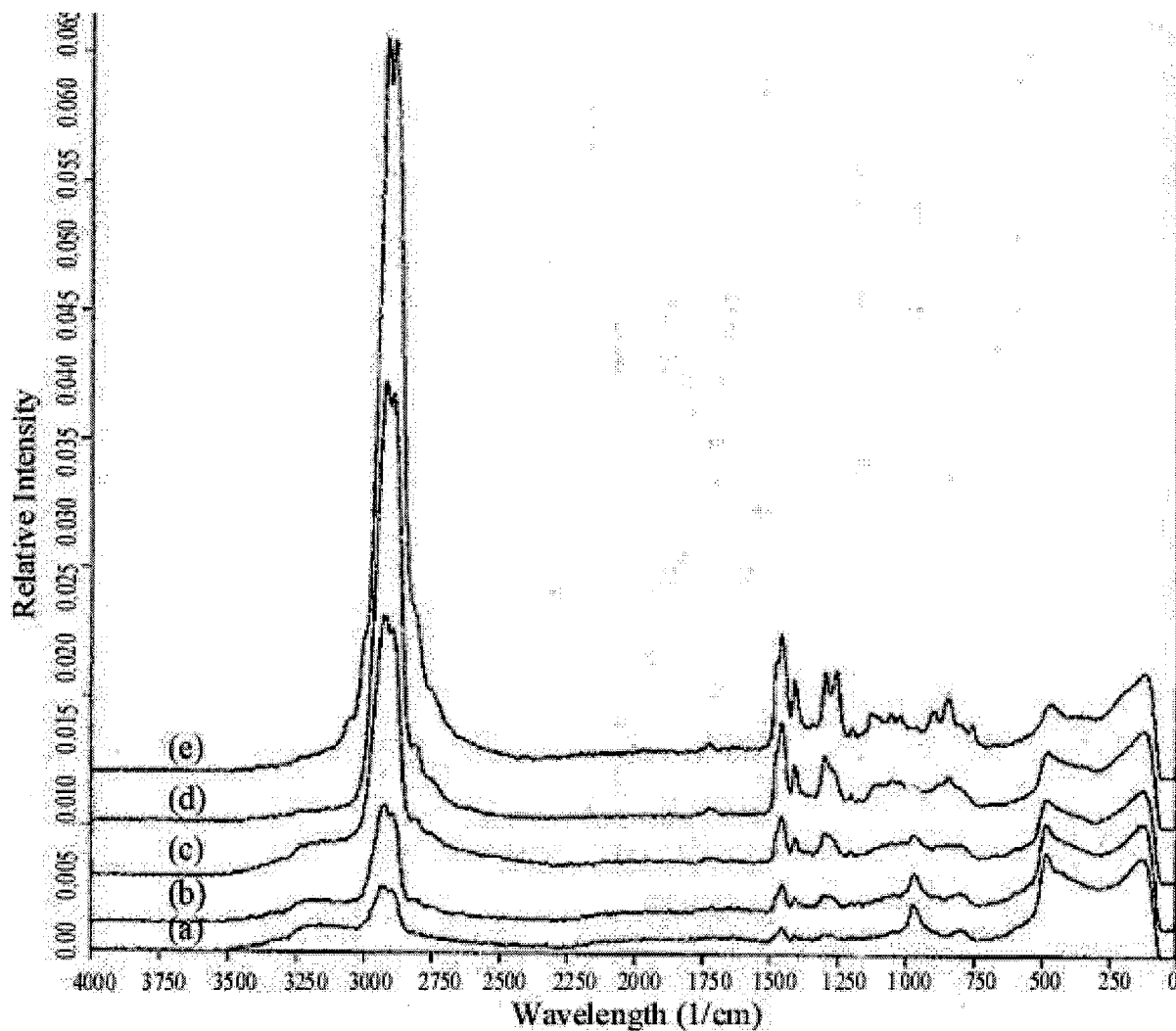


Figure E.9: Overlaid Raman spectra of epoxide hybrid gels prepared with an D value of 4 and incremental concentrations of organic content; (a) 10% hybrid, (b) 20% hybrid, (c) 40% hybrid, (d) 60% hybrid, and (e) 80% hybrid. All gels have been cured at 150 °C. Spectral intensities have been adjusted in reference to the siloxane peak.

R=24 Epoxide Ormosils cured at 150 °C

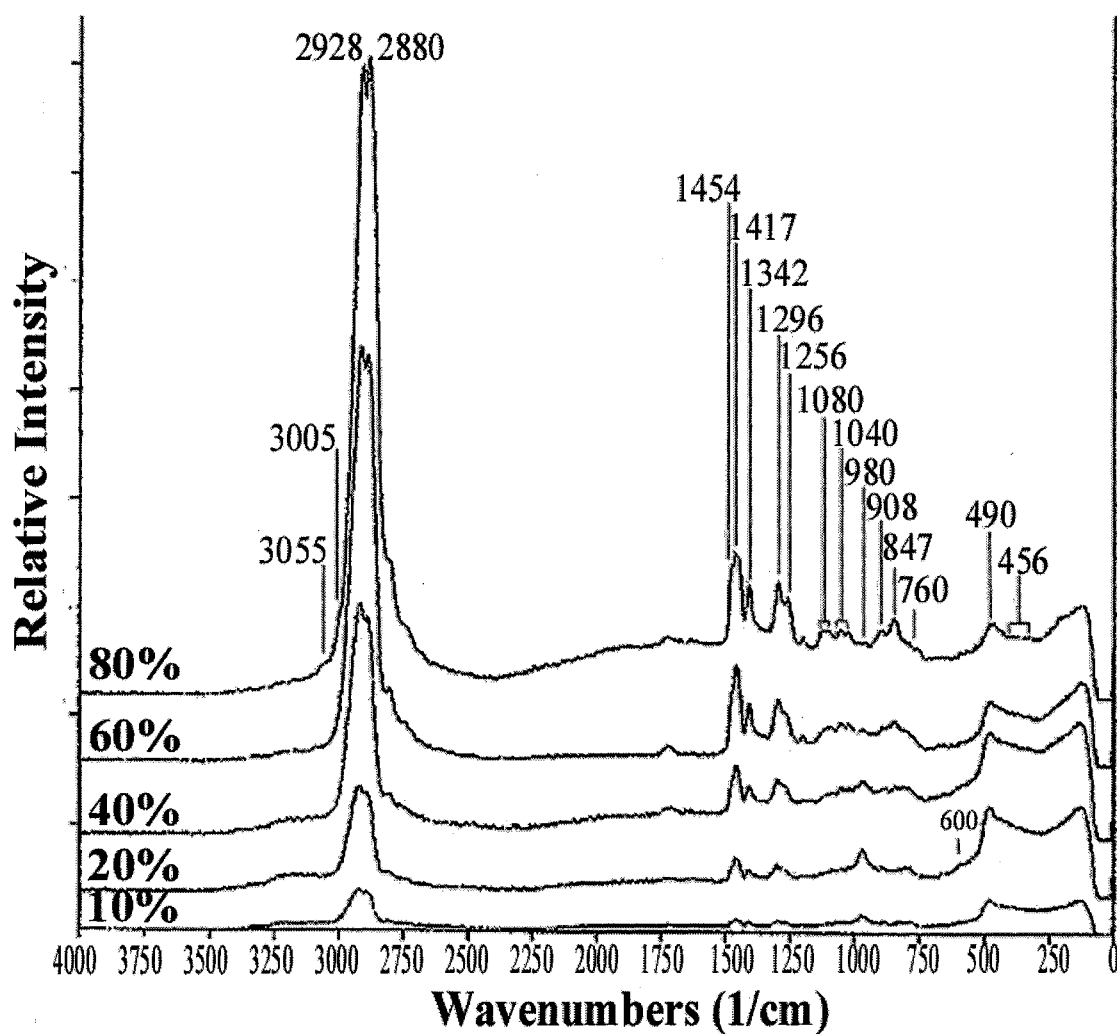


Figure E.10: Overlaid Raman Spectra for the epoxide hybrid gels prepared with D values of 6 and cured at 150 °C. Spectral intensities have been adjusted in reference to the siloxane peak.

APPENDIX F

FT-IR REFLECTANCE SPECTRA FOR HYBRID FILMS

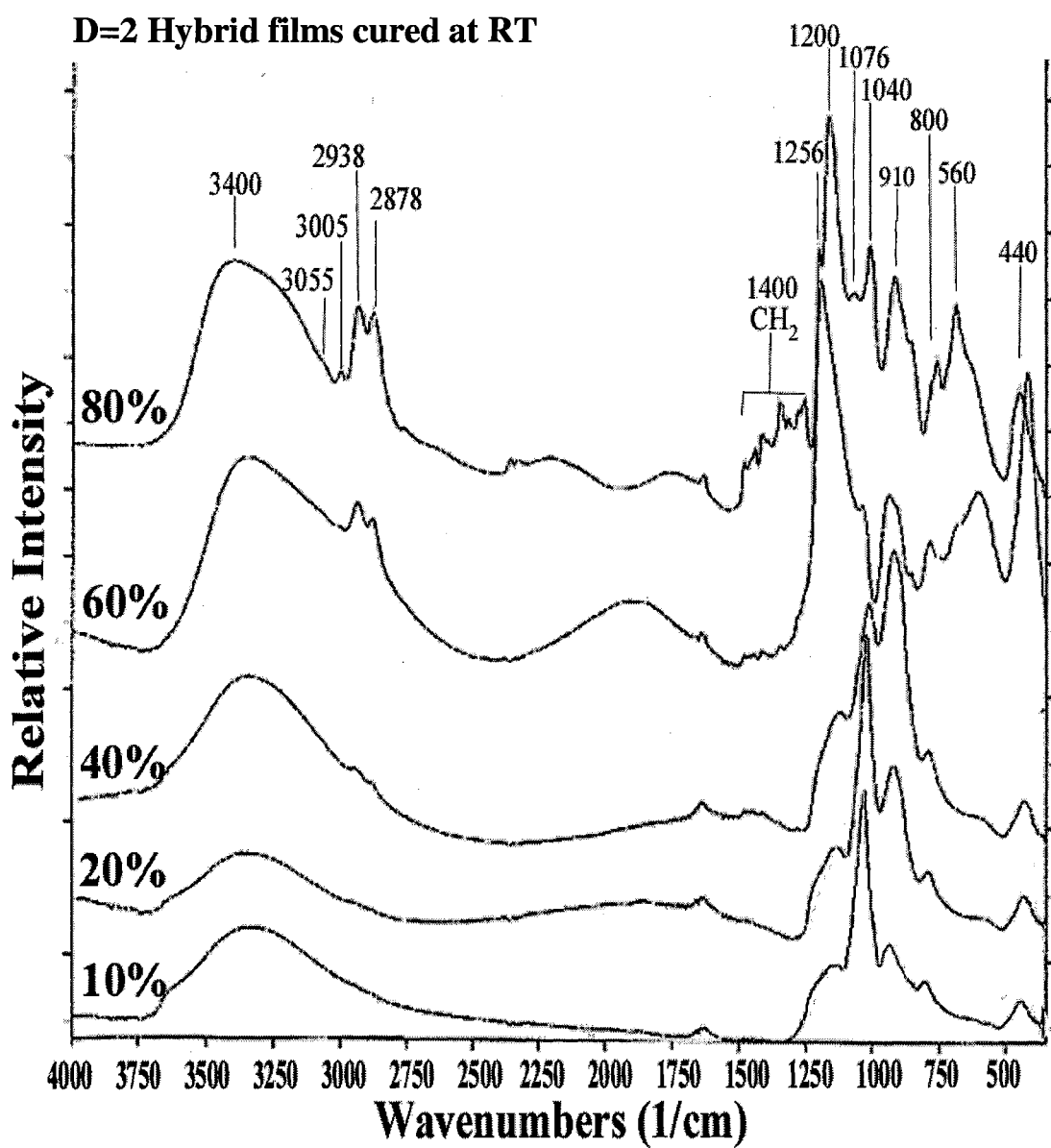


Figure F.1: Overlaid IR reflectance spectra of epoxide-based ormosil thin film prepared using an D value of 2 and cured at room temperature.

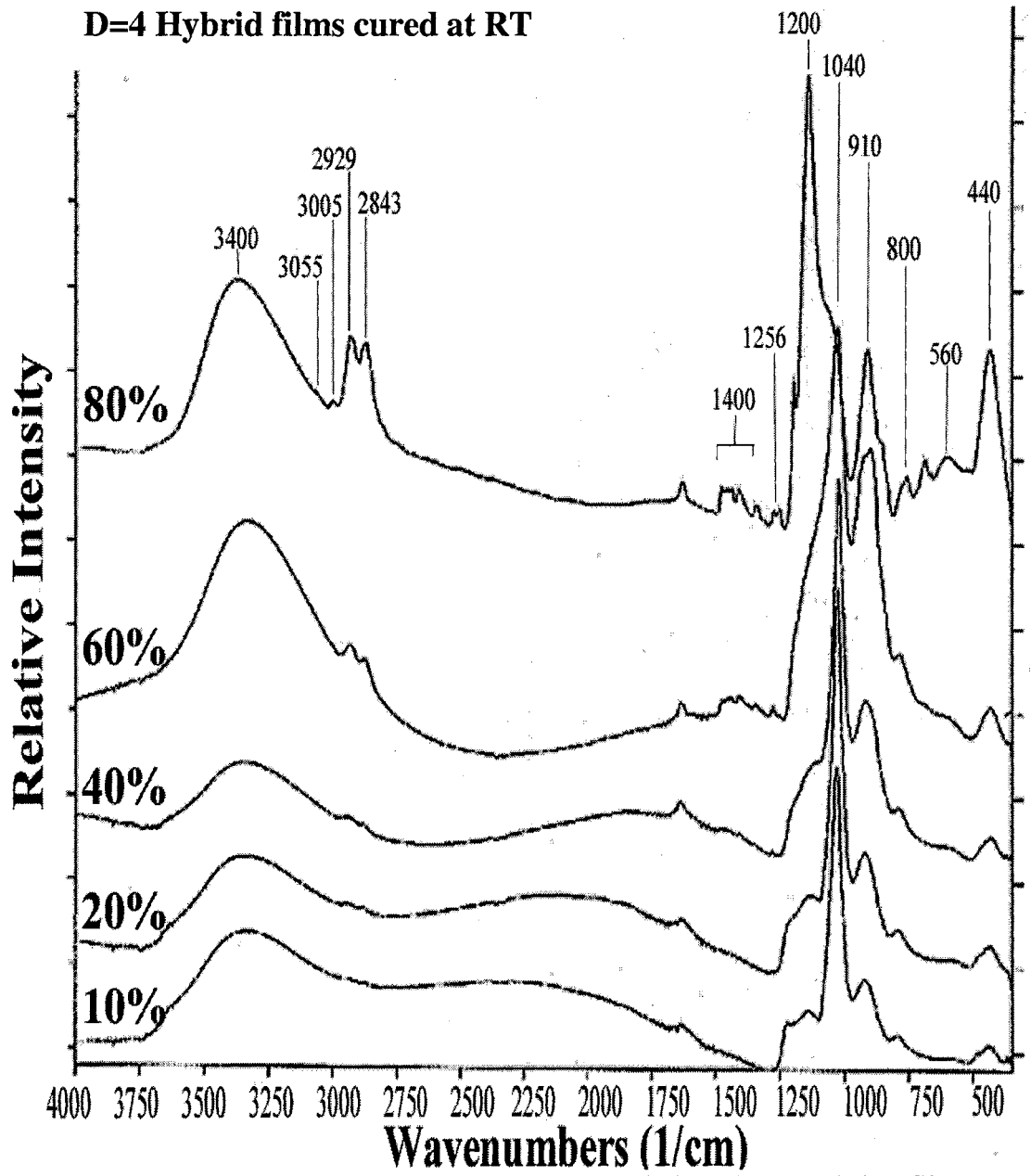


Figure F.2: Overlaid IR reflectance spectra of epoxide-based ormosil thin film prepared using an D value of 4 and cured at room temperature.

D=1 Hybrid films cured at 60°C

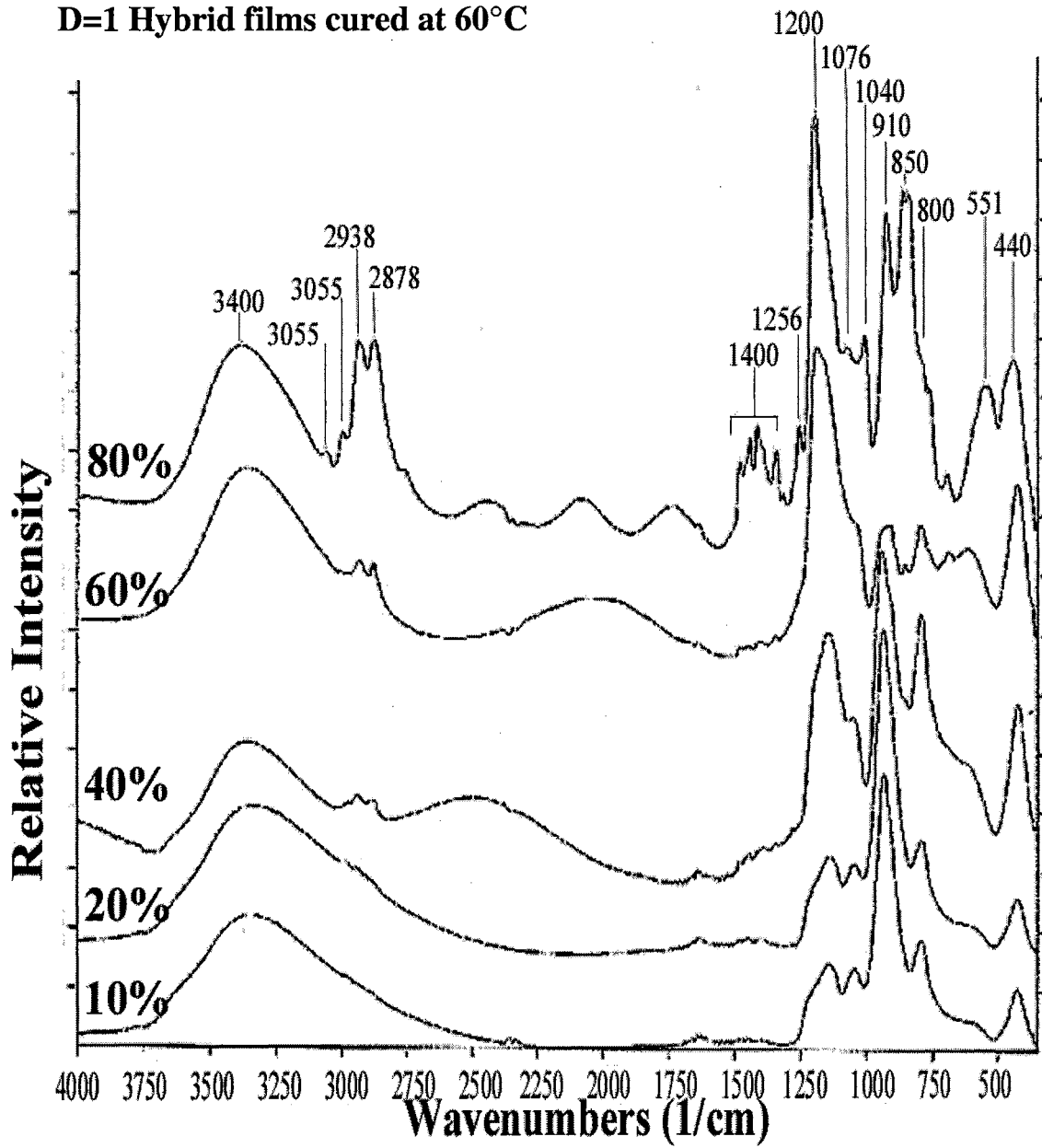


Figure F.3: Overlaid IR reflectance spectra of epoxide-based ormosil thin film prepared using an D value of 1 and cured at 60 °C.

D=2 Hybrid films cured at 60 °C

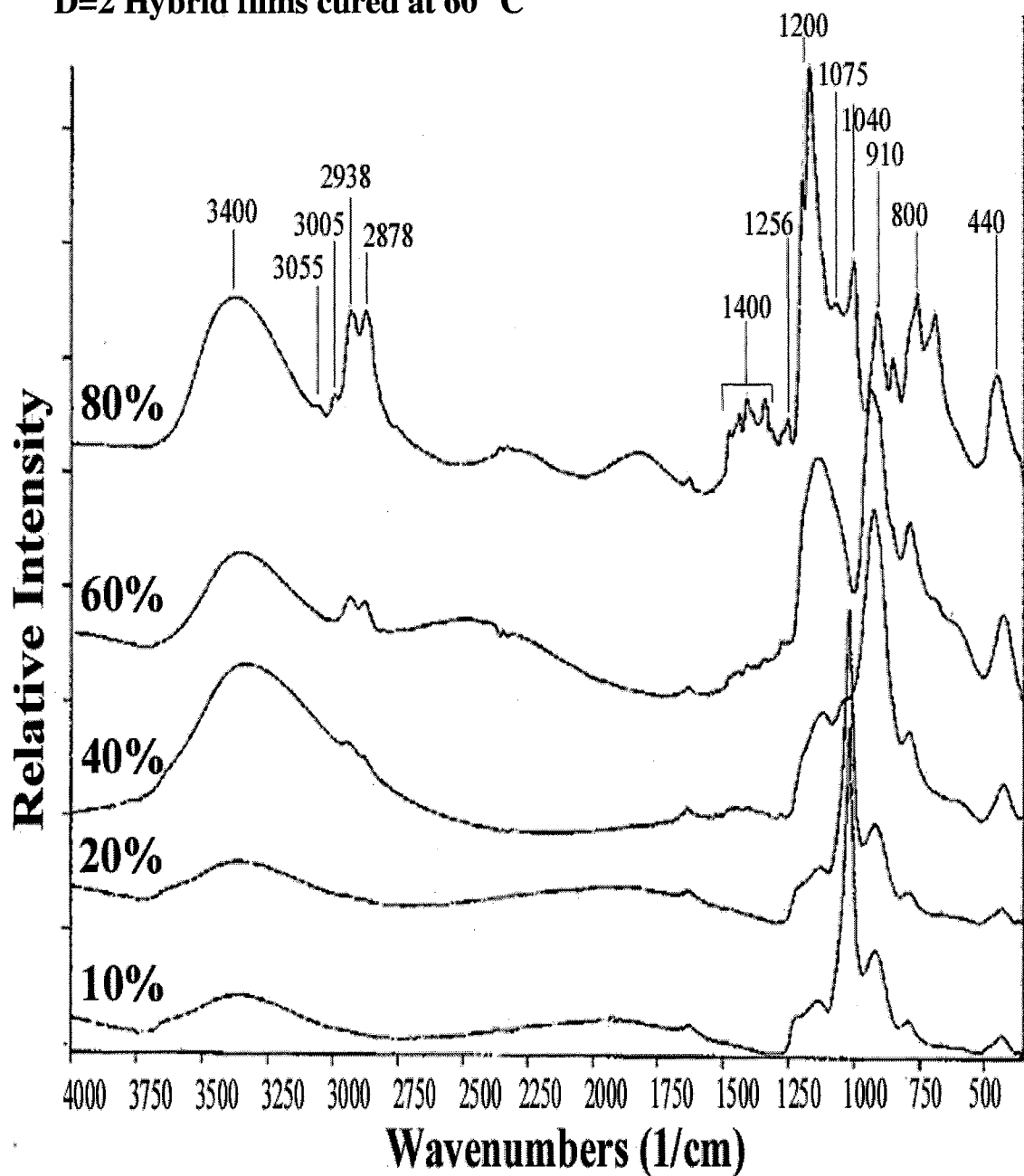


Figure F.4: Overlaid IR reflectance spectra of epoxide-based ormosil thin film prepared using an D value of 2 and cured at 60 °C.

D=4 Hybrid films cured at 60 °C

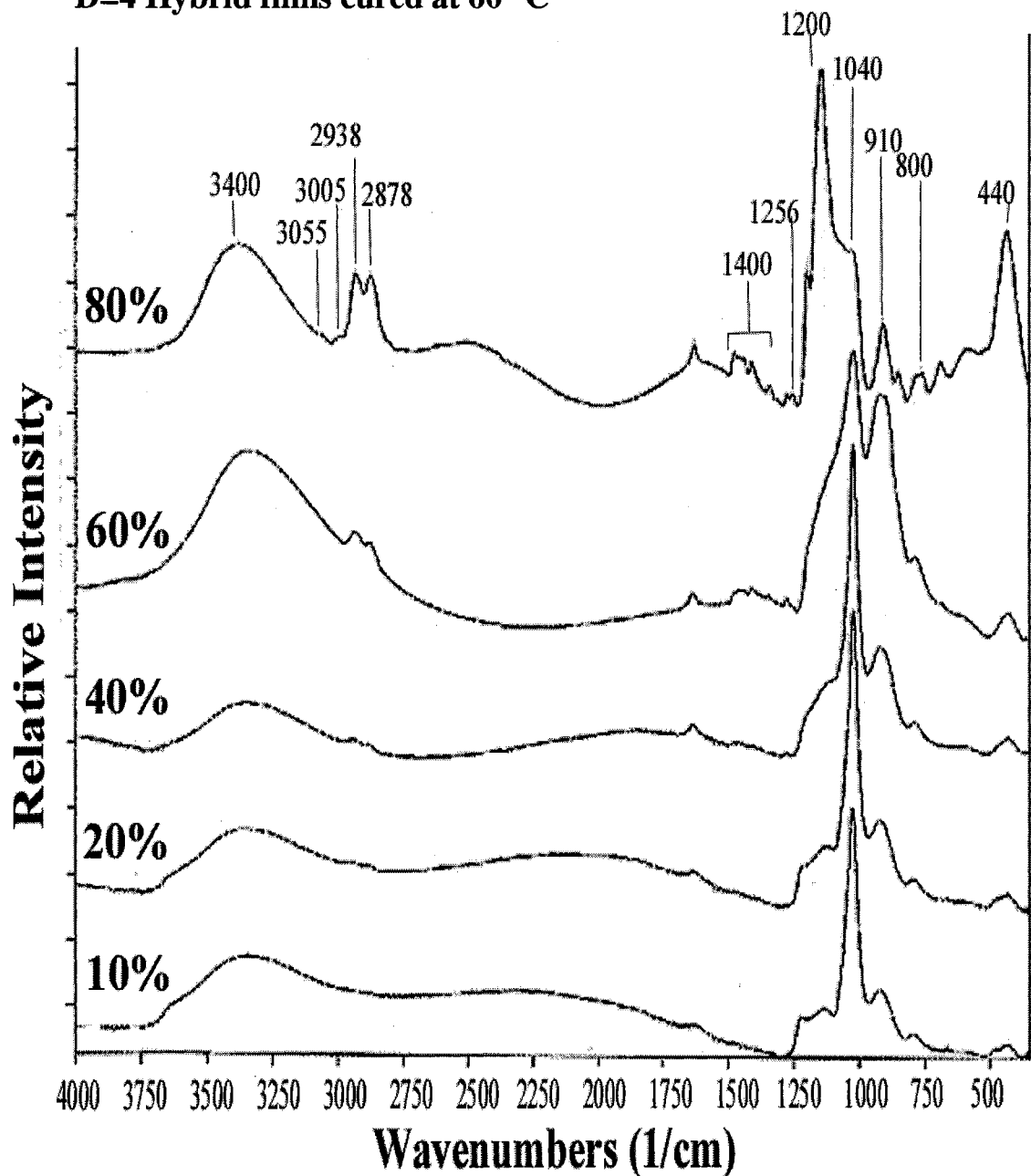


Figure F.5: Overlaid IR reflectance spectra of epoxide-based ormosil thin film prepared using an D value of 4 and cured at 60 °C.

D=6 Hybrid films cured at 60 °C

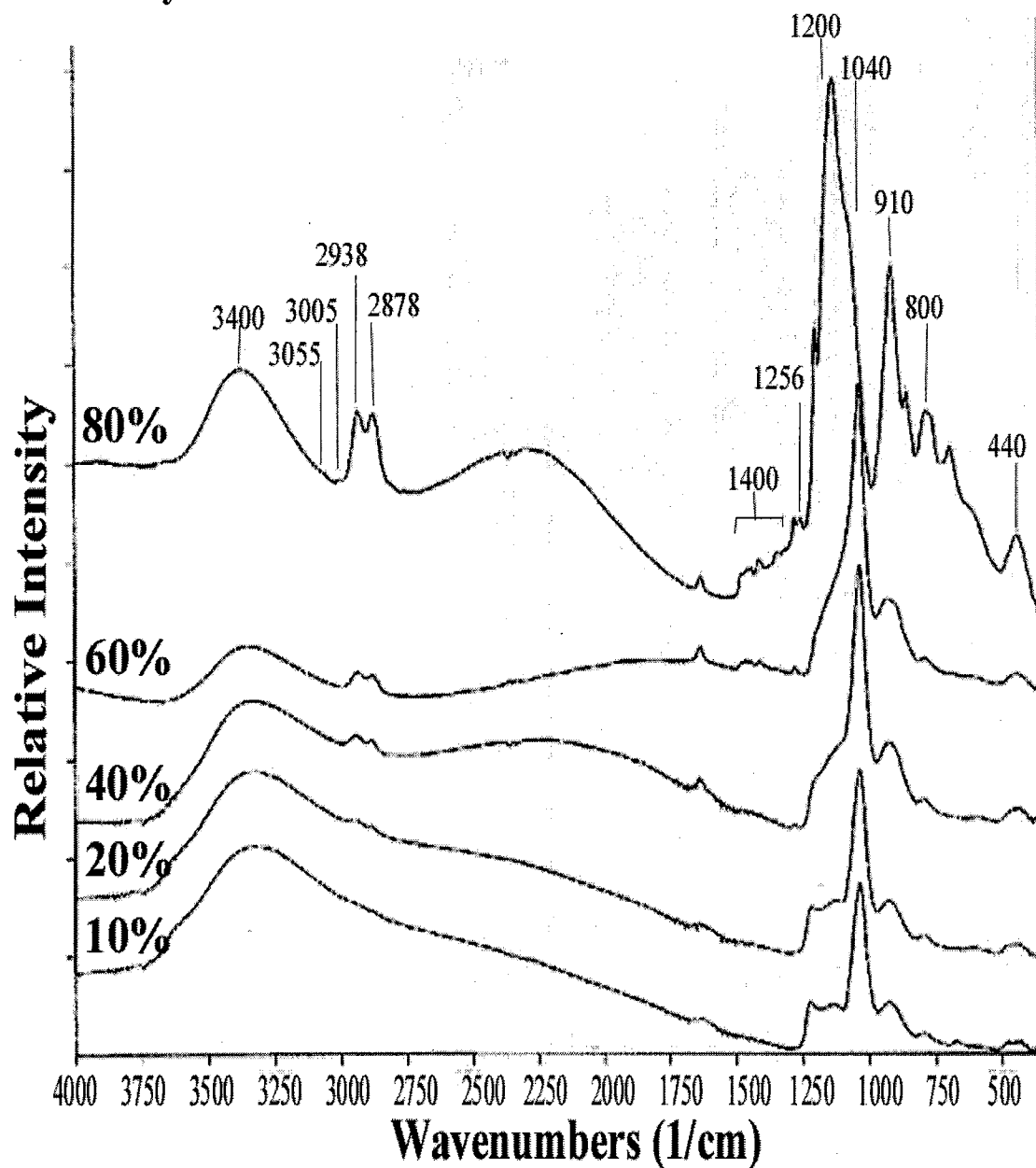


Figure F.6: Overlaid IR reflectance spectra of epoxide-based ormosil thin film prepared using an D value of 6 and cured at 60 °C.

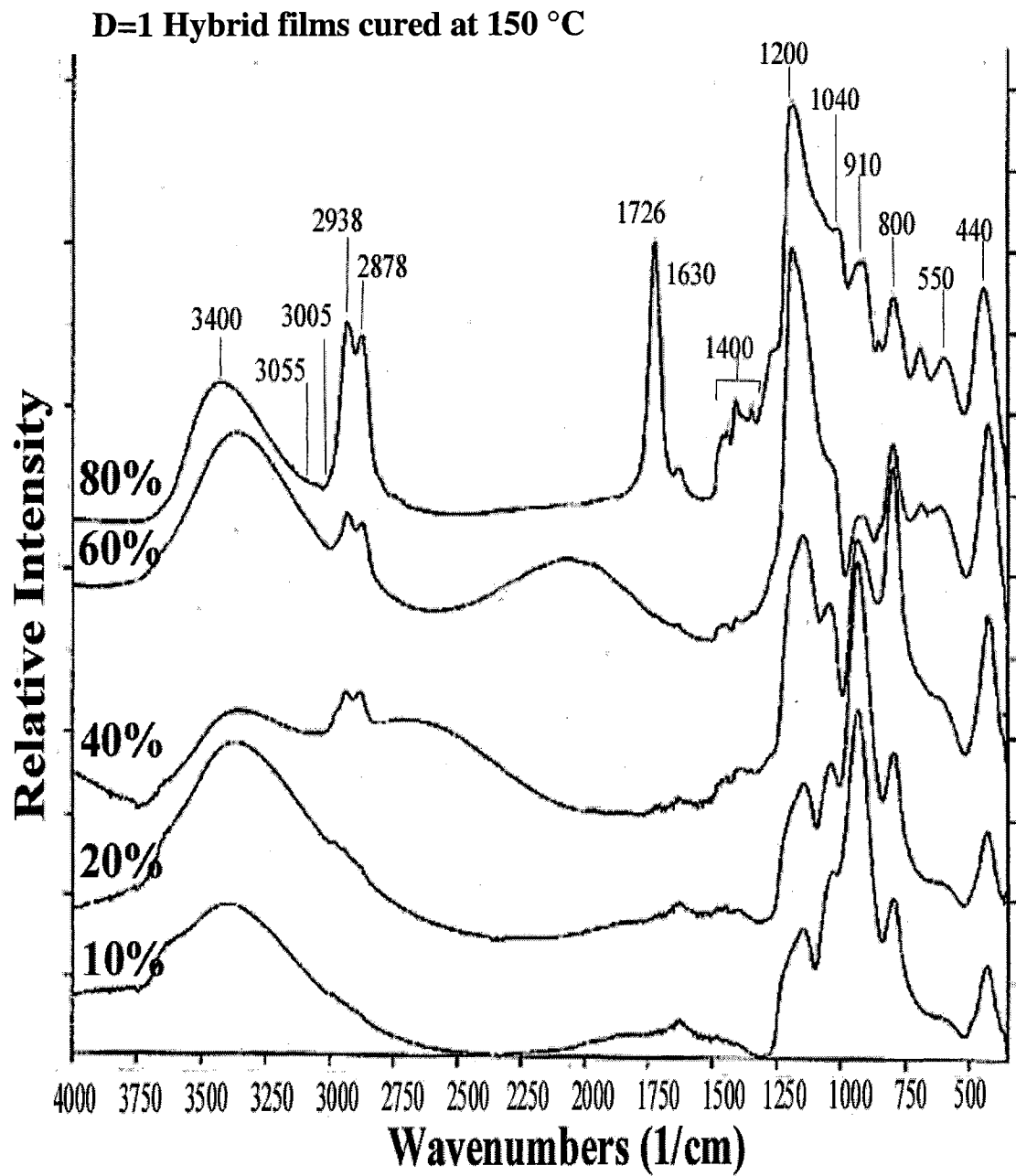


Figure F.7: Overlaid IR reflectance spectra of epoxide-based ormosil thin film prepared using an D value of 1 and cured at 150 °C.

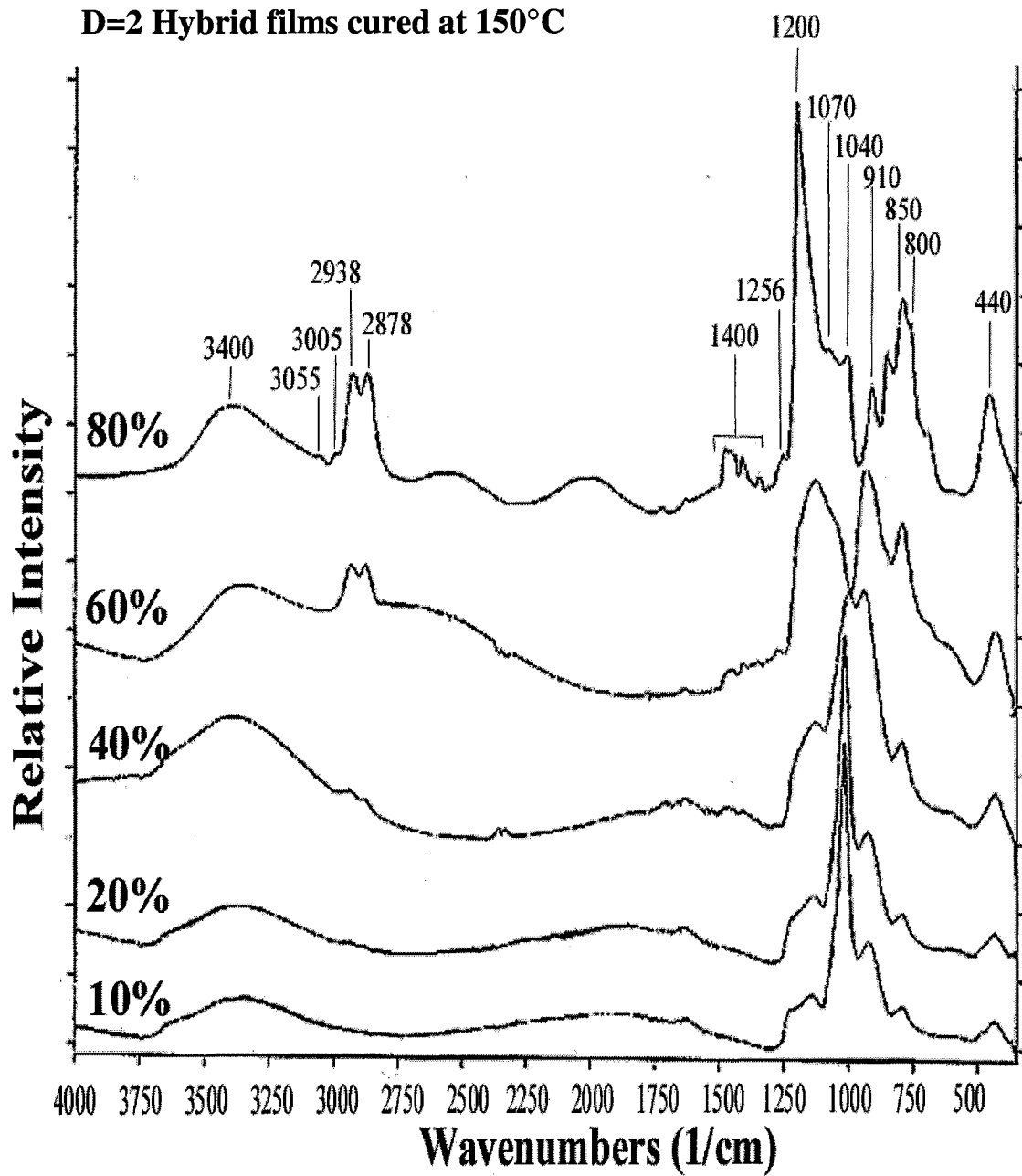


Figure 10: Overlaid IR reflectance spectra of epoxide-based ormosil thin film prepared using an D value of 2 and cured at 150 °C.

D=4 Hybrid films cured at 150 °C

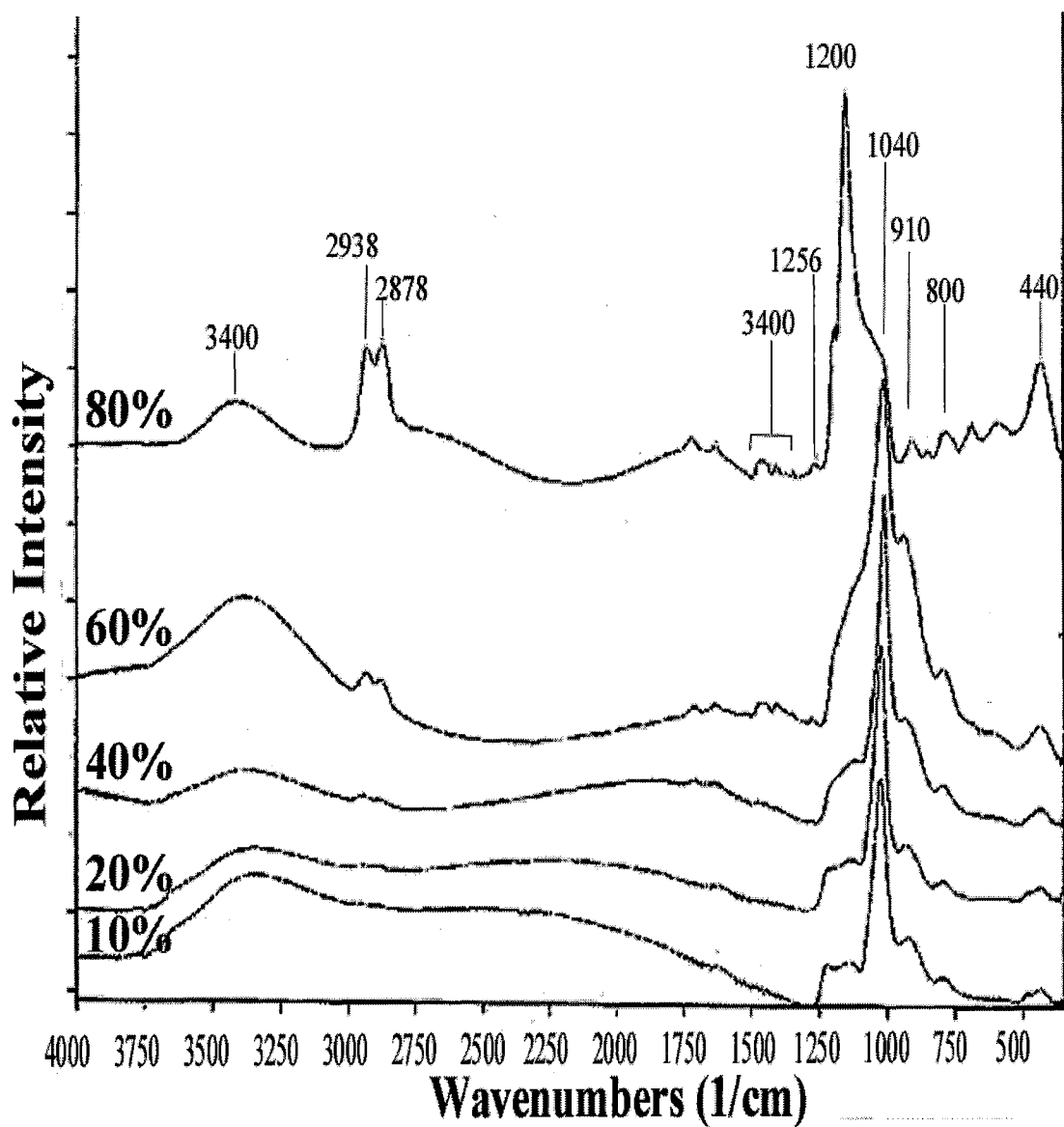


Figure 11: Overlaid IR reflectance spectra of epoxide-based ormosil thin film prepared using an D value of 4 and cured at 150 °C.

D=6 Hybrid films cured at 150 °C

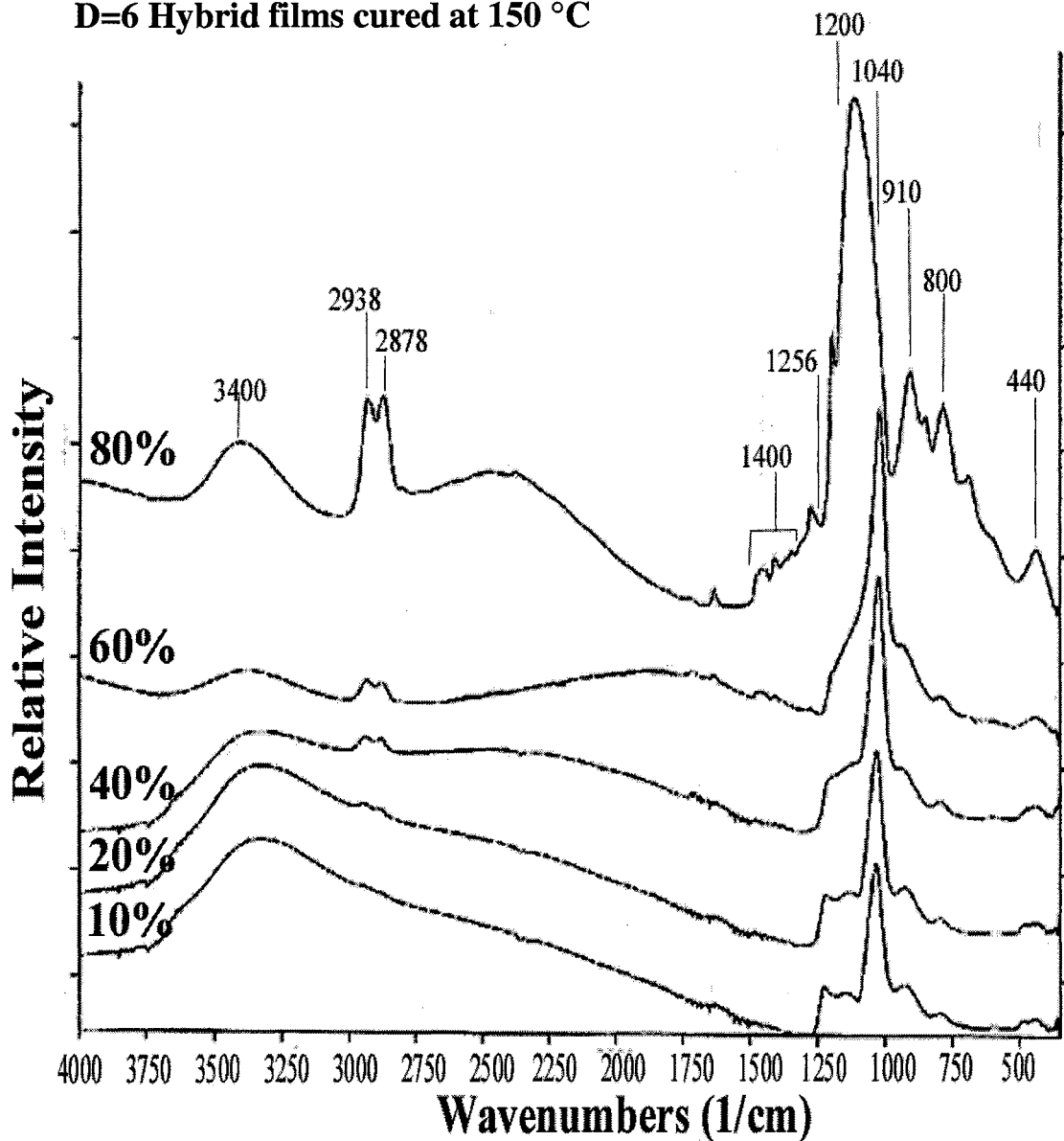


Figure 12: Overlaid IR reflectance spectra of epoxide-based ormosil thin film prepared using an D value of 6 and cured at 150 °C.

D=1 Hybrid films cured at 300 °C

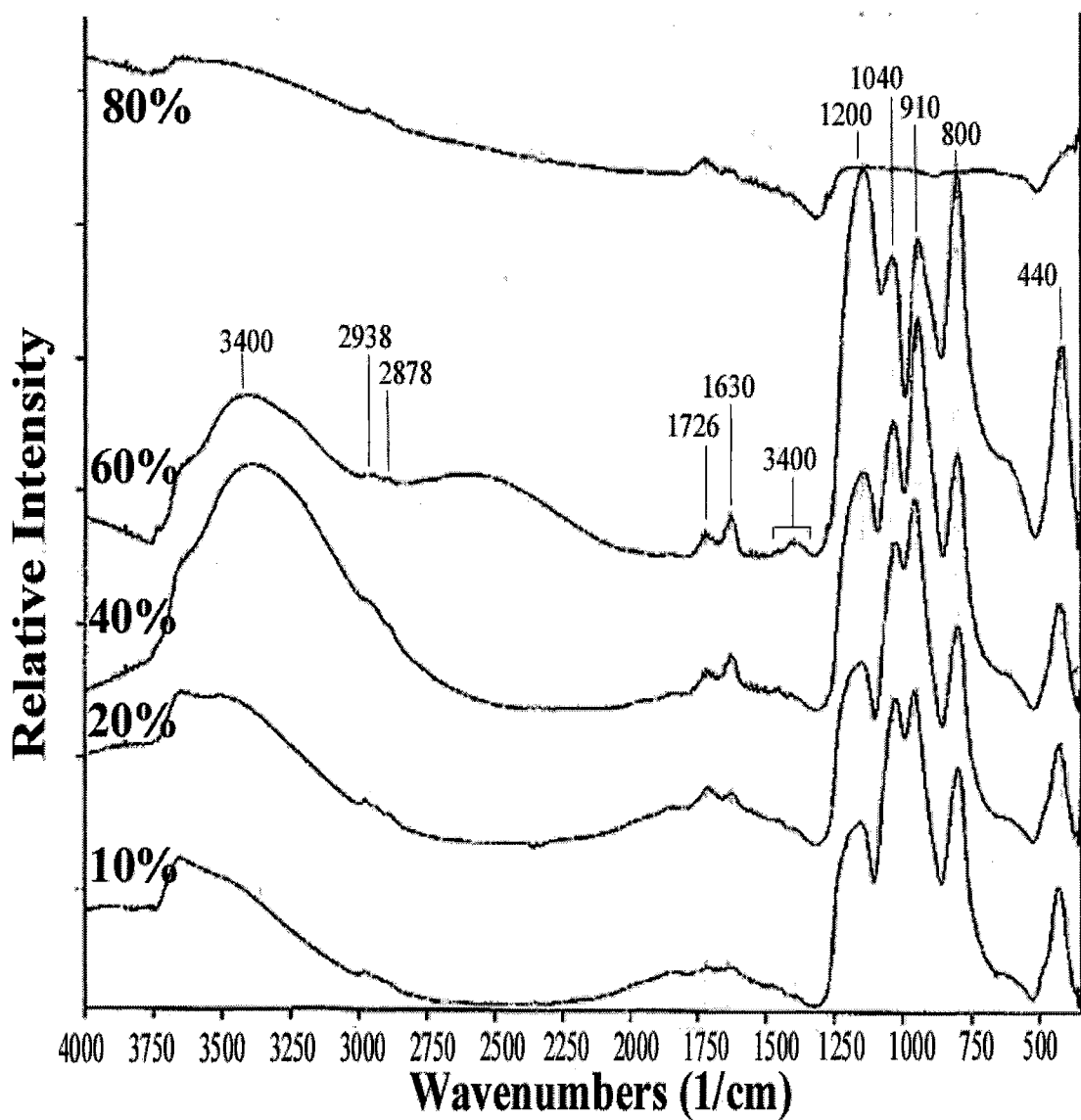


Figure 13: Overlaid IR reflectance spectra of epoxide-based ormosil thin film prepared using an D value of 1 and cured at 300 °C.

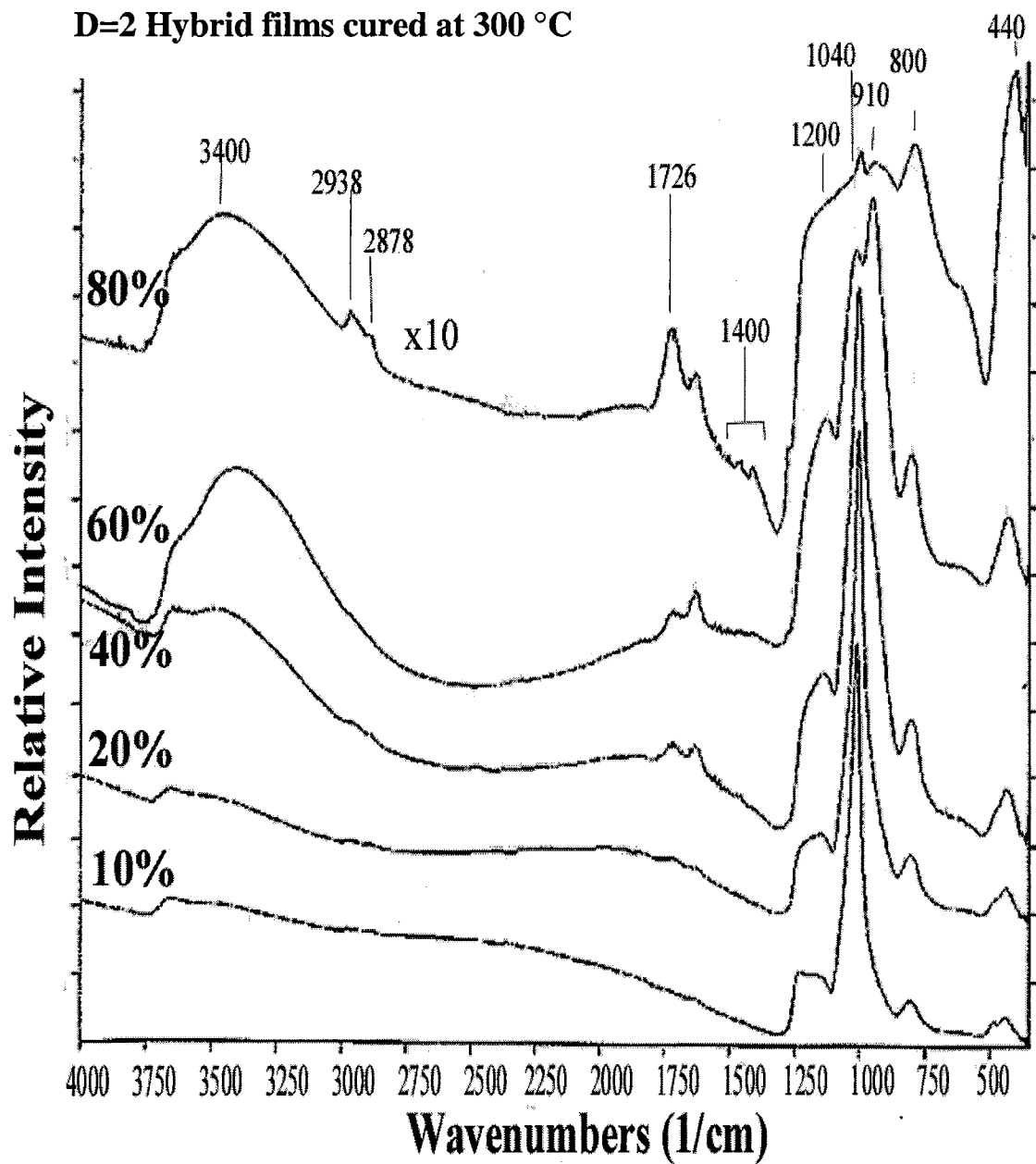


Figure 14: Overlaid IR reflectance spectra of epoxide-based ormosil thin film prepared using an D value of 2 and cured at 300 °C.

D=4 Hybrid films cured at 300 °C

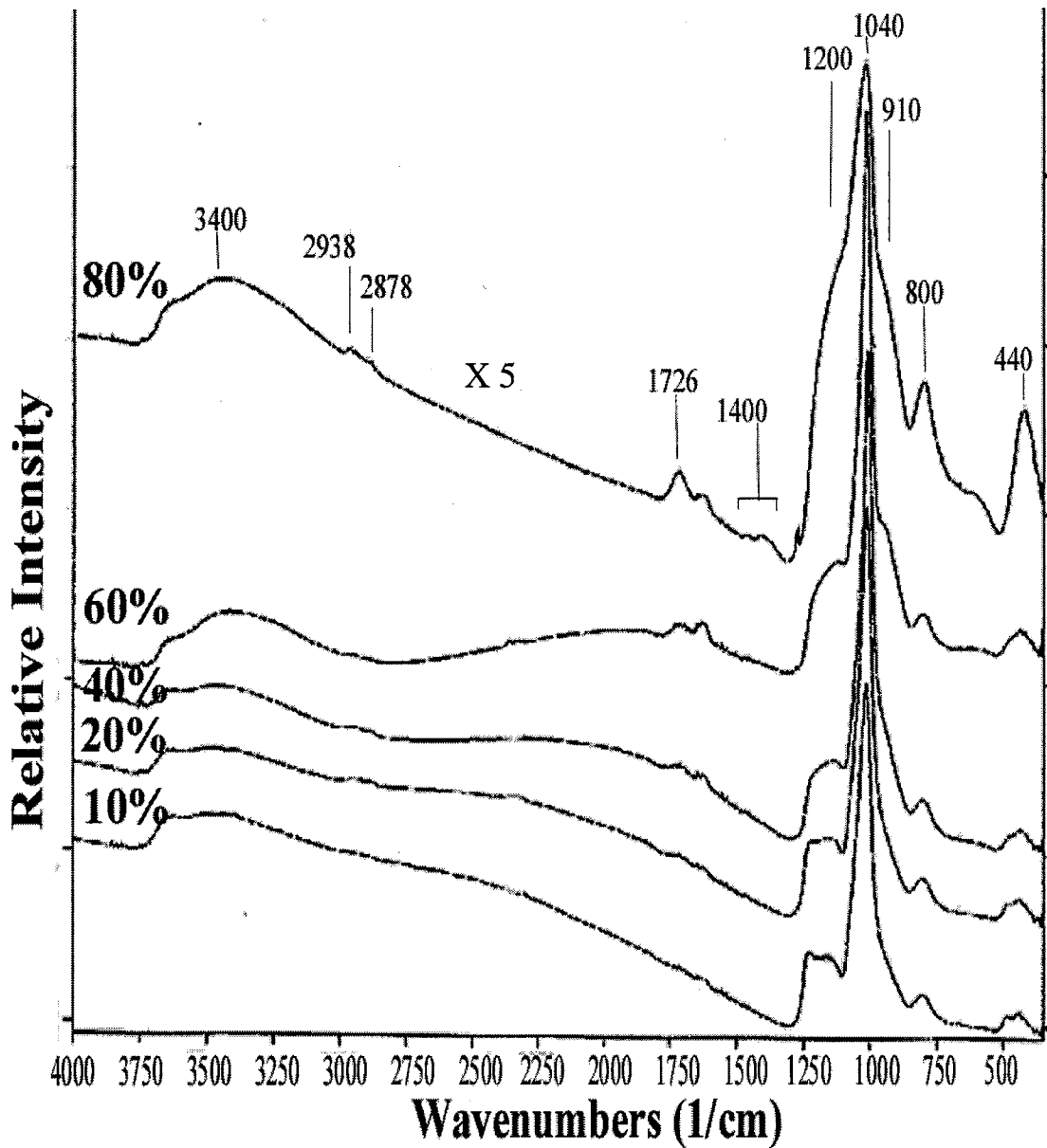


Figure 15: Overlaid IR reflectance spectra of epoxide-based ormosil thin film prepared using an D value of 4 and cured at 300 °C.

D=6 Hybrid films cured at 300 °C

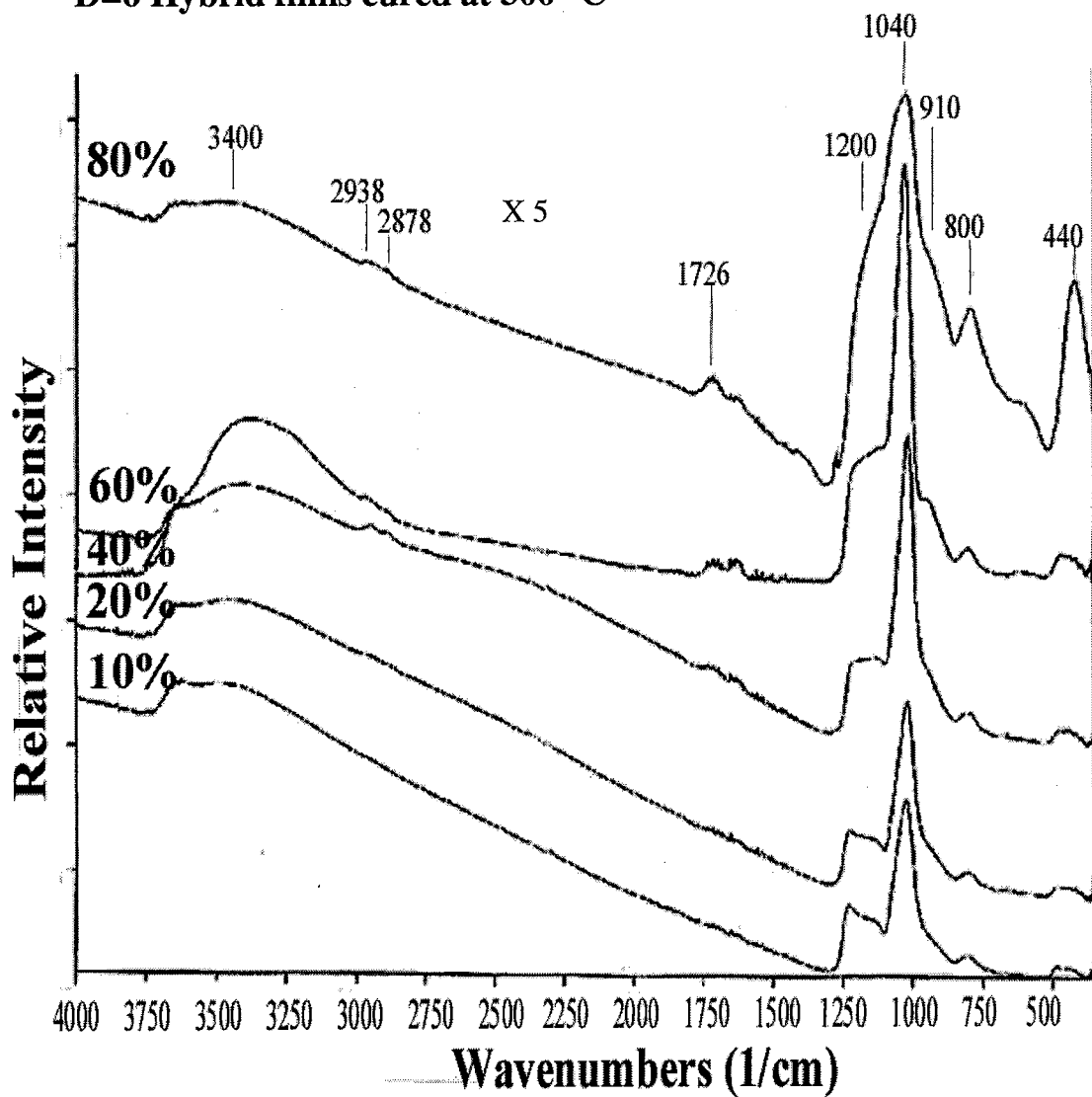


Figure 16: Overlaid IR reflectance spectra of epoxide-based ormosil thin film prepared using an D value of 6 and cured at 300 °C.

APPENDIX G

MONITORING EPOXIDE CONTENT USING RAMAN SPECTRSCOPY

Figures G.1(a)-G.1(d) represents the relative intensity decreases in epoxide peaks as function of curing temperature. Graphical representations were derived from intensity ratios between the 1256 cm^{-1} epoxide and 1295 cm^{-1} =CH₂ peaks for each of the hybrid gels. The 1295 cm^{-1} =CH₂ peak was used as an internal standard, while the intensity in the 1256 cm^{-1} peak was used to identify epoxide content. Intensity ratios were converted to a relative percentage using unreacted GPTMS epoxide as a 100% reference and the 10% R=24 epoxide ormosil gel as zero reference. The zero epoxide content in the 10% R=24 gel was confirmed by NMR analysis(Chapter 7). With the epoxide percentage based on the overall organic content, the results were directly comparable between hybrid compositions. Each graph represents the change in epoxide content as a function of curing temperature and hybrid content.

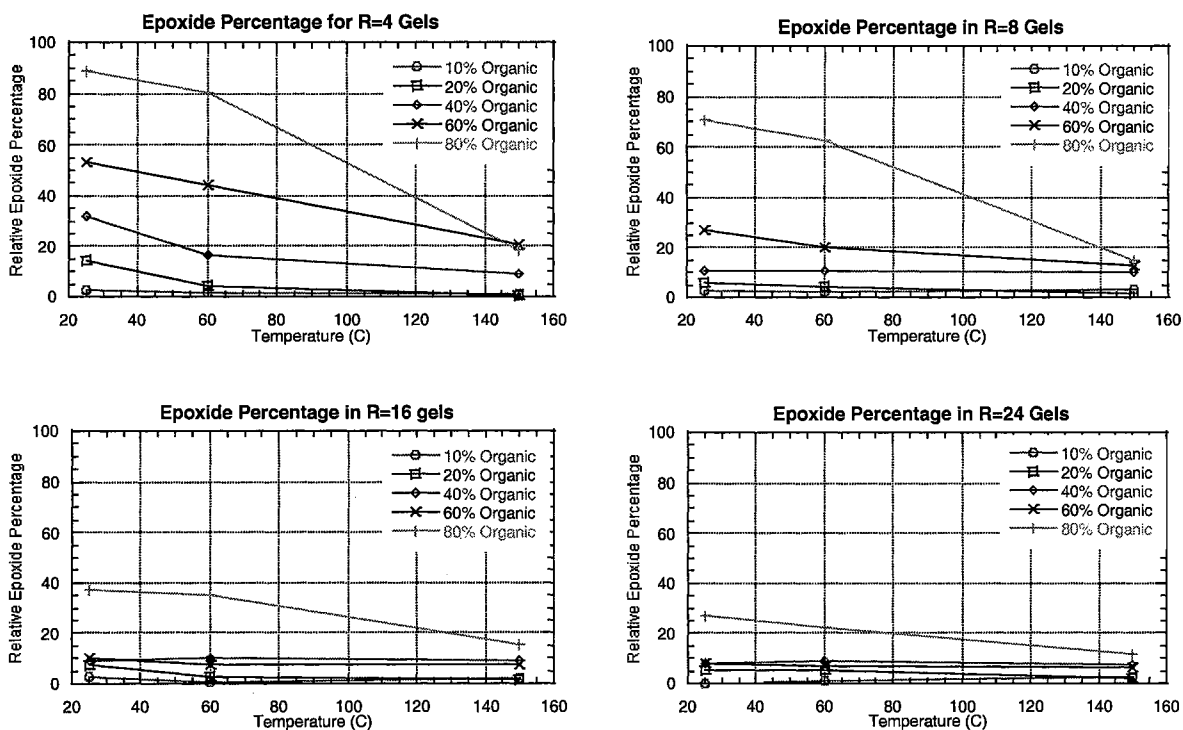


Figure G.1: Relative epoxide percentage with respect to the organic content. Graphs are represented as function of temperature and R value. The lines are only present to guide the eyes.

Comparison between the graphs revealed the epoxide content varied as functions of hybrid content, R value, and curing temperature. In all of the graphs, the concentrations of epoxide content decreased progressively with a decrease in hybrid content and curing temperature. Temperature comparisons indicated the epoxide group was relatively stable at low temperature and reacted after heating to 150°C. Comparisons between the graphs revealed dramatic losses with an increase in R value. The variations in epoxide content as a function of hybrid content and R value were consistent with the conclusion present in Chapter 7 NMR and indicated the epoxide group was unstable in an acid aqueous environment. By using the 1296 cm^{-1} and 1256 cm^{-1} epoxide vibrations, the relative epoxide content can be monitored as a function of processing conditions.

REFERENCE

1. M. Ebelmen, Ann., 57 (1846) 319.
2. M. Ebelmen, Ann. Chinn. Phys., 15 (1846) 129.
3. M. Ebelmen, Comptes Rend. De l'Acad des Science, 25 (1847) 854.
4. D.I. Meneleyev, Khim. Zhur. Sok. I. Eng., 4 (1860) 65.
5. C. Brinker and G. Scherer, Sol-gel Science: The physics and chemistry of sol-gel processing, 1990, Academic Press, San Diego, CA.
6. J. Mackenzie, Hybrid Organic-Inorganic Materials, 1995 American Chemical Society.
7. H. Schmidt, J. Non-Cryst. Solids, 100 (1988), 51-64.
8. D.R. Ulrich, J. Non.-Cryst. Solids, 121 (1990), 465-479.
9. U. Schubert, M. Husing, and A. Lorenz, Chem. Mater, 7 (1995), 2010-2027.
10. O. Lev, Z.Wu, S. Bharathi, V. Glezer, A. Modestov, J. Gun, L. Rabinovich, and S. Sampath.
11. C.J. Brinker, J. Non-Cryst. Solids, 100 (1988), 31-50.
12. J. Ying and J. Benzige, J. Am. Ceram. Soc., 76 (1993) 2571-82.
13. G.W. Scherer, Structural Evolution of Sol-gel Glasses, Yogyo Kyoka Shi, 95 (1987), 21-44.
14. J. Pope and J.D. Mackenzie, J. Non-Cryst. Solids, 87 (1986), 185-198.
15. A.H. Boonstra and J.M. Baken, J. Non-Cryst. Solids, 122 (1990), 171-182.
16. C.J. Brinker, K.D. Keefer, D.W. Schaefer, R.A. Assink, B.D. Kay, and C.S. Ashley, J. Non-Cryst. Solids, 63 (1984), 45-59.
17. M. Spinu, C. Arnold, and J.E. McGraph, Poly Pre., (19--), 125-127.

18. I. Artaki, T. Zerda, and J. Jonas, *J. Non-Cryst. Solids*, 81 (1986), 381-395.
19. J.C. Ro and I.J. Chung, *J. Non-Cryst. Solids*, 110 (1989) 26-32.
20. J.C. Pouxviel and J.P. Bolot, J.C. Beloeil, and J.Y. Lallemand, *J. Non-Cryst. Solids*, 89 (1987), 345-360.
21. A. Duran, C. Serna, V. Fornes, and J.M. Navarro, *J. Non-Cryst. Solids*, 82 (1986), 69-77.
22. J.J. Beek, D. Seykens, J. Jansen, and R. Schuiling, *J. Non-Cryst. Solids*, 134 (1991) 14-22.
23. G. Kordas, *Mat. Res. Soc. Symp. Proc.*, 61 (1986), 419-423.
24. G. Kordos and L.C. Klein, *J. Non-Cryst. Solids*, 84 (1986), 325-328.
25. F. Orgaz and H. Rawson, *J. Non-Crystalline Solids*, 82 (1986), 57-68.
26. J.C. Pouxviel and J.P. Boilet, *J. Non-Cryst. Solids*, 94 (1987), 374-386.
27. I. Strawbridge, A.F. Craievich, and P.F. James, *J. Non-Cryst. Solids*, 72 (1985), 139-157.
28. M.A. Fardad, E.M. Yeatman, E.J. Dawnay, M. Green, and F. Horowitz, *J. Non-Cryst. Solids*, 183 (1995), 260-267.
29. A. Assink and B.D. Kay, *J. Non-Cryst. Solids*, 99 (1988), 359-370.
30. C.J. Brinker and G.W. Scherer, *J. Non-Cryst. Solids*, 70 (1985) 301-322.
31. P.F. James, *J. Non-Cryst. Solids*, 100 (1988) 93-114.
32. K.C. Chen, T. Tsuchiya, and J.D. Mackenzie, *J. Non-Crystal. Solids*, 81 (1986), 227-237.
33. R. Aelion, A. Loebel, and F. Elrich, *J. Am. Chem. Soc.*, 72 (1950), 5705-5712.
34. R. Aelion, A. Loebel, and F. Elrich, *Recueil Travaux Chimiques*, 69 (1950), 61-75.
35. D. Avnir and V.R. Kaufman, *J. Non-Cryst. Solids*, 192 (1987), 180-182.
36. C.J. Brinker, K.D. Keefer, D.W. Schaefer, R.A. Assink, B.D. Kay, and C.S. Ashley, *J. Non-Cryst. Solids*, 63 (1984) 45-59.
37. 1

38. M. Yamane, S. Inoue, and A. Yasumori, *J. Non-Cryst. Solids*, 63 (1984) 13.
39. M. Shane and M.L. Mecartney, *J. Mater. Sci.*, 25 (1990), 1537-1544.
40. R.K. Iler, The Chemistry of Silica, Wiley (1979), New York.
41. R. Kasemann and H. Schmidt, *New J. Chem.*, 18 (1994) 1117-1123.
42. H. Schmidt, *J. Non-Cryst. Solids*, 178 (1994), 302-312.
43. H. Schmidt, H. Krug, B. Zeitz, and E. Geiter, *SPIE* 3136 (1997), 480-485.
44. H. Schmidt and B. Seiferling, *Mat. Res. Soc. Symp.*, 73 (1986), 739-751.
45. W. Chen, H. Feng, D. He, and C. Ye, *J. Appl. Poly. Sci.*, 67 (1998), 139-147.
46. L. Delattre and F. Babonneau, *Mater. Res. Soc. Symp. Proc.*, 346 (1994), 365.
47. B. De Witte, D. Commers, and J. Uytterhoeven, *J. Non-Cryst. Solids*, 202 (1996), 35-41.
48. A. Aelion, A. Loebel, and F. Elrich, *J. Am. Chem. Soc.*, 72 (1950), 5705.
49. 3M Industrial Chemical Products, St. Paul Minnesota, Tech. Eval.
50. D. Quere, A. de Ryck, and O. Ou Ramidane, *Europhysics Lett.*, 37(1997), 305.
51. D.R. Karsa, Additives for Water-Based Coatings, Royal Society of Chemistry, Great Brittan, (1990).
52. R. Parkhill and E.T. Knobbe, AFOSR (1996), AFRL/MLBT summer report.
53. R. Parkhill and E.T. Knobbe, AFOSR (1997), AFRL/MLBT summer report.
54. R. Parkhill, E.T. Knobbe, and M.S. Donley., submitted to Progress in Organic Coatings.
55. R. Parkhill, T.L. Metroke, M.S. Donley, and E.T. Knobbe, *Int. Conf. on Glass, Inter. Symp. on Sol-gel Tech. – III*, (1997), San Francisco, CA.
56. C.J. Brinker, A.J. Hurd, P.R. Schunk, G.C. Frye, and C.S. Ashley, *J. Non-Cryst. Solids*, 147-148 (1992), 424-436.
57. C.J. Brinker, G.C. Frye, J. Hurd, and C.S. Ashley, *Thin Solid Films*, 201 (1991), 97-108.

58. S. Zhang, C.L. Czekaj, and W.T. Ford, *J. Magnetic. Res.*, A111 (1994) 87-92.
59. D. Lin-Vien, N. B. Colthup, W. G. Fateley, J.G. Grasselli, *The Handbook of Infrared and Raman Characteristic Frequencies of Organic Molecules*, Academic, New York ©1991.
60. G. Socrates, *Infrared Characteristic Group Frequencies*, John Wiley and Sons, New York © 1980.
61. N.B. Colthup, S.E. Wiberley, and L.H. Daly, *Introduction to Infrared and Raman Spectroscopy*, Academic Press, New York © 1990.
62. F. Devreux, J.P. Boilot, F. Chaput, and A. Lecomte, *Mater. Res. Soc. Symp. Proc.*, 180 (1990), 211-216
63. W.G. Klemperer, V.V. Mainz, and D.M. Miller, *Mat. Res. Soc. Symp. Proc.*, 73 (1986), 15-25.
64. F. Devreux, J.P. Boilot, F. Chaput, and A. Lecomte, *Mater. Res. Soc. Symp. Proc.*, 180 (1990) 211-216.
65. K.L. Walther, A. Wokaun, and A. Baiker, *Mol. Phys.*, 71 (1990), 769-780
66. G. Garvey, and B. Smith, *Mat. Res. Soc. Symp. Proc.*, 180 (1990), 223-28.
67. M. Spinu, C. Arnold, and J.E. McGraph, *Poly. Pre.*
68. A.J. Vega and G.W. Scherer, *J. Non-Cryst. Solids*, 111 (1989), 153-166.
69. A.R. Grimmer, H. Rosenberger, H. Burger, and W. Vogel, *J. Non-Crystalline Solids*, 99 (1988), 371-378.
70. J. Blumel, *J. Am. Chem. Soc.*, 117 (1995). 2112-2113
71. D.W. Sindorf and G.E. Maciel, *J. Phys. Chem.*, 86 (1982), 5208-5219.
72. G.E. Maciel and D.W. Sindorf, *J. Am. Chem. Soc.*, 102 (1980), 7606-7607.
73. M. Muroya and K. Yaguchi, *Prog. in Org. Coatings*, 31 (1997) 153-156.
74. C. Fyfe, G. Gobbi, and G. Kennedy, *J. Phys. Chem.*, 89 (1985), 277-281.
L.W. Kelts and N.J. Armstrong, *Mat. Res. Soc. Symp. Proc.*, 121 (1988), 519.
75. E. Lippmaa, M. Magi, A. Samoson, G. Englehardt, and A.R. Grimmer, *J. Am. Chem. Soc.* 102, (1980), 4889.

76. G. Engelhardt, H. Jancke, E. Lippmaa, and A. Samoson, *J. Organometallic Chem.*, 210 (1981), 295.
77. M. Magi, E. Lippmaa, A. Samoson, G. Engelhardt, and A.R. Grimmer, *J. Phys. Chem.*, 88 (1984), 1518.
78. R.H. Glaser, G.L. Wilkes, and C.E. Bronnimann, *J. Non-Cryst. Solids*, 113 (1989), 73-87.
79. M.P. Peeters, W.J. Wakelkamp, and A.P. Kentgens, *J. Non-Cryst. Solids*, 189 (1995), 77-89.
80. B. Humbert, *J. Non-Crystalline Solids*, 191 (1995), 29-37.
81. L. Voon Ng, P. Thompson, J. Sanchez, C. W. Macosko, and A.V. McCormick, *Macromolecules*, 28 (1995), 6471-6476.
82. L. Voon Ng and A. V. McCormick, *J. Phys. Chem.*, 100 (1996), 12517-12531.
83. D.M. Krol and J.G. van Lierop, *J. Non-Crystalline Solids*, 63 (1984), 131-144.
84. D.M. Krol and J.G. van Lierop, *J. Non-Crystalline Solids*, 68 (1984), 163-166.
85. B. Riegel, I. Hartmann, W. Kiefer, J. Grob, and J. Fricke, *J. Non-Crystalline Solids*, 211 (1997), 294-298.
86. R. Elloitt, *J. Non-Crystalline Solids*, 182 (1995), 1-8.
87. J.C. Phillips, *J. Non-Crystalline Solids*, 63, (1984), 347-355.
88. F.L. Galeener, *Phys. Rev. B*, 19 (1979), 4292-4297.
89. C.J. Brinker, R.J. Kirkpatrick, R.K. Brow, and D.R. Tallant, *J. Non-Crystalline Solids*, 120, (1990), 26-33.
90. A. Bertoluzza, C. Fagnano, M. Morelli, V. Gottardi, and M. Guglielmi, *J. Non-Cryst. Solids*, 48 (1982), 117-128.
91. D.R. Tallant, B.C. Bunker, C.J. Brinker, and C.A. Balfe, *Mater. Res. Soc. Symp. Proc.*, 72 (1986), 261.
92. B. Humbert, A. Burneau, J.P. Gallas, and J.C. Lavalley, *J. Non-Crystalline Solids*, 143, (1992), 75-83.
93. C.J. Brinker, D.R. Tallant, E.P. Roth, and C.S. Ashley, *Mat. Res. Soc. Symp. Proc.*, 61 (1986), 387-411.

94. C.A.M. Mulder and A.A.J.M. Damen, *J. Non-Crystalline Solids*, 93, (1987), 387-394.
95. P.K. Dutta and D. Shieh, *Appl. Spect.*, 39 (1985), 343-346.
96. F.L. Galeener, *J. Non-Crystalline Solids*, 49 (1982), 53-62.
97. J.L. Lippert, S.B. Melpolder, and L.M. Kelts, *J. Non-Crystalline Solids*, 104 (1988), 139-147.
98. J. Gnado, P. Dhamelincourt, C. Pelegris, M. Traisnel, and A. Le Maguer Mayot, *J. Non-Crystalline Solids*, 208 (1996), 247-258.
99. C. Chemarin, B. Champagnon, and G. Panczer, *J. Non-Crystalline Solids*, 216 (1997), 111-115.
100. V. Gottardi, M. Guglielmi, A. Bertoluzza, C. Fagnano, and M.A. Morelli, *J. Non-Crystalline Solids*, 63 (1984), 71-80.
101. M. Yamane, S. Aso, Okano and T. Sakaino, *J. Mater. Sci*, 14 (1979) 607.
102. M. Yamane, S. Aso and T. Sakaino, *J. Mater. Sci* 13 (1978) 865.
103. M. O'Keefe and G.V. Gibbs, *J. Chem. Phys.*, 81 (1984), 876.
J.F. van Staden, M.A. Makhafola, and D. de Waal, *Appl. Spec.*, 50 (1996), 991-994.
104. F. Orgaz and H. Rawson, *J. Non-Crystalline Solids*, 82 (1986), 57-68.
105. J. Y. Ying and J. B. Benziger, *J. Non-Cryst. Solids*, 147&148 (1992), 222-231.
106. Merk Index, Merck & Co., New Jersey ©1983.
107. E.I. Kamitsos, A.P. Patsis, and G. Kordas, *Phys. Rev. B*, 48 (1993), 12499-12505.
108. R.M. Almedia, T.A. Guiton, and C.G. Pantano, *J. Non-Cryst. Solids*, 121, (1990), 193-297.
109. M.C. Matos, L.M. Ilharco, and R.M. Almeida, *J. Non-Cryst. Solids*, 147&148, (1992), 232-237.
110. C.T. Kirk, *Phys. Rev. B*, 38(2) (1988), 1255.
111. F. Terki, C. Levelut, M. Boissier, and J. Pelous, *Phys. Rev. B*, 53 (1996), 2411-2418.

112. V. Gottardi, M. Guglielmi, A. Bertoluzza, C. Fagnano, and M.A. Morelli, *J. Non-Crystalline Solids*, 63 (1984), 71-80.
113. A. Chmel, T. Pesina, and V.S. Shashkin, *J. Non-Crystalline Solids*, 210 (1997), 254-260.
114. L.M. Gan, K. Zhang, and C.H. Chew, *Colloids and Surf. A*, 110 (1996), 199-206.
115. H. Imai and H. Hirashima, *SPIE Sol-Gel Optics III*, 2288 (1994), 171.
116. C.A. Capozzi, R.A. Condrate, and L.D. Pye, *SPIE 2287* (1992) 176-182.
117. R.M. Almeida, H.C. Vasconcelos, and L.M. Ilharco, *SPIE Sol-Gel Optics III*, 2288 (1994), 678-687.
118. N. Viart and J.L. Rehspringer, *J. Non-Cryst. Solids*, 195 (1996), 223-231.
119. H.F. Poulsu, J. Newefeidud, H.B. Neuman, J.R. Schneider, M.P. Zeilder, *J. Non-Cryst. Solids*, 188 (1995) 63.
120. R. Hook, *J. Non-Cryst. Solids*, 195 (1996), 1-15.
121. F. Babonneau, *New J. Chem.*, 18 (1994), 1065-1071.
122. J.J. Yang, I.M. El-Nahhal, G.E. Maciel, *J. Non-Cryst. Solids*, 204 (1996), 105-117.
123. E. Bayer, K. Albert, J. Reiners, M. Neider, and D. Muller, *J. Chrom.*, 264 (1983), 197-213.
124. B. Riegel, W. Kiefer, S. Hofacker, and G. Schottner, *Ber. Bunsen Ges.*, 102 (1998), 1573-1576.
125. M. Templin, U. Wiesner, and H. Spiess, *Adv. Mater.*, 9 (1997), 814-817.
126. Y. Pocker, B. Ronald, L. Ferrin, *J. Am. Chem. Soc.*, 102 (1980), 7725-7732.
127. R. Nass, E. Arpac, W. Glaubitt, and H. Schmidt, *J. Non-Cryst. Solids*, 121 (1990), 370-374.
128. Y. Hsu and J. Huang, *J. Non-Cryst. Solids*, 208 (1996), 259-266.
129. E.J. Vandenberg, *Poly. Pre.* (1993), 253-254.
130. N. Husing, F. Schwetferger, W. Tappert, and U. Schubert, *J. Non-Cryst. Solids*, 186 (1995), 37-43.

131. S.A. Sojik and W.B. Moniz, *J. Appl. Poly. Sci.*, 20 (1976), 1977-1982.
132. W.W. Fleming, *J. Appl. Poly. Sci.*, 30 (1985), 2853-2862.
133. R. Kasemann, H. Schmidt, and E. Wintrich, *Mat. Res. Soc. Symp. Proc.*, 346 (1994), 915-921.
134. G. A. Sigel, R.C. Domszy, and W.C. Welch, *Mat. Res. Soc. Symp. Proc.*, 346 (1994), 135-141.
135. E.A. Williams, *Ann. Repts. NMR* 235 (1983).
136. M. Pursch, A. Jager, T. Schneller, R. Brindle, K. Albert, and E. Lindner, *Chem. Mater.*, 8 (1996), 1245-1249.
137. S. Prabakar, and R.A. Assink, *J. Non-Cryst. Solids*, 211 (1997), 39-48.
- 138.
139. C.D. Volpe, S. Dire, and E. Pagani, *J. Non-Cryst. Solids*, 209 (1997), 51-60
140. X. Li, and T. King, *J. Non-Cryst. Solids*, 204 (1996), 235-242.
141. K. Chike, M. Myrick, R. Lyon, and S. Angle, *Appl. Spec.*, 47 (1993), 1631-35.
142. N. Husing, U. Schubert, B. Riegel, and W. Kiefer, *Mat. Res. Soc. Symp. Proc.*, 435 (1996), 339-344.
143. X. Li and T.A. King, *J. Non-Cryst. Solids*, 204 (1996), 235-242.
144. Rice and Stallbaumer, *J. Am. Chem. Soc.* 64: 1527-1530 (1942).
U. Posset, M. Lankers, W. Kiefer, H. Steins, and G. Schottner, *Appl. Spec.*, 47 (1993), 1600-1603
145. V. Arslanov, L. Sheinina, R. Bulgakova, and A. Belomestnykh, *Langmuir*, 11 (1995), 3953-3958.
146. Y. Yan, Y. Hoshino, Z. Duan, S.R. Chaudhuri, and A. Sarkar, *Chem. Mater.*, 9 (1997), 2583-2587.
147. H. Lee and K. Neville, Handbook of Epoxy Resins, 1967, McGraw-Hill, New York.
148. Y. Yan, Y. Hoshino, Z. Duan, S. R. Chaudhuri, and A. Sarkar, *Mat. Res. Soc. Symp. Proc.*, 435 (1996), 307-312.

149. B. Karmakar, G. De. D. Kundu, and D. Ganguli, *J. Non-Cryst. Solids*, 135 (1991), 29-36.
150. C. Fyfe, G. Gobbi, and G. Kennedy, *J. Phys. Chem.*, 89 (1985), 277-281.
151. H. Schmidt, S. Langenfeld, and R. Nab, *Mater. And Design*, 18 (1997), 309-313.
152. H. Schmidt, *J. Non-Cryst. Solids*, 178 (1994), 302-312.
153. H. Schmidt, R. Kasemann, T. Burkhart, G. Wagner, E. Arpac, and E. Geiter, Hybrid Organic-Inorganic Composites, 1995, American Chemical Society.
154. I. Gautier-Luneau, A. Mosset, J. Galy, and H. Schmidt, *J. Mater. Sci.*, 25 (1990), 3739-3745.
155. X. Ming Chen, B. Ellis, F. Wang, A. Seddon, *J. Non-Cryst. Solids*, 185 (1995), 1-17.
156. H. Schmidt, H. Krug, B. Zeitz, and E. Geiter, *SPIE*, 3136 (1997), 220-228.
157. T. Iwamoto and J. Mackenzie, *J. Mater. Sci.*, 30 (1995), 2566-2570.
158. T. Suratwala, K. Davidson, Z. Gardlund, and D. Uhlmann, *SPIE*, 3136 (1997), 36-47.

VITAE

Robert Parkhill

Candidate for the Degree of

Doctor of Philosophy

Thesis: INVESTIGATION OF WATER-BASED SILICA AND ORGANICALLY
MODIFIED SLICATE SOL-GEL SYSTEMS

Major Field: Chemistry

Biographical

Education: Graduated from Dickson High School, Ardmore, Oklahoma, in May of 1989; received Bachelor of Science degree in Chemistry from the University of Central Oklahoma, Edmond, Oklahoma in July 1993. Completed the requirements for the Doctor of Philosophy degree with a major in Chemistry at Oklahoma State University in July 1999.

Experience: Employed as a teaching and research assistant at Oklahoma State University, Department of Chemistry, 1993 to 1995; employed as a research assistant at Oklahoma State University under a Environmental Institute Presidential Fellowship, 1996 to 1998; employed as a visiting scientist at Wright Patterson Air Force Base, Materials Directorate, Dayton Ohio, summer of 1996 and 1997; employed as a materials engineer at Air Force Research Laboratory, Materials Directorate, Dayton, Ohio, June 1998 to present. My teaching responsibilities have included laboratory courses in introductory chemistry for majors and non-major students. My research responsibilities have included advanced synthesis of alkoxide precursors, design and construction of pulse laser deposition system, development of advanced sol-gel based coating systems, and general laboratory safety.

Professional Memberships: Phi Lambda Epsilon and Materials Research Society